Technische Universität Braunschweig

Experimental and theoretical analyses of the metabolic role of the 262-kb plasmid in the context of the endogenously produced antibiotic tropodithietic acid in *Phaeobacter inhibens* DSM 17395

Von der Fakultät für Lebenswissenschaften

der Technischen Universität Carolo-Wilhelmina zu Braunschweig

zur Erlangung des Grades

einer Doktorin der Naturwissenschaften

(Dr. rer. nat.)

genehmigte

D i s s e r t a t i o n

von Sabine Eva Will

aus Koblenz

1. Referent: Professor Dr. Dietmar Schomburg
2. Referent: Professor Dr. Dieter Jahn
eingereicht am: 28.03.2018
mündliche Prüfung (Disputation) am: 18.06.2018

Druckjahr 2018

Vorveröffentlichungen der Dissertation

Teilergebnisse aus dieser Arbeit wurden mit Genehmigung der Fakultät für Lebenswissenschaften, vertreten durch den Mentor der Arbeit, in folgenden Beiträgen vorab veröffentlicht:

Publikationen

Trautwein, K., Will, S.E., Hulsch, R., Maschmann, U., Wiegmann, K., Hensler, M., Michael, V., Ruppersberg, H., Wünsch, D., Feenders, C., Neumann-Schaal, M., Kaltenhäuser, S., Ulbrich, M., Schmidt-Hohagen, K., Blasius, B., Petersen, J., Schomburg, D., Rabus, R. (2016). Native plasmids restrict growth of *Phaeobacter inhibens* DSM 17395: Energetic costs of plasmids assessed by quantitative physiological analyses. *Environ. Microbiol*., 18, 4817-4829.

Will, S.E., Neumann-Schaal, M., Heydorn, R.L., Bartling, P., Petersen, J., Schomburg, D. (2017). The limits to growth – energetic burden of the endogenous antibiotic tropodithietic acid in *Phaeobacter inhibens* DSM 17395. *PLoS ONE* 12 (5), e0177295.

Reimer, L.C., Will, S.E., Schomburg, D. (2017). The fate of lysine: Non-targeted stable isotope analysis reveals parallel ways for lysine catabolization in *Phaeobacter inhibens*. *PLoS ONE* 12 (10), e0186395.

Tagungsbeiträge (Vorträge)

Trautwein, K., Will, S.E. (2015). Growth control by plasmids in *Phaeobacter inhibens* DSM 17395. 10. Statusseminar des SFB TRR 51, 07.-08.05.15, Oldenburg.

Posterbeiträge

Will, S.E., Majer, E.V.I., Bartling, P., Petersen, J., Schomburg, D. (2016). Dependency between growth, substrate and antibiotic production in *Phaeobacter inhibens* DSM 17395. EMBO Conference: From Functional Genomics to Systems Biology. 12.-15.11.2016, Heidelberg.

Table of contents

Abbreviations

Abbreviation	Explanation
AHL	*N*-acyl homoserine lactone
ADP	Adenosine-5'-diphosphate
AMP	Adenosine-5'-monophosphate
APCI	Atmospheric pressure chemical ionization
ATP	Adenosine-5'-triphosphate
BLAST	Basic local alignment search tool
CDW	Cell dry weight
CDW_{max}	Maximal cell dry weight
CoA	Coenzyme A
DMSP	Dimethylsulfoniopropionate
DNA	Deoxyribonucleic acid
DO	Dissolved oxygen
DSMZ	German Collection for Microorganisms and Cell Cultures (Braunschweig, Germany)
EC	Enzyme commission number
EDTA	Ethylenediaminetetraacetic acid
EI	Electron ionization
ESI	Electrospray ionization
et al.	Latin: *et alii*, and others
FAD	Flavine adenine dinucleotide
FBA	Flux balance analysis
FLD	Fluorescence detector
FMOC	fluorenylmethylchloroformate
GAM	Growth-associated maintenance energy
GC	Gas chromatography
HPLC	High performance liquid chromatography
ICBM	Institute for Chemistry and Biology of the Marine Environment (Carl von Ossietzky University Oldenburg)
kb	kilobase
LC	Liquid chromatography
LTA	Lipoteichoic acid
m/z	Mass to charge ration
MB medium	Marine bouillon medium
MS	Mass spectrometry
MSTFA	*N*-methyl-*N*-(trimethylsilyl)-trifluoro-acetamide
MTBE	Methyl-*tert*-butylether
NAD^+/NADH	Nicotinamide adenine dinucleotide (oxidized/reduced)

Abbreviation	Explanation
$NADP^+$/NADPH	Nicotinamide adenine dinucleotide phosphate (oxidized/reduced)
NGAM	Non-growth-associated maintenance energy
OD_{600}	Optical density, measured at 600 nm
OD_{max}	Maximal optical density, measured at 600 nm
OPA	O-phthalaldehyde
OTR	Oxygen transfer rate
OUR	Oxygen uptake rate
PHB	Poly-(*R*)-3-hydroxybutanoate
q_{O2}	Specific oxygen uptake rate
q_S	Specific substrate uptake rate
RI	Retention index
RNA	Ribonucleic acid
rpm	Rotations per minute
RPKM	Reads per kilobase of gene per million reads
SDS	Sodium dodecyl sulphate
SPE	Solid phase extraction
TDA	Tropodithietic acid
TMS	Trimethylsilyl
TOF	Time of flight
x g	x-fold acceleration
μ	Specific growth rate
μ_{lin}	Linear growth rate

Units were abbreviated according to the international unit system (SI, Systéme international d'unités), except for molar concentrations (mol L^{-1}), which were abbreviated with the capital letter M. Furthermore, chemical elements were abbreviated by their symbols of the periodic table of elements.

Summary

Extrachromosomal elements play a crucial role in adaptation and survival of many marine bacteria in their natural habitat providing essential features and facilitating lateral gene transfer. *Phaeobacter inhibens* DSM 17395 carries three plasmids with advantageous functions: 65-kb (biofilm, motility), 78-kb (siderophores) and 262-kb (tropodithietic acid).

The metabolic role of the 262-kb plasmid of *P. inhibens* DSM 17395 with a focus on biosynthesis of TDA were studied as part of this thesis applying both, non-targeted GC- and LC-MS based analyses. Experimental data were complemented by *in silico* analyses with the reconstructed metabolic model *i*Pin571.

Deletion of the 262-kb plasmid improved growth efficiency with only minor changes on metabolic level which can be attributed to the pipecolate oxidase-dependent lysine catabolism encoded by the plasmid.

Combined metabolomics and transcriptomics showed that the wild-type strain entered stationary growth phase due to the inhibitory effect by its own produced TDA. Sufficient carbon provided by amino acids were still available in the medium. Contrary to that, the Δ262-kb plasmid-cured mutant strain was carbon-limited. Detailed analyses indicated the degradation of the storage compound polyhydroxybutanoate to produce a proposed lipoteichoic acid as a response to a starvation triggered phage.

A new biosynthetic pathway for TDA was proposed based on metabolome and transcriptome data revealing an unexpected strategy for sulfur incorporation via an episulfide. Furthermore, a methylated ("pre"-) TDA was observed with a proposed associated methyltransferase, encoded on the chromosome, for conversion into TDA.

Metabolic model-based analyses showed that growth efficiency for TDA-free cultivations were optimal while TDA biosynthesis decreased biomass yield and increased oxygen consumption. The major drawback is based on the inhibitory effect by the disruption of the proton gradient.

Taken together, this study clearly shows that TDA production by *P. inhibens* DSM 17395 and some closely related strains is an advantage in its natural habitat despite the consequences for its own energy metabolism.

Zusammenfassung

Extrachromosomale Elemente spielen eine essentielle Rolle in der Adaptation und den Überlebensstrategien mariner Bakterien in ihrem natürlichen Habitat und können sich über lateralen Gentransfer zwischen Stämmen verbreiten. *Phaeobacter inhibens* DSM 17395 besitzt drei Plasmide unterschiedlicher Größe mit relevanten Funktionen: 65-kb (Biofilm, Motilität), 78-kb (Siderophore) und 262-kb (Tropodithietsäure).

Die metabolische Funktion des 262-kb Plasmids von *P. inhibens* DSM 17395 wurde in Bezug auf die Biosynthese von TDA im Rahmen dieser Arbeit untersucht, indem ungezielte GC- und LC-MS basierte Analysen angewendet wurden. Zudem wurde das metabolische Modell *i*Pin571 erstellt und für *in silico* Analysen genutzt.

Die Deletion des 262-kb Plasmids verbesserte die Wachstumseffizienz während nur geringfügige Unterschiede auf Metabolomebene sichtbar waren. Diese Änderungen können im Wesentlichen auf den Plasmid-codierten und Pipecolatoxidase-abhängigen Lysinabbau zurückgeführt werden.

Die Kombination von Metabolomics und Transcriptomics zeigte, dass der Wildtyp auf Grund des inhibitorischen Effekts des vom Organismus selbst produzierten TDAs in die stationäre Wachstumsphase übergeht. Im Gegensatz dazu war die Δ262-kb Plasmidmutante am Ende der Kultivierung kohlenstofflimitiert. Detaillierte Analysen deuten darauf hin, dass der Speicherstoff Polyhydroxybutanoat abgebaut wurde, um eine Verbindung ähnlich zu Lipoteichonsäuren als Antwort auf einen Phagen zu produzieren, der durch den Nährstoffmangel induziert wurde.

Basierend auf Metabolom- und Transkriptomdaten wurde ein neuer Stoffwechselweg für die TDA-Biosynthese mit einem Schwefeleinbau über ein Episulfid postuliert. Außerdem konnte ein methyliertes („Pre“-) TDA beobachtet werden, welches durch eine putative Methyltransferase, die auf dem Chromosom codiert ist, in TDA umgewandelt werden kann.

Metabolische, modellbasierte Analysen zeigten, dass die Wachstumseffizienz für TDA-freie Kultivierungen optimal war, während die TDA-Biosynthese die Biomasseausbeute verringerte und den Sauerstoffverbrauch erhöhte. Der größte Effekt basiert dabei auf dem inhibitorischen Effekt durch die Zerstörung des Protonengradienten.

Zusammengefasst zeigt dies, dass die Produktion von TDA durch *P. inhibens* DSM 17395 und einiger nah verwandter Stämme, unabhängig von den Auswirkungen auf den eigenen Energiemetabolismus, einen Vorteil im natürlichen Habitat bietet.

1 Introduction

1.1 The marine environment as habitat for *Rhodobacteraceae*

The most important ecosystem on the earth - the ocean with a volume of 1.3 x 10^9 km^3 (Charette and Smith 2010) - covers about 70% of the earth's surface and provides habitats for over 240000 different species with over 2000 species classified as bacteria (WoRMS, 11/2017). However, the absolute number for bacteria species is underestimated (Appeltans *et al.* 2012) and even more species are expected. *Alphaproteobacteria* (37%), *Gammaproteobacteria* (14%) and *Bacteroidetes* (12%) form the majority of the marine bacterioplankton with the SAR11 clade as the most abundant marine group of the *Alphaproteobacteria* (Wietz *et al.* 2010). Marine *Rhodobacteraceae*, designated as *Roseobacter* group (Simon *et al.* 2017) and belonging to the *Alphaproteobacteria*, is another major marine group and represents up to 20% of coastal and 15% of mixed-layer ocean bacterioplankton communities (Buchan *et al.* 2005). In contrast to the SAR11 clade, many members of the *Roseobacter* group are cultivable. Furthermore, they are ecological all-rounder (Newton *et al.* 2010) and one of the most abundant and most active bacterial clade upon seasonal collapse of algae blooms (Alonso-Sáez *et al.* 2007; Alonso-Sáez, Gasol 2007).

Ecological niches in the marine habitat are diverse due to differences in temperature, pressure, pH, salinity, light, dissolved gases and nutrient supply dependent on the distance to coastal regions, the sea layer and the latitude (Fuhrman *et al.* 2008). Thus, bacteria developed different strategies for successful survival in the various marine environment. For *Alphaproteobacteria*, a variety of features to adapt to different niches are found on extrachromosomal elements, especially within the *Rhodobacteraceae* (Pradella *et al.* 2010; Petersen *et al.* 2011; Petersen *et al.* 2013; Trautwein *et al.* 2016; Kleist *et al.* 2016; Wagner-Döbler *et al.* 2010; Thole *et al.* 2012; Frank *et al.* 2014; Michael *et al.* 2016).

1.2 Extrachromosomal elements of the *Rhodobacteraceae*

Microbial evolution is dominated by horizontal gene transfer including plasmid transfer by conjugation, transformation by direct DNA uptake and transduction by phages or gene transfer agents (Koonin 2016). Extrachromosomal elements are widely spread within the *Rhodobacteraceae* with species carrying up to 12 plasmids per cell (Pradella *et al.* 2010). They provide the possibility for rapid adaptation to ecological niches by genetic flexibility and horizontal exchange (Petersen *et al.* 2013).

1.2.1 Classification of extrachromosomal elements

Extrachromosomal elements can be classified according to their replication modules RepABC, RepA, RepB and DNA-like (Petersen *et al.* 2011; Petersen *et al.* 2013). Plasmids with a RepABC module are only found in *Alphaproteobacteria* (Pinto *et al.* 2012), DNA-like replicons are restricted to *Rhodobacterales* and RepA- and RepB-type plasmids are further observable in *Beta*- and *Gammaproteobacteria* (Petersen *et al.* 2013). Chromids, extrachromosomal elements with genetic footprint similar to those of the chromosome (Harrison *et al.* 2010), were identified in *Rhodobacterales* species additionally to the chromosome and plasmids. While plasmids often contain the RepABC-type replication system, chromids are mainly replicated by RepA, RepB and DNA-like modules (Petersen *et al.* 2013). For example, the three extrachromosomal elements of the model organism *Phaeobacter inhibens* DSM 17395 containing RepA-I (65-kb), RepB-I (78-kb) and DNA-like I (262-kb) replication types and were all classified as chromids by Petersen *et al.* (2013). The model organism *Dinoroseobacter shibae* DFL12^T carries five extrachromosomal elements, two of them are chromids (153-kb and 72-kb) and three are plasmids (86-kb, 191-kb, 126-kb). Harrison *et al.* (2010) assumes that chromids are essential for the bacterial host. However, all three chromids of *P. inhibens* DSM 17395 were curable (Petersen *et al.* 2013; Trautwein *et al.* 2016). Thus, chromids that a curable have to be considered as essential in their natural habitat but not as essential per se. For reasons of simplicity, “chromids” will be further on designated as “plasmids”.

1.2.2 Functional role of extrachromosomal elements

A variety of functions of the extrachromosomal elements were observed within the *Rhodobacteraceae*. Most of these functions are associated with the habitat and provide benefits for the successful survival in the marine habitat. The 153-kb plasmid of *D. shibae* DFL12^T was shown to be essential for dealing with high salinity (Kleist *et al.* 2016) and encodes a gene cluster for degradation of aromatic compounds. Furthermore, its 86-kb plasmid harbors genes for sugar metabolism and the 72-kb plasmid carries *cox* operons contributed to energy production (Wagner-Döbler *et al.* 2010). Wagner-Döbler *et al.* (2010) identified three copies of *thiC*, essential for thiamine (vitamin B_1) biosynthesis, on three plasmids (191-kb, 153-kb and 86-kb) while all other genes of this pathway are localized on the chromosome. Furthermore, heavy metal resistance genes were found on plasmids of *D. shibae* DFL12^T and other *Rhodobacteracea*, e.g. *Roseobacter litoralis* OCh149 or *Rosevarius nubinhibens* ISM (Kalhoefer *et al.* 2011). Kalkhoefer *et al.* (2011) identified the photosynthesis gene cluster (PGC) encoded on the 94-kb plasmid of *R. litoralis* which was found on the chromosome of *Roseobacter denitrificans* OCh114 indicating a translocation of these genes in *R. litoralis* from the chromosome to the plasmid. This translocation of the PGC could explain the dispersed presence of the aerobic anoxygenic photosynthesis amongst the *Rhodobacteraceae* (Petersen *et al.* 2013). The 65-kb plasmid of *P. inhibens* DSM 17395 is crucial for motility and colonization of marine algae associated with a functional biofilm formation (Frank *et al.* 2014). These RepA-I-type biofilm plasmids are widely distributed amongst *Rhodobacteraceae* (Michael *et al.* 2016). *P. inhibens* DSM 17395 and the closely related *P. inhibens* 2.10 produce siderophores under iron-limiting conditions. The gene clusters for biosynthesis and transport of these iron-chelating siderophores are located on the 78-kb or 95-kb plasmid, respectively (Thole *et al.* 2012). *P. inhibens* DSM 17395 and some closely related *Rhodobacteracea* produces the antibacterial compound tropodithietic acid (TDA). The biosynthetic gene cluster is encoded on the 262-kb plasmid of *P. inhibens* DSM 17395 (Thole *et al.* 2012) .

Overall, some features are widespread amongst the *Rhodobacteraceae* but others are specific for only a few species. Thus, every species within the *Roseobacter* group

developed its own successful survival strategy and obtained some of these functions by horizontal gene transfer.

1.3 The model organism *Phaeobacter inhibens* DSM 17395

Phaeobacter species are strictly aerobe, motile, brown-pigmented, Gram-negative ovoid rods with chemoheterotrophic metabolism. The optimal salinity ranges from 0.51 to 0.68 M, the optimum pH is 7.5 and the optimal temperature is 27-29 °C (Martens 2006).

P. inhibens DSM 17395 was originally reclassified from *Roseobacter gallaeciensis* (Ruiz-Ponte *et al.* 1998) to *P. gallaeciensis* DSM 17395 (Martens 2006). However, the alleged type strains *P. gallaeciensis* CIP 105210 and *P. gallaeciensis* DSM 17395 are not identical. The strain CIP 105210 most likely corresponds to the original *P. gallaeciencsis* type strain BS107^T while strain DSM 17395 shows a closer relation to *P. inhibens* DSM 16374^T (T5^T) resulting in reclassification to *P. inhibens* DSM 17395 (Buddruhs *et al.* 2013).

The genome of *P. inhibens* DSM 17395 comprises a 3.8 million basepairs (bp) long chromosome and three plasmids of 65-kb, 78-kb and 262-kb described in chapter 1.2. *P. inhibens* DSM 17395 is a nutritionally versatile organism with a broad substrate range including amino acids, carbohydrates and further different short-chain carboxylic acids (Zech *et al.* 2009; Zech *et al.* 2013a; Zech *et al.* 2013b; Drüppel *et al.* 2014; Wiegmann *et al.* 2014). *P. inhibens* DSM 17395 catabolizes glucose via the Entner-Douderoff pathway. The 6-phosphofructokinase is missing in the genome of *P. inhibens* DSM 17395, but all necessary genes for gluconeogenesis are annotated (Zech *et al.* 2009). Furthermore, Zech *et al.* (2009) identified the enzymes to produce the storage compound polyhydroxybutanoate (PHB).

P. inhibens DSM 17395 shows different morphotypes depending on the substrate (Drüppel *et al.* 2014). Furthermore, the typical rosette formation is correlated with the ability of surface attachment (Frank *et al.* 2014).

The organism is able to synthesize different secondary metabolites like quorum sensing molecules (acyl homoserine lactones), roseobacticides or the antibaterial compound TDA (Berger et al. 2011; Thole et al. 2012).

1.4 The antibacterial compound tropodithietic acid

Tropodithietic acid was firstly described as its isomer thiotropocin which was isolated from *Pseudomonas* sp. CB-104 (Kintaka *et al.* 1984). A thicarbonyl-enol tautomerism between both structures is assumed based on computational studies (Greer *et al.* 2008) (figure 1.1). Greer *et al.* (2008) suggest a barrierless process in the gas phase. In aqueous solution a stabilization relative to a transition state is anticipated to produce a small barrier for tautomerization of thiotropocin to the more stable TDA (figure 1.1).

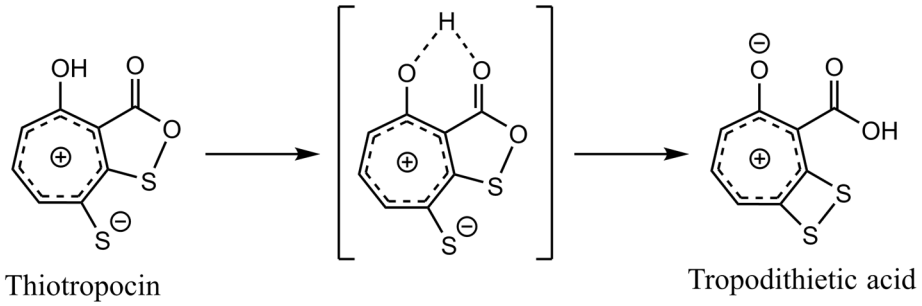

Figure 1.1 Suggested tautomerization of thiotropocin to tropodithietic acid via a transition state by Greer *et al*. 2008.

In the presence of Fe^{3+}, TDA forms a $[Fe^{III}(TDA)_2]_x$ complex which shows a characteristic brown color and could be precipitated by acidification (D'Alvise *et al.* 2015) explaining the co-occurrence of the yellow-brown pigment and TDA (Brinkhoff *et al.* 2004; Bruhn *et al.* 2007; Bruhn *et al.* 2005; Geng and Belas 2010, 2011; Geng *et al.* 2008; Berger *et al.* 2011).

TDA shows antibacterial activity against a broad range of Gram-negative and Gram-positive bacteria including human-pathogenic bacteria, e.g. *Staphylococcus aureus* NCTC 12493 (Porsby *et al.* 2011). TDA is proposed to disrupt the proton gradient by a proton antiport mechanism, in which extracellular protons are exchanged for cytoplasmic cations (Wilson *et al.* 2016). Furthermore, Wilson *et al.* (2016) suggests a self-resistance mechanism of *P. inhibens* DSM 17395 by uptake of glutamate and export of γ-aminobutyric acid for proton export catalyzed by enzymes encoded on the 262-kb plasmid neighboring the TDA biosynthetic gene cluster (figure 1.2). Attempts by Porsby *et al.* (2011) to isolate stable TDA resistant or tolerant strains were not successful. Even more, the TDA-producing *Phaeoabacter* strain 27-4 itself was also

inhibited by TDA. In studies by Harrington *et al.* (2014) observed tolerances were not associated with native TDA production.

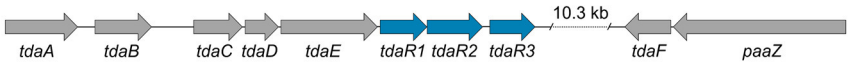

Gene	Predicted gene products
tdaA	Transcriptional regulator, LysR family
tdaB	Putative beta etherase
tdaC	Prephenate dehydratase TdaC-like protein
tdaD	Thioesterase superfamily protein
tdaE	Acyl-CoA dehydrogenase
tdaR1	Uncharacterized protein
tdaR2	Uncharacterized protein
tdaR3	Gamma-glutamylcyclotransferase
tdaF	Putative flavoprotein, HFCD family
paaZ	Phenylacetic acid degradation protein

Figure 1.2 TDA biosynthetic gene cluster. Resistance genes proposed by Wilson *et al.* (2016) are shown in blue.

TDA was recently described as signaling molecule in global gene regulation of *P. inhibens* DSM 17395 and causes a regulatory effect similar to the effect of the quorum sensing molecule AHL (Beyersmann *et al.* 2017). Both, TDA and AHL, were proposed to positively regulate TDA and AHL biosynthesis and negatively regulate motility and biofilm associated genes. In *Pseudovibrio* neither autoinduction nor AHL mediated induction of TDA production was observed (Harrington *et al.* 2014).

Furthermore, TDA shows a cytotoxic effect on mammalian cells of the nervous system resulting in oxidative stress and cell death (Wichmann *et al.* 2015). DMSP was shown to be protective against TDA induced cytotoxicity (Wichmann *et al.* 2016). Thus, DMSP provided by the algal host might be essential for resistance of TDA producing marine bacterial strains.

Phenylacetyl-CoA was shown to be the precursor for TDA biosynthesis and is mainly produced by degradation of phenylalanine (Berger *et al.* 2012; Thole *et al.* 2012). Brock *et al.* (2014) proposed a biosynthetic pathway starting with phenylacetyl-CoA resulting in a tropone ring (figure 1.3) followed by dehydrogenation and water elimination.

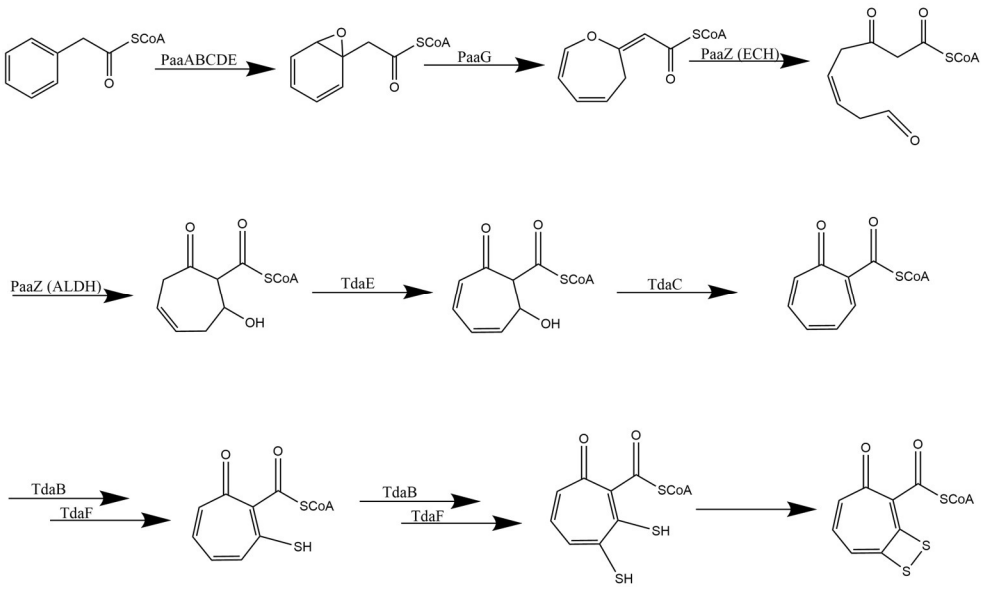

Figure 1.3 Proposed TDA biosynthetic pathway. The proposed biosynthetic steps by Brock *et al.* (2014) starting from phenylacetyl-CoA is shown with associated involved enzymes.

Recently, the L-cystine β-Lyase PatB from *P. inhibens* DSM 17395 was characterized and shown to be active with L-cystine resulting in the unstable compound S-thio-L-cysteine (Dickschat *et al.* 2017). Sulfur incorporation was proposed by transfer of sulfur from S-thio-L-cysteine to the TDA precursor (Brock et al. 2014).

1.5 Metabolome analyses

1.5.1 Metabolomics

The metabolome is the set of metabolites produced by a biological system as a result of its metabolism (Fiehn 2002; Villas-Bôas *et al.* 2005). The analysis of the metabolome is an essential step on functional genomics because the metabolome is the most predictive of a phenotype (Dettmer *et al.* 2007). Genetic or environmental changes lead to different metabolite levels which can be regarded as the ultimate response of a biological system (Fiehn 2002). The metabolic fingerprinting is used to compare patterns of metabolites without identifying each metabolite in a response to a treatment. Furthermore, the metabolic profiling could be used if only a small number of metabolites are identified and quantified based on e.g. same biochemical pathway or compound class (Fiehn 2002; Dettmer *et al.* 2007).

A metabolome analysis should be fast, reliable, sensitive, amenable for automation and it should cover a significant number of metabolites (Strelkov *et al.* 2004; Fiehn 2002). Currently, there is no single or combined analytical method to cover the whole metabolome (Allwood, Goodacre 2010). Thus, the choice of the right analytical method depends on the aim of the analysis.

1.5.2 Sample preparation

Sample preparation is the most challenging step in metabolomics. Remaining enzyme activity could lead to metabolic changes as stress response while sampling. Thus, metabolism has to be stopped immediately. Plant tissues can be easily frozen in liquid nitrogen (Fiehn 2002), but this technique is not transferrable to aqueous cell suspensions. There are mainly two possible methods to stop the metabolome of bacterial cell cultures: i) separation and ii) quenching. The separation can be conducted by filtration (Bolten *et al.* 2007) or centrifugation (Spura *et al.* 2009) followed by washing of the cells with an appropriate solution. A faster method is quenching with cold-buffered organic solutes, e.g. methanol, leading to protein degradation. However, this method has to be adapted to the respective organism. Quenching can lead to cell leakage resulting in loss of metabolites (Bolten *et al.* 2007; Spura *et al.* 2009) .

Usually, a liquid-liquid or solid phase extraction is performed after metabolism is stopped depending on the targeted metabolite class. The analytes are concentrated to facilitate the detection of low abundant metabolites (Dettmer *et al.* 2007).

1.5.3 Gas chromatography – mass spectrometry

Gas chromatography (GC) coupled to mass spectrometry (MS) is one of the most used techniques for high-throughput metabolomics (Dettmer *et al.* 2007). Volatile compounds can be directly analyzed by the headspace technique. However, many metabolites are not volatile and need a derivatization procedure prior to vaporization. In this study a two-step derivatization procedure is performed using methoxyamine-hydrochloride for stabilization of the open-chain structure of sugars and MSTFA for silylation of functional chemical groups resulting in volatile compounds (figure 1.4). Silylation is sensitive to moisture. Thus, samples and agents

have to be completely dry to prevent degradation or less effective derivatization (Dettmer *et al.* 2007). Derivatization often results in several derivatives of one analyte containing different amounts of silyl-groups. These derivatives have to be combined because distribution pattern can differ (Kanani and Klapa 2007).

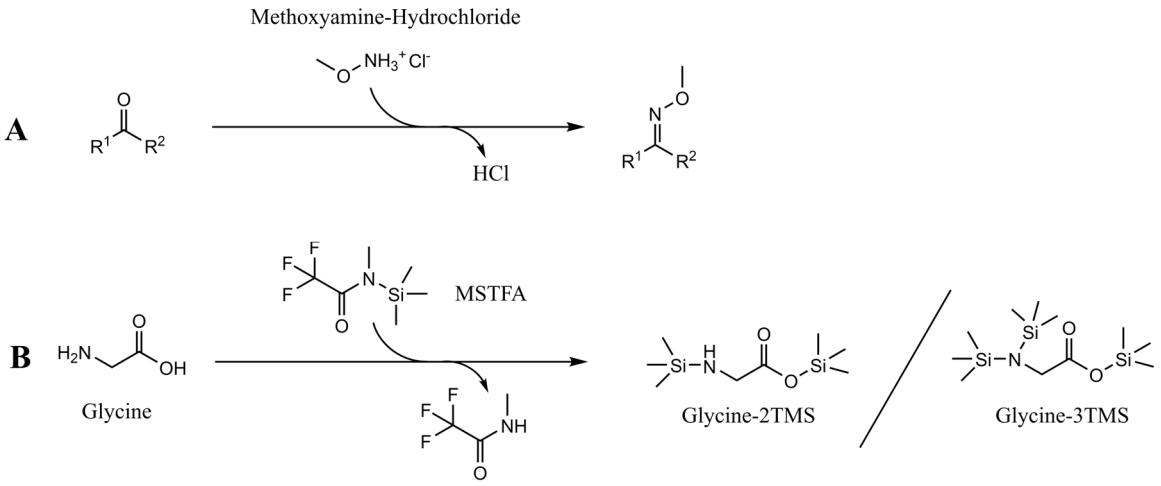

Figure 1.4 Derivatization reaction for GC-MS analysis. Shown is the two-step derivatization reaction with (A) methoxymation of carbonyl-groups and (B) silylation of exchangeable protons from glycine (example). MSTFA: *N*-Methyl-*N*-(trimethylsilyl)-trifluoro-acetamide, TMS: trimethylsilyl

Vaporization of the derivatized metabolites is conducted by a programmed temperature vaporizing (PTV) injector. The vaporized compounds are transported by the mobile phase (an inert gas, e.g. helium) over a coated separation column. The compounds interact with the column material (e.g. silicon) depending on their structure and functional groups. Thus, the analytes have different retention times according to their interaction with the column, their mass and steric configuration. Usually, a temperature gradient is applied for elution of the compounds from the column.

The analytes have to be ionized prior to the MS detection. This is usually conducted by the standardized and reproducible electron ionization (EI) with an electron energy of 70 eV. This hard ionization techniques results in fragmentation reactions characteristic for each analyte. Identification of the compounds is possible by comparison with several open and commercial MS libraries (Dettmer *et al.* 2007).

1.5.4 Liquid chromatography - mass spectrometry

The major advantage of liquid chromatography coupled to mass spectrometry (LC-MS) compared to GC-MS is the possibility to analyze larger molecules. In the field of metabolomics, it is suitable for the analysis of for example coenzyme A intermediates. Furthermore, with different columns and mobile phases a broad range of substance classes can be analyzed. Usually, a soft ionization method as electrospray ionization (ESI) is used for ionization of the analytes. These are vaporized into fine aerosol and molecular ions with either a positive $[M+H]^+$ or negative $[M+H]^-$ charge could be detected. Thus, with the information of the accurate mass and isotopic pattern it is possible to predict molecule formula. This information can help at structure elucidation of so far unidentified compounds. The major drawback of the method is the lack of standardization and libraries. Due to a higher instrument-dependent variability, the comparison of ionization, spectra and retention times is difficult (Dettmer *et al.* 2007).

1.6 Metabolic model-based analyses

Metabolic models can be used for applications like metabolic engineering, identification of metabolic capabilities or analysis of the growth efficiency of bacteria (Becker *et al.* 2011; Imam *et al.* 2011; Lee *et al.* 2014; Orth *et al.* 2011; Puchałka *et al.* 2008; Hintermayer and Weuster-Botz 2017). Combining experimental and theoretical data can help to understand the complex adaptation strategies of bacteria to their natural habitat with respect to utilization of carbon sources and maintenance energy requirements.

1.6.1 Metabolic model reconstruction

The most common approach is the constraint-based reconstruction and analysis (COBRA) (Price *et al.* 2003). These models, created in a bottom-up manner, can be used for a variety of predictions such as simulating the growth of a cell for a given condition (Thiele, Palsson 2010; Varma, Palsson 1994a; Schilling *et al.* 2000).
Stoichiometric models can be used to describe a metabolic network as a numerical matrix of the stoichiometric coefficients of each reaction (Orth *et al.* 2010). A steady

state is assumed for constraint-based models to reduce the set of differential equations (Schilling *et al.* 2000).

1.6.2 Flux-balance and flux-variability analyses

Flux-balance analysis (FBA) calculates the flow of metabolites through a metabolic network with linear optimization to a defined biological objective. For prediction of growth the objective function is the biomass production represented by a biomass reaction including precursor metabolites. Usually, this reaction is scaled and equal to the growth rate μ (Orth *et al.* 2010).
The flux-variability analysis (FVA) is used for prediction of maximum and minimum of a flux to analyze the solution space. Thus, it is possible to identify variable fluxes with still the optimal solution or a solution near the optimum (e.g. 95%) (Mahadevan, Schilling 2003).

1.6.3 Growth efficiency and maintenance energy

The basic concept to quantitively describe bacterial growth was given by Monod (1949). He introduced the growth rate as a constant for the exponential growth phase. This growth phase is a steady state where all metabolites and all enzymes are constant (Monod 1949). Energy requirements for maintenance were neglected by this classical approach and the concept of energy maintenance was introduced by Pirt (1965). Pirt (1982) proposed a model which accounts for the energy requirement for growth including a constant maintenance energy term independent of the specific growth rate and a term which decreases linearly with increase in specific growth rates. Based on these concepts, energy requirements are considered as growth- and non-growth-associated maintenance energy (GAM and NGAM) in metabolic models. NGAM is defined as $mmol_{ATP}\ g_{CDW}^{-1}\ h^{-1}$ and GAM is defined as additional $mmol_{ATP}$ required per unit of biomass produced (Varma *et al.* 1993). The experimental determination of both parameters is generally performed using continuous cultivation based on the relationship between substrate concentration and growth rate (Schulze, Lipe 1964; Varma *et al.* 1993; Varma, Palsson 1994b). FBAs usually predict the maximal possible growth rate dependent on an experimentally determined substrate uptake rate (Orth *et al.* 2010). Based on these data it is possible to calculate the optimal biomass yield

(Y). However, predicted biomass yield obtained by FBA could be unrealistic high, but is well suited for organisms which show no overflow metabolism (Adadi *et al.* 2012; Hintermayer, Weuster-Botz 2017). This begs the question of which expression is describing growth efficiency more accurate. Many review articles discuss the complex relationship between growth rate and growth yield (Lipson 2015). The biomass yield is the simplest term to express growth yield (Lele and Gwatve 2014). A positive relationship between bacterial growth rate and bacterial growth efficiency (BGE) was described for natural planktonic bacteria (del Giorgio, Cole 1998). BGE was defined as bacterial production divided by the sum of production and respiration. Lipson (2015) proposed a relationship between growth rate and yield across a broad range of environmental conditions and ecological strategies. He described a positive relationship from a stress tolerance strategy (low biomass yield, slow growth rate) to a high efficiency strategy (high biomass, average growth rate) followed by a negative relationship after Beardmore *et al.* (2011) to the rapid growth strategy (low biomass yield, high growth rate). Thus, for marine bacteria like the *Rhodobacteracea*, biomass yields should be compared to analyze the growth efficiency dependent on nutrient supply.

1.7 Objectives

The alphaproteobacterial *Roseobacter* group (marine *Rhodobacteraceae*) is one of the most abundant lineages of the oceans and members of the group carry a variety of extrachromosomal elements. The nutritionally versatile model organism *Phaeobacter inhibens* DSM 17395 harbors three extrachromosomal elements (262-kb, 78-kb and 65-kb plasmid) and has been widely analyzed regarding to metabolic abilities.
This study focuses on the metabolic role of the 262-kb plasmid in the context of the endogenously produced antibiotic TDA.

Initially, all three plasmids should be characterized with respect to their influence on the growth efficiency of *P. inhibens* DSM 17395 to analyze a possible energetic burden by carrying these plasmids.
One main part is the detailed characterization of the largest plasmid (262-kb) on metabolomic and transcriptomic level to study the features with respect to successful survival in the natural habitat. These studies include the analysis of the biosynthetic

pathway of TDA which is not yet fully described with experimental evidence. Furthermore, structures for so far unknown metabolites should be proposed based on mass spectra data.
The second study should investigate the theoretical and actual growth efficiency of *P. inhibens* DSM 17395 with different amino acids regarding maintenance energy requirements. This study includes analysis of possible decreasing biomass yields due to costs for the biosynthesis of TDA.

Overall, these studies should provide new insights into the function of the 262-kb plasmid of *P. inhibens* DSM 17395 and should clarify the benefit of carrying this plasmid in the natural habitat.

2 Material and methods

Experiments including cultivation in process-controlled bioreactors were conducted in cooperation with the research group of Prof. Ralf Rabus (ICBM, Carl von Ossietzky University Oldenburg) whose co-workers performed cultivation and sampling. Associated transcriptomic analyses (RNA-seq) were conducted by the group of Robert Geffers (Helmholtz centre for infection research, Braunschweig). All experiments conducted in Erlenmeyer flasks were independently realized as part of this work.

2.1 Chemicals

Chemicals and reagents with highest quality ("purest" or "for analytical purpose") purchased from the manufacturers Carl Roth (Karlsruhe, Germany), Sigma-Aldrich (Steinheim, Germany), Fisher Scientific (Schwerte, Germany) and CS GmbH (Langerwehe, Germany) were used.

2.2 Bacterial strains

All strains of *Phaeobacter inhibens* DSM 17395 used in this study are listed in table 2.1 and 2.2. For long-time storage marine bouillon medium (chapter 2.3.1) was inoculated with colonies from the agar plates. 800 µL of growing cells were mixed with 200 µL 100% glycerol, incubated for 20 minutes on ice and stored at -80 °C.

Table 2.1 Wild-type and plasmid-cured mutant strains of *P. inhibens* DSM 17395 used in this work. All strains were provided by the (DMSZ) German Collection of Microorganisms and Cell Cultures, Braunschweig, Germany.

Strain	Genetic modification	Reference
DSM 17395	Wild-type strain	DSMZ
Δ262-kb	Curation of the 262-kb plasmid	Trautwein *et al.* 2016
Δ78-kb	Curation of the 78-kb plasmid	Trautwein *et al.* 2016
Δ65-kb	Curation of the 65-kb plasmid	Trautwein *et al.* 2016
Δ78Δ65-kb	Curation of the 78- and 65-kb plasmid	Trautwein *et al.* 2016
Δ262Δ78-kb	Curation of the 262- and 78-kb plasmid	Trautwein *et al.* 2016
Δ262Δ65-kb	Curation of the 262- and 65-kb plasmid	Trautwein *et al.* 2016
Δ262Δ78Δ65-kb	Curation of all three plasmids	Trautwein *et al.* 2016

Transposon mutants were transferred twice to fresh marine bouillon agar plates containing 120 µg mL^{-1} kanamycin and incubated for 2-3 days to exclude

contaminations with wild-type cells attached to the antibiotic resistant transposon mutant strains. Then marine bouillon containing 120 µg mL^{-1} kanamycin was inoculated with colonies from the agar plates and glycerol stocks were prepared as previously described.

Table 2.2 Transposon mutant strains of *P. inhibens* DSM 17395 used in this work. Transposon mutants were taken from a transposon library of *P. inhibens* DSM 17395 provided by Pascal Bartling (working group of Jörn Petersen, DSMZ).

Strain	Insertion site	Insertion locus	Reference
Tm1693	107502+	PGA1_262p00980	Will *et al.* 2017
Tm2750	106916-	PGA1_262p00970	Will *et al.* 2017
Tm3519	105936+	PGA1_262p00960	Will *et al.* 2017
Tm2690	104157-	PGA1_262p00940	Will *et al.* 2017
Tm2361	389043+	PGA1_c04030	this work
Tm510	390721-	PGA1_c04040	this work
Tm4090	390914-	PGA1_c04050	this work
Tm970	393104-	PGA1_c04080	this work
Tm2428	394153+	PGA1_c04090	this work
Tm3938	1205517+	PGA1_c11650	this work
Tm2456	1700287+	PGA1_c16390	this work
Tm774	2353034+	PGA1_c22710	this work
Tm225	2799630+	PGA1_c26830	this work
Tm3860	3305902+	PGA1_c31650	this work
Tm3922	3413439-	PGA1_c32550	this work
Tm757	3412773-	PGA1_c32550	this work
Tm1215	3462719-	PGA1_c33040	this work
Tm2415	90491-	PGA1_262p00800	this work
Tm2567	238764-	PGA1_262p02210	this work
Tm299	256398-	PGA1_262p02330	this work

2.3 Media and solutions

Salt-free, particle filtered water (ddH_2O) from ultra pure water systems (Arium, Sartorius) was used for all media and solutions. Autoclaving of media was conducted for 20 min at 121 °C and 1 bar overpressure.

2.3.1 Marine Bouillon

For complex medium 40.1 g L^{-1} Marine-Bouillon (Carl Roth, Karlsruhe, Germany) was prepared and autoclaved. 15 g L^{-1} agar was added prior to autoclaving if solid medium was used.

2.3.2 Defined salt water medium

The defined salt water medium was prepared immediately before inoculation with the respective carbon source. The medium always consisted of Basic A, Basic B, trace elements, a carbon source and was filled up with ddH_2O. For transposon mutant strains kanamycin was added in the precultures.

Basic A

Basic A was prepared as 5x stock solution with ddH_2O. The Stock solution was autoclaved for sterilization. Final concentration in the medium:

NaCl	20.0 g L^{-1}
Na_2SO_4	4.0 g L^{-1}
$MgCl_2$ x 6 H_2O	3.0 g L^{-1}
KCl	0.5 g L^{-1}
NH_4Cl	0.25 g L^{-1}
KH_2PO_4	0.2 g L^{-1}
$CaCl_2$ x 2 H_2O	0.15 g L^{-1}

Basic B

Basic B was prepared as 10x stock solution with ddH_2O. The stock solution was sterile filtrated. Final concentration in the medium:

$NaHCO_3$	0.19 g L^{-1}

Trace element stock solution

Trace elements were prepared as 1000x stock solution as follows:

H_2O	25 mL
Fe(II)SO_4 x 7 H_2O	1.05 g
HCl, 25% (w/v)	6.5 mL
Tritiplex III (Na2EDTA)	2.6 g

Dissolved and pH adjusted to 6.0-6.5 before adding next components.

H_3BO_3	15 mg
$MnCl_2$ x 4 H_2O	50 mg

$CoCl_2$ x 6 H_2O	95 mg
$NiCl_2$ x 6 H_2O	12 mg
$CuCl_2$ x 2 H_2O	1 mg
$ZnSO_4$ x 7 H_2O	72 mg
Na_2MoO_4 x 2 H2O	18 mg

The stock solution was filled up to 500 mL with ddH_2O and sterile filtrated.

Carbon sources

Carbon sources were prepared as 5x stock solutions with ddH_2O. pH was adjusted to 6.5 and stock solutions were sterile filtrated. Final concentrations in the medium:

Casamino acids	10 g L^{-1}
L-alanine	30 mM
L-phenylalanine	10 mM
L-leucine	15 mM
L-lysine	15 mM
L-threonine	22.5 mM

Kanamycin stock solution

Kanamycin was prepared as 1000x stock solution (120 mg mL^{-1}), sterile filtered, aliquoted and stored at -20 °C.

2.3.3 Solutions for HPLC analysis

Sodium tetraphenylborate

0.25 M sodium tetraphenylborate was prepared prior to usage for precipitation of ammonium.

Eluent A (sodium acetate)

10 mM, 25 mM or 100 mM sodium acetate was prepared prior to usage, pH was adjusted to 6.5 and the solution was filtered.

Derivatization reagents

OPA reagent (10 mg mL^{-1} each of O-phthalaldehyde and 3-mercaptopropoinic acid in 0.4 M borate buffer) and FMOC reagent (2.5 mg mL^{-1} of 9-fluorenylmethylchloroformate in acetonitrile) were purchased from Agilent Technologies (Waldbronn, Germany). One vial was opened and aliquoted prior to usage. Aliquots were stored at 4 °C and used for maximal 7-10 days. Furthermore,

borate buffer (0.4 N, pH 10.2) was purchased from Agilent Technologies (Waldbronn, Germany) and stored at 4 °C.

Injection diluent

100 mL solution containing Na_2HPO_4 and $Na_2B_4O_7$ (10 mM each) was prepared and 0.4 mL concentrated H_3PO_4 was added. The solution was stored at 4 °C.

Amino acid standard mix

The purchased 1 mM amino acid standard mix (Agilent Technologies, Waldbronn, Germany) was diluted to obtain calibration curves in the range of 5-500 µM. The diluted amino acid standard was stored at -20 °C.

Internal standard mix

A stock solution with 1 mM norvaline and 1 mM sarcosine was prepared, aliquoted and stored at -20 °C.

2.3.4 Solutions for GC-MS analysis

Ribitol stock solution

0.2 g L^{-1} ribitol stock solution was prepared, sterile filtered, aliquoted and stored at -20 °C.

Methoxyamine/pyridine solution

20 mg mL^{-1} methoxyamine hydrochloride (dissolved in pyridine) was prepared prior to use.

Alkan time standard (retention index calibration mix)

Decane, $C_{10}H_{22}$	12.5 mg (17.1 µL)
Dodecane, $C_{12}H_{26}$	12.5 mg (16.7 µL)
Pentadecane, $C_{15}H_{32}$	12.5 mg (16.2 µL)
Nonadecane, $C_{19}H_{40}$	12.5 mg
Docosane, $C_{22}H_{46}$	12.5 mg
Octacosane, $C_{28}H_{58}$	12.5 mg
Dotriacontane, $C_{32}H_{66}$	12.5 mg
Hexatriacontane, $C_{36}H_{74}$	12.5 mg

The alkanes were dissolved in 25 mL cyclohexane (0.5 g L^{-1} for each alkane). For GC-MS measurement 6 µL of this stock solution were added to 48 µL cyclohexane.

2.3.5 Solutions for LC-MS analysis

Eluent A (50 mM ammoniumformiate, pH 8.1)

450 mL ddH_2O was mixed with 943 µL formic acid. Subsequently, the pH was adjusted to 8.1 with 1:2 diluted ammonium hydroxide solution and filled up to 500 mL with ddH_2O. The eluent was freshly prepared prior to use and degassed for 30 min in an ultrasonic bath.

Eluent B (methanol), Eluent C (ddH_2O), Eluent D (acetonitrile)

Eluents were freshly filled up and degassed for 30 min in an ultrasonic bath prior to usage.

Calibrationmix (Na-formiate cluster)

ddH_2O	4.95 mL
Isopropyl alcohol	4.95 mL
Formic acid	10 µL
1 M NaOH	100 µL

Components were mixed and stored at 4 °C.

Sample buffer (25 mM ammoniumformiate, pH 3.5, 2% methanol)

40 mL ddH_2O were mixed with 47.2 µL formic acid. Subsequently, pH was adjusted to 3.5 with 1:2 diluted ammonium hydroxide solution. 1 mL methanol were added and the solution was filled up to 50 mL with ddH_2O. The buffer was stored at 4°C.

2.4 Microbial techniques

2.4.1 Measurement of cell density and cell dry weight

The cell density was determined photometrically at a wavelength of 600 nm (OD_{600}). Samples were diluted in Basic A if OD_{600} values were above 0.5. To transfer OD_{600} values into cell dry weight (CDW) correlations between both values were determined. Cells were grown according to 2.4.2 in Erlenmeyer flasks with at least 4 biological replicates. Each biological replicate was harvested at a different time point to get OD-CDW correlations over the complete growth curves. From each biological replicate 2 x 40 mL culture volume was harvested by centrifugation (12000 x g, 5 min, 4 °C). Cells were resuspended in 1 mL 3.7% sodium chloride and transferred into dry, weighted 2 mL reaction tubes. Sodium chloride was discarded after centrifugation (12000 x g,

5 min, 20 °C) and the cell pellets were dried to constant weight (80 °C, 72 h). Determined OD-CDW correlations for the different carbon sources and strains are listed in table 2.3.

Table 2.3 Determined OD-CDW correlations for casamino acids and single amino acids.

Carbon source	Strain	OD-CDW correlation
Casamino acids	WT	OD = 2.43 * CDW – 0.23
	Δ262-kb	OD = 1.70 * CDW
	tdaE (Tm2690)	OD = 2.00 * CDW
L-phenylalanine	WT	OD = 2.30 * CDW
	Δ262-kb	OD = 2.07 * CDW
	tdaE (Tm2690)	OD = 1.92 * CDW
L-alanine	WT	OD = 1.87 * CDW
	Δ262-kb	OD = 1.73 * CDW
	tdaE (Tm2690)	not determined
L-leucine	WT	OD = 2.61 * CDW
	Δ262-kb	OD = 2.03 * CDW
	tdaE (Tm2690)	OD = 2.14 * CDW

2.4.2 Cultivation procedure

Cultivations were performed in Erlenmeyer flasks with three baffles filled to 1/5 of their maximum volume with medium. Cultures were incubated at 28 °C and 150 rpm (Certomat BS-1, orbit 50 mm, Sartorius).

For every cultivation precultures with casamino acids containing defined salt water medium were inoculated with colonies from MB agar plates. Second precultures containing defined salt water medium with the respective carbon source were inoculated with the casamino acids preculture to an OD_{600} of 0.01. Then, main cultures (100 mL medium in 500 mL Erlenmeyer flasks) were inoculated with the second preculture to an OD_{600} of 0.01.

Adaptation to single amino acids

For adaptation to single amino acids, two consecutive transfers into cultures containing the respective amino acids were performed starting with a casamino acids preculture. Glycerol stocks according to chapter 2.2 were generated from growing

cells of the second culture with the single amino acids. One glycerol stock was used for inoculation of a preculture with defined salt water medium containing the respective single amino acid. Then, main cultures were inoculated with growing cells from the preculture.

Cultivation of transposon mutant strains

For cultivation of transposon mutant strains 120 µg mL^{-1} kanamycin was added to the medium in the precultures. Main cultures were then realized without addition of antibiotics.

Medium exchange

For the medium exchange experiment (chapter 3.2.2), cultivations were performed in 250 mL Erlenmeyer flasks containing 50 mL defined salt water medium with casamino acids as carbon source. At about ½ OD_{max}, cultures were transferred into 50 mL reaction tubes and harvested by centrifugation. Culture supernatants were sterile filtered and cells were resuspended in either their own (references) or the culture supernatant of another strain. Subsequently, cultivation was continued and growth was determined by OD measurement for calculation of linear growth rates (figure 2.1).

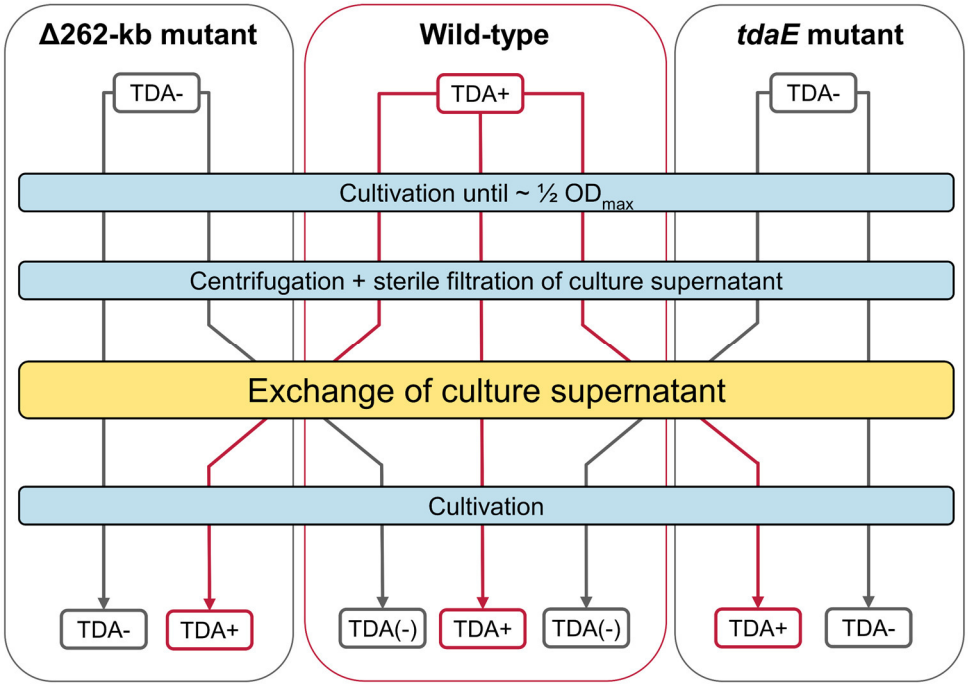

Figure 2.1 Medium exchange experiment. Shown is the scheme for the exchange of culture supernatant between the wild-type and TDA-free mutant strains. Arrows indicate the medium (red: with TDA, grey: without TDA).

2.4.3 Determination of growth parameters

Specific growth rate μ

The specific growth rate μ is the increase of biomass over time:

$$\mu = \frac{dCDW}{dt} \cdot \frac{1}{CDW} \quad (1)$$

Integration yields:

$$\mu = \frac{ln(CDW) - ln(CDW_0)}{t - t_0} \quad (2)$$

Thus, the specific growth rate μ is constant over the exponential growth phase and μ was determined by a linear fit of the logarithmized CDW value over time. For cultures growing not exponentially, μ was determined by fitting the logarithmized growth curve followed by differentiation of the fit using OriginPro 2016G yielding specific growth rates μ (h^{-1}) at each specific time point.

Linear growth rate μ_{lin}

Additionally, the linear growth rate μ_{lin} ($g\,L^{-1}\,h^{-1}$) was determined for cultures showing a section with linear growth achieved by linear fits of the CDW values over time.

Specific substrate uptake rate q_S

The specific substrate uptake rate is described by formula 3.

$$q_S = \frac{d[S]}{dt} \cdot \frac{1}{CDW} \quad (3)$$

Due to the changing specific growth rate of cultures growing not exponentially, the specific substrate uptake rates were also not necessarily constant. Thus, the substrate uptake rate was determined by differentiation of the fitted substrate concentrations. Afterwards, the determined substrate uptake rates ($mmol_S\,L^{-1}\,h^{-1}$) were related to the CDW at the specific time point yielding the specific substrate uptake rate q_S ($mmol_S\,g_{CDW}^{-1}\,h^{-1}$).

Biomass yield $Y_{X/C}$

The biomass yield $Y_{X/C}$ is defined as produced CDW per mol carbon. Therefore, the consumed carbon was determined by measurement of the substrate and transfer of $mol_{substrate}$ into mol_{carbon}.

2.4.4 Online measurement of dissolved oxygen

Erlenmeyer flasks with attached optical oxygen sensor spots (SP-PSt3-YAU-D7-YOP; PreSens, Regensburg, Germany) were used for determination of the oxygen consumption. The incubator was equipped with an online oxygen monitoring device (Shake Flask Reader; PreSens, Regenburg, Germany) and dissolved oxygen (DO) was measured based on fluorescing quenching (Schneider *et al.* 2010). Data acquisition was carried out with the *Shake Flask Reader Software v2.0.0* (PreSens, Regenburg, Germany). Measured DO as % air saturation was transferred into absolute concentrations with an estimation of the oxygen solubility in the used salt water medium to 6.8 mg L^{-1} based on values for different temperatures and salt concentrations (PreSens, Regensburg, Germany). Oxygen transfer rates (OTR) were determined for each data point according to formula 4. Oxygen uptake rates (OUR) were then calculated with formula 5 and a k_La value of 132 h^{-1} which was estimated with the *Presens k_La Calculator* (PreSens, Regensburg, Germany).

$$OTR = \frac{d[O_2]}{dt} \tag{4}$$

$$OUR = k_L a \cdot ([O_2^*] - [O_2]) - OTR \tag{5}$$

For selected data points calculated OUR in $mmol_{O_2}$ L^{-1} h^{-1} were referred to the associated CDW to obtain the respective specific oxygen uptake rate q_{O2} in $mmol_{O_2}$ g_{CDW}^{-1} h^{-1}. Absolute oxygen consumption ($mmol_{O_2}$ g_{CDW}^{-1}) at the specific time point was calculated with the respective growth rate (h^{-1}).

2.4.5 Determination of biomass composition

For determination of the biomass composition cells of 6 biological replicates were harvested and centrifuged at 4 °C and 10000 x g for 5 min. Supernatant was discarded and cells were resuspended in 3.7% sodium chloride. Suspended cells were split to get 1-3 mg CDW for DNA, RNA, protein content, protein composition and PHB each, 10-30 mg for lipid and 10-30 mg for determination of CDW, followed by centrifugation. Supernatant was discarded and cell pellets were frozen in liquid nitrogen. Cell pellets for determination of lipids were resuspended in 1.5 mL

methanol prior to freezing. Cell pellets for determination of CDW were resuspended in 1 mL 3.7% sodium chloride and transferred into dried weighted 2 mL reaction tubes and were dried for 72 h at 80°C.

Protein content

Cells were resuspended in protein lysis buffer (0.5 M NaOH, 2% SDS). Volume of lysis buffer was adjusted to harvested CDW to obtain a final concentration of 1 g_{CDW} L^{-1}. Resuspended cells were incubated at 80 °C for 30 min in an ultrasonic bath followed by centrifugation (12000 x g, 5 min, 20 °C). Cell lysate was diluted 1:5 with ddH_2O. Protein concentration in the cell lysate was determined using *the Bicinchoninic acid Protein Assay Kit* (Sigma-Aldrich, Germany). A calibration curve with bovine serum albumin was prepared for each measurement in 96-well plates using the *Tecan infinite Reader* (Tecan GmbH, Germany).

DNA

Isolation of DNA was performed using the *Genomic DNA from tissue Kit* (Macherey&Nagel, Düren, Germany) according to the protocol of the manufacturer. The isolated DNA was quantified by measuring the absorbance at 260 using *Tecan NanoQuant Plate* (Tecan GmbH, Germany).

RNA

Isolation of RNA was performed using the *RNA Isolation Kit* (Macherey&Nagel, Düren, Germany) according to the protocol of the manufacturer with minor modification. Homogenization was performed for 10 min at room temperature to minimize degradation of RNA. The isolated RNA was quantified by measuring the absorbance at 260 using *Tecan NanoQuant Plate* (Tecan GmbH, Germany).

Lipids

The lipid content was determined by extraction with methyl-*tert*-butyl ether (MTBE) adapted from Matyash *et al.* (2008). Cell lysis was performed at 70 °C for 15 min in an ultrasonic bath. 5 mL MTBE was added and incubated for 1 h at room temperature under shaking. Then, 1.25 mL ddH_2O was added followed by incubation for another 10 min at room temperature and shaking. Phase separation was conducted by centrifugation (10 000 x g, 10 min, 20 °C). The upper organic phase was transferred

step by step into dried, weighted glas vials and dried under vacuum and with rotation. A mix of 1.29 mL MTBE and 0.387 mL methanol was added to the bottom phase and was incubated for 1 h at room temperature under shaking. Subsequently, 0.323 mL ddH_2O was added, incubated for another 10 min (room temperature, shaking), centrifuged (10 000 x g, 10 min, 20 °C) and the upper organic phase was added to the prior dried organic phase. Lipids were quantified by determination of difference in weight of the dried vials with and without lipids.

Polyhydroxybutanoate (PHB)

For hydrolyzation of polyhydroxybutanoate (PHB) cell pellets were resuspended in 1 mL 2 M NaOH and incubated at 95 °C and 350 rpm for 60 min. The suspension was neutralized with 1 mL 2 M HCl and centrifuged for 5 min and 12 000 x g. The content of 3-hydroxybutanoate in the lysate was then quantified with *the D-3-Hydroxybutyric acid enzymatic assay* (r-biopharm, Darmstadt, Germany).

Protein composition and peptidoglycan

For determination of protein composition and estimation of peptidoglycan content, cells were hydrolyzed with 200 µL 6 M HCl for 24 h at 95 °C followed by neutralization. Amino acids of the proteins and total diaminopimelate were quantified by HPLC-FLD (chapter 2.5).

2.4.6 Cell harvesting for metabolome analysis

Harvesting for cultivations in processed-controlled bioreactors (chapter 3.1.1-3.1.3) were performed as previously described (Zech *et al.* 2013a) by the working group of Prof. Ralf Rabus (ICBM).

For analyses in Erlenmeyer flasks, cultures were grown according to chapter 2.4.2 with the strains and carbon source of interest. Cells were harvested in 50 mL reaction tubes by centrifugation (12 000 x g, 3 min, 4 °C). For cells growing on L-lysine as sole carbon source the first centrifugation step was performed in 250 mL bottles with 30 000 x g for 10 min at 4 °C (Beckmann Coulter, Krefeld, Germany) followed by transfer of the cells into 50 mL reaction tubes. 1 mL of the supernatant was transferred into 2 mL reaction tubes and stored at -20 °C. The remaining supernatant was discarded. Cell pellets for LC-MS analyses were resuspended in 1 mL methanol,

frozen in liquid nitrogen and stored at -80 °C. Cells for GC-MS analysis were washed twice with 20 mL ice cold 3.7% NaCl with centrifugation steps of 3 min at 4 °C and 12 000 x g. Afterwards cell pellets were frozen in liquid nitrogen and stored at -80 °C. At least 20 mg CDW for GC-MS and 10 mg CDW for LC-MS analyses were harvested. Higher amounts were harvested as backup if sufficient amount of biomass was available. Harvesting volume was calculated by OD-CDW correlations (table 2.3).

2.5 Amino acid analysis by HPLC-FLD

2.5.1 Sample preparation

To precipitate ammonia in the samples, 100 µL 0.25 M sodium tetraphenylborate were added to 100 µL of the sample, mixed vigorously for 5 min and centrifuged (10 min, 12 000 x g, 20 °C). When necessary, the clear supernatant was diluted in ddH_2O prior to analysis.
Cell hydrolysates were filtered to remove residual cell fragments.

2.5.2 HPLC-FLD analysis

Amino acids were quantified with a 1260 Infinity HPLC system equipped with a fluorescence detector (Agilent Technologies, Waldbronn, Germany). Separation was conducted with a Poroshell HPH-C18 separation column (4.6 x 100 mm, particle size 2.7 mm; Agilent Technologies, Germany). Derivatization of the amino acids were performed online in the sample loop with OPA and FMOC as derivatization reagents prior to injection as follows: 2.5 µL borate buffer was mixed with 1 µL sample and 0.1 µL internal standard followed by incubation with 0.5 µL OPA reagent and afterwards with 0.4 µL FMOC reagent. To stop derivatization 32 µL injection diluent was drawn, mixed and then 20 µL were injected. Separation was performed at 25 °C with a flow rate of 1.5 mL min^{-1}. Gradients were adjusted depending on the used concentration of sodium acetate (table 2.4). Fluorescence of OPA derivatives were measured with an excitation wavelength of 340 nm and an emission wavelength of 450 nm. After elution of lysine, wavelengths were switched to detect FMOC derivatives (excitation 266 nm, emission 305 nm).

Table 2.4 Gradients for amino acid analysis for different used sodium acetate concentrations (100 mM, 25 mM, 10 mM). Listed are the runtime with corresponding % of mobile phase A (sodium acetate) and B (acetonitrile).

100 mM			25 mM			10 mM		
min	**% A**	**% B**	**min**	**% A**	**% B**	**min**	**% A**	**% B**
0.00	97	3	0.00	97	3	0.00	97	3
5.30	97	3	5.30	97	3	5.30	97	3
5.35	94	6	5.35	96	4	5.35	94	6
10.00	90	10	10.00	93	7	10.00	93	7
11.00	90	10	12.00	85	15	11.00	93	7
12.00	85	15	22.00	85	15	12.00	85	15
25.00	85	15	22.50	75	25	22.00	85	15
35.00	65	35	24.50	75	25	22.50	75	25
35.10	0	100	27.00	70	30	24.50	75	25
38.00	0	100	27.10	0	100	27.00	70	30
			30.00	0	100	27.10	0	100
						30.00	0	100

For analyses of single amino acids, the method was shortened to 20 min with a gradient as follows: 15 min from 3% B to 30% B followed by 2 min increasing B to 100% and 3 min isocratic at 100% B. Furthermore, derivatization procedure was conducted without FMOC reagent because only OPA derivatives were analyzed.

2.6 Analysis of polar metabolites by GC-EI-MS

2.6.1 Sample preparation

Extraction of intracellular metabolites

Cell pellets were resuspended in methanol containing 4% ribitol stock solution. 1.5 mL of the methanol/ribitol solution was used per 20 mg_{CDW}. Cell lysis was performed in an ultrasonic bath for 15 min at 70 °C followed by cooling on ice. 1.5 mL ddH_2O per 20 mg_{CDW} was added and mixed vigorously for 1 min. Then, 1 mL chloroform was added followed by another 1 min of mixing for extraction of non-polar compounds. Phase separation was conducted by centrifugation (12 000 x g, 5 min, 4 °C). 500 µL of the polar phase was transferred into glass vials, dried in a vacuum concentrator with rotation at 4°C, capped and stored at -20 °C until GC-MS analysis. The residual polar phase was transferred into 2 mL reaction tubes and stored at -80 °C as backup samples.

Preparation of culture supernatants

10 µL of the culture supernatants were transferred into glas vials and spiked with 200 µL of ethanol containing 3.5% ribitol stock solution (193 µL ethanol + 7 µL ribitol). The samples were dried in a vacuum concentrator with rotation at 4°C, capped and stored at -20 °C until GC-MS analysis.

Derivatization procedure

The two-step automated derivatization was performed prior to injection with the MPS 2 XL autosampler equipped with a mVorx unit (Gerstel, Mülheim a.d. Ruhr, Germany) coupled to the Leco Pegasus 4D GC x GC TOF MS (Leco Instruments, Mönchengladbach, Germany). 40 µL methoxyamine/pyridine solution were added to the dried samples, mixed at 1300 rpm for 1 min with the mVorx unit and incubated for 90 min at 30 °C with constant agitation. In this step carbonyl groups are substituted with a methoxyl group. Then, silylation of amino- and hydroxyl groups was achieved by adding 60 µL MSTFA and incubation for 30 min at 37 °C under constant shaking followed by 1 h incubation at 18 °C without shaking.

2.6.2 GC-EI-MS analysis

Samples were analyzed using a Leco Pegasus 4D GC x GC TOF MS (Leco Instruments, Mönchengladbach, Germany) equipped with a MPS 2 XL autosampler (Gerstel, Mülheim a.d. Ruhr, Germany) and operated in GC-TOF mode. 1 µL of the sample was injected into a programmed temperature vaporizing (PTV) injector (Gerstel, Mülheim a.d. Ruhr, Germany) equipped with a 71 x 1 mm CIS 4 glass liner filled with silanized glass wool. Injection was performed in splitless mode. Vaporizing was conducted with initial 70 °C for 0.02 min and stepwise increase with 12 K s^{-1} up to 330 °C followed by 5 min at a constant temperature of 330 °C. Separation was conducted with a 7890 Agilent GC equipped with a ZB-5MS column (Phenomenex, Aschaffenburg, Germany) or a DB5MS (Agilent Technologies, Waldbronn, Germany) and a constant helium flow of 1.2 or 1.8 mL min^{-1}. The temperature of the transfer line was set to 275 °C. Inoization was performed with an electron impact mode at 70 eV and an ion source temperature of 250 °C. The detector voltage was adjusted to the daily performance of the instrument (about 200 V higher than the output of automatic tuning). Solvent

delay was adjusted according to the deterioration of the column. Full mass spectra were collected from 45 to 600 *m/z* with 8 scans/s.

2.6.3 GC-EI-MS data processing and analysis

Raw data was exported using the ChromaTOF software as NetCDF (network common data format) files. Data were further processed with the software MetaboliteDetector (Hiller *et al.* 2009). The by Christian Nieke (TU Braunschweig) further developed version *2.2N-2013-01-15* was used for all analyses. The software automatically deconvolutes all mass spectra from the imported chromatograms and calculates the retention indices (RI) based on formula (6) using the measured alkane mix as RI marker.

$$RI^{(T)} = 100 \cdot \left[(y - x) \cdot \left(\frac{log(t_i) - log(t_x)}{log(t_y) - log(t_x)} \right) + x \right] \quad (6)$$

with $RI^{(T)}$ = retention index in a temperature gradient,
x = number of carbon atoms of the alkane eluting before the analyte,
y = number of carbon atoms of the alkane eluting after the analyte,
t_i = retention time of the analyte,
t_x = retention time of the alkane eluting before the analyte,
t_y = retention time of the alkane eluting after the analyte.

Additionally, the calculated RIs of the analytes were corrected by alignment to the internal standard ribitol. Automatic identification of compounds was achieved by comparison of mass spectra and RI with a defined library and a cut-off score for similarity of 70%. Quantification was performed with an appropriate, specific fragment ion for the respective compound. The library also includes unidentified compounds which were reproducibly detected in different strains analyzed at the institute labeled with the prefix “Unknown”. Unidentified compounds originated from the Golm Metabolome Database are labeled with the prefix “NA” or “D”.
Data were checked and if necessary peak areas were added manually. The data were normalized to the peak area of the internal standard ribitol. The different derivatives of one compound were summed using the institute intern script *itool*.

2.6.4 Statistical data analysis

Significance test was conducted with OriginPro 2016G using the implemented non-parametric Wilcoxon-Mann-Whitney test (Mann, Whitney 1947). Differences

between two conditions were regarded as significant for p-values < 0.001. Furthermore, fold changes (quotient of the mean values “test state” and “reference state”) were calculated and values ≥ 2 or ≤ 0.5 were considered when the Wilcoxon-Mann-Whitney test was significant. Errors of fold changes (fc) were determined using propagation of uncertainty (formula 7).

$$s_e(fc) = \sqrt{\left(\left(\frac{s_e(t)}{mean(t)}\right)^2 + \left(\frac{s_e(r)}{mean(r)}\right)^2\right)} \cdot \left(\frac{mean(t)}{mean(r)}\right) \quad (7)$$

with t = test state,
r = reference state,
s_e = standard error

2.7 Analysis of CoA derivatives by LC-ESI-MS

2.7.1 Extraction of CoA-esters

10 mg CDW were harvested and resuspended in 1 mL methanol. The suspension was transferred into 2 mL reaction tubes containing 0.6 g glass beads (70 - 110 µM diameter). Cell lysis was realized with the oscillating mill MM400 (Retsch GmbH, Haan, Germany) using -80 °C cold milling cups for 2 mL reaction tubes. Three cycles of 1 min and 30 Hz were carried out for homogenization. The lysate was transferred into 15 mL reaction tubes containing 10 mL ice cold ammonium acetate (25 mM, pH 6), centrifuged for 5 min at 10 000 x g and 4 °C and stored on ice until solid phase extraction.

The solid phase extraction columns Strata XL-AW (Phenomenex, Aschaffenburg, Germany) were conditioned by sequential application of 1 mL methanol, 1 mL methanol/water/formic aicd (50:45:5) and 1 mL water. The supernatants of the cell lysates were loaded onto the conditioned columns with 800 – 900 mbar vacuum. Afterwards, the columns were washed with 1 mL ammonium acetate (25 mM) and 1 mL methanol and dried at 700 mbar for 5 min. Elution was performed using 1 mL methanol containing 0.5 % ammonia. Subsequently, the samples were dried in a vacuum concentrator with rotation at 4 °C and stored at -80 °C until measurement.

2.7.2 LC-ESI-MS analysis

For measurement, the samples were dissolved in 200 µL sample buffer and transferred into vials for HPLC. Analysis was performed on a Dionex ultimate 3000 system (Thermo Scientific Inc., Schwerte, Germany) coupled to a Bruker MicroTOF QII mass spectrometer (Bruker Daltonik GmbH, Bremen, Germany) equipped with an electrospray ionization interface. 50 µL of the sample were injected and separated based on the protocol described by Peyraud *et al.* (2009) with a C_{18} analytical column (Gemini 150 x 2.0 mm, particle size 3 µm; Phenomenex, Aschaffenburg, Germany) at 35 °C and a flow rate of 220 µL min^{-1}. Following stepwise gradient was applied: 0-1 min 5% B, 1-19 min increase to 30% B, 19-26 min increase to 95%B, 26-30 min 95%B followed by reequilibration of the column. MS analysis was performed in ESI+ mode with a rate of 3 Hz for data acquisition and automated MS/MS acquisition. Mass range was set to *m/z* 90-1178 with an end plate offset of -500 V and capillary voltage of 4500 V. Nebulizer pressure of 1.2 bar, dry gas flow rate of 8 L min^{-1} and dry temperature at 200 °C were used.

2.7.3 LC-ESI-MS data processing and analysis

The raw data was recalibrated to the sodium formate cluster and data was exported as MZXML files using *DataAnalysis* automation scripting (Bruker Daltonic, Bremen, Deutschland). Peak detection and alignment was conducted with the R package XCMS. Identification of CoA derivatives was conducted by comparison of the accurate masses and retention times with commercial available coenzyme A standards. Furthermore, sum formula predictions were performed for unidentified compounds using SmartFormula implemented in the *DataAnalysis* software.

2.8 Transcriptomic analysis

Transcriptomic analyses were conducted by the group of Robert Geffers (Helmholtz centre for infection research, Braunschweig) using RNA-seq technology. The quality and integrity of total RNA was controlled on Agilent Technologies 2100 Bioanalyzer (Agilent Technologies, Waldbronn, Germany). The RNA sequencing library was generated from 100 ng total RNA using *TruSeq RNA Sample Prep Kits v2* (Illumina) for

mRNA purification followed by *ScriptSeq v2 RNA-Seq Library Preparation Kit* (Epicentre) according to manufacturer's protocols. The libraries were sequenced on Illumina HiSeq2500 using TruSeq SBS Kit v3-HS (50 cycles, single ended run) with an average of 3 x 10^7 reads per RNA sample. The data was provided as *Rockhopper* output (expression levels).

2.9 Metabolic model reconstruction

2.9.1 Metabolic Pathways

The metabolic model *i*Pin571 was reconstructed based on genome and experimental data (Thole *et al.* 2012; Berger *et al.* 2012; Berger *et al.* 2011; Brock *et al.* 2014; Drüppel *et al.* 2014; Wiegmann *et al.* 2014; Zech *et al.* 2013a; Zech *et al.* 2013b; Zech *et al.* 2009). The web service EnzymeDetector was used for prediction of enzyme functions for implemented reactions (Quester and Schomburg 2011). The bottom-up approach was used to reconstruct the model step-by-step from central carbon metabolism up to all necessary biosynthetic pathways and known degradation pathways for 32 different substrates including 20 amino acids, some carbohydrates and further carboxylic acids. TDA biosynthesis was included as overall reaction based on the published proposed biosynthesis pathway by Brock *et al.* (2014). Non-sequenced based reactions were added to fill necessary gaps in the model. The model was checked for internal cycles and reversibility was changed if necessary.
The inhouse program *simia* (Rex 2013), further developed by Helge Stark, was used to export reactions based on EC numbers from the database *BKM-react* (Lang *et al.* 2011) and transfer them into the *metano* format (Riemer 2013). Reactions which were not included in one of the databases were manually added to the model.

2.9.2 Biomass composition

The biomass reaction includes experimental, literature and genome data. The content of DNA, RNA, protein, PHB and lipids were experimentally determined as described in chapter 2.4.5. Total concentrations of amino acids and diaminopimelate (free and bonded) in cell hydrolysates were determined by HPLC-FLD measurement (chapter 2.5).

The content of peptidoglycan was estimated with the assumption that total diaminopimelate is bonded in the peptidoglycan. For the protein composition determined glutamate and alanine were corrected for the content in peptidoglycan based on diaminopimelate. Furthermore, glutamate was corrected for intracellular levels based on quantification for *D. shibae* by Kleist *et al.* (2016). Estimation of asparagine, glutamine, tryptophan and cysteine was based on ratio assumptions in the protein sequence.
The shares of nucleotides in DNA and RNA were estimated based on GC-content. Further biomass components were estimated based on literature data (table S15).

2.9.3 Determination of GAM and NGAM

Growth rates μ and specific substrate uptake rates q_S were determined as described in chapter 2.4.3. The q_S were referred to 1 mol carbon. Thus, an amino acid overarching determination of GAM and NGAM with TDA-free cultivations was possible (see chapter 3.3.5).
NGAM is included as separate ATP hydrolyzation reaction. GAM is included as ATP hydrolyzation in the biomass reaction.

2.10 *In silico* analyses

FBAs were performed with the *metano* software (Riemer 2013) to calculate optimal biomass production with experimentally determined substrate uptake rates q_S. Maximal possible ATP yields were determined by optimizing NGAM reaction instead of the biomass reaction. The upper bound of the biomass reaction was set to the experimentally determined growth rate for calculations of TDA dependent carbon flux.

3 Results and discussion

3.1 Metabolic role of the 262-kb plasmid

The 262-kb plasmid encodes several genes with a variety of functions including transporter for substrates and dipeptides as well as biosynthesis genes for an exopolysaccharide and the antibiotic TDA. First studies with plasmid-cured mutant strains and casamino acids as substrate showed that the deletion of the 262-kb plasmid led to a higher growth efficiency associated with higher amino acid consumption compared to the wild-type strain (Hensler 2014). All possible mutant strains missing one (Δ262-kb, Δ78-kb, Δ65-kb), two (Δ262Δ78-kb, Δ262Δ65-kb, Δ78Δ65-kb) or all three (Δ262Δ78Δ65-kb) plasmids were cultivated in process-controlled bioreactors in collaboration with the working group of Prof. Dr. Ralf Rabus (ICBM, Oldenburg) for physiological analyses. Furthermore, a systems biology approach of the Δ262-kb mutant strain was performed in process-controlled bioreactors to get a deeper understanding of the function of the 262-kb plasmid. Cultivation in process-controlled bioreactors and sampling were performed by the working group of Prof. Dr. Ralf Rabus (ICBM, Oldenburg). Here, the results on metabolic level will be discussed and compared with changes on transcriptomic level. Data for analysis of growth physiology of plasmid-cured mutant strains were published in Trautwein *et al.* (2016). The observation of L-pipecolate as L-lysine degradation intermediate was published in Will *et al.* (2017) and Reimer *et al.* (2017).

3.1.1 Growth physiology of plasmid-cured mutant strains

Growth characteristics at OD_{max} were compared for all plasmid-cured mutant strains and the wild-type strain to analyze the effect on the growth behavior of lacking single, double or all three plasmids. Maximally reached optical densities (OD) and cell dry weights (CDW) were dependent on the available plasmids (figure 3.1). Deletion of the 262-kb plasmid led to more than 2-fold higher CDWs. Maximal OD values were not correlating with maximal CDW values which might be due to disturbance of OD measurement by nonviable cells and the production of an exopolysaccharide. Thus, only trends are identifiable but not exact differences as determination of living cells

would be necessary. It is noticeable that the deletion of the 65-kb or the 78-kb plasmid only, did not influence the maximally reached CDW compared to the wild-type strain. The 65-kb plasmid is known as the "biofilm plasmid" as it is required for biofilm formation, motility and the colonization of marine algae (Frank *et al.* 2014). In process-controlled bioreactors, *P. inhibens* DSM 17395 does not grow in biofilms. Consequently, the smallest plasmid is not crucial which is represented by the similar CDW values. However, the Δ65-kb mutant strain depleted less available carbon compared to the wild-type strain. Thus, the lack of the biofilm-related polysaccharide production increased the biomass yield but not the maximally reached CDW. This effect is only slightly observable between the Δ262-kb and the Δ262Δ65-kb mutant strains. In previous studies with Erlenmeyer flask cultivations the difference between both strains was more pronounced (Hensler 2014).

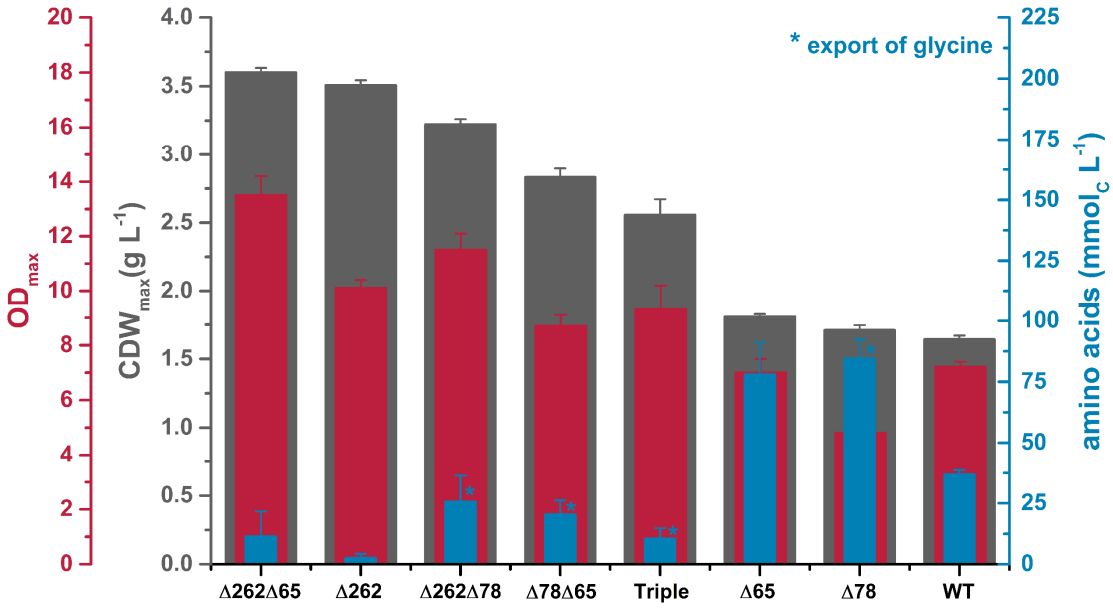

Figure 3.1 Growth characteristics at OD_{max} of the wild-type and plasmid-cured mutant strains for cultivation in process-controlled bioreactors with casamino acids as carbon source. Shown are maximal OD (red) and CDW (grey) values with corresponding $mmol_C\ L^{-1}$ (provided by amino acids) left in the medium (blue). Cultivation, sampling and measuring of OD and CDW were performed by the working group of Ralf Rabus (ICBM) (Trautwein et al. 2016).

For the Δ78-kb mutant strain similar amounts of carbon were detected in the supernatant compared to the Δ65-kb mutant strain. However, lacking the 78-kb plasmid led to secretion of glycine due to the missing glycine cleavage system (Zech *et al.* 2013b). Threonine, which is degraded via glycine (Drüppel *et al.* 2014), is

exported as glycine leading to higher glycine levels at OD_{max} compared to the initial medium. Besides the necessity for glycine catabolism the 78-kb plasmid encodes the only known copy for the catalase (PGA1_78p00050). Thus, this plasmid might be important for detoxification of reactive oxygen species. Comparison of mutant strains lacking the 78-kb plasmid with the other strains is difficult due to the secreted glycine and different ratios between OD_{max} and CDW_{max} values. As mentioned above, determination of living cells would be necessary because the missing detoxification by the catalase might increase the number of nonviable cells.

Analysis of the plasmid-cured mutant strains revealed one important information: the 262-kb plasmid shows a growth restriction effect leading to stop of growth even though there are still amino acids left in the medium. Thus, the 262-kb plasmid plays the key role in growth differences with casamino acids as carbon source and will be analyzed in the following.

3.1.2 Metabolome analysis of the Δ262-kb plasmid-cured mutant strain compared to the wild-type strain

Metabolome analysis was performed for cells harvested at ½ OD_{max} and OD_{max} of the wild-type strain and the Δ262-kb plasmid-cured mutant strain, respectively. Different unidentified compounds were only detectable in the Δ262-kb mutant strain (figure 3.2 A and C) and will be discussed in chapter 3.1.3. Besides these unidentifed compounds there are only a few noticeable differences in the metabolome at ½ OD_{max}. Higher amounts of pipecolate and cadaverine but smaller amounts of 2-aminoadipate were detected when the 262-kb plasmid was missing (figure 3.2 A). Furthermore, 5-aminopentanoate was lower in the Δ262-kb mutant strain at OD_{max} (figure 3.2 C). Cadaverine, 5-aminopentanoate and 2-aminoadipate are intermediates of L-lysine catabolism of *P. inhibens* DSM 17395 (Drüppel *et al.* 2014). Pipecolate was accumulating over time in the Δ262-kb mutant strain until OD_{max} (figure 3.2 A and C). It was about 3.5-fold higher in the Δ262-kb mutant strain at ½ OD_{max} (table 3.1) and about 5-fold higher at OD_{max} (table 3.2) compared to the wild-type strain. Furthermore, pipecolate was already secreted at ½ OD_{max} by the Δ262-kb mutant strain while it was only detected in smaller amounts in the wild-type strain supernatant at OD_{max} (figure 3.2 B and D). A degradation pathway of L-lysine via

pipecolate was found to be active in *Pseudomonas putida* KT2440 (Revelles *et al.* 2005) but is not yet described for *P. inhibens* DSM 17395 and will be discussed in chapter 3.1.4.

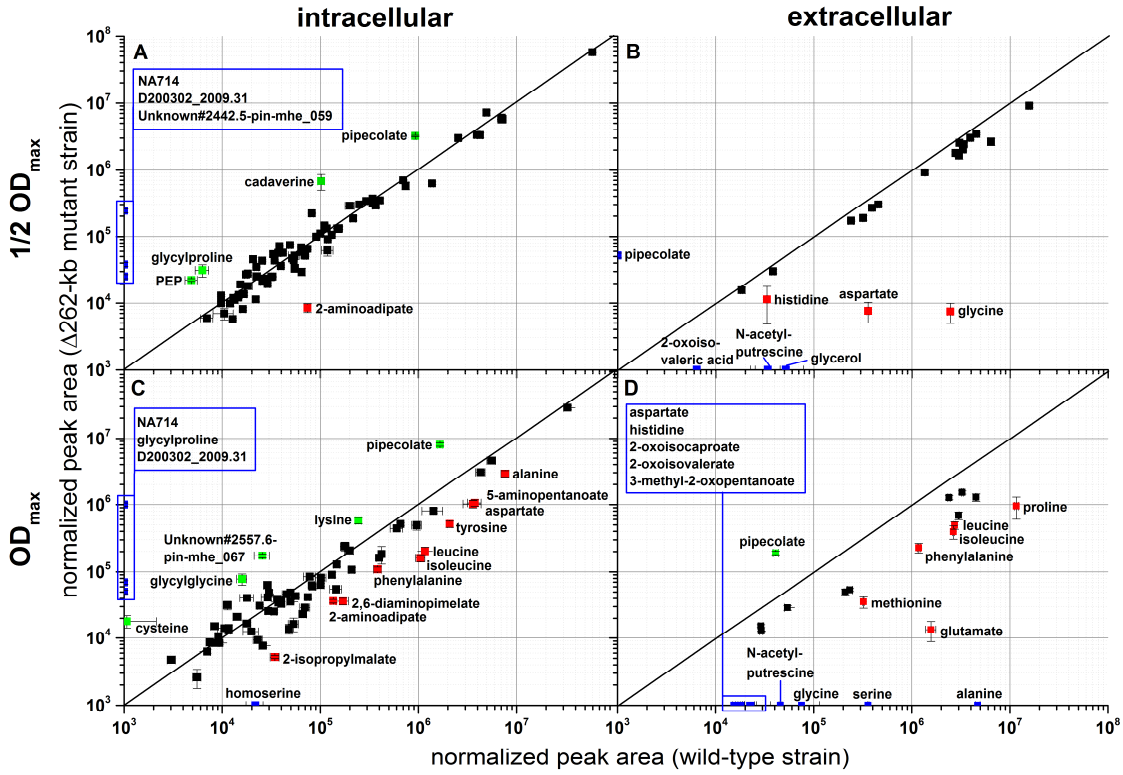

Figure 3.2 Comparison of intracellularly and extracellularly detected metabolites by GC-MS analysis in the wild-type and Δ262-kb plasmid-cured mutant strains at ½ OD_{max} and OD_{max} with casamino acids as carbon source (process-controlled bioreactors). Shown are logarithmized, normalized peak areas of intracellularly (A and C) and extracellularly (B and D) detected metabolites for cells harvested at ½ OD_{max} (A and B) and OD_{max} (C and D). Values of the Δ262-kb mutant strain are plotted over the wild-type strain. Shown are mean values of four biological replicates with standard errors. Metabolites detected only in one strain are labeled in blue. Furthermore, metabolites with significantly higher (green) and significantly lower (red) abundance in the Δ262-kb mutant strain are highlighted. All detected metabolites are listed in table S1 (intracellular) and S2 (extracellular). Cultivation and sampling were performed by the working group of Ralf Rabus (ICBM). PEP: phosphoenolpyruvate.

Higher amounts of dipeptides, e.g. glycylproline and glycylglycine, in the Δ262-kb mutant strain could be related to missing genes coding for dipeptide transport relating proteins (table S4). Serine, as the precursor for cysteine biosynthesis, was about 2.7-fold higher in the Δ262-kb the mutant strain at ½ OD_{max} (figure 3.2 A, table 3.1). At OD_{max} serine was lower, but cysteine was about 17-fold higher in the Δ262-kb mutant strain because it was only detectable in one of the wild-type replicates (figure

3.2 C, table 3.2). Cysteine is discussed as one possible source for the incorporation of sulfur in TDA catalyzed by enzymes encoded on the 262-kb plasmid (Brock *et al.* 2014). Thus, cysteine is maybe produced in higher amounts than necessary in the Δ262-kb mutant strain which led to accumulation at OD_{max}.

Table 3.1 Fold changes of selected intracellularly detected metabolites at ½ OD_{max} with casamino acids as carbon source (process-controlled bioreactors). Shown are metabolites with fold changes ≥2.0 or ≤0.5 compared to the wild-type strain and p-values < 0.001 (Wilcoxon-Mann-Whitney test). Metabolites only detected in the Δ262-kb mutant strain are listed with "+". Fold changes with corresponding p-values for all metabolites are listed in table S3. Cultivation and sampling were performed by the working group of Ralf Rabus (ICBM).

Higher abundance in Δ262-kb mutant strain		Lower abundance in Δ262-kb mutant strain	
Metabolite	**Fold change**	**Metabolite**	**Fold change**
D200302_2009.31	+	2-aminoadipate	0.12 ± 0.02
NA714	+	Uric acid	0.45 ± 0.03
Unknown#2442.5-pin-mhe_059	+	Tyrosine	0.46 ± 0.03
Cadaverine	7 ± 2	Putrescine	0.46 ± 0.06
Glycylproline	5 ± 1	2-isopropylmalate	0.50 ± 0.04
Phosphoenolpyruvate	4.6 ± 0.7		
Pipecolate	3.5 ± 0.1		
Serine	2.7 ± 0.1		
NA_1703.1	2.2 ± 0.2		

Phosphoenolpyruvate was about 4.6-fold more abundant in the Δ262-kb mutant strain compared to the wild-type strain at ½ OD_{max} (figure 3.2 A, table 3.1). The Δ262-kb mutant strain already depleted the complete available aspartate (figure 3.3) which can be easily degraded via oxaloacetate to phosphoenolpyruvate to feed gluconeogenesis. Thus, a higher phosphoenolpyruvate level is explainable by the higher aspartate consumption.

Previous studies showed a time-resolved utilization of the available amino acids by *P. inhibens* DSM 17395 (Zech *et al.* 2013b). Zech *et al.* (2013b) divided the amino acids in four groups according to their depletion rate. Thus, different amino acids availability could have an influence on the metabolome at ½ OD_{max} and OD_{max}. Besides aspartate, also glycine is almost completely consumed at ½ OD_{max} by the Δ262-kb mutant strain (figure 3.2 B, figure 3.3). These two amino acids are also preferred by the wild-type strain while all other amino acids were not completely depleted.

Especially glutamate and alanine as easy accessible amino acids were not completely consumed by the wild-type strain, which indicates a massive growth restriction by the 262-kb plasmid as previously mentioned (chapter 3.1.1).

Table 3.2 Fold changes of selected intracellularly detected metabolites at OD_{max} with casamino acids as carbon source (process-controlled bioreactors). Shown are metabolites with fold changes ≥2.0 or ≤0.5 compared to the wild-type strain and p-values < 0.001 (Wilcoxon-Mann-Whitney test). Metabolites only detected in the Δ262-kb mutant strain are listed with "+" and metabolites only detected in the wild-type strain with n.d. (not detected). Fold changes with corresponding p-values for all metabolites are listed in table S3. Cultivation and sampling were performed by the working group of Ralf Rabus (ICBM).

Higher abundance in Δ262-kb mutant		**Lower abundance in Δ262-kb mutant**	
Metabolite	**Fold change**	**Metabolite**	**Fold change**
NA714	+	Homoserine	n.d.
D200302_2009.31	+	Unknown#2260-cgl-sst_001	n.d.
Glycylproline	+	Isoleucine	0.15 ± 0.03
Cysteine	17 ± 17	2-isopropylmalate	0.15 ± 0.02
Unknown#2557.6-pin-mhe_067	7 ± 1	Leucine	0.17 ± 0.03
Glycylglycine	5 ± 1	2,6-diaminopimelate	0.21 ± 0.04
Pipecolate	4.9 ± 0.4	Tyrosine	0.25 ± 0.03
Lysine	2.4 ± 0.3	2-Aminoadipate	0.27 ± 0.02
3-Hydroxybutanoate	2.3 ± 0.4	5-Aminopentanoate	0.28 ± 0.06
Ethanolamine	2.2 ± 0.3	Phenylalanine	0.28 ± 0.04
		NA199017_1996.71	0.29 ± 0.05
		Glutarate	0.30 ± 0.03
		2,4-diaminobutanoate	0.30 ± 0.08
		Serine	0.35 ± 0.04
		Alanine	0.38 ± 0.06
		Alanyl-alanine	0.41 ± 0.03
		Putrescine	0.41 ± 0.06
		Malate	0.42 ± 0.05

Interestingly, the classification groups of Zech et al (2013b) are not entirely reflecting the observed depletion order. Here, only 50% of arginine and lysine were used by the Δ262-kb mutant strain and even less by the wild-type strain. This could indicate a problem with excess nitrogen since both amino acids provide more nitrogen compared to the other available amino acids. Furthermore, arginine and lysine are

alkaline amino acids. Glutamate and aspartate as acidic amino acids were completely depleted by the Δ262-kb mutant. Thus, uptake of alkaline substrates might be limited due to intracellular pH.

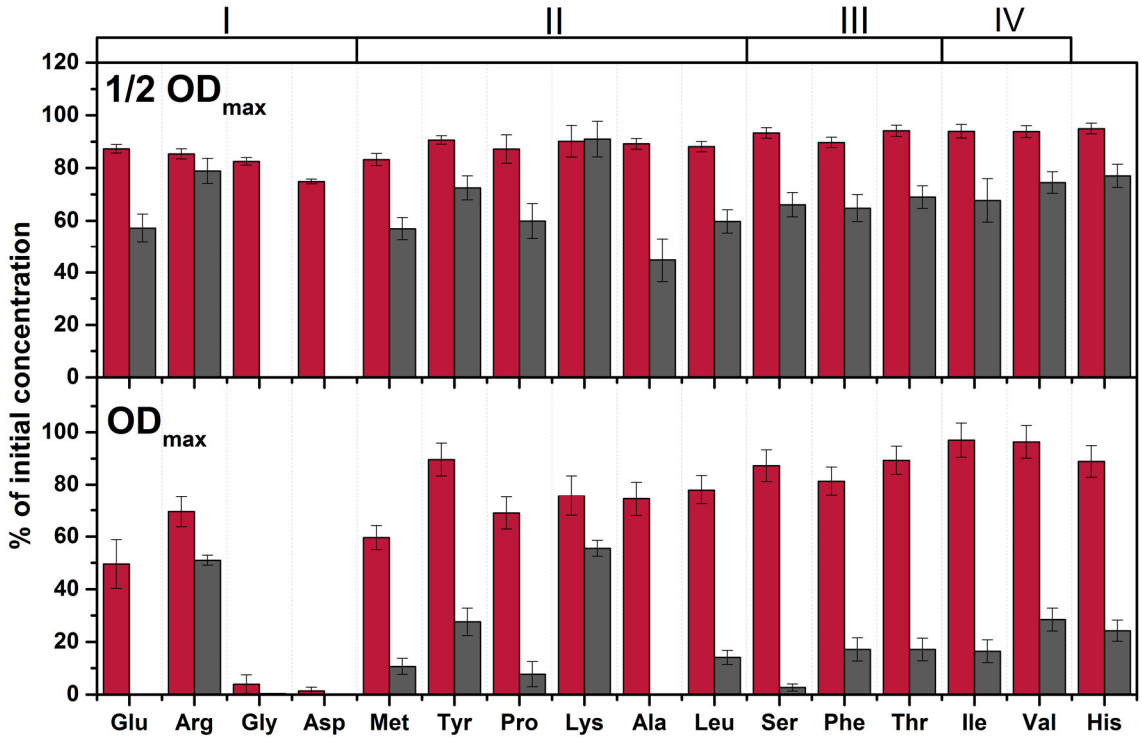

Figure 3.3 Amino acid depletion profiles at ½ OD_{max} and OD_{max} for cultivations in process-controlled bioreactors with casamino acids as carbon source. Shown are the available amino acids in the medium at ½ OD_{max} and OD_{max} for the wild-type (red bars) and the Δ262-kb mutant (grey bars) strains determined by HPLC as percentage of the initial concentration. Absolute concentrations are listed in table S5. Cultivation and sampling were performed by the working group of Ralf Rabus (ICBM). Classification groups I to IV were abstracted by Zech *et al.* (2013b).

Overall, the wild-type strain has only consumed about 10% of the available carbon at ½ OD_{max} while the Δ262-kb mutant strain already depleted 40% of the available carbon (table 3.3). This difference is connected to the stage of growth which means ½ OD_{max} for the wild-type strain is lower than for the Δ262-kb mutant strain. At OD_{max} the Δ262-kb mutant strain had only 16% of the carbon left while the wild-type strain entered stationary growth phase with still 72% carbon available in the medium.

The Δ262-kb mutant strain and the wild-type strain had more amino acids left compared to the previous study (chapter 3.1.1). Here, the medium contains about 280 $mmol_C\ L^{-1}$ which is about 55 $mmol_C\ L^{-1}$ more than in the previous study and could be attributed to a different casamino acid batch used in this study. However, in both

studies deletion of the 262-kb plasmid led to higher growth efficiency compared to the wild-type strain.

Table 3.3 Available carbon at ½ OD_{max} and OD_{max} for cultivations in process-controlled bioreactors with casamino acids as carbon source. Listed are the $mmol_C\ L^{-1}$ in the medium at ½ OD_{max} and OD_{max} for the Δ262-kb mutant strain and the wild-type strain based on quantification of all amino acids in the supernatant with HPLC. Cultivation and sampling were performed by the working group of Ralf Rabus (ICBM).

Strain	0.5 OD_{max}		OD_{max}	
	$mmol_C\ L^{-1}$	% of initial concentration	$mmol_C\ L^{-1}$	% of initial concentration
Wild-type	248 ± 4	89 ± 1	200 ± 14	72 ± 5
Δ262-kb	172 ± 13	61 ± 5	45 ± 8	16 ± 3

The minor differences observed at ½ OD_{max} could also be confirmed by analysis of certain nucleotides and cofactors which revealed no differences at ½ OD_{max} between the wild-type and the Δ262-kb mutant strain (figure 3.4). Higher levels of NAD^+ and lower levels of $NADP^+$ at OD_{max} in the Δ262-kb mutant strain are in accordance with the growth state indicating a lack of energy.

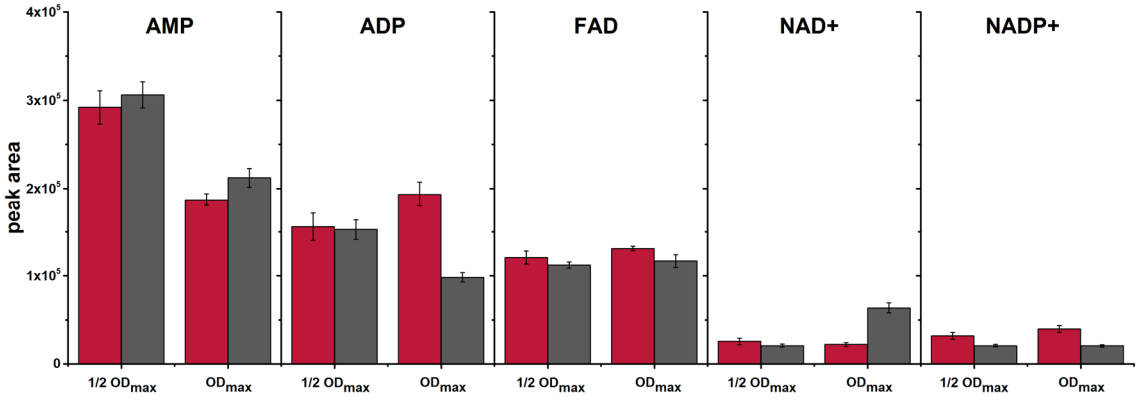

Figure 3.4 Intracellularly detected nucleotides and cofactors at ½ OD_{max} and OD_{max} for the wild-type and Δ262-kb mutant strains for cultivations in process-controlled bioreactors with casamino acids as carbon source. Shown are peak areas of intracellular nucleotides and cofactors of the wild type (red bars) and the Δ262-kb mutant (grey bars) of four biological replicates with standard errors at ½ OD_{max} and OD_{max}. Cultivation and sampling were performed by the working group of Ralf Rabus (ICBM).

Thus, differences on the metabolic level due to different growth states associated with different amino acid availability should be considered. Many amino acids are degraded via CoA intermediates (Drüppel *et al.* 2014) which are analyzed in the following.

Intermediates of the branched chain amino acid (valine, leucine, isoleucine) degradation pathways (2-oxoisovalerate, 2-oxoisocaproate, and 3-methyl-2-oxopentanoate) are secreted by the wild-type strain at OD_{max} (figure 3.2 D). Corresponding CoA intermediates of the further degradation (isobutanoyl-CoA, isovaleryl-CoA, 2-methylbutanoyl-CoA, 3-hydroxy-2-methylbutanoyl-CoA) were accumulating in the wild-type strain at ½ OD_{max} (figure 3.5, figure 3.6). On transcriptomic level genes coding for enzymes involved in the degradation of the CoA intermediates (isovaleryl-CoA dehydrogenase, methylcrotonyl-CoA carboxylase, 3-hydroxyacyl-CoA dehydrogenase, acyl-CoA dehydrogenase, 3-hydroxyisobutyryl-CoA hydrolase, 3-hydroxyisobutyrate dehydrogenase) were down-regulated in the wild-type strain at OD_{max} (table S6, figure 3.6) which is in accordance with the observations on metabolic level. 2-isopropylmalate is a sideproduct of 2-oxoisovalerate (valine degradation) which led to higher intracellular levels at OD_{max} in the wild-type strain compared to the Δ262-kb mutant strain (figure 3.2 C, table 3.2, figure 3.6). Propanoyl-CoA as degradation intermediate of different amino acids is also accumulating at ½ OD_{max}. Furthermore, the affected lysine degradation pathways due to the missing 262-kb plasmid is also reflected by higher levels of glutaryl-CoA in the wild-type strain at both harvesting points (figure 3.5).

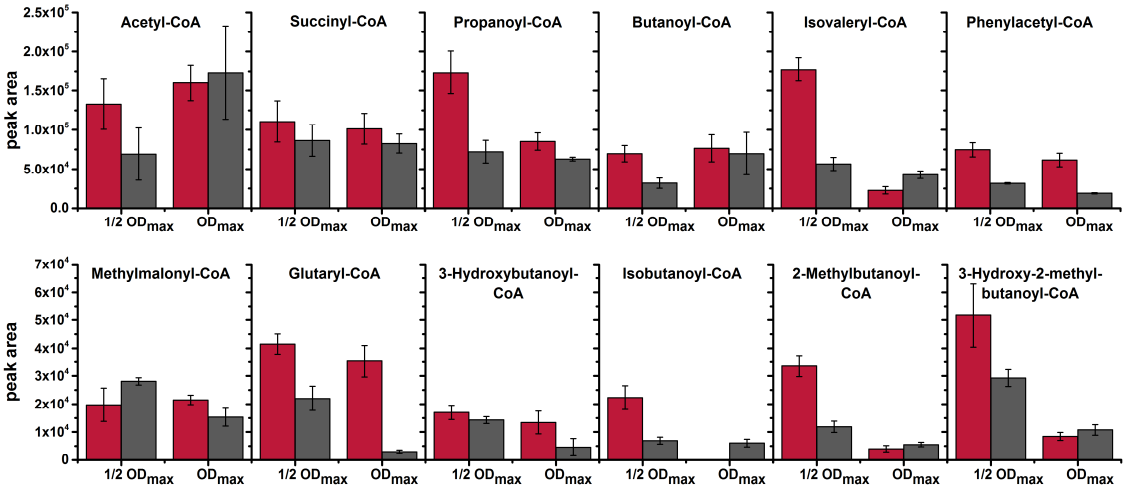

Figure 3.5 Identified CoA intermediates at ½ OD_{max} and OD_{max} for the wild-type and Δ262-kb mutant strains for cultivations in process-controlled bioreactors with casamino acids as carbon source. Shown are peak areas of intracellularly detected CoA intermediates of the wild-type (red bars) and the Δ262-kb mutant (grey bars) of four biological replicates with standard errors at ½ OD_{max} and OD_{max}. Cultivation and sampling were performed by the working group of Ralf Rabus (ICBM).

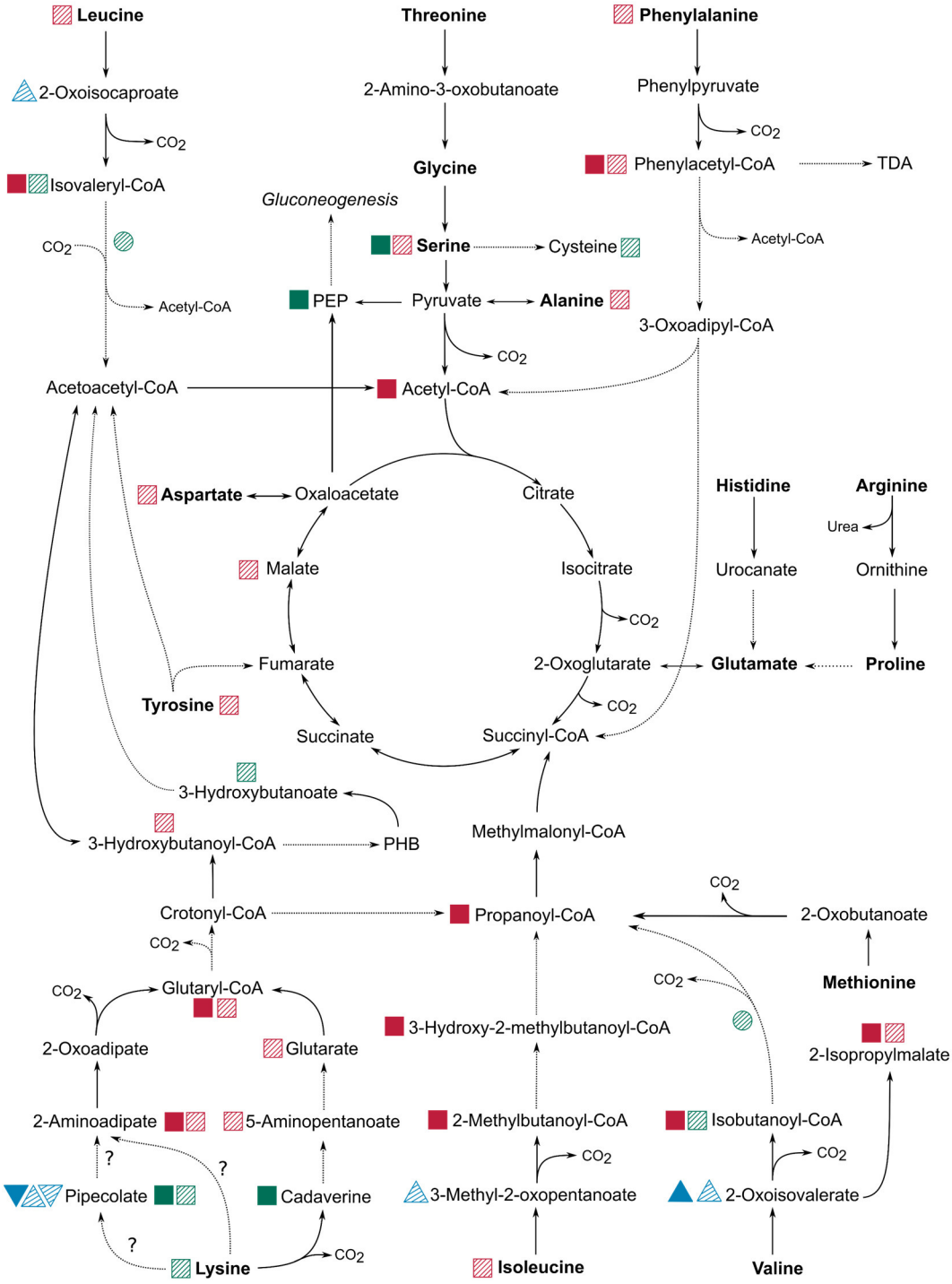

Figure 3.6 Overview of the degradation pathways of all amino acids present in casamino acids and differences on metabolic and transcriptomic level between the Δ262-kb mutant strain and the wild-type strain. Intracellular metabolites significantly higher (green squares) and lower (red squares) in the Δ262-kb mutant strain compared to the wild-type strain are labeled for ½ OD_{max} (filled) and OD_{max} (striped). Transcriptomic data is analogously represented by circles. Extracellularly detected intermediates are labeled with blue triangles for the wild-type and blue reversed triangles for the Δ262-kb mutant strain. PEP: phosphoenolpyruvate. The overview of the pathways was reconstructed based on published data (Zech et al. 2009; Drüppel et al. 2014). Dashed lines represent more than one reaction.

A lower level of 3-hydroxybutanoyl-CoA and a higher level of 3-hydroxybutanoate could be observed in the Δ262-kb mutant strain at OD_{max} indicating a possible PHB degradation due to starvation (table 3.2, figure 3.5, figure 3.6).

Phenylacetyl-CoA, an intermediate of the phenylalanine degradation and precursor of TDA biosynthesis (Berger *et al.* 2012), is more abundant in the wild-type strain compared to the Δ262-kb mutant strain (figure 3.5). Intracellular levels of phenylacetyl-CoA and TDA (figure 3.7) were similar in the wild-type strain at ½ OD_{max} and OD_{max} indicating similar TDA production per g_{CDW} independent of the growth phase. The Δ262-kb mutant strain is not able to produce any TDA due to the missing TDA biosynthesis gene cluster *tdaABCDE* coding on the 262-kb plasmid (Geng *et al.* 2008; Brock *et al.* 2014; Thole *et al.* 2012).

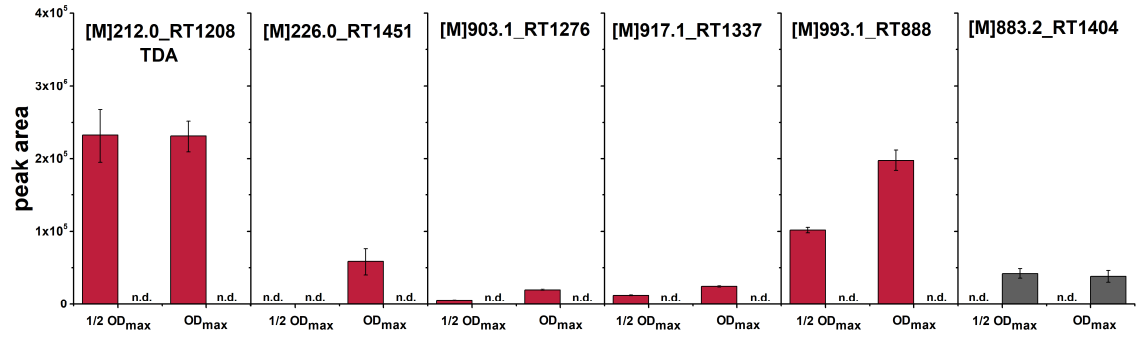

Figure 3.7 Intracellularly detected TDA and unidentified sulfur-containing compounds at ½ OD_{max} and OD_{max} for the wild-type and Δ262-kb mutant strains for cultivations in process-controlled bioreactors with casamino acids as carbon source. Shown are peak areas of intracellular TDA, one compound similar to TDA with additional methyl-moiety and four unidentified CoA intermediates of the wild type strain (red bars) and the Δ262-kb mutant strain (grey bars) of four biological replicates with standard errors at ½ OD_{max} and OD_{max}. Cultivation and sampling were performed by the working group of Ralf Rabus (ICBM).

A similar compound to TDA was detectable at OD_{max} in the wild-type strain with an additional CH_3-moiety ([M]226.0_RT1451) and might be the "pre-TDA" observed by D'Alvise *et al.* (2015). Furthermore, four unidentified CoA derivatives could be detected (figure 3.7). Sum formula predictions revealed sulfur containing moieties bound to the CoA indicating a relation to TDA biosynthesis (table 3.4). The CoA-bonded structure of [M]993.1_RT888 is similar to TDA ($C_8H_4O_3S_2$) but includes one more carbon and an additional oxygen. The lower retention time (RT) might indicate an open structure, because a higher RT compared to the other compounds would be expected due to additional moieties. The predicted sum formula is contrary to the

proposed biosynthesis pathway of TDA by Brock *et al.* (2014) where water elimination and cyclization were proposed to be prior to sulfur incorporation.

Table 3.4 Postulated sum formula for TDA-related unidentified compounds detected in the wild-type and Δ262-kb mutant strains with casamino acids as carbon source. Predictions were performed with SmartFormula, implemented in DataAnalysis 4.0. Cultivation and sampling were performed by the working group of Ralf Rabus (ICBM).

Compound	m/z measured	mSigma	m/z	Sum Formula
[M]226.0_RT1451	226.9836	14.3	226.9831	$C_9H_6O_3S_2$
[M]903.1_RT1276	452.5608	12.7	425.564	$C_{28}H_{40}N_7O_{17}P_3S_2$
[M]917.1_RT1337	459.5717	16.1	459.5718	$C_{29}H_{42}N_7O_{17}P_3S_2$
[M]993.1_RT888	497.5493	8.2	497.5528	$C_{30}H_{42}N_7O_{19}P_3S_3$
[M]883.2_RT1404	442.5821	12.6	442.5797	$C_{26}H_{44}N_7O_{17}P_3S_2$

Furthermore, S-thio-L-cysteine was used as sulfur donor in their hypothesis. However, no compound with the *m/z* of a TDA precursor with a bounded S-thio-L-cysteine could be detected. Furthermore, no differences between the wild-type and the Δ262-kb mutant strain could be observed for *patB* (PGA1_c00860) on transcriptomic level (figure 3.8, table S7). PatB was recently characterized as L-cystine β-lyase catalyzing the reaction of cystine to L-thio-L-cysteine but might also act on L-methionine resulting in methanethiol (Dickschat *et al.* 2017). Methionine is a component of casamino acids which was used in the systems biology approach. Interestingly, [M]883.2_RT1404 was only detectable in the Δ262-kb mutant strain and the predicted sum formula would fit to 4-methylthiobutanoyl-CoA indicating a possible relation to the degradation of a methionine-related sulfur donor. S-thio-L-cysteine is not stable (Dickschat *et al.* 2017) and thus, methanethiol might be a more effective sulfur donor in the described set-up. Two neighboring genes to *patB* showed different expression levels. PGA1_c00840 (glutathione transferase-like protein) was higher expressed in the wild-type strain at OD_{max} and PGA1_00850 (hypothetical protein) was higher expressed in the Δ262-kb mutant strain at OD_{max} (figure 3.8, table S7) indicating a possible role in the degradation or biosynthesis of the respective sulfur donor compound.

[M]903.1_RT1276 and [M]917.1_RT1337 include only one sulfur atom and might be intermediates of the first sulfur incorporation step.

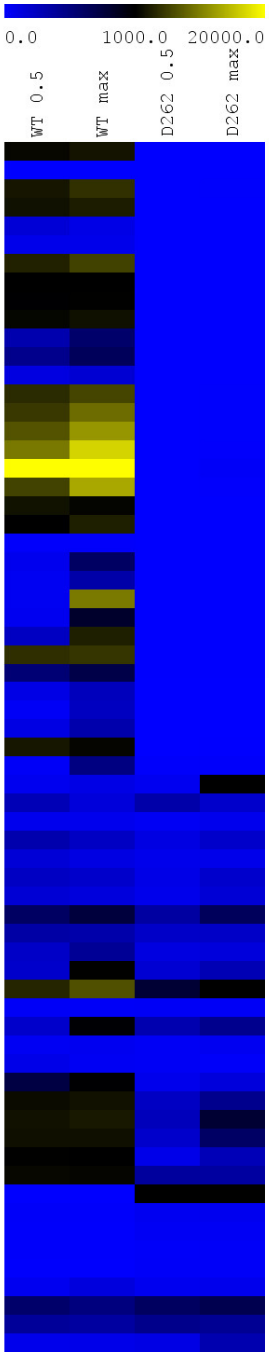

PGA1_262p00780: NAD dependent epimerase/dehydratase
PGA1_262p00790: hypothetical protein
PGA1_262p00800: phenylacetic acid degradation protein PaaZ
PGA1_262p00810: flavoprotein, HFCD family
PGA1_262p00820: hypothetical protein
PGA1_262p00830: hypothetical protein
PGA1_262p00840: hypothetical protein
PGA1_262p00850: sodium dependent symporter
PGA1_262p00860: hypothetical protein
PGA1_262p00870: ABC transporter, extracellular solute-binding protein
PGA1_262p00880: ABC transporter, integral inner membrane component
PGA1_262p00890: ABC transporter, integral inner membrane component
PGA1_262p00900: ABC transporter ATP-binding protein
PGA1_262p00910: cation transport protein
PGA1_262p00920: hypothetical protein
PGA1_262p00930: hypothetical protein
PGA1_262p00940: acyl-CoA dehydrogenase TdaE
PGA1_262p00950: thioesterase superfamily protein TdaD
PGA1_262p00960: prephenate dehydratase TdaC-like protein
PGA1_262p00970: beta etherase TdaB
PGA1_262p00980: LysR family transcriptional regulator
PGA1_262p00990: LysR family transcriptional regulator
PGA1_262p01320: hypothetical protein
PGA1_262p01330: MarR family transcriptional regulator
PGA1_262p01340: hypothetical protein
PGA1_262p01580: metal ion uptake regulator
PGA1_262p01590: hypothetical protein
PGA1_262p01890: hypothetical protein
PGA1_262p01900: hypothetical protein
PGA1_262p01910: NADH:flavin oxidoreductase / NADH oxidase
PGA1_262p01920: NADH:flavin oxidoreductase / NADH oxidase
PGA1_262p01930: ArsR family transcriptional regulator
PGA1_262p01940: hypothetical protein
PGA1_c00840: glutathione transferase-like protein
PGA1_c00850: hypothetical protein
PGA1_c00860: cystathionine beta-lyase PatB
PGA1_c04030: phenylacetic acid degradation protein paaA-like protein
PGA1_c04040: phenylacetic acid degradation NADH oxidoreductase PaaE
PGA1_c04050: phenylacetic acid degradation protein PaaD
PGA1_c04060: phenylacetic acid degradation protein PaaC
PGA1_c04070: phenylacetic acid degradation protein PaaB
PGA1_c04080: phenylacetic acid degradation protein PaaA
PGA1_c04090: beta-ketoadipyl-CoA thiolase PaaJ
PGA1_c04490: indolepyruvate oxidoreductase
PGA1_c07050: methyltransferase domain-containing protein
PGA1_c07610: 4-hydroxyphenylpyruvate dioxygenase
PGA1_c11690: thioesterase domain-containing protein
PGA1_c11700: 5,10-methylenetetrahydrofolate reductase
PGA1_c11710: LysR family transcriptional regulator
PGA1_c20730: AsnC family transcriptional regulator
PGA1_c20740: uroporphyrinogen-III C-methyltransferase CobA
PGA1_c20750: hypothetical protein
PGA1_c20760: nitrite/sulfite reductase
PGA1_c20770: phosphoadenosine phosphosulfate reductase
PGA1_c20780: hypothetical protein
PGA1_c20790: ferredoxin--NADP reductase Fpr
PGA1_c22710: acyl-CoA dehydrogenase
PGA1_c26800: phenylacetate-CoA ligase PaaK
PGA1_c26810: phenylacetic acid degradation protein PaaI
PGA1_c26820: enoyl-CoA hydratase
PGA1_c26830: phenylacetic acid degradation protein PaaZ
PGA1_c26840: phenylacetic acid degradation operon negative regulatory protein
PGA1_c29420: aromatic-amino-acid aminotransferase TyrB
PGA1_c29430: 3-mercaptopyruvate sulfurtransferase
PGA1_c32550: phenylacetate-CoA ligase PaaK

Figure 3.8 Heat map of expression levels of putative TDA biosynthesis related genes. Data was plotted using MultiExperiment Viewer. Expression levels for putative TDA biosynthesis related genes of the wild-type (WT) and the Δ262-kb mutant strain (D262) at ½ OD_{max} (0.5) and OD_{max} (max) are shown. Expression levels are indicated by a two-color scale: Blue to black (0-1000) and black to yellow (1000-20000). For detailed values see table S7. Cultivation and sampling were performed by the working group of Ralf Rabus (ICBM).

The transcriptome data showed very high expression levels (over 10000) for the TDA biosynthetic gene cluster *tdaABCDE* (figure 3.8). Genes coding for the phenylacetic acid degradation proteins had significantly lower expression levels (about 100-300)

except for *paaA* with expression levels of 600-700 at OD_{max}. Genes coding for enzymes necessary for L-phenylalanine degradation (*paaI*, *paaG*, *paaZ*) showed no significant expression levels (about 20) indicating that L-phenylalanine is not catabolized for energy but only used as precursor for TDA production. Analyses of cultures spiked with $^{13}C_9$-^{15}N-labeled L-phenylalanine proved that L-phenylalanine degradation is not active in the wild type strain because acetyl-CoA and succinyl-CoA were unlabeled (figure 3.9). In contrast, the transposon mutant affecting the TDA biosynthetic gene *tdaE* showed an active L-phenylalanine degradation (labeled acetyl-CoA and succinyl-CoA). Furthermore, TDA and two unidentified compounds ([M]993.1_RT867 and [M]899.2_RT982) could be detected and were labeled. [M]993.1_RT867 is the previously described sulfur-containing TDA precursor ([M]993.1_RT888) with a retention time shift. [M]899.2_RT982 was matched with phenylglyoxylyl-CoA but could also be another isomeric structure.

The annotated 4-hydroxyphenylpyruvate dioxygenase *hpd* (PGA1_c07610) showed unexpected high expression levels for the wild-type strain (about 4000-7000) and the Δ262-kb mutant strain (about 800-1100) indicating a major role in TDA biosynthesis and early L-phenylalanine degradation. Overall, *hpd* is one of the highest expressed chromosome genes in the wild-type strain. This enzyme is involved in the degradation of tyrosine and additionally it is proposed to catalyze the reaction of phenylpyruvate to 2-hydroxyphenylacetate in *P. inhibens* DSM 17395 (Drüppel et al. 2014). In the study by Drüppel *et al.* (2014) 2-hydroxyphenylacetate was described as dead-end product because there is no known L-phenylalanine degradation pathway via 2-hydroxyphenylacetate and the compound was detected extracellularly. However, in the described study *P. inhibens* DSM 17395 was adapted to L-phenylalanine as sole carbon source and on proteomic level the 4-hydroxyphenylpyruvate dioxygenase showed the highest fold change of all L-phenylalanine related proteins (Drüppel et al. 2014). Thus, expression of *hpd* is independent of available tyrosine and the high expression levels observed with casamino acids as carbon source might be connected to an active TDA biosynthesis.

Furthermore, the uroporphyrinogen-III-C-methyltransferase CobA (PGA1_c20740) is noticeable because the gene was up-regulated in the wild-type strain compared to the Δ262-kb mutant strain (figure 3.8, table S7). Thole *et al.* (2012) observed an

interruption of the TDA biosynthesis for a transposon mutant strain affecting this methyl transferase.

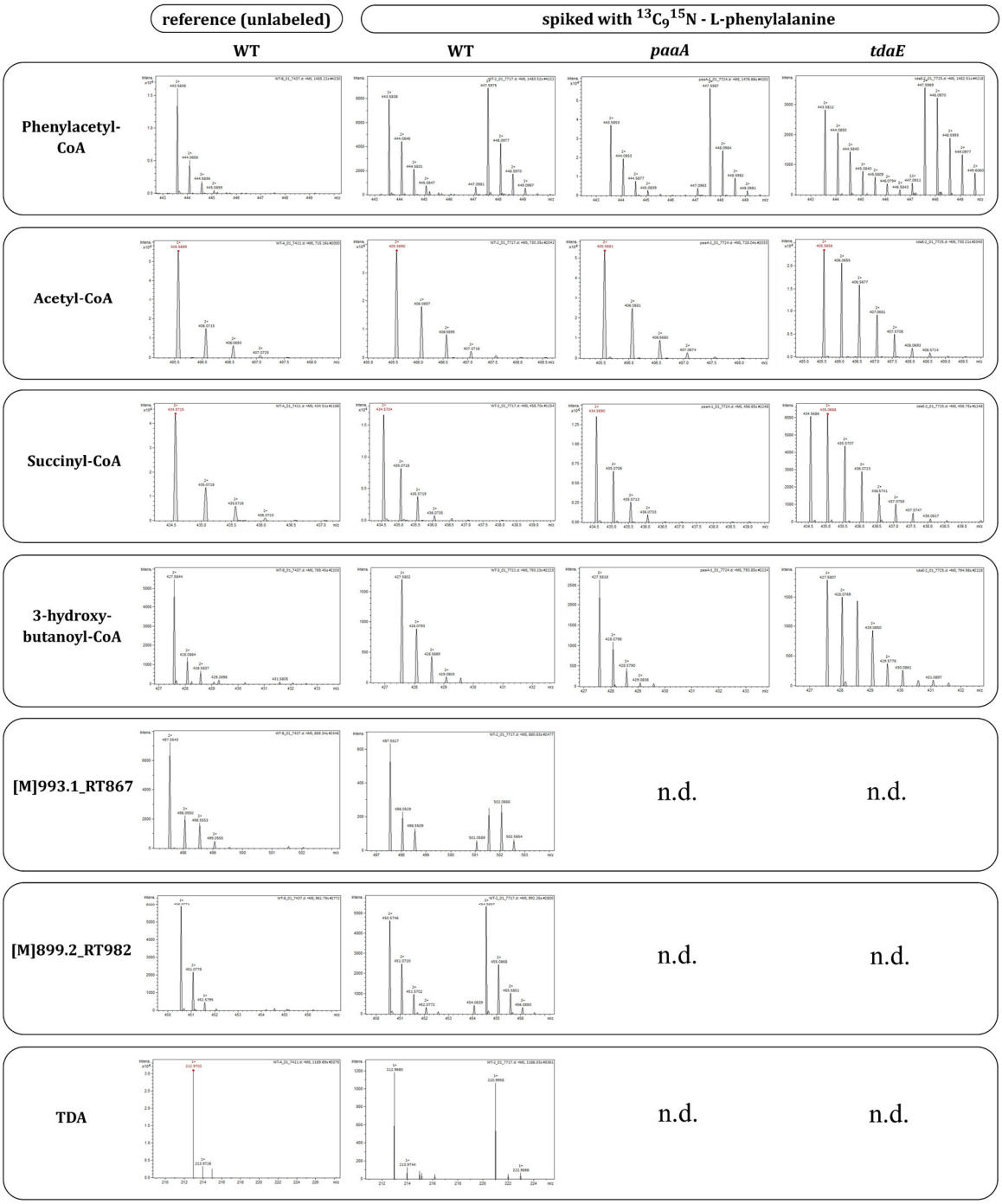

Figure 3.9 Isotope labeling patterns of L-phenylalanine degradation and proposed TDA biosynthesis intermediates. The wild-type, the *paaA* and *tdaE* transposon mutant strains were cultivated with casamino acids supplemented with $^{13}C_9{}^{15}N$-L-phenylalanine. n.d: not detected

These results clarify the necessity of further experiments to understand the uncommon biosynthesis pathway for TDA. Thus, LC-MS-analysis was performed with transposon mutant strains of the *tdaABCDE* gene cluster and of the phenylacetic acid degradation pathway (table 3.5).

Table 3.5 Analyzed transposon mutant strains with corresponding locus tag and proposed enzyme function. Enzyme functions were proposed based on literature, SwissProt and InterPro hits.

Gene	Locus tag	Enzyme function or domains
paaZ_c	PGA1_c26830	Bifunctional protein PaaZ
paaZ_p	PGA1_262p00800	Aldehyde dehydrogenase, Hot-Dog superfamily
paaJ	PGA1_c04090	beta-ketoadipyl-CoA thiolase PaaJ
paaA	PGA1_c04080	1,2-phenylacetyl-CoA epoxidase subunit PaaA
paaD	PGA1_c04050	1,2-phenylacetyl-CoA epoxidase subunit PaaD
paaE	PGA1_c04040	1,2-phenylacetyl-CoA epoxidase subunit PaaE
tdaA	PGA1_262p00980	Transcriptional regulator, LysR family
tdaB	PGA1_262p00970	Thioredoxin-like superfamily, glutathionine S-transferase
tdaC	PGA1_262p00960	*no hit*
tdaE	PGA1_262p00940	acyl-CoA dehydrogenase/oxidase

Based on the previously predicted sum formula, the expression levels and the associated observed differences for the transposon mutant strains a new TDA biosynthesis pathway was suggested (figure 3.10). Similar amounts of TDA were produced in the wild-type and *paaZ_c* transposon mutant strains. TDA production was reduced in the *paaZ_p* and *paaJ* transposon mutant strains showing that both are involved in the TDA biosynthesis. The observation of *paaJ* as involved gene is contrary to the TDA biosynthesis pathway proposed by Brock *et al.* (2012). The ^{13}C-labeled data and the expression levels already showed that phenylalanine degradation via the pathway by Teufel *et al.* (2010) is inactive in the wild-type strain. Three isomeric structures with a molecular mass of 902.1 Da were detected at a retention time of 1338, 1423 and 1563 s. Probably, two of them are oxepin-CoA ([M]901.2_RT1423) and 1,2-epoxyphenylacetyl-CoA ([M]901.2_RT1338). The third one ([M]901.2_RT1563) might be 2-hydroxyphenylacetyl-CoA which would fit to the observed high expression level of *hpd*.

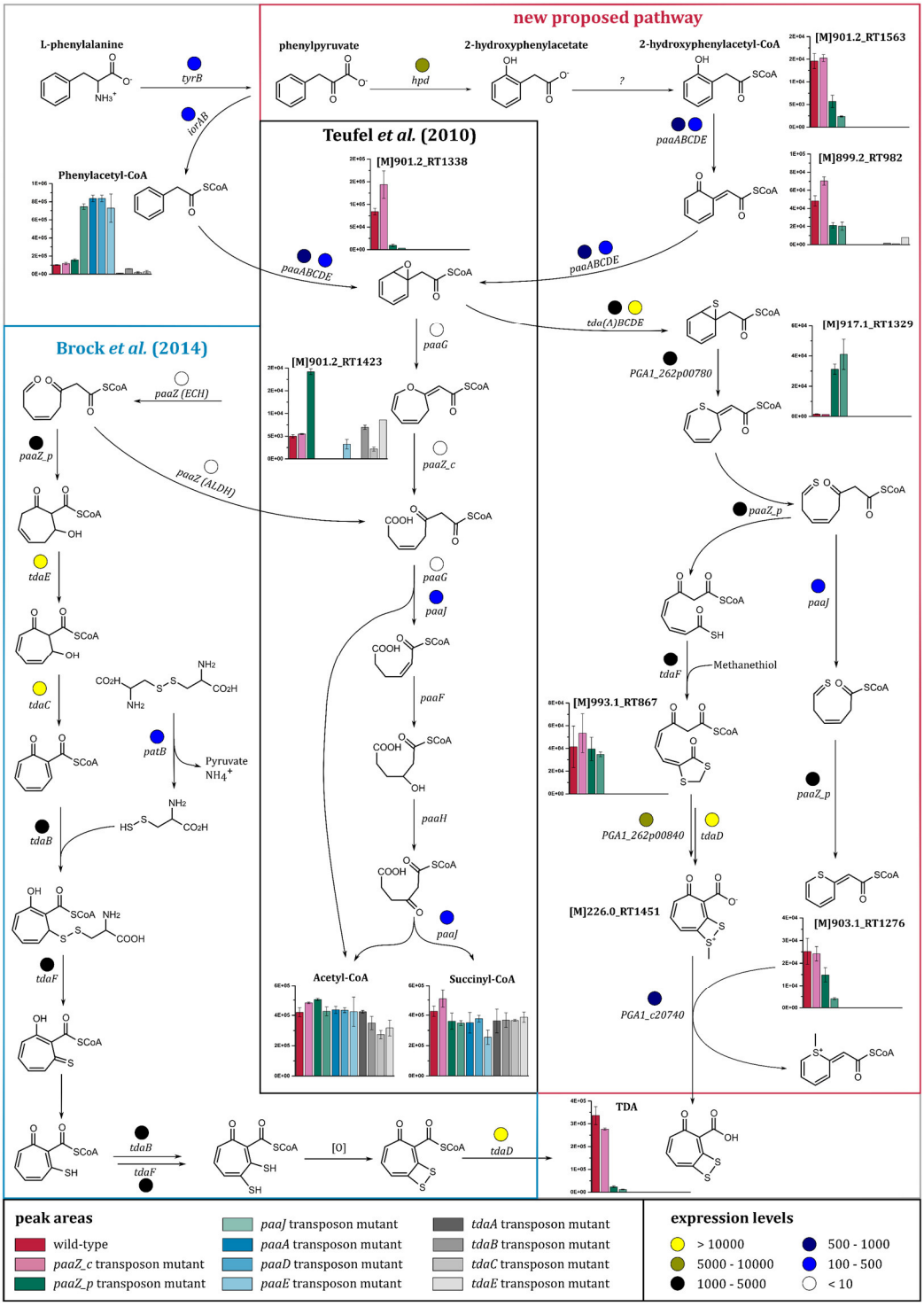

Figure 3.10 Proposed TDA biosynthesis pathway. Shown are the degradation steps of phenylacetyl-CoA by Teufel *et al.* (2010) which were proposed to provide the precursor for TDA biosynthesis by Brock *et al.* (2014). The new proposed biosynthesis pathway is shown with newly detected so far unidentified sulfur-containing compounds with proposed structures based on sum formula predictions. Furthermore, peak areas for different transposon mutant strains are shown for the detectable compounds compared to the wild-type strain. Expression levels at OD_{max} in the wild-type strain are labeled with colored circles. For detailed expression levels see figure 3.8 and table S7.

PaaA, *paaD* and *paaE* were necessary to produce TDA. Thus, 1,2-epoxyphenylacetyl-CoA could be a possible precursor for the first sulfur incorporation step to [M]917.1_RT1329 which might be catalyzed by enzymes of the *tdaABCDE* gene cluster. There is no reliable annotation for these genes and bioinformatic analyses only revealed some domain structures (table 3.5). TdaB might catalyze the transfer of sulfur from a sulfur donor compound to 1,2-epoxyphenylacetyl-CoA. The further steps might be catalyzed by TdaF, PaaZ_p and enzymes coded on two neighbouring genes (PGA1_262p00780 and PGA1_262p00840). [M]917.1_RT1329 was higher abundant in the *paaZ_p* and *paaJ* transposon mutant strains. [M]903.1_RT1276 was less abundant in both strains compared to the other TDA-producing strains. This effect was stronger in the *paaJ* transposon mutant strain and the decreased TDA production seems to be connected to the decreased production of [M]903.1_RT1276 indicating an important role of this observed "degradation" compound. A demethylation step is necessary to obtain TDA and [M]903.1_RT1276 might act as methyl-acceptor.

Overall, the presented data revealed new insights into the TDA biosynthesis pathway of *P. inhibens* DSM 17395 and is the first experimental evidence of sulfur-containing TDA precursors. Contrary to previous proposed TDA biosynthesis pathways the actual data suggest sulfur incorporation prior to cyclization and water elimination. However, further experiments will be necessary to prove the proposed pathway.

3.1.3 Identification of unidentified compounds

One major difference between the wild-type and the Δ262-kb mutant strain was the detection of so far unidentified compounds by GC-EI-MS analysis (figure 3.2 A and C). Three of them (NA714, D200302_2009.31, Unknown#2442.5-pin-mhe_059) were only detectable in the Δ262-kb mutant strain and showed similar EI fragmentation pattern (figure 3.11). EI fragmentation pattern of compound 3 is also found in compound 2 and 1. Furthermore, all ions of compound 2 were found in compound 1. The basic fragmentation pattern involved typical ions for a pyranose (Simoneit et al. 2004; Kleist et al. 2016), glycerate and 3-hydroxybutanoate, the degradation product of the storage compound PHB (table 3.6). Glycerate could be detected at OD_{max} and was 1.6-fold higher abundant (p-value < 0.005) in the Δ262-kb mutant strain

compared to the wild-type strain (table S1) and 3-hydroxybutanoate was 2.3-fold higher (table 3.2).

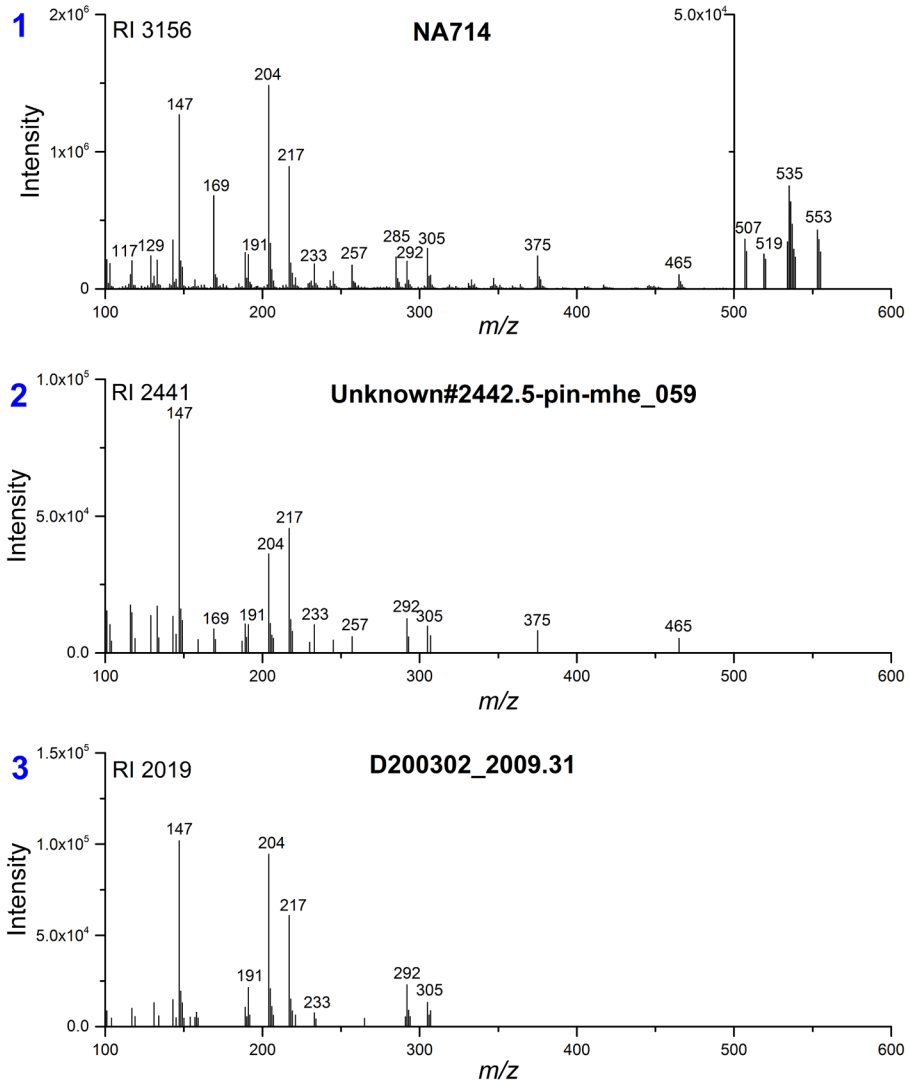

Figure 3.11 EI spectra of unidentified compounds detected in the Δ262-kb mutant strain by GC-MS analysis. Numbers in blue were used in the text for better traceability.

Additionally, in compound 1 and 2 the ions at *m/z* 169 and 375 were characteristic. Fragments at *m/z* 169 and 361 are typically found in compounds with glycosidic bonds as disaccharides (Simoneit *et al.* 2004) or also pyranoses bond to glycerate like 2-*O*-(α-D-glucopyranosyl)-glycerate, an osmoprotectant found in *D. shibae* DFL12 (Kleist *et al.* 2016). Thus, the detected ions at *m/z* 169 and 375 could indicate a glycosidic bond with a structure containing one nitrogen atom which would explain the shift from *m/z* 361 to 375 (table 3.6).

Table 3.6 Observed fragmentation patterns with corresponding structure properties. 1: NA417, 2: Unknown#2442.5-pin-mhe_059, 3: D200302_2009.31, 4: Unknown#2557.6-pin-mhe_067, 5: NA1703.1, 6: Unknown#2260-cgl-sst_001. Italic: only some ions were found in the respective compound. Bold: characteristic ions found in compound 1.

Fragmentation pattern (*m/z*)	Found in	Possible structure properties
147, 191, 204, 217	1 ,2, 3	Pyranose
117, 133, 147, **189**, 217, **292**	1, 2, 3	Glyceric acid 3TMS
169	1, 2, 4	Sugar with glycosidic bond
375	1, 2	Glycosidic bond (361) + nitrogen
117, 147, 191, **233**	1, 2, 3	3-hydroxybutanoate 2TMS
147, 211, 227, 243, **285**, 299, 315	*1*, 5	Glycerol-2-phosphate 4TMS
147, 241, **257**, 299, 329, 357, 387	*1, 2, 4*	Glycerol-3-phosphate 4TMS
128, 147, 156, 174, 200, 317	6	Lysine 4TMS

Three other so far unidentified compounds were detected in both strains (figure 3.12). Compound 4 and 6 were more abundant in the Δ262-kb mutant strain and compound 5 was only detectable in the wild-type strain at OD_{max} (table 3.1 and 3.2). Compound 6 is a lysine containing compound (table 3.6) which is in accordance with higher levels of lysine in the Δ262-kb mutant strain (table 3.2). Furthermore, 2,6-diaminopimelate was lower which could imply a role of compound 6 in the peptidoglycan structure. However, this compound is independent from the other 5 compounds because the typical ions at *m/z* 156 and 174 were not found in any other compound. Compounds 4 and 5 are of peculiar interest because the EI spectra includes parts of the typical fragmentation pattern for glycerol-2-phosphate and glycerol-3-phosphate (table 3.6). Furthermore, the specific ion at *m/z* 257 is found in compound 1 and 2 as well as ion at *m/z* 285 is also present in compound 1. This led to the assumption that addition of compound 4 to compound 3 results in compound 2. Further addition of compound 5 would then end in compound 1, the most abundant so far unidentified metabolite with the highest RI.

Overall, NA714 is supposed to be a nitrogen containing, glycosidic-bonded pyranose-glycerate structure with glycerol and 3-hydroxybutanoate residues.

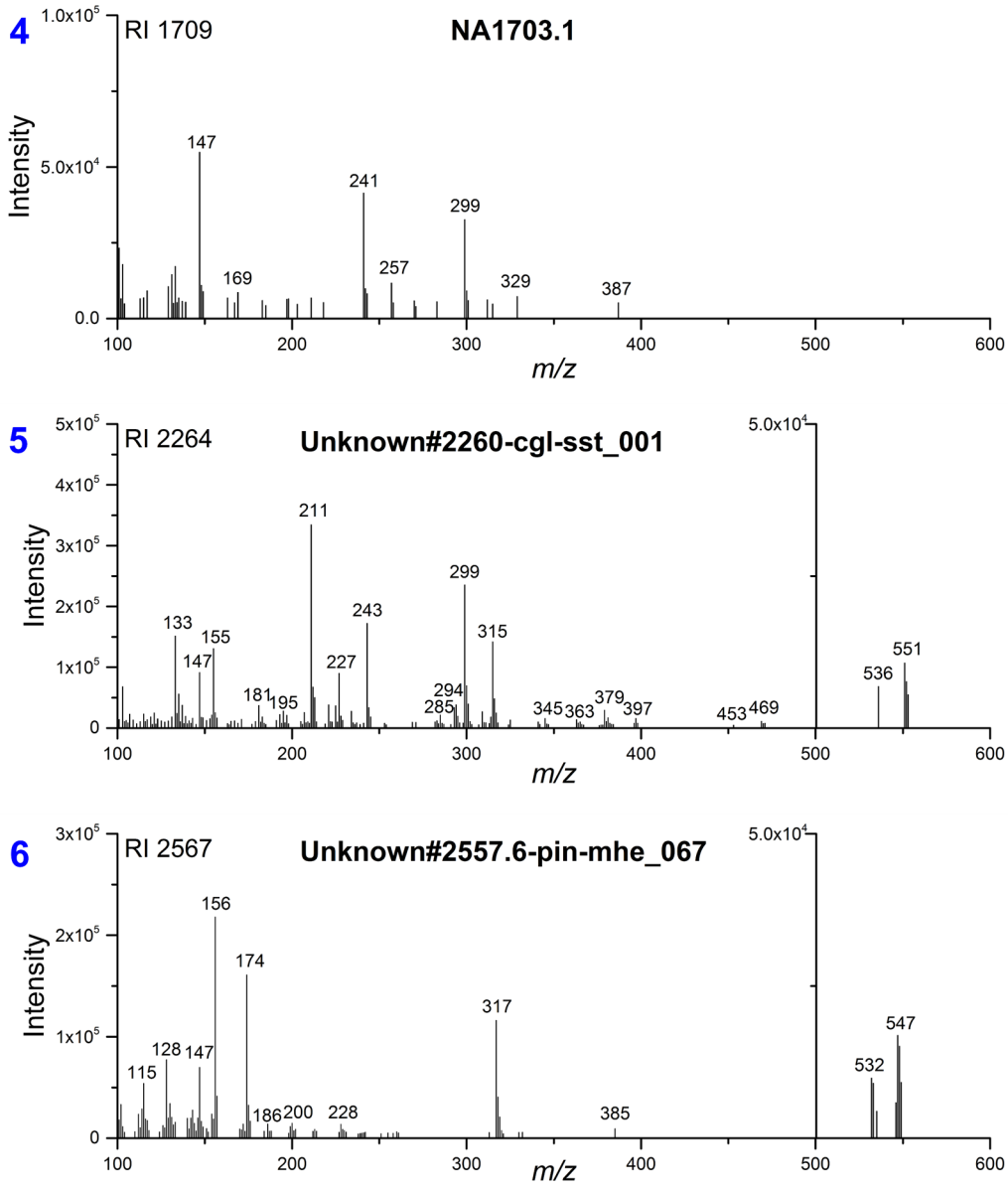

Figure 3.12 EI spectra of unidentified compounds detected in the wild-type and Δ262-kb mutant strain by GC-MS analysis. Numbers in blue were used in the text for better traceability.

The high molecular weight and the low abundance of this compound impeded a successful analysis with GC-APCI-MS. Thus, it was not possible to identify a molecule ion for this compound. However, besides CoA thioesters it is also possible to detect other acidic compounds by the previously used LC-ESI-MS analytics. With this method compounds without a bonded CoA were detected which were accumulating in the Δ262-kb mutant strain at OD_{max} (figure 3.13) indicating a relation to the unidentified compounds detected by GC-EI-MS. ESI is a soft ionization technique generating mass

spectra with a detectable molecule ion which could be used for sum formula predictions due to the high resolution of the qTOF detector.

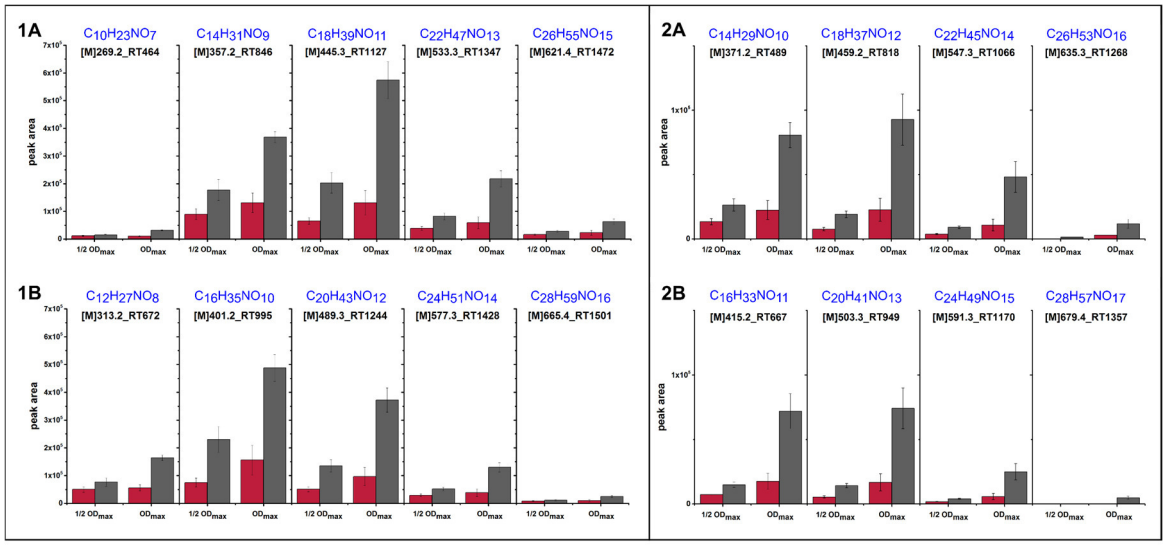

Figure 3.13 Intracellularly detected unidentified compounds at ½ OD_{max} and OD_{max} for the wild-type and Δ262-kb mutant strains by LC-MS-analysis. Shown are peak areas of unidentified polymeric compounds of the wild type (red bars) and the Δ262-kb mutant (grey bars) of four biological replicates with standard errors at ½ OD_{max} and OD_{max} and associated predicted sum formula (table S8). Cultivation and sampling were performed by the working group of Ralf Rabus (ICBM).

Sum formula predictions revealed similar structures for all compounds with iterating units and include a single nitrogen atom (table S8). Detected components could be divided in two groups which differ by one carbonyl group (figure 3.13 and figure 3.14). Furthermore, within a group the residue bound to 3-hydroxybutanoate as iterating units differ by one acetyl residue. Proposed structures for the detected compounds are glucosamine-PHB, N-acetylglucosamine-PHB, glucosaminate-PHB and N-acetylglucosaminate-PHB (figure 3.14). Retention times (RT) were higher for compounds of group 1 when components of the same length are compared indicating that glucosamine and N-acetylglucosamine were present in cyclic form but the ring opened while ionization. 3-hydroxybutanoate as iterating unit is in accordance with the observed higher abundance in the Δ262-kb mutant strain at OD_{max} (table 3.2) and the observed fragmentation patterns in unidentified compounds detected by GC-MS (table 3.6).

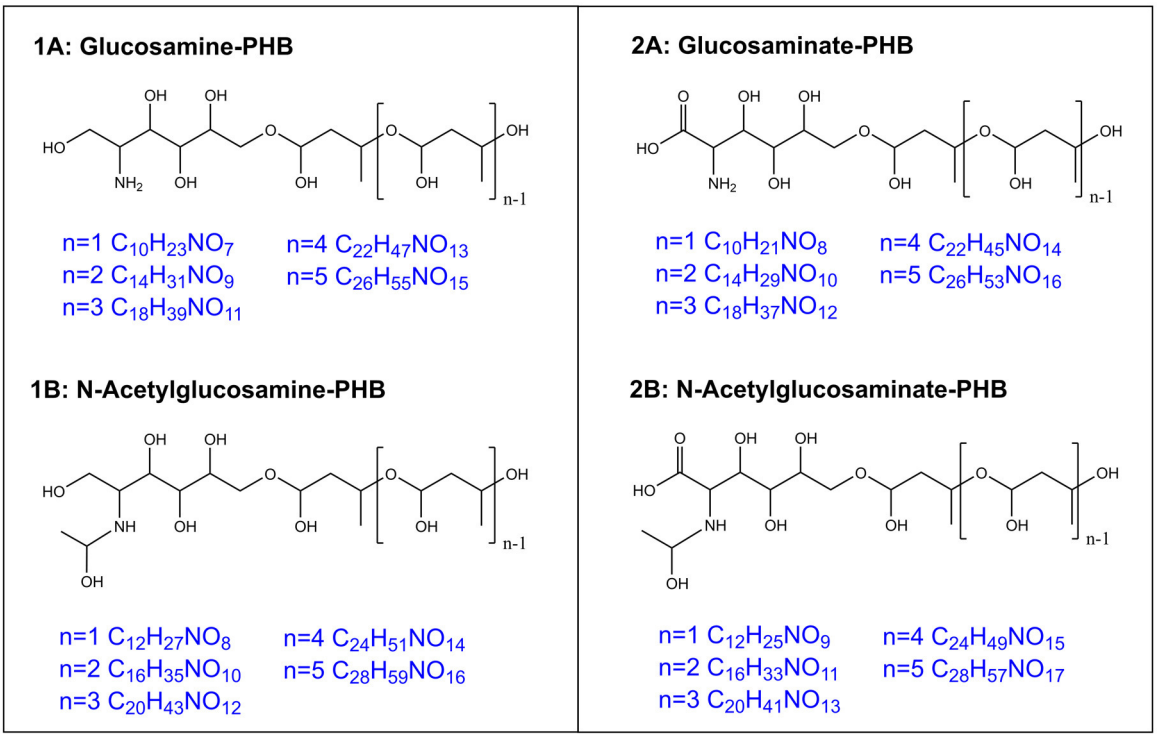

Figure 3.14 Proposed structures for the detected unidentified compounds by LC-MS analysis.

However, the GC-MS analysis revealed also fragmentation patterns indicating glycerate and glycerol involved in the polymeric structures. On transcriptomic level a gene cluster (PGA1_c13580 to PGA1_c13830) which was highly up-regulated in the Δ262-kb mutant strain at OD_{max} could be related to the detected compounds. This cluster is coding for proteins like D-alanine-poly(phosphoribitol) ligase, long-chain-fatty-acid-CoA ligase, long-chain specific acyl-CoA dehydrogenase, phosphopantetheine binding protein, 4'-phosphopantetheinyl transferase-like protein and a monooxygenase. Furthermore, this cluster includes a secretion protein and an ABC transporter ATP-binding protein. Thole *et al.* (2012) already described this gene cluster and assumed an uncommon cell envelope composition as D-alanine-poly(phosphoribitol) ligase is an enzyme known to be involved in the biosynthesis of D-alanyl-lipoteichoic acid, a compound in the cell wall of Gram-positive bacteria (Neuhaus and Baddiley 2003). *Sulfitobacter brevis* KMM 6006, a marine Gram-negative bacterium, produces a teichoic acid containing poly(glycosylribitophosphate) and poly(glycerophosphate) (Gorshkova *et al.* 2007). For the linkage of each unit phosphate is required. Genes coding for phosphate transport proteins (PGA1_c15730 to PGA1_c15800) were up-regulated at OD_{max} in the

Δ262-kb mutant strain. The units forming the basis of the teichoic acid could be similar to the teichoic aicd found in *S. brevis* KMM 6006 with glycerate instead of ribitol. This teichoic acid could be then bound via phosphate to the four detected PHB-bounded amino sugars/sugar acids (figure 3.14), resulting in a lipoteichoic acid (LTA). The PHB residues indicating that the possible LTA is probably not anchored in the membrane as the chain is too polar with the hydroxy groups. Thus, this polymeric structure could have another function than a usual membrane compound. The LTA of *Lactococcus lactis* subsp. *cremoris* SK110 and SK112 consist of glycerol, glucose, rhamnose, alanine, fatty acids and protein (Sijtsma *et al.* 1990). Sijtsma *et al.* (1990) showed that the LTA of the phage-resistant strain SK110 additionally includes galactose which was not detected in the phage-sensitive strain SK112. Furthermore, inactivation of phages by LTAs is dependent on the substitution (Räisänen *et al.* 2007). This is interesting because a gene cluster containing a phage (PGA1_c18210 to PGA1_c18560) is up-regulated in the Δ262-kb mutant strain at OD_{max}. Thus, production of LTA could be a reaction to a starvation triggered phage. The expression of the phage would also explain the rapid die off at OD_{max} observed for the Δ262-kb mutant strain (Trautwein *et al.* 2016).

3.1.4 Refinement of L-lysine catabolism

The metabolome analysis revealed differences in intermediates of lysine catabolism. While the L-lysine degradation via cadaverine was well described by Drüppel *et al.* (2014) nothing is known for a degradation via L-pipecolate in *P. inhibens* DSM 17395 ecxept for the observation of an accumulation of L-pipecolate in the Δ262-kb mutant strain (Reimer *et al.* 2017, Will *et al.* 2017). Thus, further studies were performed with help of bioinformatic approaches and transposon mutant strains to propose a degradation pathway via L-pipecolate. Furthermore, enzymes necessary for growth on L-lysine as sole carbon source were identified.

Degradation via L-pipecolate

The degradation of L-lysine via L-pipecolate is not well-known for bacteria. In *Streptomyces hygroscopicus* the direct conversion of L-lysine to L-pipecolate by a lysine cyclodeaminase (EC 4.3.1.28) is part of the rapamycin gene cluster (Gatto *et al.* 2006). BLASTp analysis revealed PGA1_c16390 as possible gene locus coded for an

enzyme in *P. inhibens* DSM 17395 analogous to *S. hygroscopicus* (table S9, figure 3.15). This gene is annotated as ornithine cyclodeaminase (EC 4.3.1.12). Gatto *et al.* (2006) observed a cyclization of ornithine by the lysine cyclodeaminase of *S. hygroscopicus* but with a reduced rate compared to lysine. Thus, besides ornithine also L-lysine could be a possible substrate of the ornithine cyclodeaminase of *P. inhibens* DSM 17395.

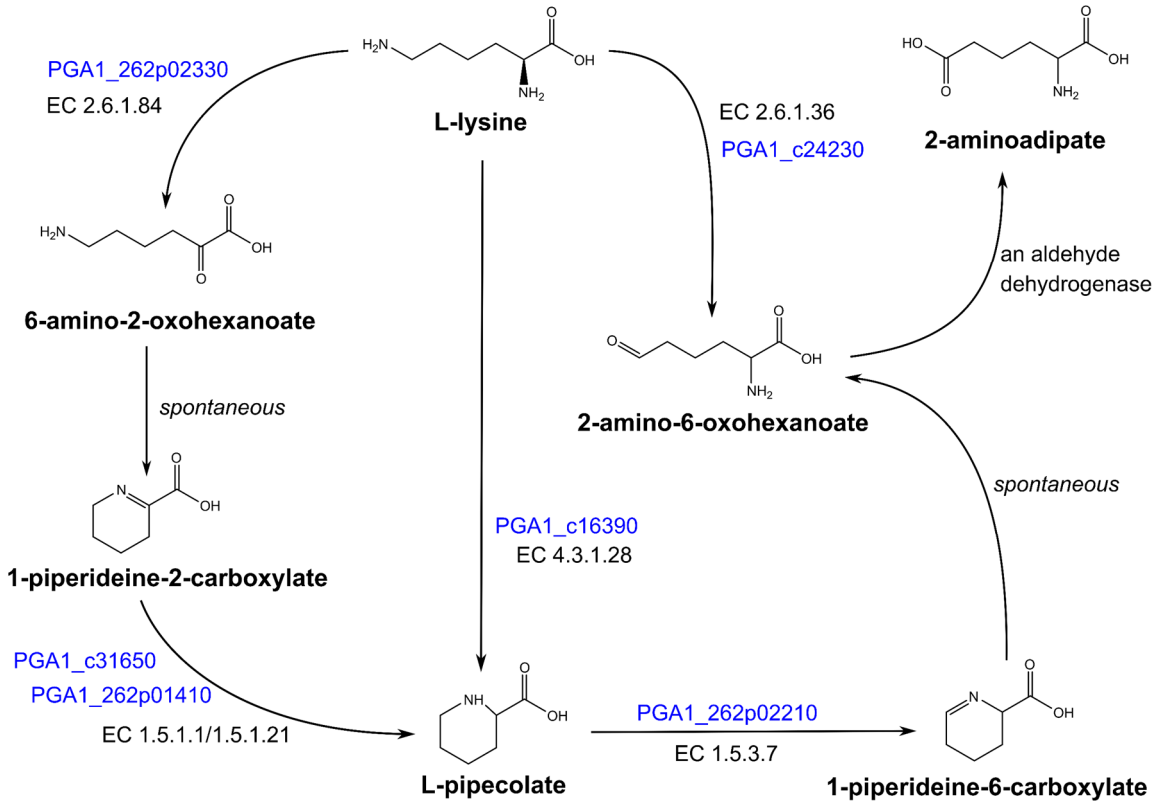

Figure 3.15 Postulated degradation pathways via L-pipecolate to 2-aminoadipate. Possible enzymes involved in the degradation of L-lysine via L-pipecolate were predicted based on bioinformatic analyses (table S9).

The BLASTp analysis provided also a putative Δ1-piperideine-2-carboxylate reductase (1.5.1.21) (*Paracoccus denitrificans* PD1222) as predicted protein function for PGA1_c31650. This enzyme catalyzes the conversion of Δ1-piperideine-2-carboxylate to L-pipecolate and is well described for *Pseudomonas putida* ATCC 12633 and *Pseudomonas syringae* pv. tomato DSM 50315 (Muramatsu *et al.* 2005; Goto *et al.* 2005). Furthermore, the BLASTp analyses revealed PGA1_262p01410 as possible Δ1-piperideine-2-carboxylate reductase. Δ1-piperideine-2-carboxylate is formed by spontaneously cyclization of 6-amino-2-oxohexanoate (Revelles *et al.* 2007). A transamination reaction is necessary to obtain 6-amino-2-oxohexanoate. One

possible enzyme for this reaction is the annotated arginine-pyruvate transaminase (PGA1_262p02330). For *Pseudomonas aeruginosa* PAO1 this enzyme is well characterized, and L-lysine is an alternative substrate to L-arginine resulting in Δ1-piperideine-2-carboxylate as product (Yang and Lu 2007). Thus, besides the direct conversion of L-lysine to L-pipecolate another pathway via Δ1-piperideine-2-carboxylate could be possible (figure 3.15).

For *Pseudomonas putida* KT2440, two enzymes necessary for L-pipecolate degradation were identified (L-pipecolate oxidase AmaA and Δ1-piperideine-6-carboxylate dehydrogenase AmaB). In mutant strains lacking these enzymes L-pipecolate was accumulating (Revelles *et al.* 2005). An accumulation of L-pipecolate was observed for the Δ262-kb mutant strain of *P. inhibens* DSM 17395 (table 3.1 and 3.2) indicating a gene locus on this plasmid coding for an oxidoreductase for the conversion of L-pipecolate to Δ1-piperideine-6-carboxylate. BLASTp analyses revealed PGA1_262p02210 as possible gene locus coding for an oxidoreductase similar to AmaA in *P. putida* (table S9). The pipecolate oxidase (EC 1.5.3.7) is well known for eukaryotic organisms. However, the occurrence of this enzyme in prokaryotic organisms is still new. A genome-wide analysis of lysine catabolism in bacteria revealed genes similar to *amaA* gene in 61 organisms. These organisms belong all to the phylum proteobacteria (Neshich *et al.* 2013). Thus, the transposon mutant Tm2567 of *P. inhibens* DSM 17395 without a functional predicted pipecolate oxidase (PGA1_262p02210) was cultivated on casamino acids and additionally with L-lysine as sole carbon source compared to the Δ262-kb mutant strain and the wild-type strain. An accumulation of L-pipecolate could be observed in the transposon mutant strain for both carbon sources (figure 3.16). The effect is higher if more L-lysine is available (2.1 mM in casamino acids and 15 mM if L-lysine is used as sole carbon source) underlying the assumption that L-pipecolate is a degradation product of L-lysine and that PGA1_262p02210 is coding for an enzyme with pipecolate oxidase function.

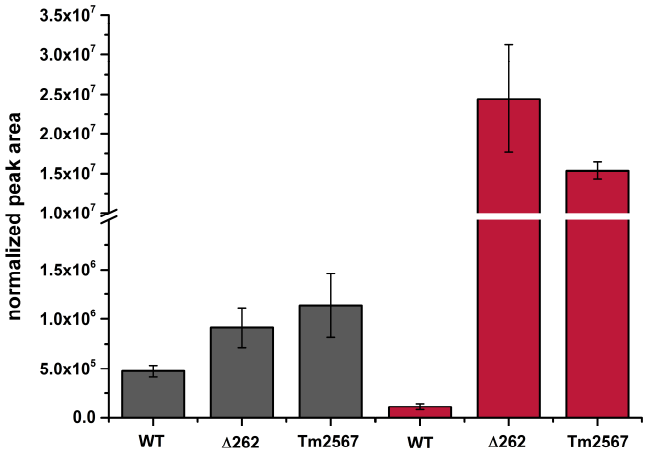

Figure 3.16 Accumulation of L-pipecolate in the Δ262-kb mutant strain and transposon mutant strain Tm2567 (PGA1_262p02210). Shown are normalized peak areas of intracellularly detected L-pipecolate for cultures with casamino acids (grey) and 15 mM L-Lysine as carbon source (red). Cultures with casamino acids were harvested at approximately half-maximal OD and with L-Lysine at maximal OD.

The conversion of Δ1-piperideine-6-carboxylate to 2-amino-6-oxohexanoate is spontaneous followed by a dehydrogenation to 2-aminoadipate (figure 3.15). In *P. putida* this step is catalyzed by the Δ1-piperideine-6-carboxylate dehydrogenase AmaB (Revelles *et al.* 2005). Neshich *et al.* (2013) could identify 177 proteobacteria having a gene coding for a similar enzyme described as α-aminoadipic semialdehyde dehydrogenase (EC 1.2.1.31). No distinct aldehyde dehydrogenase could be identified in *P. inhibens* DSM 17395 for this reaction step. In previous studies of the degradation pathways of amino acids in *P. inhibens* DSM17395 an aldehyde dehydrogenase (PGA1_c33040) was identified in the proteome which was slightly up regulated with L-lysine as carbon source compared to other amino acids (Drüppel *et al.* 2014). However, this aldehyde dehydrogenase could also be only active in the degradation pathway via cadaverine.

Degradation via cadaverine

To analyze whether the degradation pathway via L-pipecolate is a possible alternative pathway, transposon mutant strain of the cadaverine pathway were analyzed. In previous studies by Drüppel *et al.* (2014) the lysine/ornithine decarboxylase (PGA1_c11650) was identified on proteomic level for the first degradation step. Furthermore, PGA1_c33040 was identified as an important aldehyde dehydrogenase involved in L-lysine catabolism. Transposon mutant strains affected those two genes could not be adapted to L-lysine as sole carbon source (figure 3.17 A).

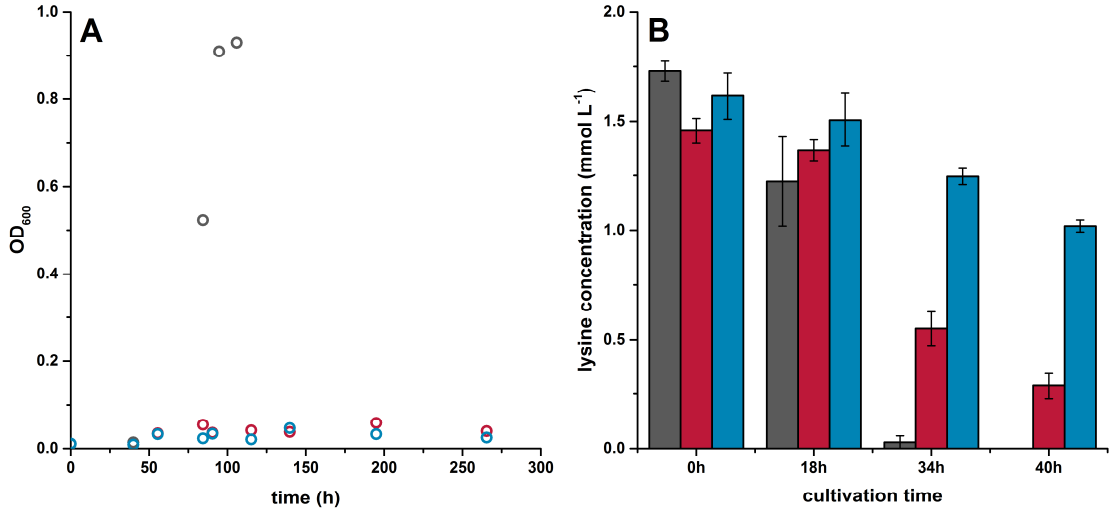

Figure 3.17 Adaptation of the wild-type strain and the transposon mutant strains affecting PGA1_c33040 (aldehyde dehydrogenase) and PGA1_c11650 (lysine/ornithine decarboxylase) to L-lysine as sole carbon source and L-lysine uptake by those strains with casamino acids as carbon source. Shown are OD_{600} values of cultures with 15 mM L-Lysine which were inoculated with growing cells of casamino acids cultures (A) and uptake of L-lysine for cultures growing on casamino acids (B) for the wild-type (grey), the transposon mutant strain Tm1215 (PGA1_c33040, red) and the transposon mutant strain Tm3938 (PGA1_c11650, blue). Adaptation of transposon mutant strains was attempted twice. All cultures already reached OD_{max} at 34 h.

Both mutant strains grew on casamino acids and showed a decreased lysine uptake compared to the wild-type strain (figure 3.17 B). This effect is higher for the transposon mutant strain Tm3938 lacking the lysine/ornithine decarboxylase (PGA1_c11650) which is necessary for the first L-lysine degradation step to cadaverine (Drüppel *et al.* 2014). Metabolome analysis of Tm1215 (PGA1_c33040) revealed a bottleneck in the conversion of cadaverine to 5-aminopentanoate (figure 3.18) which is in accordance with the proposed function of this aldehyde dehydrogenase by Drüppel *et al.* (2014). The detected 5-aminopentanoate and glutarate could be explained by another, less specific aldehyde dehydrogenase. However, this activity is not sufficient for a growth with L-lysine as sole carbon source. Thus, growth with L-lysine is only possible via the cadaverine pathway and both analyzed genes (PGA1_c11650 and PGA1_33040) are essential for this degradation pathway.

Overall, L-pipecolate is not a possible alternative to obtain biomass and L-pipecolate might have another function and it should be more regarded as a biosynthesis of L-

pipecolate. Neshich *et al.* (2013) observed an accumulation of L-pipecolate under high salt concentrations. L-pipecolate as osmoprotectant was already described in 1992 and 1994 (Gouesbet *et al.* 1992; Gouesbet *et al.* 1994). Therefore, the biosynthesis of L-pipecolate by marine bacteria could be an advantage in their natural habitat.

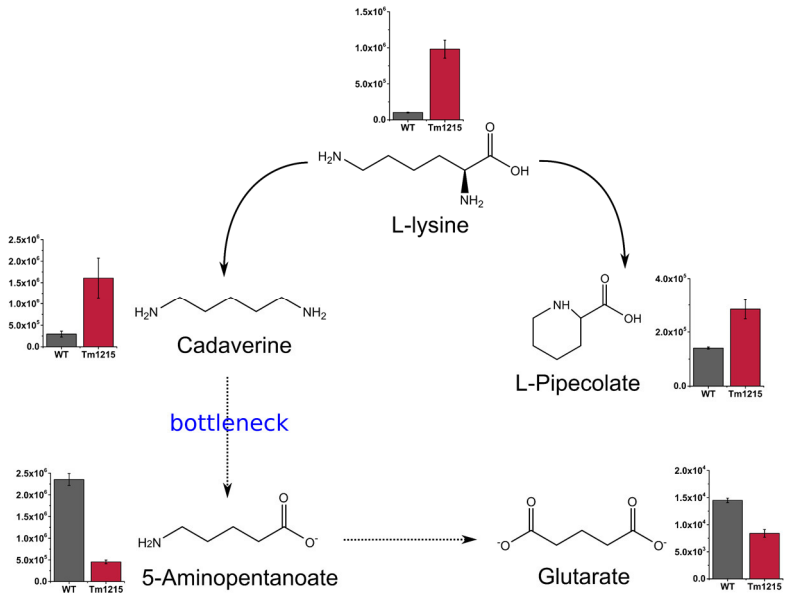

Figure 3.18 Intracellularly detected lysine degradation metabolites for the wild-type and the transposon mutant Tm1215 (PGA1_c33040). Shown are normalized peak areas for the wild-type strain (grey) and the transposon mutant strain Tm1215 (PGA1_c33040, red).

Overall, the main metabolome is similar for the wild-type and the Δ262-kb mutant strain. Different levels of amino acids and corresponding degradation intermediates are mainly attributed to different growth states which are caused by the growth restriction. Small differences in lysine catabolism could be observed which have only minor influence on the growth behavior. Accumulation of sugar-containing compounds in the Δ262-kb mutant strain at OD_{max} could be connected to a possible lipoteichoic acid production which might be a response to a starvation triggered phage. However, these observations could not explain the growth inhibition of the wild-type strain by the 262-kb plasmid. On the contrary, main differences in the metabolome at OD_{max} could be connected to highly different amino acid depletion profiles which are caused by the growth inhibition of the wild-type strain. Thus, the missing TDA production in the Δ262-kb mutant strain has to be considered and will be discussed in the next chapter.

3.2 Growth inhibition by TDA

The antibacterial compound TDA acts by disruption of the proton motive force (Wilson *et al.* 2016). Efforts by Porsby *et al.* (2011) to generate TDA resistant strains were not successful and in their study the TDA-producing *P. inhibens* strain 24-7 was inhibited by TDA. Thus, the influence of the endogenously produced TDA on the growth behavior was analyzed aided by transposon mutant strains missing enzymes of the TDA biosynthesis (TDA-free strains).
Data presented here were published in Will *et al.* (2017).

3.2.1 Growth physiology and metabolome of TDA-free mutant strains

Four transposon mutant strains (*tdaA, tdaB*, *tdaC* and *tdaE*) were cultivated in addition to the wild-type and the Δ262-kb mutant strains with casamino acids as carbon source to analyze if the observed growth inhibition by the 262-kb plasmid is connected to the TDA production. A similar growth behavior could be observed for the transposon mutant strains and the Δ262-kb mutant strain (figure 3.19). In absence of a functional TDA biosynthesis, maximal biomass was reached after 15-20 h while the wild-type strain entered the stationary growth phase after 30 h. Besides a 2 h longer lag phase the transposon mutant strains reached 10% lower CDW_{max} and $Y_{X/C}$ compared to the Δ262-kb mutant strain (figure 3.19). These minor differences might be attributed to the necessary replication of the plasmid and production of an exopolysaccharide with encoding genes on the 262-kb plasmid and sequence similarities to the succinoglycan biosynthesis of *Rhizobium meliloti* 1021 (Reuber, Walker 1993) (table S10). Furthermore, the TDA-free mutant strains showed the same amino acid depletion as the Δ262-kb mutant strain (table S12). The wild-type strain reached only 50% of the CDW_{max} and 60% of the biomass yield $Y_{X/C}$ compared to the Δ262-kb mutant strain. Thus, only minor effects can be attributed to plasmid carriage and exopolysaccharide production and the major growth restriction effect described in chapter 3.1.1 and 3.1.2 is connected to the TDA biosynthesis.

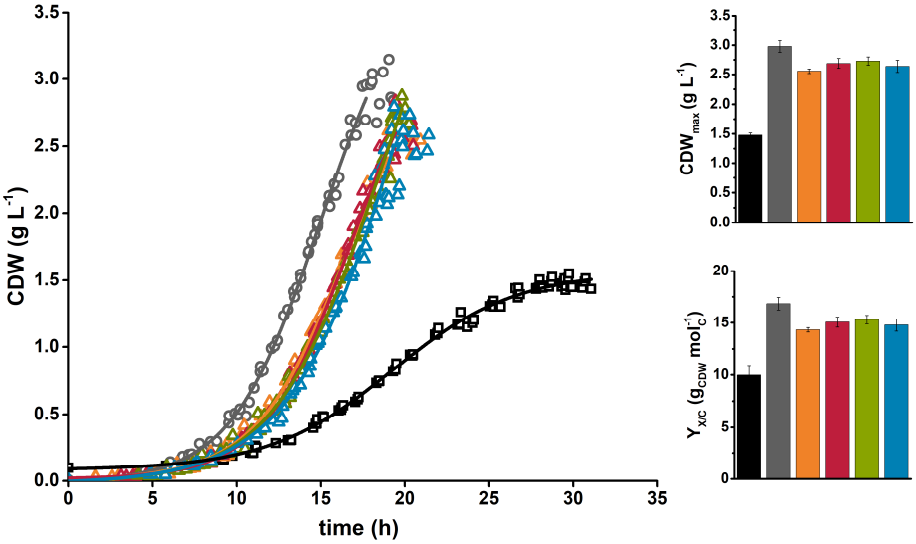

Figure 3.19 Growth characteristic of the wild-type strain, Δ262-kb mutant strain and transposon mutant strains (*tdaA*, *tdaB*, *tdaC* and *tdaE*) on casamino acids. Shown are cell dry weights (CDW) over time for the wild-type strain (black squares), Δ262-kb mutant strain (grey circles), *tdaA* (orange triangles), *tdaB* (red triangles), *tdaC* (green triangles) and *tdaE* (blue triangles) transposon mutant strain with corresponding CDW_{max} and $Y_{X/C}$. Lag phases were corrected. Data were published in Will et al. (2017).

No conspicuous metabolites, which would explain the growth restriction, could be identified by metabolome analysis of the *tdaE* transposon mutant strain in addition to the Δ262-kb mutant and wild-type strains (which were already analyzed in chapter 3.1). As previously discussed, the wild-type strain shows higher levels of amino acids and their degradation intermediates (valine, tyrosine, isoleucine, leucine, 2-isopropylmalate), especially from the branched chain amino acids (figure 3.20 A). These differences are mainly attributed to the different amino acid availability (table S13). This effect is also observed with higher amounts of valine, isoleucine and 3-aminoisobutanoate (side product of valine degradation) in the Δ262-kb mutant strain. The differences in lysine degradation (discussed in chapter 3.1.2 and 3.1.4) were only observed when the complete 262-kb plasmid was missing (figure 3.20 B) reinforcing the assumption that the changes in lysine degradation are not responsible for the growth restriction. The unidentified compound D2003002 described in chapter 3.1.3 was only detectable in the Δ262-kb mutant strain. However, the intensity was low and it could not be excluded that this compound is also present in the *tdaE* transposon mutant strain but below the detection limit.

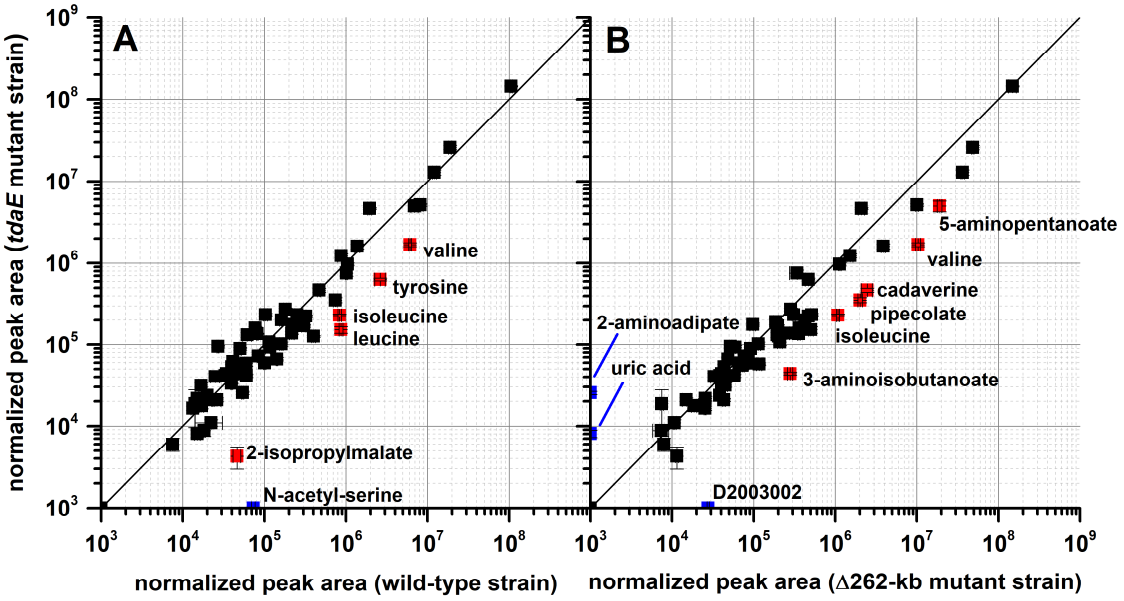

Figure 3.20 Metabolome analysis dependent on TDA production. Shown are normalized peak areas of intracellularly detected metabolites by GC-MS analysis in the *tdaE* transposon mutant strain compared to the wild-type strain (A) and the Δ262-kb mutant strain (B) at ½ OD_{max}. Peak areas are listed in table S11. Data were published in Will et al. (2017).

The only noticeable difference between the wild-type and the TDA-free mutant strains is N-acetyl-serine which was only found in the wild-type strain (figure 3.20 A). In the previous analysis, homoserine was only detectable in the wild-type strain at OD_{max} (figure 3.2 C). Both metabolites might be connected to a production of N-acyl homoserine lactones (AHLs). These quorum sensing molecules were shown to induce TDA biosynthesis in *P. inhibens* DSM 17395 (Berger *et al.* 2011).

3.2.2 Medium exchange between wild-type and TDA-free mutant strains

A medium exchange experiment was performed in order to analyze whether costs for the TDA biosynthesis itself or the presence of TDA and consequently the antibacterial effect is crucial for the observed growth restriction. TDA-free mutant strains showed a drastic growth inhibition effect after transferring the cells into the sterile filtered, TDA containing medium of the wild-type strain (table 3.7). In presence of TDA, linear growth rates decreased about 68% (Δ262-kb) or 58% (*tdaE*) to approximately 0.15 g $L^{-1}h^{-1}$. Additionally, a control experiment with a medium exchange between the Δ262-kb mutant and the *tdaE* mutant strains was performed to exclude growth inhibition effects due to the exchange procedure. Linear growth rates remained

similar for both strains underlying the assumption that the growth inhibition effect is directly connected to the presence of TDA (table 3.7). The growth rate of the wild-type strain increased about 55% to an average of 0.17 $g\,L^{-1}h^{-1}$ with "TDA-free medium". This is similar to the growth rate of the TDA-free mutant strains with TDA-containing medium. As previously shown, TDA production per g_{CDW} is similar at different growth phases (chapter 3.1.2, figure 3.7) assuming half-maximal TDA concentration at the time point of medium exchange. Thus, the presence of a half-maximal TDA concentration led to the same growth inhibition effect as TDA production by the wild-type cells itself in a "TDA-free medium". This means that growing cells are directly affected by the freshly produced TDA and, due to accumulation in the medium, growth inhibition is increasing leading to decreasing growth rates in the wild-type strain until reaching maximal TDA tolerance at CDW_{max}.

Table 3.7 Linear growth rates ($g\,L^{-1}h^{-1}$) for the medium exchange. Shown are linear growth rates of the reference and the exchanged culture for the wild-type, the Δ262-kb mutant and the *tdaE* mutant strains, respectively. Growth rates were determined after the exchange procedure between the wild-type and TDA-free mutant strains. Furthermore, growth rates for the control experiment (exchange between the TDA-free mutant strains) were determined. For detailed cultivation procedure see chapter 2.4.2. Complete growth curves are shown in figure S1. Data were published in Will et al. (2017).

Condition	WT vs. Δ262	WT vs. *tdaE*	Δ262 vs. *tdaE*
WT reference	0.09 ± 0.01	0.06 ± 0.01	-
WT exchange	0.20 ± 0.02	0.14 ± 0.02	-
Δ262 reference	0.47 ± 0.05	-	0.43 ± 0.01
Δ262 exchange	0.15 ± 0.05	-	0.53 ± 0.06
tdaE reference	-	0.33 ± 0.01	0.34 ± 0.03
tdaE exchange	-	0.14 ± 0.02	0.30 ± 0.01

Growth of the *tdaE* transposon mutant strain was tested with TDA containing culture supernatant of the stationary growth phase to analyze the hypothesis that growth is not possible with the maximal reached TDA concentration. Casamino acid containing medium was supplemented with different dilutions of culture supernatant of the wild-type strain. Medium containing 20% and 40% of the wild-type supernatant did not influence the growth behavior compared to the reference (figure 3.21 A). Cultures with more TDA in the medium showed a prolonged lag phase and variable growth of the three biological replicates. No growth was observable after transfer of these cells into medium containing wild-type culture supernatant from a later time point (late

stationary growth phase) to increase TDA concentration (figure 3.21 B). The reference (TDA-free supernatant) showed normal growth behavior. Porsby *et al.* (2011) explained the inhibition effect of *P. inhibens* strain 24-7 by a not yet active TDA production when cells were tested. However, *P. inhibens* DSM 17395 wild-type cells from a fresh TDA-producing preculture were unable to grow in the TDA containing supernatant medium (figure 3.21 B), indicating that this effect is independent from a TDA production by the strain itself. An adaptation to TDA by selecting and transfer of more tolerant cells was not possible. Thus, the unsuccessful attempts by Porsby *et al.* (2011) to generate TDA tolerant or resistant strains were also transferable to *P. inhibens* DSM17398 as a TDA-producing strain.

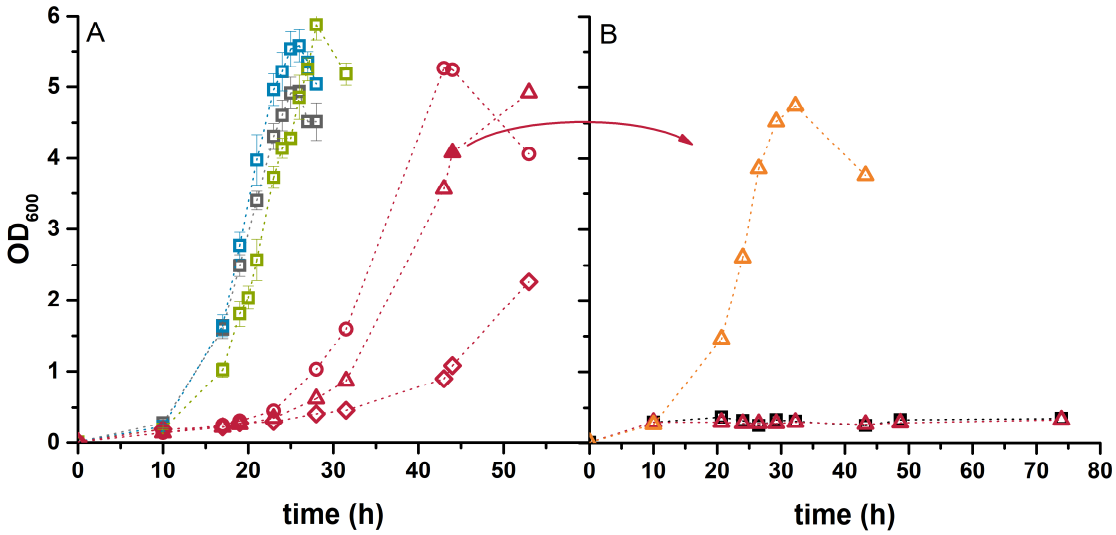

Figure 3.21 Analysis of TDA tolerance. (A) Shown are cultivations of the *tdaE* transposon mutant strain with casamino acid medium containing different dilutions of supernatant from wild-type cultivations (OD_{max}). Supernatant was diluted with salt water medium to obtain final TDA concentration of 80% (red), 40% (green), 20% (blue) and 0% (grey) of the initial concentration of the wild-type at OD_{max}. (B) Supposed TDA tolerant cells (closed red triangle) were transferred into fresh casamino acids medium with 80% of wild-type supernatant (red) and 80% of the *tdaE* transposon mutant supernatant (orange). Furthermore, 80% of the wild-type supernatant medium was inoculated with the wild-type strain from fresh precultures (black).

Wilson *et al.* (2016) identified possible resistance genes located on the 262-kb plasmid in *P. inhibens* DSM 17395. However, no experimental evidence for a resistance mechanism is given so far. The presented data clearly show an inhibition effect by TDA under shaken culture conditions. Furthermore, the wild-type strain is not limited by carbon but enters stationary growth phase because maximal tolerable

TDA concentration is reached indicating insufficient energy supply by respiration due to the disruption of the proton gradient.

3.2.3 TDA dependent respiratory activity

In chapter 3.1.2 similar intracellular amounts of TDA per g_{CDW} were detected at ½ OD_{max} and at OD_{max}. Here, TDA concentration in the supernatant was relatively determined by measurement of absorption at 302 nm (free TDA) and 398 nm (TDA-iron complex). TDA concentration increased in the supernatant of the wild-type strain (figure 3.22). Both, TDA-iron complex and free TDA are correlated with the biomass but increase further when entering stationary growth phase indicating TDA production without a coupled biomass production at CDW_{max}. Thus, the respiratory metabolism is probably still active, but carbon is completely turned into TDA and CO_2.

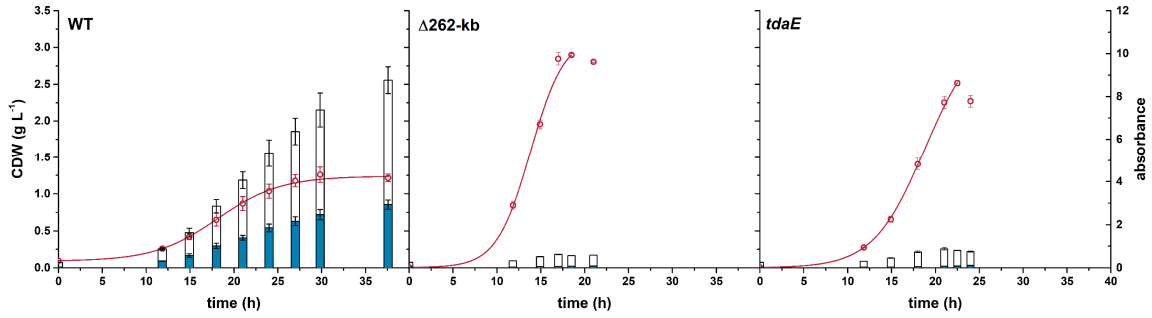

Figure 3.22 Relative TDA concentration for cultivations with casamino acids. Shown are growth curves (red) and absorption measured in the culture supernatants at 302 nm (white bars, TDA) and 398 nm (blue bars, TDA-iron complex) for the wild-type, the Δ262-kb mutant strain and the *tdaE* transposon mutant strain. Data were published in Will et al. (2017).

To analyze the respiratory activity dependent on TDA production, dissolved oxygen (DO) was measured online in Erlenmeyer flasks cultivations to calculate oxygen uptake rates (figure S2, table S14). Specific oxygen uptake rates q_{O_2} of approximately 11.5 $mmol_{O_2} g_{CDW}^{-1} h^{-1}$ were similar and constant for all strains over the complete culture time (figure 3.23). For TDA-free mutant strains growth was mainly linear while the wild-type strain only showed a short linear growth around ½ OD_{max}. Thus, μ is decreasing over time for all strains with corresponding increasing oxygen consumption per g_{CDW} due to a constant q_{O2}. For the wild-type strain μ is decreasing to about 20% compared to ½ CDW_{max} while the TDA-free mutant strains only drop to about 50% of their μ at ½ CDW_{max}.

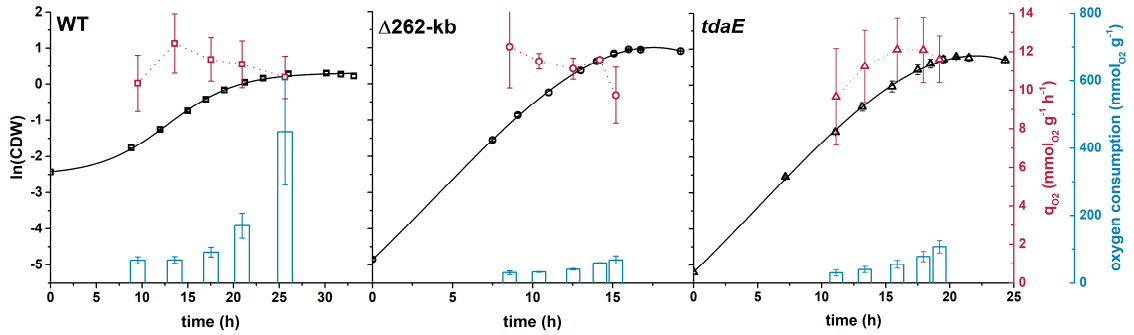

Figure 3.23 Oxygen consumption dependent on TDA presence. Shown are determined specific oxygen uptake rates q_{O2} and absolute oxygen consumption at different time points with corresponding logarithmized CDW. For detailed values see table S14.

The absolute oxygen consumption at ½ OD_{max} were similar to those determined in process-controlled bioreactors (Trautwein *et al.* 2016). The overall oxygen consumption per g_{CDW} is increasing with accumulation of TDA because the respiratory activity remains constant. The presence of TDA led to lower ATP yield due to the disruption of the proton gradient resulting in a less active ATP synthase. Thus, *P. inhibens* DSM 17395 is not able to increase respiratory activity to fully counteract the antibacterial effect of TDA.

Taken together, the observed growth restriction of *P. inhibens* DSM 17395 by the 262-kb plasmid is attributed to the disruption of the proton motive force by its own produced antibacterial compound TDA. This effect was observed for shaken cultures in Erlenmeyer flasks as well as for process-controlled bioreactor cultivations with 1% casamino acid containing defined salt water medium. Thus, the wild-type strain is not producing maximal possible biomass under the given conditions. Cultivations with single amino acids will be discussed in the following supported by simulations with the reconstructed metabolic model *i*Pin571 to analyze energetic efficiency dependent on substrate and TDA production.

3.3 Metabolic model-based analyses of the TDA dependent growth restriction

P. inhibens DSM 17395 was previously analyzed by Drüppel *et al.* (2014) with respect to reconstruction of degradation pathways for nine single amino acids. Growth physiology and morphology differed dependent on the amino acid. Further studies combining experimental data with metabolic model-based flux predictions were performed in order to analyze whether these differences are based on the inhibition effect by TDA or due to different growth efficiency (determined as biomass yield $Y_{X/C}$). Furthermore, in the study by Drüppel *et al.* (2014) cells were adapted to each amino acid by five consecutive transfers. The influence of the adaptation process on the growth behavior was included in the following analyses.

3.3.1 The metabolic model *i*Pin571

The metabolic model *i*Pin571 consists of 486 genes, 571 metabolic reactions (13 not sequenced based, 7 spontaneous), 17 biomass reactions, 35 transport reactions, 22 exchange reactions and 564 metabolites. The model was analyzed for essential, non-variable and variable reactions. Optimal FVAs were performed with glucose and casamino acids as theoretical carbon sources (Table 3.8). 53% (glucose) or 58% (casamino acids) of the reactions were identified as essential. 36 of the variable reactions were independent from the scenario. 4 variable reactions (threonine and proline biosynthesis) could be identified in the glucose scenario which had a flux of 0 mmol $g_{CDW}^{-1}h^{-1}$with casamino acids as substrate. 22 of the variable reactions were specific for the casamino acid scenario. These are mainly reactions of the citric acid cycle, gluconeogenesis and amino acid degradation steps via CoA intermediates.

Table 3.8 Essential, non-variable and variable reactions for glucose and casamino acids. Theoretical scenarios with glucose or casamino acids as carbon source were used for optimal FVA prediction; flux in mmol $g_{CDW}^{-1}h^{-1}$.

	Glucose		**Casamino acids**	
	number	%	number	%
Essential (Flux ≠ 0)	368	53%	403	58%
Non-variable	652	94%	634	92%
Non-variable (Flux of 0 possible)	298	43%	256	37%
Variable	40	6%	58	8%
Variable (Flux of 0 possible)	25	4%	26	4%

P. inhibens DSM 17395 is able to grow with a variety of different carbon sources. The metabolic model *i*Pin571 contains degradation pathways and transporter for 32 of them.

3.3.2 Theoretical analyses of energetic efficiency of different carbon sources

The 32 implemented carbon sources were analyzed for their energetic efficiency. *In silico* predictions of the theoretical maximal ATP yield without any biomass production showed a range from 2.8 $mol_{ATP}\ mol_C^{-1}$ (L-aspartate, L-asparagine, L-methionine) up to 4.3 $mol_{ATP}\ mol_C^{-1}$ (L-isoleucine, L-lysine, mannitol, 4-aminobutanoate, butanoate) (figure 3.24). Furthermore, the consumed oxygen was calculated and for sugars, L-alanine, L-threonine and acetate exactly 1 mol O_2 was consumed per 1 mol carbon. The degradation of the aromatic amino acids L-tryptophan, L-tyrosine and L-phenylalanine involve dioxygenase catalyzed reaction steps explaining the higher oxygen consumption observed for these three amino acids. Except for these carbon sources, a tendency of a higher respiratory activity for higher ATP yields is observable.

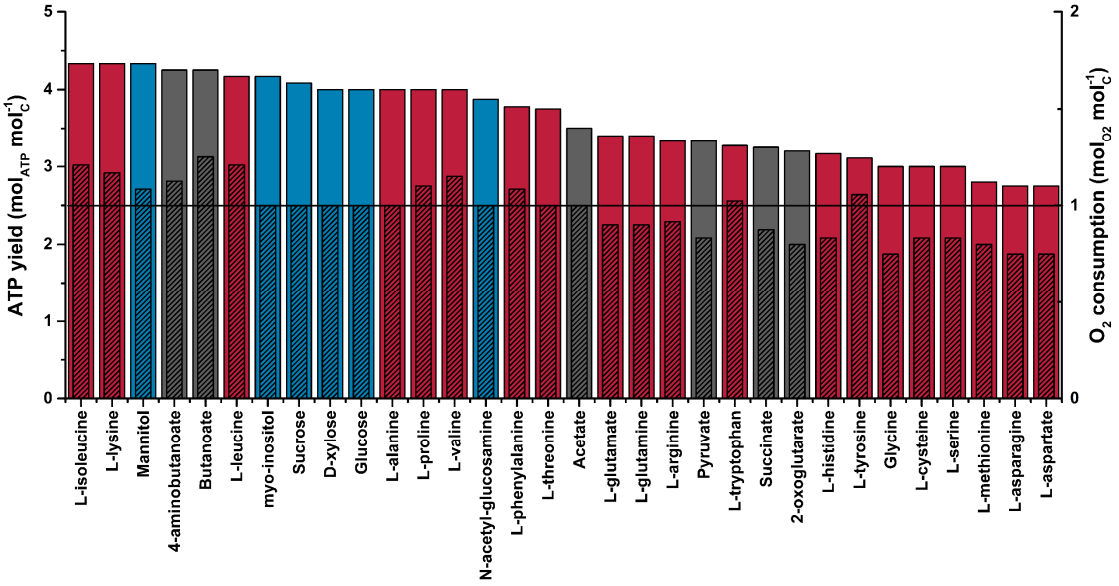

Figure 3.24 *In silico* predicted energetic efficiency for 32 carbon sources. Shown are theoretical maximal possible ATP yield (colored bars) and corresponding oxygen consumption (striped bars) without biomass production. Both values were referred to 1 mol carbon for better comparability. Sugar and sugar alcohols are marked in blue, amino acids in red and other short chain carboxylic acids in grey.

The branched chain amino acids (L-valine, L-leucine and L-isoleucine) belong to the six amino acids with the highest possible ATP yield but are not preferred by *P. inhibens* DSM 17395 with casamino acids as carbon source (chapter 3.1.2) (Zech *et al.* 2013b). In previous studies by Drüppel *et al.* (2014) growth with the branched chain amino acids as single carbon source was slower compared to e.g. L-threonine or succinate. These differences could indicate less efficient transporter for the branched chain amino acids, differences in maintenance energy or biomass composition. Furthermore, TDA production might be dependent on the respective carbon source and should be considered for comparison of theoretical and actual energetic efficiency.

3.3.3 Growth characteristics with single amino acids as carbon source

P. inhibens DSM 17395 was adapted by two consecutive transfers to each amino acid (L-alanine, L-threonine, L-phenylalanine, L-lysine or L-leucine) for determination of growth characteristics. Growth was similar for L-alanine and L-threonine with a longer lag phase observed for L-threonine (figure 3.25). The biomass yields $Y_{X/C}$ of both substrates were only about 1-2 $g_{CDW}\ mol_C^{-1}$ lower compared to those determined in chapter 3.2.1 for the wild-type strain with casamino acids as carbon source ($10 \pm 0.9\ g_{CDW}\ mol_C^{-1}$). The similarity between L-alanine and L-threonine is in accordance with the similar possible ATP yields (figure 3.24). Cultures with L-phenylalanine showed slightly decreased CDW_{max} and biomass yield $Y_{X/C}$. The highest growth efficiency under the given conditions was observed with L-leucine and the lowest with L-lysine as carbon source. The low growth efficiency observed for L-lysine is contrary to the predicted possible ATP yield which was similar to L-leucine. Thus, the low growth efficiency with L-lysine might be connected to the in chapter 3.1.4 described pipecolate production which is probably not catabolized for energy and biomass generation.

Cultures with L-leucine as carbon source showed only a weak yellow-brownish color (TDA-iron complex) in the late stage of growth while all other cultures already produced TDA at an early stage of growth. Thus, the lower biomass yield compared to L-leucine might be connected to the TDA production. However, it is not distinct if less carbon is available for biomass production due to the costs for TDA biosynthesis

and/or due to the inhibitory effect by TDA because the available carbon source was completely depleted.

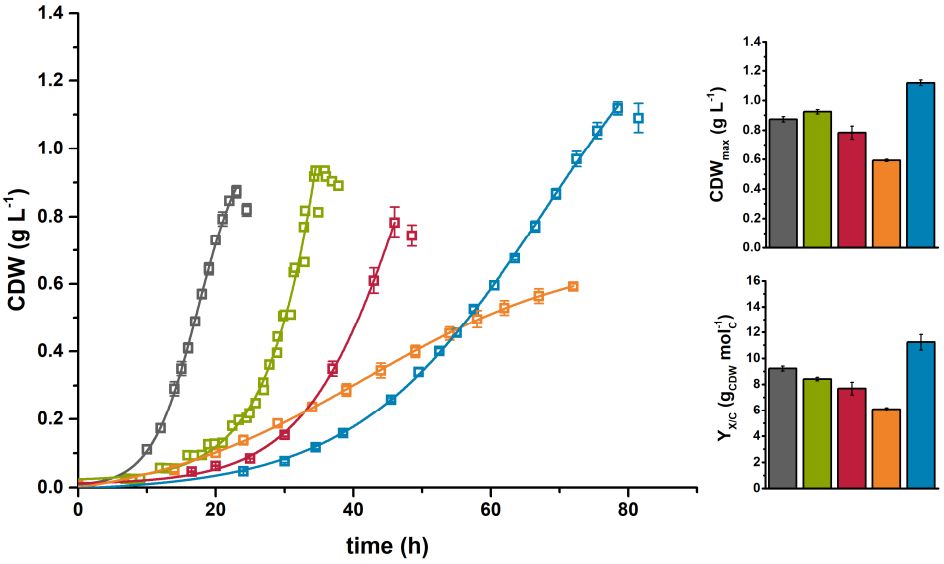

Figure 3.25 Growth characteristic of the wild-type strain adapted to single amino acids. Shown are CDW over time and corresponding CDW_{max} and $Y_{X/C}$ for the wild-type strain with L-alanine (grey), L-threonine (green), L-phenylalanine(red), L-lysine (orange) and L-leucine (blue) as sole carbon source. Lag phases were corrected for L-threonine.

Thus, L-phenylalanine as the TDA-precursor, L-alanine as an amino acid with immediate access to the central carbon metabolism and L-leucine as an amino acid with a more complex degradation pathway, slower growth and less TDA production were chosen for further experiments with TDA-free mutant strains. To exclude growth differences due to the adaptation process all cultivations were performed with only one preculture in the respective single amino acid. Without a functional TDA biosynthesis growth efficiency with L-alanine and L-leucine was similar to casamino acids (figure 3.26). Furthermore, with L-phenylalanine $Y_{X/C}$ were slightly decreased compared to L-alanine and L-leucine for both TDA-free mutant strains. This could be explained by the less energetic efficiency determined by the maximal possible ATP yield (figure 3.24). The wild-type strain only reached about 55% (L-alanine and L-leucine) or 30% (L-phenylalanine) of the $Y_{X/C}$ of the TDA-free mutant strains. Only 50% of the $Y_{X/C}$ of the adapted L-phenylalanine cultures were reached without adaptation. The observed drawback in growth efficiency due to TDA production was analyzed in the context of energy requirements and carbon flux aided by *in silico* analyses with the metabolic model *i*Pin571.

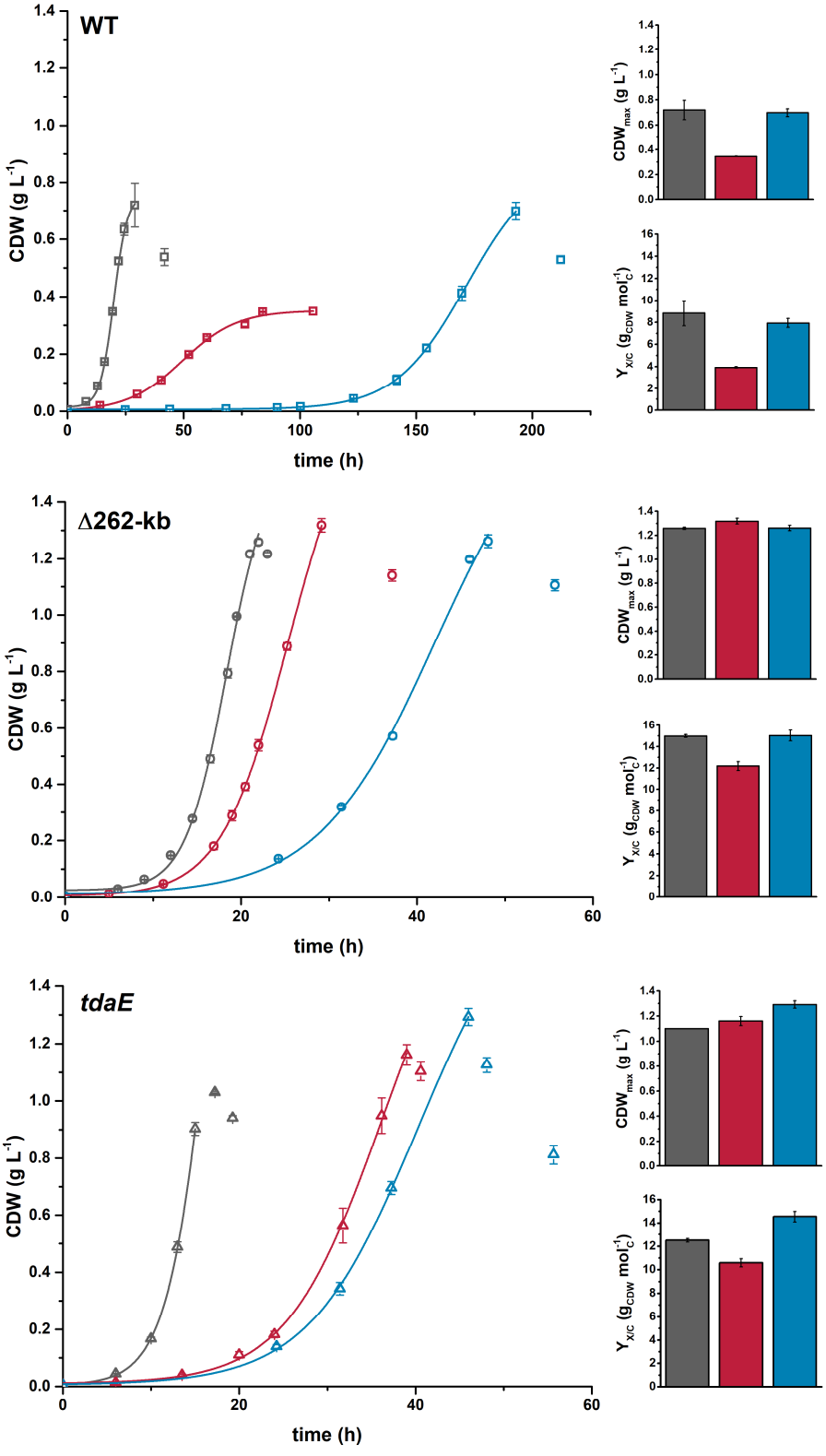

Figure 3.26 Growth characteristics of the wild-type, the Δ262-kb and *tdaE* mutant strains with single amino acids. Shown are cell dry weights (CDW) over time and corresponding CDW_{max} and $Y_{X/C}$ with L-alanine (grey), L-phenylalanine(red) and L-leucine (blue) as sole carbon source. Cells were not adapted to the amino acids.

3.3.4 Biomass composition

In silico analyses of growth efficiency based on biomass production require reliable data for the biomass composition. Thus, experimental determination for the biomass composition was conducted as accurately as possible with the available analytics (figure 3.27). It was possible to determine DNA, RNA, lipids, protein and PHB content. Furthermore, the content of peptidoglycan was estimated to approximately 12% based on measurement of total diaminopimelate in samples with L-alanine, L-phenylalanine and L-leucine as carbon sources. This estimated peptidoglycan content is unusual for Gram-negative bacteria and almost 5-fold higher compared to *E. coli* (Feist *et al.* 2007). A thicker murein layer could maintain a higher turgor pressure and might be a strategy of *P. inhibens* DSM 17395 to the higher salt concentrations.

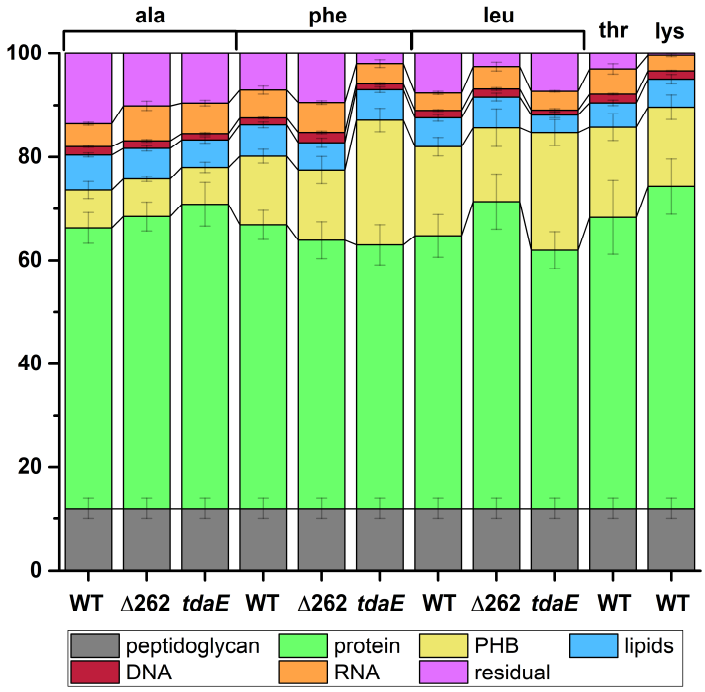

Figure 3.27 Determined biomass composition. Shown are experimentally determined biomass components as % of the complete CDW. For detailed values see table S15.

Main differences between the substrates were observed in PHB content which was least abundant with L-alanine as carbon source. In contrast to the higher accumulation of PHB in the Δ262-kb mutant strain with casamino acids at OD_{max} (Trautwein *et al.* 2016) no differences related to the 262-kb plasmid could be observed for cultivations with single amino acids. The transposon mutant strain *tdaE*

produced more PHB with L-phenylalanine and L-leucine compared to the wild-type and Δ262-kb mutant strain. The difference is more distinct with L-phenylalanine as carbon source and might indicate a use of degradation products of the accumulating TDA biosynthesis intermediates for PHB production. The highest protein content was observed with L-lysine as carbon source. L-lysine was not included in the estimation of the peptidoglycan content and the content seems to be overestimated as 100% biomass is reached but the residual includes lipopolysaccharide (~3.4%) and soluble metabolites (~2%). The L-lysine degradation product pipecolate was already discussed as possible compatible solute in chapter 3.1.4. Thus, due to production of pipecolate a thinner murein layer might be possible. Furthermore, L-glutamate was implemented in the biomass composition (all carbon sources) for the metabolic model with about 4% based on quantification for *D. shibae* DFL12 (Kleist *et al.* 2016). RNA content is correlating with the growth rates. Thus, lowest RNA could be isolated with L-leucine as carbon source.

3.3.5 Determination of GAM and NGAM

Usually, growth-and non-growth-associated maintenance energy (GAM and NGAM) are determined by chemostat cultivations. Most metabolic models are reconstructed with GAM and NGAM values published for hardly related organisms. Here, the different observed growth rates for the different amino acids as carbon source were used instead of adjusted dilution rates in chemostat cultivations for the experimental determination of GAM and NGAM. As described in chapter 3.3.3, TDA-free cultures showed optimal growth while the wild-type strain is inhibited by TDA when grown on L-alanine or L-phenylalanine. Thus, only TDA-free cultures were included in the determination of GAM and NGAM. The y-intercept is representing NGAM costs while the slope can be used for determination of GAM.

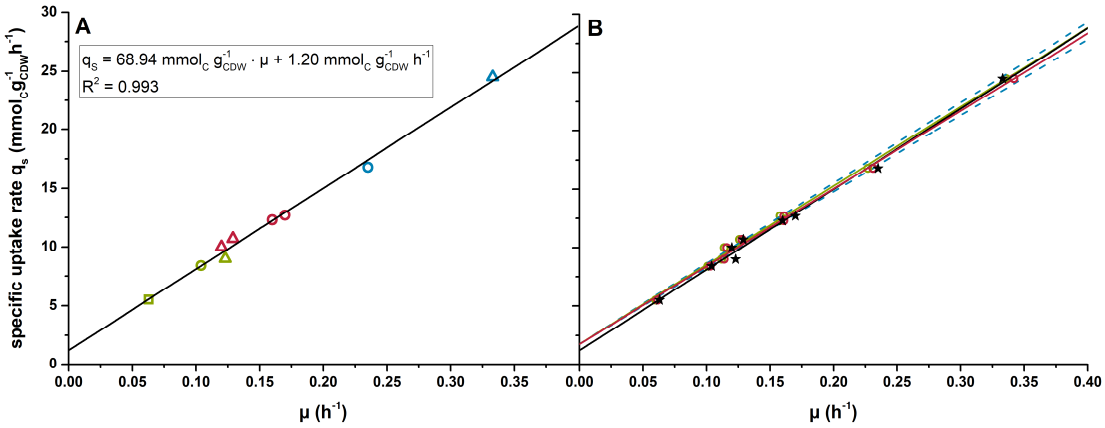

Figure 3.28 Determination of NGAM (A) and GAM (B). (A) Specific uptake rates q_S in $mmol_C\ g^{-1}_{CDW}h^{-1}$ were plotted over the corresponding growth rates for L-alanine (blue), L-phenylalanine (red) and L-leucine (green) for the wild-type strain (squares), the Δ262-kb mutant strain (circle) and the *tdaE* transposon mutant strain (triangle). (B) Shown are experimental data from A (black line, stars) compared to predicted data in a range from 80-95 $mmol_{ATP}\ g^{-1}_{CDW}$ (blue dash lines). Predicted values for 85 $mmol_{ATP}\ g^{-1}_{CDW}$ (red line, circles) and 90 $mmol_{ATP}\ g^{-1}_{CDW}$ (green line, circles) are shown for each simulated data point.

Transfer of the determined specific uptake rate q_S at a growth rate of 0 h^{-1} yields 4.8 (L-alanine), 4.5 (L-phenylalanine) and 5.0 (L-leucine) $mmol_{ATP}\ g^{-1}_{CDW}h^{-1}$ as NGAM values (figure 3.28 A, table 3.9). Thus, NGAM costs are higher compared to *P. putida* (3.96 $mmol_{ATP}\ g^{-1}_{CDW}h^{-1}$) but lower compared to *E. coli* (7.6 to 8.39 $mmol_{ATP}\ g^{-1}_{CDW}h^{-1}$) which were determined by chemostat cultivations (van Duuren *et al.* 2013; Feist *et al.* 2007; Varma, Palsson 1994b).

Table 3.9 Determination of NGAM. The determined specific uptake rate q_S ($mmol_C\ g^{-1}_{CDW}h^{-1}$) at a growth rate of 0 h^{-1} was transferred into $mmol_{ATP}\ g^{-1}_{CDW}h^{-1}$ for L-alanine, L-phenylalanine and L-leucine.

Amino acid	$mmol_C\ g^{-1}_{CDW}h^{-1}$	$mmol_S\ g^{-1}_{CDW}h^{-1}$	$mmol_{ATP}\ g^{-1}_{CDW}h^{-1}$
L-alanine	1.2	0.40	4.8
L-phenylalanine	1.2	0.13	4.5
L-leucine	1.2	0.20	5.0

GAM was estimated by FBA with the respective experimentally determined specific substrate uptake rate q_S. Different values for GAM within a range from 80 to 95 $mmol_{ATP}\ g^{-1}_{CDW}$ were used for the simulations and the predicted growth rates were compared to the experimental data (figure 3.28 B). Changes in GAM have only a minor effect on the predictions with lower substrate uptake rates/growth rates and increase

with increasing growth rates and corresponding higher substrate uptake rates. Overall, a GAM value of 85 $mmol_{ATP}\ g_{CDW}^{-1}$ was chosen for further analyses and thus GAM is equal to the determined value of *P. putida* (van Duuren *et al.* 2013). GAM was estimated to 59.81 and 71 $mmol_{ATP}\ g_{CDW}^{-1}$ in chemostat cultivations for *E. coli* ((Feist *et al.* 2007; Varma, Palsson 1994b). Thus, the maintenance for non-growth-associated processes are lower compared to *E. coli* but the growth-associated maintenance requirements are higher.

Overall, the determination of GAM and NGAM for *P. inhibens* DSM 17395 with batch cultivations in Erlenmeyer flasks resulted in values which suit to literature data. This determination was possible with optimal growing (TDA-free) cultures with different growth rates achieved by combining amino acid overarching growth data. Wild-type strain cultivations with L-alanine and L-phenylalanine as carbon source could not be implemented in the determination of GAM and NGAM due to growth inhibition by TDA on both substrates (figure 3.25, figure 3.26). Thus, the drawback of TDA production on the growth efficiency will be analyzed aided by the metabolic model.

3.3.6 Carbon flux and energy supply dependent on TDA production

Experimental and theoretical biomass yield $Y_{X/C}$ and oxygen consumption for cultivations with single amino acids were compared (figure 3.29). The TDA-free mutant strains showed optimal growth and experimental and theoretical biomass yields were similar, which was already observed in chapter 3.3.5 for determination of GAM and NGAM. The predicted oxygen consumption was least with L-alanine and increased with L-phenylalanine and highest were observed with L-leucine which is similar to the predictions for maximal possible ATP yields (figure 3.24). However, the experimentally determined oxygen consumption were about 20-30% higher with L-alanine and L-leucine compared to the predicted values indicating a higher respiratory activity than theoretically necessary. The wild-type strain reached only 67% (L-alanine), 42% (L-phenylalanine) or 77% (L-leucine) of the theoretically possible biomass yield. Experimentally determined oxygen consumptions were higher in the wild-type strain compared to the TDA-free mutant strains. The higher absolute oxygen consumption per g_{CDW} with decreasing growth rates and almost constant specific oxygen uptake rates q_{O2} was already described in chapter 3.2.3 and

is explainable by the disruption of the proton motive force by TDA (Wilson *et al.* 2016).

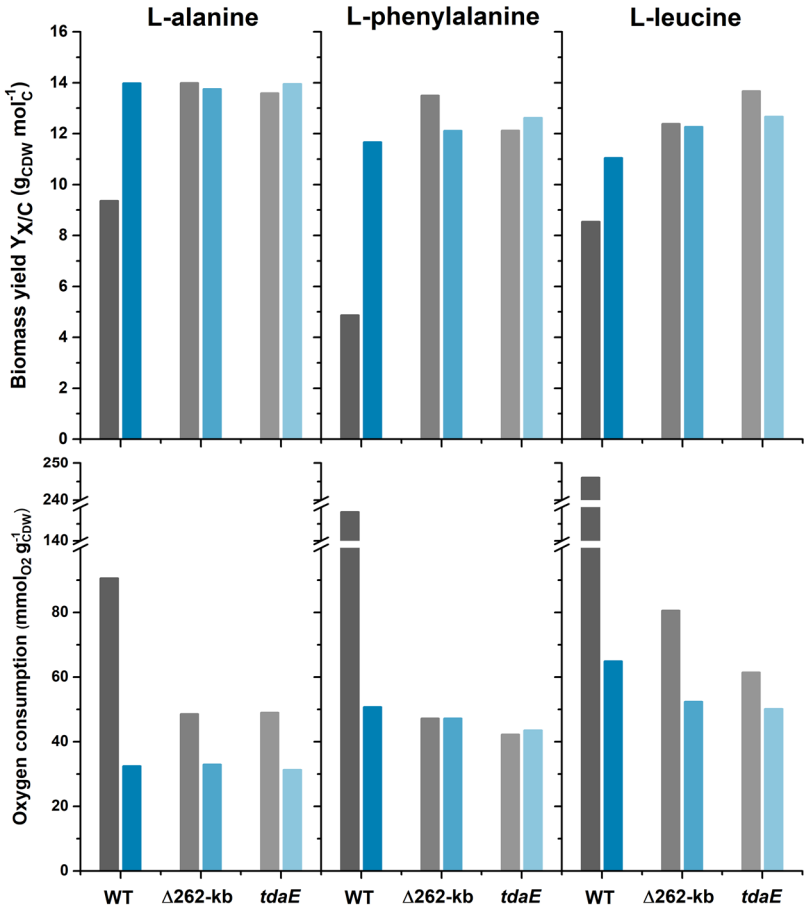

Figure 3.29 Comparison of experimental and theoretical biomass yield and oxygen consumption for L-alanine, L-phenylalanine and L-leucine. Shown are experimental (grey) and predicted (blue) biomass yield $Y_{X/C}$ and oxygen consumption for cultivations with L-alanine, L-phenylalanine and L-leucine as single carbon sources. Experimental q_S from ½ CDW_{max} (growth curves shown in figure 3.26) were used for FBA analyses.

Furthermore, observed biomass yield and oxygen consumption with L-alanine as carbon source were similar as with casamino acids (figure 3.23, table S14) indicating similar TDA production. With the TDA precursor L-phenylalanine, biomass yield decreased about 48% compared to L-alanine and oxygen consumption increased about 42% indicating a higher TDA production. The inhibition by TDA might be represented by a higher NGAM resulting in less available ATP for biomass production. This is only an approximation because the proton gradient is disrupted and thus, the ATP hydrolyzed in NGAM reaction is not actually produced. However, this is the easiest way to implement higher oxygen consumption into the model. With

experimental data from L-alanine and two L-phenylalanine cultivations (adapted cells) NGAM could be determined with the method described in chapter 3.3.5.

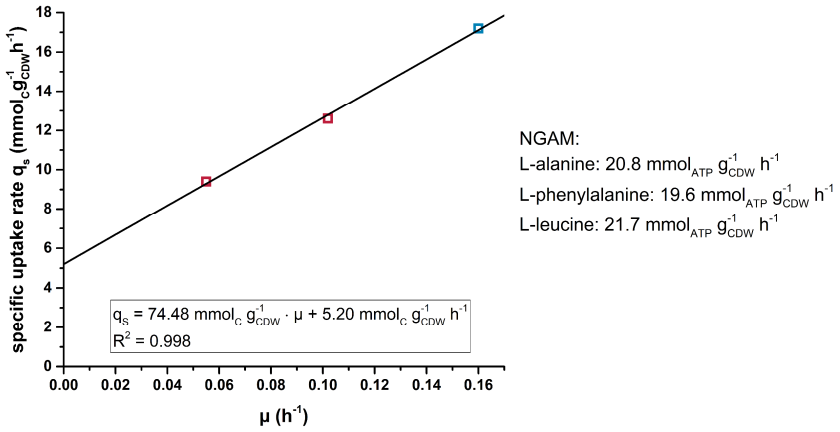

Figure 3.30 Determination of NGAM for representing the inhibition effect by TDA. Specific uptake rates q_S in mmol$_C$ g^{-1} h^{-1} were plotted over the corresponding growth rates for L-alanine (blue) and L-phenylalanine (red) for the wild-type strain.

FBAs with the determined NGAM values and restricted biomass production predicted TDA production with L-alanine as carbon source of about 0.47 mmol$_{TDA}$ g$^{-1}_{CDW}$ which is corresponding to 170 µM TDA (table 3.10). In previous studies by Berger *et al.* (2011) approximately 400 µM TDA was maximally reached with MB medium. However, with L-phenylalanine the experimental µ of 0.035 h^{-1} could not be reached and no production of TDA was possible with this scenario. TDA production was observed for all cultivations with L-phenylalanine which is the precursor for TDA production. Thus, using an estimation of NGAM determined by specific uptake rates of the carbon sources is not possible. Furthermore, it indicates that the higher specific uptake rates are not entirely reflecting the higher energetic costs due to higher oxygen consumption and consequently higher CO_2 production. In this experimental set-up, it might be considered that costs for the TDA biosynthesis itself reduces the available carbon.

Table 3.10 Predicted oxygen consumption, CO_2 and TDA production for the wild-type strain with higher NGAM costs. The upper bound of the biomass reaction was restricted to the experimentally determined growth rate and NGAM was set to 20.8 (L-alanine) and 19.6 (L-phenylalanine) mmol$_{ATP}$ g$^{-1}_{CDW}$h^{-1}. All simulations were performed with the respective experimental q_S.

Amino acid	µ [h^{-1}]	mmol$_{O2}$ g$^{-1}_{CDW}$	mmol$_{CO2}$ g$^{-1}_{CDW}$	mmol$_{TDA}$ g$^{-1}_{CDW}$
L-alanine	0.16	63	67	0.47
L-phenylalanine	0.028	236	21	0

In casamino acid containing medium the variety and availability of carbon sources is high. Thus, probably only a minor effect of decreased biomass yield is attributed to less available carbon due to TDA production. However, for L-phenylalanine cultures, inoculated with growing cells from casamino acids cultures, mainly TDA production was observed and first considerably biomass production initiated at about 100 h (figure 3.31). After already one transfer lag phase was shortened to 30 h and CDW_{max} was almost doubled. Both cultivations showed a stationary growth phase while for adapted cells no transient and stationary phase could be observed. Overall, these results indicate the use of L-phenylalanine mainly as a TDA precursor in casamino acid cultures.

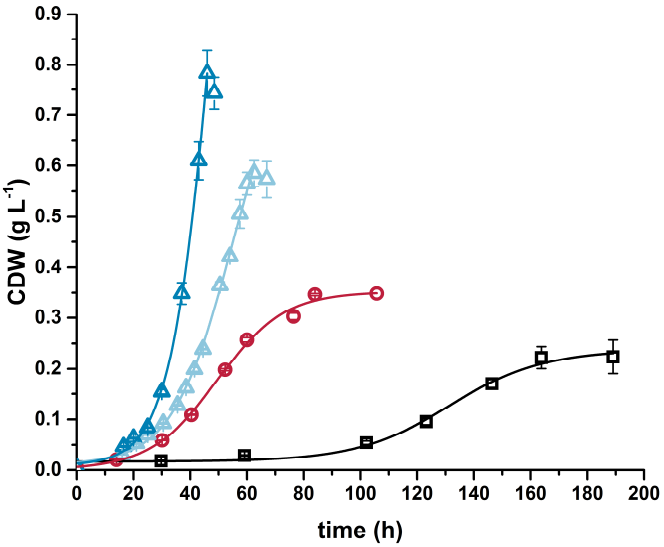

Figure 3.31 Adaptation of the wild-type strain to L-phenylalanine as carbon source. Shown are growth curves from cultures directly inoculated with a casamino acid preculture (black), cultures inoculated with one preculture in L-phenylalanine (red) and two independent cultures with adapted glycerol-stocks (blue).

To analyze this adaptation effect, the carbon flux distribution was calculated based on the experimentally determined specific substrate uptake rates and growth rates. The theoretically possible TDA production was predicted by restriction of the biomass reaction to the experimentally observed growth rate. Thus, excess carbon could be catabolized to TDA and CO_2. The overall oxygen consumption and CO_2 production increased with increasing TDA production (table 3.11). No TDA production for wild-type cells adapted to L-leucine as substrate was possible. This is the only analyzed wild-type culture showing similar growth efficiency compared to the TDA-free mutant strains.

Table 3.11 Predicted oxygen consumption, CO_2 and TDA production for the wild-type strain with restricted growth and normal NGAM costs. The upper bound of the biomass reaction was restricted to the experimentally determined growth rate and NGAM was set to the values determined in chapter 3.3.5. All simulations were performed with the respective experimental q_S. a: adapted

Amino acid	strain	$mmol_{O2}\ g_{CDW}^{-1}$	$mmol_{CO2}\ g_{CDW}^{-1}$	$mmol_{TDA}\ g_{CDW}^{-1}$	mM TDA
L-alanine	WT	46	55	2.0	0.7
	Δ262-kb	33	36	0	0
	tdaE	31	34	0	0
L-phenylalanine	WT	104	109	7.3	1.4
	WT-a1	81	84	5.1	1.5
	WT-a2	61	62	2.9	1.2
	Δ262-kb	43	40	0	0
	tdaE	47	43	0	0
L-leucine	WT	83	68	1.2	0.4
	WT-a	61	48	0	0
	Δ262-kb	52	40	0	0
	tdaE	50	39	0	0

50% of the available carbon is used for biomass production and 50% is respired to CO_2 in TDA-free mutant strains (table 3.12). For the wild-type strain slightly increased CO_2 production is predicted with L-leucine as carbon source. If TDA production is active, CO_2 production remained approximately at 50% but carbon incorporated into biomass decreased. The adaptation process of the wild-type strain to L-phenylalanine increased carbon flux to biomass from 19.1 to 31.6% with decreasing of TDA from 28.2 to 18.9%. Thus, cells with already one preculture in L-phenylalanine had only 19.1% of the carbon available for biomass production.

A higher CO_2 flux and less TDA production might be possible due to the disruption of the proton gradient. Thus, the method is restricted and absolute quantification of TDA would be necessary. However, TDA quantification is challenging due to the TDA-iron complex which is precipitated while extraction procedure and the available standard substance which showed a different behavior.

Table 3.12 Predicted carbon flux distribution dependent on TDA production. Listed are the theoretically carbon flux distributions for L-alanine, L-phenylalanine and L-leucine for the wild-type strain and TDA-free mutant strains. The flux values for CDW, CO_2 and TDA were referred to the specific uptake rate q_S (both values transferred into $mmol_C$). a: adapted

Amino acid	strain	% CDW	% CO_2	% TDA
L-alanine	WT	34.1	51.1	14.8
	Δ262-kb	51.0	49.0	0
	tdaE	52.5	47.5	0
L-phenylalanine	WT	19.1	52.7	28.2
	WT-a1	27.3	48.9	23.8
	WT-a2	31.6	49.5	18.9
	Δ262-kb	49.5	50.5	0
	tdaE	49.6	50.4	0
L-leucine	WT	28.3	62.8	8.9
	WT-a	45.5	54.5	0
	Δ262-kb	51.0	49.0	0
	tdaE	50.7	49.3	0

Overall the presented metabolic model-based analyses showed a high growth efficiency of *P. inhibens* DSM 17395 for many different substrates if growth is not inhibited by TDA. Observed biomass yields were independent from the growth rate. Thus, with L-leucine similar biomass yield was observed as for L-alanine and L-phenylalanine. Lipson (2015) already discussed the complex relationship between microbial growth rate and yield. One explanation for differences in growth rates and yields are different maintenance requirements. However, for the tested substrates the differences in NGAM were negligibly. Instead, L-leucine showed slower growth rates due to slower substrate uptake.

P. inhibens DSM 17395 is highly adapted to its habitat with energetically efficient use of many substrates. Furthermore, within some days or hours this organism is able to adapt to carbon sources to improve efficiency. However, TDA production is a drawback on energy supply due to degradation of the proton gradient. This effect is probably lower in the marine environment due to higher dilution. Furthermore, *P. inhibens* DSM 17395 is producing less TDA in stagnant cultures (Berger *et al.* 2011) indicating less production when growing attached to marine algae.

4 Conclusion

Extrachromosomal elements with a broad range of functions are widely spread amongst *Rhodobacteraceae* and enable optimal adaptation and survival in the natural habitat. For example, the 153-kb plasmid of *D. shibae* has an essential role in dealing with salinity extremes (Kleist *et al.* 2016) and the 65-kb (biofilm)plasmid of *P. inhibens* DSM 17395 is crucial for motility and colonization of the marine algal host (Frank *et al.* 2014).

One metabolic role of the 262-kb plasmid is the uptake of glucose and xylose (Wiegmann *et al.* 2014). Deletion of the 262-kb plasmid resulted in enhanced growth with casamino acids as substrate. Metabolic analyses showed that this plasmid is not involved in the uptake and degradation of amino acids. Only minor changes in lysine catabolism could be attributed to the missing plasmid due to accumulation of pipecolate which is synthesized from L-lysine. The 262-kb plasmid encodes for a pipecolate oxidase which was shown to be necessary for further use of pipecolate with unknown final product. The main degradation pathway via cadaverine is crucial for biomass production from L-lysine. Pipecolate might originally function as compatible solute and with receipt of the 262-kb plasmid pipecolate is further degraded.

The main function of the 262-kb plasmid is the biosynthesis of the antibacterial compound TDA. Based on the obtained data, it was possible to propose an updated biosynthetic pathway involving sulfur incorporation steps via an episulfide structure. Besides the TDA biosynthetic gene cluster on the 262-kb plasmid, further proteins encoded on the chromosome are crucial for TDA biosynthesis. Thus, *P. inhibens* DSM 17395 developed a high specific and unusual biosynthetic pathway for a sulfur containing antibiotic. Recently, TDA was shown to be active as signaling molecule in global gene regulation (Beyersmann *et al.* 2017). Lacking the complete 262-kb plasmid resulted in various changes on transcriptomic level. Several of them could be related to the TDA biosynthesis and one methyltransferase was newly proposed to be involved in the conversion of “pre”-TDA to TDA.

Furthermore, deletion of the 262-kb plasmid led to high expression levels of a putative lipoteichoic acid (LTA) biosynthetic gene cluster observed at maximally reached biomass. Possible components of this putative LTA could be identified and structures were proposed to include 3-hydroxybutanoate units originated from the

accumulated storage compound PHB. At the same time point expression levels of a gene cluster including phage relevant genes increased. Thus, starvation might trigger a phage and LTA is produced in return to counteract the phage. This observation is only indirectly connected to the 262-kb plasmid. The wild-type strain did not reach a starvation phase due to the immense growth restriction by TDA.

It was shown that this observation is connected to an inhibitory effect of TDA on the wild-type strain due to disruption of the proton gradient. *P. inhibens* DSM 17395 is not able to fully counteract by higher respiratory activity to this effect. Furthermore, *in silico* analyses showed optimal growth efficiency for different substrates without an active TDA production. However, if TDA biosynthesis is active more oxygen is consumed per g_{CDW} due to the inhibitory effect resulting in decreased biomass yield. L-phenylalanine, the precursor for TDA, was shown to be mainly used for TDA production if no adaptation to this carbon source for biomass production is ensued resulting in decreasing biomass yield due to less available carbon.

Thus, despite the drawback on energetic level, TDA production and consequently carrying the 262-kb plasmid seem to provide benefits in the natural habitat. For the more complex substrate range while algal bloom (represented in this work by casamino acids) only a minor effect of less available carbon due to TDA production is expected. Furthermore, less TDA is produced in stagnant cultures (Berger *et al.* 2011). Thus, the inhibitory effect could be lower when *P. inhibens* DSM 17395 is growing attached to the algae.

Growth efficiency and nutritionally versatility combined with production of an antibacterial compound to inhibit competitors is the successful survival strategy of *P. inhibens* DSM 17395. Consequently, growth efficiency in extreme habitats is not represented by a high growth rate but a high biomass yield.

References

Adadi, R; Volkmer, B; Milo, R; Heinemann, M; Shlomi, T (2012): Prediction of microbial growth rate versus biomass yield by a metabolic network with kinetic parameters. In *PLoS Comput Biol* 8 (7), e1002575. DOI: 10.1371/journal.pcbi.1002575.

Allwood, JW; Goodacre, R (2010): An introduction to liquid chromatography-mass spectrometry instrumentation applied in plant metabolomic analyses. In *Phytochemical analysis : PCA* 21 (1), pp. 33–47. DOI: 10.1002/pca.1187.

Alonso-Sáez, L; Balagué, V; Sà, EL; Sánchez, O; González, JM; Pinhassi, J *et al.* (2007): Seasonality in bacterial diversity in north-west Mediterranean coastal waters. Assessment through clone libraries, fingerprinting and FISH. In *FEMS microbiology ecology* 60 (1), pp. 98–112. DOI: 10.1111/j.1574-6941.2006.00276.x.

Alonso-Sáez, L; Gasol, JM (2007): Seasonal variations in the contributions of different bacterial groups to the uptake of low-molecular-weight compounds in northwestern Mediterranean coastal waters. In *Appl. Environ. Microbiol.* 73 (11), pp. 3528–3535. DOI: 10.1128/AEM.02627-06.

Appeltans, W; Ahyong, ST; Anderson, G; Angel, MV; Artois, T; Bailly, N *et al.* (2012): The magnitude of global marine species diversity. In *Current biology : CB* 22 (23), pp. 2189–2202. DOI: 10.1016/j.cub.2012.09.036.

Beardmore, RE; Gudelj, I; Lipson, DA; Hurst, LD (2011): Metabolic trade-offs and the maintenance of the fittest and the flattest. In *Nature* 472 (7343), pp. 342–346. DOI: 10.1038/nature09905.

Becker, J; Zelder, O; Häfner, S; Schröder, H; Wittmann, C (2011): From zero to hero--design-based systems metabolic engineering of *Corynebacterium glutamicum* for L-lysine production. In *Metabolic engineering* 13 (2), pp. 159–168. DOI: 10.1016/j.ymben.2011.01.003.

Berger, M; Brock, NL; Liesegang, H; Dogs, M; Preuth, I; Simon, M *et al.* (2012): Genetic Analysis of the Upper Phenylacetate Catabolic Pathway in the Production of Tropodithietic Acid by *Phaeobacter gallaeciensis*. In *Applied and Environmental Microbiology* 78 (10), pp. 3539–3551. DOI: 10.1128/AEM.07657-11.

Berger, M; Neumann, A; Schulz, S; Simon, M; Brinkhoff, T (2011): Tropodithietic Acid Production in *Phaeobacter gallaeciensis* Is Regulated by N-Acyl Homoserine Lactone-Mediated Quorum Sensing. In *Journal of Bacteriology* 193 (23), pp. 6576–6585. DOI: 10.1128/JB.05818-11.

Beyersmann, PG; Tomasch, J; Son, K; Stocker, R; Goker, M; Wagner-Dobler, I *et al.* (2017): Dual function of tropodithietic acid as antibiotic and signaling molecule in global gene regulation of the probiotic bacterium *Phaeobacter inhibens*. In *Scientific reports* 7 (1), p. 730. DOI: 10.1038/s41598-017-00784-7.

Bolten, CJ; Kiefer, P; Letisse, F; Portais, J-C; Wittmann, C (2007): Sampling for metabolome analysis of microorganisms. In *Anal. Chem.* 79 (10), pp. 3843–3849. DOI: 10.1021/ac0623888.

Brinkhoff, T; Bach, G; Heidorn, T; Liang, L; Schlingloff, A; Simon, M (2004): Antibiotic Production by a Roseobacter Clade-Affiliated Species from the German Wadden Sea and Its Antagonistic Effects on Indigenous Isolates. In *Applied and Environmental Microbiology* 70 (4), pp. 2560–2565. DOI: 10.1128/AEM.70.4.2560-2565.2003.

Brock, NL; Nikolay, A; Dickschat, JS (2014): Biosynthesis of the antibiotic tropodithietic acid by the marine bacterium *Phaeobacter inhibens*. In *Chem. Commun.* 50 (41), p. 5487. DOI: 10.1039/c4cc01924e.

Bruhn, JB; Gram, L; Belas, R (2007): Production of Antibacterial Compounds and Biofilm Formation by Roseobacter Species Are Influenced by Culture Conditions. In *Applied and Environmental Microbiology* 73 (2), pp. 442–450. DOI: 10.1128/AEM.02238-06.

Bruhn, JB; Nielsen, KF; Hjelm, M; Hansen, M; Bresciani, J; Schulz, S; Gram, L (2005): Ecology, inhibitory activity, and morphogenesis of a marine antagonistic bacterium belonging to the Roseobacter clade. In *Applied and Environmental Microbiology* 71 (11), pp. 7263–7270. DOI: 10.1128/AEM.71.11.7263-7270.2005.

Buchan, A; Gonzalez, JM; Moran, MA (2005): Overview of the Marine Roseobacter Lineage. In *Applied and Environmental Microbiology* 71 (10), pp. 5665–5677. DOI: 10.1128/AEM.71.10.5665-5677.2005.

Buddruhs, N; Pradella, S; Goker, M; Pauker, O; Pukall, R; Sproer, C *et al.* (2013): Molecular and phenotypic analyses reveal the non-identity of the *Phaeobacter gallaeciensis* type strain deposits CIP 105210T and DSM 17395. In *International Journal of Systematic and Evolutionary Microbiology* 63 (Pt 11), pp. 4340–4349. DOI: 10.1099/ijs.0.053900-0.

Charette, M; Smith, W (2010): The Volume of Earth's Ocean. In *Oceanog.* 23 (2), pp. 112–114. DOI: 10.5670/oceanog.2010.51.

D'Alvise, PW; Phippen, CB; Nielsen, KF; Gram, L (2015): Influence of iron on the production of the antibacterial compound tropodithietic acid and its non-inhibitory analog in *Phaeobacter inhibens*. In *Appl. Environ. Microbiol.*, p. 2992. DOI: 10.1128/AEM.02992-15.

del Giorgio, PA; Cole, JJ (1998): BACTERIAL GROWTH EFFICIENCY IN NATURAL AQUATIC SYSTEMS. In *Annu. Rev. Ecol. Syst.* 29 (1), pp. 503–541. DOI: 10.1146/annurev.ecolsys.29.1.503.

Dettmer, K; Aronov, PA; Hammock, BD (2007): Mass spectrometry-based metabolomics. In *Mass spectrometry reviews* 26 (1), pp. 51–78. DOI: 10.1002/mas.20108.

Dickschat, JS; Rinkel, J; Klapschinski, T; Petersen, J (2017): Characterisation of the l-Cystine β-Lyase PatB from *Phaeobacter inhibens*. An Enzyme Involved in the Biosynthesis of the Marine Antibiotic Tropodithietic Acid. In *ChemBioChem. DOI:* 10.1002/cbic.201700358.

Drüppel, K; Hensler, M; Trautwein, K; Koßmehl, S; Wöhlbrand, L; Schmidt-Hohagen, K *et al.* (2014): Pathways and substrate-specific regulation of amino acid degradation in *Phaeobacter inhibens* DSM 17395 (archetype of the marine Roseobacter clade). In *Environ Microbiol* 16 (1), pp. 218–238. DOI: 10.1111/1462-2920.12276.

Feist, AM; Henry, CS; Reed, JL; Krummenacker, M; Joyce, AR; Karp, PD *et al.* (2007): A genome-scale metabolic reconstruction for *Escherichia coli* K-12 MG1655 that accounts for 1260 ORFs and thermodynamic information. In *Mol Syst Biol* 3. DOI: 10.1038/msb4100155.

Fiehn, Oliver (Ed.) (2002): Metabolomics - the link between genotypes and phenotypes. Dordrecht: Springer Netherlands.

Frank, O; Michael, V; Päuker, O; Boedeker, C; Jogler, C; Rohde, M; Petersen, J (2014): Plasmid curing and the loss of grip–The 65-kb replicon of *Phaeobacter inhibens* DSM 17395 is required for biofilm formation, motility and the colonization of marine algae. In *Systematic and Applied Microbiology. DOI:* 10.1016/j.syapm.2014.12.001.

Fuhrman, JA; Steele, JA; Hewson, I; Schwalbach, MS; Brown, MV; Green, JL; Brown, JH (2008): A latitudinal diversity gradient in planktonic marine bacteria. In *Proceedings of the National Academy of Sciences of the United States of America* 105 (22), pp. 7774–7778. DOI: 10.1073/pnas.0803070105.

Gatto, GJ; Boyne, MT; Kelleher, NL; Walsh, CT (2006): Biosynthesis of Pipecolic Acid by RapL, a Lysine Cyclodeaminase Encoded in the Rapamycin Gene Cluster. In *J. Am. Chem. Soc.* 128 (11), pp. 3838–3847. DOI: 10.1021/ja0587603.

Geng, H; Belas, R (2010): Expression of Tropodithietic Acid Biosynthesis Is Controlled by a Novel Autoinducer. In *Journal of Bacteriology* 192 (17), pp. 4377–4387. DOI: 10.1128/JB.00410-10.

Geng, H; Belas, R (2011): TdaA Regulates Tropodithietic Acid Synthesis by Binding to the tdaC Promoter Region. In *Journal of Bacteriology* 193 (15), pp. 4002–4005. DOI: 10.1128/JB.00323-11.

Geng, H; Bruhn, JB; Nielsen, KF; Gram, L; Belas, R (2008): Genetic Dissection of Tropodithietic Acid Biosynthesis by Marine Roseobacters. In *Applied and Environmental Microbiology* 74 (5), pp. 1535–1545. DOI: 10.1128/AEM.02339-07.

Gorshkova, RP; Isakov, VV; Shevchenko, LS; Ivanova, EP; Denisenko, VA; Nazarenko, EL (2007): Structure of teichoic acid from the marine proteobacterium *Sulfitobacter brevis* KMM 6006. In *Chem Nat Compd* 43 (6), pp. 643–647. DOI: 10.1007/s10600-007-0218-7.

Goto, M; Muramatsu, H; Mihara, H; Kurihara, T; Esaki, N; Omi, R *et al.* (2005): Crystal Structures of 1-Piperideine-2-carboxylate/ 1-Pyrroline-2-carboxylate Reductase Belonging to a New Family of NAD(P)H-dependent Oxidoreductases: CONFORMATIONAL CHANGE, SUBSTRATE RECOGNITION, AND STEREOCHEMISTRY OF THE REACTION. In *Journal of Biological Chemistry* 280 (49), pp. 40875–40884. DOI: 10.1074/jbc.M507399200.

Gouesbet, G; Blanco, C; Hamelin, J; Bernard, T (1992): Osmotic adjustment in *Brevibacterium ammoniagenes*: pipecolic acid accumulation at elevated osmolalities. In *Journal of General Microbiology* 138 (5), pp. 959–965. DOI: 10.1099/00221287-138-5-959.

Gouesbet, G; Jebbar, M; Talibart, R; Bernard, T; Blanco, C (1994): Pipecolic acid is an osmoprotectant for *Escherichia coli* taken up by the general osmoporters ProU and ProP. In *Microbiology* 140 (9), pp. 2415–2422. DOI: 10.1099/13500872-140-9-2415.

Greer, EM; Aebisher, D; Greer, A; Bentley, R (2008): Computational Studies of the Tropone Natural Products, Thiotropocin, Tropodithietic Acid, and Troposulfenin. Significance of Thiocarbonyl−Enol Tautomerism. In *J. Org. Chem.* 73 (1), pp. 280–283. DOI: 10.1021/jo7018416.

Harrington, C; Reen, F; Mooij, M; Stewart, F; Chabot, J-B; Guerra, A *et al.* (2014): Characterisation of Non-Autoinducing Tropodithietic Acid (TDA) Production from Marine Sponge *Pseudovibrio* Species. In *Marine Drugs* 12 (12), pp. 5960–5978. DOI: 10.3390/md12125960.

Harrison, PW; Lower, RPJ; Kim, NKD; Young, JPW (2010): Introducing the bacterial 'chromid'. Not a chromosome, not a plasmid. In *Trends in microbiology* 18 (4), pp. 141–148. DOI: 10.1016/j.tim.2009.12.010.

Hensler, M (2014): Metabolic characterisation of the nutritional versatile marine bacterium *Phaeobacter inhibens* DSM 17395 via gas chromatography – mass spectrometry. Technische Universität Carolo-Wilhelmina zu Braunschweig.

Hiller, K; Hangebrauk, J; Jäger, C; Spura, J; Schreiber, K; Schomburg, D (2009): MetaboliteDetector: Comprehensive Analysis Tool for Targeted and Nontargeted GC/MS Based Metabolome Analysis. In *Anal. Chem.* 81 (9), pp. 3429–3439. DOI: 10.1021/ac802689c.

Hintermayer, SB; Weuster-Botz, D (2017): Experimental validation of in silico estimated biomass yields of *Pseudomonas putida* KT2440. In *Biotechnology journal* 12 (6). DOI: 10.1002/biot.201600720.

Imam, S; Yilmaz, S; Sohmen, U; Gorzalski, AS; Reed, JL; Noguera, DR; Donohue, TJ (2011): iRsp1095: a genome-scale reconstruction of the *Rhodobacter sphaeroides* metabolic network. In *BMC Syst Biol* 5, p. 116. DOI: 10.1186/1752-0509-5-116.

Kalhoefer, D; Thole, S; Voget, S; Lehmann, R; Liesegang, H; Wollher, A *et al.* (2011): Comparative genome analysis and genome-guided physiological analysis of *Roseobacter litoralis*. In *BMC Genomics* 12, p. 324. DOI: 10.1186/1471-2164-12-324.

Kanani, HH; Klapa, MI (2007): Data correction strategy for metabolomics analysis using gas chromatography-mass spectrometry. In *Metabolic engineering* 9 (1), pp. 39–51. DOI: 10.1016/j.ymben.2006.08.001.

Kintaka, K; Ono, H; Tsubotani, S; Harada, S; Okazaki, H (1984): Thiotropocin, a new sulfur-containing 7-membered-ring antibiotic produced by a *Pseudomonas* sp. In *The Journal of antibiotics* 37 (11), pp. 1294–1300.

Kleist, S; Ulbrich, M; Bill, N; Schmidt-Hohagen, K; Geffers, R; Schomburg, D (2016): Dealing with salinity extremes and nitrogen limitation - an unexpected strategy of the marine bacterium *Dinoroseobacter shibae*. In *Environmental microbiology. DOI:* 10.1111/1462-2920.13266.

Koonin, EV (2016): Horizontal gene transfer. Essentiality and evolvability in prokaryotes, and roles in evolutionary transitions. In *F1000Research* 5. DOI: 10.12688/f1000research.8737.1.

Lang, M; Stelzer, M; Schomburg, D (2011): BKM-react, an integrated biochemical reaction database. In *BMC biochemistry* 12, p. 42. DOI: 10.1186/1471-2091-12-42.

Lee, N-R; Lakshmanan, M; Aggarwal, S; Song, J-W; Karimi, IA; Lee, D-Y; Park, J-B (2014): Genome-scale metabolic network reconstruction and in silico flux analysis of the thermophilic bacterium *Thermus thermophilus* HB27. In *Microbial cell factories* 13, p. 61. DOI: 10.1186/1475-2859-13-61.

Lele, UN; Gwatve, M (2014): Bacterial Growth Rate and Growth Yield. Is There A Relationship? In *Proceedings of the Indian National Science Academy* 80 (3), p. 537. DOI: 10.16943/ptinsa/2014/v80i3/55129.

Lipson, DA (2015): The complex relationship between microbial growth rate and yield and its implications for ecosystem processes. In *Frontiers in microbiology* 6, p. 615. DOI: 10.3389/fmicb.2015.00615.

Mahadevan, R; Schilling, CH (2003): The effects of alternate optimal solutions in constraint-based genome-scale metabolic models. In *Metabolic engineering* 5 (4), pp. 264–276.

Mann, HB; Whitney, DR (1947): On a Test of Whether one of Two Random Variables is Stochastically Larger than the Other. In *Ann. Math. Statist.* 18 (1), pp. 50–60. DOI: 10.1214/aoms/1177730491.

Martens, T (2006): Reclassification of *Roseobacter gallaeciensis* Ruiz-Ponte *et al.* 1998 as *Phaeobacter gallaeciensis* gen. nov., comb. nov., description of *Phaeobacter inhibens* sp. nov., reclassification of *Ruegeria algicola* (Lafay *et al.* 1995) Uchino *et al.* 1999 as *Marinovum algicola* gen. nov., comb. nov., and emended descriptions of the genera *Roseobacter, Ruegeria* and *Leisingera*. In *International Journal of Systematic and Evolutionary Microbiology* 56 (6), pp. 1293–1304. DOI: 10.1099/ijs.0.63724-0.

Matyash, V; Liebisch, G; Kurzchalia, TV; Shevchenko, A; Schwudke, D (2008): Lipid extraction by methyl-tert-butyl ether for high-throughput lipidomics. In *Journal of lipid research* 49 (5), pp. 1137–1146. DOI: 10.1194/jlr.D700041-JLR200.

Michael, V; Frank, O; Bartling, P; Scheuner, C; Göker, M; Brinkmann, H; Petersen, J (2016): Biofilm plasmids with a rhamnose operon are widely distributed determinants of the 'swim-or-stick' lifestyle in roseobacters. In *ISME J. DOI:* 10.1038/ismej.2016.30.

Monod, J (1949): The Growth of Bacterial Cultures. In *Annu. Rev. Microbiol.* 3 (1), pp. 371–394. DOI: 10.1146/annurev.mi.03.100149.002103.

Muramatsu, H; Mihara, H; Kakutani, R; Yasuda, M; Ueda, M; Kurihara, T; Esaki, N (2005): The putative malate/lactate dehydrogenase from *Pseudomonas putida* is an NADPH-dependent delta1-piperideine-2-carboxylate/delta1-pyrroline-2-carboxylate reductase involved in the catabolism of D-lysine and D-proline. In *The Journal of biological chemistry* 280 (7), pp. 5329–5335. DOI: 10.1074/jbc.M411918200.

Neshich, IAP; Kiyota, E; Arruda, P (2013): Genome-wide analysis of lysine catabolism in bacteria reveals new connections with osmotic stress resistance. In *ISME J* 7 (12), pp. 2400–2410. DOI: 10.1038/ismej.2013.123.

Neuhaus, FC; Baddiley, J (2003): A Continuum of Anionic Charge. Structures and Functions of D-Alanyl-Teichoic Acids in Gram-Positive Bacteria. In *Microbiology and Molecular Biology Reviews* 67 (4), pp. 686–723. DOI: 10.1128/MMBR.67.4.686-723.2003.

Newton, RJ; Griffin, LE; Bowles, KM; Meile, C; Gifford, S; Givens, CE *et al.* (2010): Genome characteristics of a generalist marine bacterial lineage. In *ISME J* 4 (6), pp. 784–798. DOI: 10.1038/ismej.2009.150.

Orth, JD; Conrad, TM; Na, J; Lerman, JA; Nam, H; Feist, AM; Palsson, BO (2011): A comprehensive genome-scale reconstruction of *Escherichia coli* metabolism--2011. In *Molecular Systems Biology* 7 (1), p. 535. DOI: 10.1038/msb.2011.65.

Orth, JD; Thiele, I; Palsson, BØ (2010): What is flux balance analysis? In *Nat Biotechnol* 28 (3), pp. 245–248. DOI: 10.1038/nbt.1614.

Petersen, J; Brinkmann, H; Berger, M; Brinkhoff, T; Päuker, O; Pradella, S (2011): Origin and evolution of a novel DnaA-like plasmid replication type in *Rhodobacterales*. In *Molecular biology and evolution* 28 (3), pp. 1229–1240. DOI: 10.1093/molbev/msq310.

Petersen, J; Frank, O; Göker, M; Pradella, S (2013): Extrachromosomal, extraordinary and essential—the plasmids of the Roseobacter clade. In *Appl Microbiol Biotechnol* 97 (7), pp. 2805–2815. DOI: 10.1007/s00253-013-4746-8.

Peyraud, R; Kiefer, P; Christen, P; Massou, S; Portais, J-C; Vorholt, JA (2009): Demonstration of the ethylmalonyl-CoA pathway by using 13C metabolomics. In *Proceedings of the National Academy of Sciences of the United States of America* 106 (12), pp. 4846–4851. DOI: 10.1073/pnas.0810932106.

Pinto, UM; Pappas, KM; Winans, SC (2012): The ABCs of plasmid replication and segregation. In *Nature reviews. Microbiology* 10 (11), pp. 755–765. DOI: 10.1038/nrmicro2882.

Pirt, SJ (1965): The Maintenance Energy of Bacteria in Growing Cultures. In *Proceedings of the Royal Society B: Biological Sciences* 163 (991), pp. 224–231. DOI: 10.1098/rspb.1965.0069.

Pirt, SJ (1982): Maintenance energy. A general model for energy-limited and energy-sufficient growth. In *Arch. Microbiol.* 133 (4), pp. 300–302. DOI: 10.1007/BF00521294.

Porsby, CH; Webber, MA; Nielsen, KF; Piddock, L. J. V.; Gram, L (2011): Resistance and Tolerance to Tropodithietic Acid, an Antimicrobial in Aquaculture, Is Hard To Select. In *Antimicrobial Agents and Chemotherapy* 55 (4), pp. 1332–1337. DOI: 10.1128/AAC.01222-10.

Pradella, S; Päuker, O; Petersen, J (2010): Genome organisation of the marine Roseobacter clade member *Marinovum algicola*. In *Arch. Microbiol.* 192 (2), pp. 115–126. DOI: 10.1007/s00203-009-0535-2.

Price, ND; Papin, JA; Schilling, CH; Palsson, BO (2003): Genome-scale microbial in silico models. The constraints-based approach. In *Trends in Biotechnology* 21 (4), pp. 162–169. DOI: 10.1016/S0167-7799(03)00030-1.

Puchałka, J; Oberhardt, MA; Godinho, M; Bielecka, A; Regenhardt, D; Timmis, KN *et al.* (2008): Genome-scale reconstruction and analysis of the *Pseudomonas putida* KT2440 metabolic network facilitates applications in biotechnology. In *PLoS Comput Biol* 4 (10), e1000210. DOI: 10.1371/journal.pcbi.1000210.

Quester, S; Schomburg, D (2011): EnzymeDetector: an integrated enzyme function prediction tool and database. In *BMC Bioinformatics* 12 (1), p. 376. DOI: 10.1186/1471-2105-12-376.

Räisänen, L; Draing, C; Pfitzenmaier, M; Schubert, K; Jaakonsaari, T; Aulock, S von *et al.* (2007): Molecular interaction between lipoteichoic acids and *Lactobacillus delbrueckii* phages depends on D-alanyl and alpha-glucose substitution of poly(glycerophosphate) backbones. In *Journal of Bacteriology* 189 (11), pp. 4135–4140. DOI: 10.1128/JB.00078-07.

Reimer, LC; Will, SE; Schomburg, D (2017): The fate of lysine. Non-targeted stable isotope analysis reveals parallel ways for lysine catabolization in *Phaeobacter inhibens*. In *PLoS ONE* 12 (10), e0186395. DOI: 10.1371/journal.pone.0186395.

Reuber, T; Walker, GC (1993): Biosynthesis of succinoglycan, a symbiotically important exopolysaccharide of *Rhizobium meliloti*. In *Cell* 74 (2), pp. 269–280. DOI: 10.1016/0092-8674(93)90418-P.

Revelles, O; Espinosa-Urgel, M; Fuhrer, T; Sauer, U; Ramos, JL (2005): Multiple and Interconnected Pathways for L-Lysine Catabolism in *Pseudomonas putida* KT2440. In *Journal of Bacteriology* 187 (21), pp. 7500–7510. DOI: 10.1128/JB.187.21.7500-7510.2005.

Revelles, O; Wittich, R-M; Ramos, JL (2007): Identification of the Initial Steps in D-Lysine Catabolism in *Pseudomonas putida*. In *Journal of Bacteriology* 189 (7), pp. 2787–2792. DOI: 10.1128/JB.01538-06.

Rex, R (2013): Towards a new view on metabolic networks: Automated reconstruction and large-scale computational analysis applied to *Dinoroseobacter shibae*. Technische Universität Carolo-Wilhelmina zu Braunschweig.

Riemer, SA (2013): metano - An open-source toolbox for the reconstruction and analysis of genome-scale metabolic models. Technische Universität Carolo-Wilhelmina zu Braunschweig.

Ruiz-Ponte, C; Cilia, V; Lambert, C; Nicolas, JL (1998): *Roseobacter gallaeciensis* sp. nov., a new marine bacterium isolated from rearings and collectors of the scallop *Pecten maximus*. In *International journal of systematic bacteriology* 48 Pt 2, pp. 537–542. DOI: 10.1099/00207713-48-2-537.

Schilling, CH; Edwards, JS; Letscher, D; Palsson, BØ (2000): Combining pathway analysis with flux balance analysis for the comprehensive study of metabolic systems. In *Biotechnology and bioengineering* 71 (4), pp. 286–306.

Schneider, K; Schütz, V; John, GT; Heinzle, E (2010): Optical device for parallel online measurement of dissolved oxygen and pH in shake flask cultures. In *Bioprocess and biosystems engineering* 33 (5), pp. 541–547. DOI: 10.1007/s00449-009-0367-0.

Schulze, KL; Lipe, RS (1964): Relationship between substrate concentration, growth phase, and respiration rate of *Escherichia coli* in continuous culture. In *Archiv fur Mikrobiologie* 48, pp. 1–20.

Sijtsma, L; Wouters, JT; Hellingwerf, KJ (1990): Isolation and characterization of lipoteichoic acid, a cell envelope component involved in preventing phage adsorption, from *Lactococcus lactis* subsp. cremoris SK110. In *Journal of Bacteriology* 172 (12), pp. 7126–7130. DOI: 10.1128/jb.172.12.7126-7130.1990.

Simon, M; Scheuner, C; Meier-Kolthoff, JP; Brinkhoff, T; Wagner-Döbler, I; Ulbrich, M *et al.* (2017): Phylogenomics of *Rhodobacteraceae* reveals evolutionary adaptation to marine and non-marine habitats. In *ISME J* 11 (6), pp. 1483–1499. DOI: 10.1038/ismej.2016.198.

Simoneit, BRT; Elias, VO; Kobayashi, M; Kawamura, K; Rushdi, AI; Medeiros, PM *et al.* (2004): SugarsDominant Water-Soluble Organic Compounds in Soils and Characterization as Tracers in Atmospheric Particulate Matter. In *Environ. Sci. Technol.* 38 (22), pp. 5939–5949. DOI: 10.1021/es0403099.

Spura, J; Reimer, LC; Wieloch, P; Schreiber, K; Buchinger, S; Schomburg, D (2009): A method for enzyme quenching in microbial metabolome analysis successfully applied to gram-positive and gram-negative bacteria and yeast. In *Analytical biochemistry* 394 (2), pp. 192–201. DOI: 10.1016/j.ab.2009.07.016.

Strelkov, S; Elstermann, M von; Schomburg, D (2004): Comprehensive analysis of metabolites in *Corynebacterium glutamicum* by gas chromatography/mass spectrometry. In *Biological chemistry* 385 (9), pp. 853–861. DOI: 10.1515/BC.2004.111.

Thiele, I; Palsson, BØ (2010): A protocol for generating a high-quality genome-scale metabolic reconstruction. In *Nat Protoc* 5 (1), pp. 93–121. DOI: 10.1038/nprot.2009.203.

Thole, S; Kalhoefer, D; Voget, S; Berger, M; Engelhardt, T; Liesegang, H *et al.* (2012): *Phaeobacter gallaeciensis* genomes from globally opposite locations reveal high similarity of adaptation to surface life. In *ISME J* 6 (12), pp. 2229–2244. DOI: 10.1038/ismej.2012.62.

Trautwein, K; Will, SE; Hulsch, R; Maschmann, U; Wiegmann, K; Hensler, M *et al.* (2016): Native plasmids restrict growth of *Phaeobacter inhibens* DSM 17395: Energetic costs of plasmids assessed by quantitative physiological analyses. In *Environmental microbiology. DOI:* 10.1111/1462-2920.13381.

van Duuren, JBJH; Puchałka, J; Mars, AE; Bücker, R; Eggink, G; Wittmann, C; Dos Santos, VAPM (2013): Reconciling in vivo and in silico key biological parameters of *Pseudomonas putida* KT2440 during growth on glucose under carbon-limited condition. In *BMC biotechnology* 13, p. 93. DOI: 10.1186/1472-6750-13-93.

Varma, A; Boesch, BW; Palsson, BO (1993): Stoichiometric interpretation of *Escherichia coli* glucose catabolism under various oxygenation rates. In *Appl. Environ. Microbiol.* 59 (8), pp. 2465–2473.

Varma, A; Palsson, BO (1994a): Metabolic Flux Balancing. Basic Concepts, Scientific and Practical Use. In *Nat Biotechnol* 12 (10), pp. 994–998. DOI: 10.1038/nbt1094-994.

Varma, A; Palsson, BO (1994b): Stoichiometric flux balance models quantitatively predict growth and metabolic by-product secretion in wild-type *Escherichia coli* W3110. In *Applied and Environmental Microbiology* 60 (10), pp. 3724–3731.

Villas-Bôas, SG; Mas, S; Akesson, M; Smedsgaard, J; Nielsen, J (2005): Mass spectrometry in metabolome analysis. In *Mass spectrometry reviews* 24 (5), pp. 613–646. DOI: 10.1002/mas.20032.

Wagner-Döbler, I; Ballhausen, B; Berger, M; Brinkhoff, T; Buchholz, I; Bunk, B *et al.* (2010): The complete genome sequence of the algal symbiont *Dinoroseobacter shibae*. A hitchhiker's guide to life in the sea. In *ISME J* 4 (1), pp. 61–77. DOI: 10.1038/ismej.2009.94.

Wichmann, H; Brinkhoff, T; Simon, M; Richter-Landsberg, C (2016): Dimethylsulfoniopropionate Promotes Process Outgrowth in Neural Cells and Exerts Protective Effects against Tropodithietic Acid. In *Marine Drugs* 14 (5). DOI: 10.3390/md14050089.

Wichmann, H; Vocke, F; Brinkhoff, T; Simon, M; Richter-Landsberg, C (2015): Cytotoxic Effects of Tropodithietic Acid on Mammalian Clonal Cell Lines of Neuronal and Glial Origin. In *Marine Drugs* 13 (12), pp. 7113–7123. DOI: 10.3390/md13127058.

Wiegmann, K; Hensler, M; Wohlbrand, L; Ulbrich, M; Schomburg, D; Rabus, R (2014): Carbohydrate Catabolism in *Phaeobacter inhibens* DSM 17395, a Member of the Marine Roseobacter Clade. In *Applied and Environmental Microbiology* 80 (15), pp. 4725–4737. DOI: 10.1128/AEM.00719-14.

Wietz, M; Gram, L; Jørgensen, B; Schramm, A (2010): Latitudinal patterns in the abundance of major marine bacterioplankton groups. In *Aquat. Microb. Ecol.* 61 (2), pp. 179–189. DOI: 10.3354/ame01443.

Will, SE; Neumann-Schaal, M; Heydorn, RL; Bartling, P; Petersen, J; Schomburg, D (2017): The limits to growth – energetic burden of the endogenous antibiotic tropodithietic acid in *Phaeobacter inhibens* DSM 17395. In *PLoS ONE* 12 (5), e0177295. DOI: 10.1371/journal.pone.0177295.

Wilson, MZ; Wang, R; Gitai, Z; Seyedsayamdost, MR (2016): Mode of action and resistance studies unveil new roles for tropodithietic acid as an anticancer agent and the γ-glutamyl cycle as a proton sink. In *Proceedings of the National Academy of Sciences of the United States of America. DOI:* 10.1073/pnas.1518034113.

Yang, Z; Lu, C-D (2007): Characterization of an Arginine:Pyruvate Transaminase in Arginine Catabolism of *Pseudomonas aeruginosa* PAO1. In *Journal of Bacteriology* 189 (11), pp. 3954–3959. DOI: 10.1128/JB.00262-07.

Zech, H; Hensler, M; Koßmehl, S; Drüppel, K; Wöhlbrand, L; Trautwein, K *et al.* (2013a): Adaptation of *Phaeobacter inhibens* DSM 17395 to growth with complex nutrients. In *Proteomics*, pp. n/a. DOI: 10.1002/pmic.201200513.

Zech, H; Hensler, M; Koßmehl, S; Drüppel, K; Wöhlbrand, L; Trautwein, K *et al.* (2013b): Dynamics of amino acid utilization in *Phaeobacter inhibens* DSM 17395. In *Proteomics*, pp. n/a. DOI: 10.1002/pmic.201200560.

Zech, H; Thole, S; Schreiber, K; Kalhöfer, D; Voget, S; Brinkhoff, T *et al.* (2009): Growth phase-dependent global protein and metabolite profiles of *Phaeobacter gallaeciensis* strain DSM 17395, a member of the marine Roseobacter -clade. In *Proteomics* 9 (14), pp. 3677–3697. DOI: 10.1002/pmic.200900120.

Supplementary material

Table S1a Normalized peak areas of intracellularly detected metabolites of the wild-type and Δ262-kb mutant strain at ½ OD_{max} with casamino acids as carbon source (cultivation in process-controlled bioreactors). Normalized peak areas are listed with corresponding standard error for all identified metabolites detectable at least in one of both strains. n.d.: not detected. Cultivation and sampling were performed by the working group of Ralf Rabus (ICBM).

Metabolite	½ OD_{max}	
	WT	Δ262-kb
2,4-diaminobutanoate	$4.2x10^4 \pm 8.3x10^2$	$5.7x10^4 \pm 2.6x10^3$
2,6-diamino-pimelate	$1.1x10^5 \pm 4.5x10^3$	$1.4x10^5 \pm 8.3x10^3$
2-aminoadipic-acid	$7.4x10^4 \pm 2.7x10^3$	$8.5x10^3 \pm 1.3x10^3$
2-isopropylmalic acid	$1.6x10^4 \pm 8.8x10^2$	$8.1x10^3 \pm 3.9x10^2$
2-oxoglutarate	$1.5x10^4 \pm 7.6x10^2$	$1.3x10^4 \pm 4.8x10^2$
3-aminoisobutanoate	$2.3x10^4 \pm 2.1x10^3$	$2.6x10^4 \pm 3.1x10^3$
3-hydroxybutanoate	$3.7x10^4 \pm 2.3x10^3$	$5.7x10^4 \pm 2.6x10^3$
3-hydroxy-decanoate	$1.3x10^4 \pm 8.7x10^2$	$1.2x10^4 \pm 7.1x10^2$
3-phosphoglycerate	$2.6x10^4 \pm 1.6x10^3$	$4.3x10^4 \pm 1.4x10^3$
5-aminopentanoic-acid	$4.9x10^6 \pm 1.8x10^5$	$7.2x10^6 \pm 5.8x10^5$
6-phospho-gluconate	$7.0x10^3 \pm 1.0x10^3$	$5.9x10^3 \pm 3.1x10^2$
Adenine	$1.2x10^5 \pm 3.5x10^3$	$9.1x10^4 \pm 2.4x10^3$
Alanine	$7.1x10^6 \pm 7.5x10^5$	$5.8x10^6 \pm 7.1x10^5$
AMP	$7.0x10^5 \pm 2.2x10^4$	$7.0x10^5 \pm 1.4x10^4$
Arginine	$9.7x10^3 \pm 3.4x10^2$	$1.3x10^4 \pm 5.0x10^2$
Asparagine	$1.8x10^4 \pm 8.4x10^2$	$2.8x10^4 \pm 1.5x10^3$
Aspartate	$2.5x10^6 \pm 1.4x10^5$	$3.0x10^6 \pm 2.3x10^5$
Beta-alanine	$5.5x10^4 \pm 5.0x10^3$	$3.4x10^4 \pm 4.5x10^3$
Cadaverine	$1.0x10^5 \pm 7.6x10^3$	$6.8x10^5 \pm 1.8x10^5$
Cis-vaccenic acid	$1.8x10^4 \pm 1.9x10^3$	$1.8x10^4 \pm 1.5x10^3$
Citrate	$2.2x10^4 \pm 1.1x10^3$	$3.5x10^4 \pm 8.5x10^2$
Cysteine	$1.0x10^4 \pm 2.4x10^3$	$6.9x10^3 \pm 1.4x10^3$
Cysteinylglycine	$6.5x10^4 \pm 5.2x10^3$	$5.9x10^4 \pm 5.8x10^3$
Cytosine	$1.6x10^5 \pm 7.7x10^3$	$1.3x10^5 \pm 6.0x10^3$
D200302_2009.31	n.d.	$3.8x10^4 \pm 2.4x10^3$
D-glucosaminate	$2.2x10^4 \pm 1.3x10^3$	$1.1x10^4 \pm 9.3x10^2$
Ethanolamine	$3.8x10^4 \pm 1.9x10^3$	$7.2x10^4 \pm 2.8x10^3$
Fructose-1,6-bisphosphate	$5.5x10^4 \pm 7.2x10^3$	$5.2x10^4 \pm 6.6x10^3$
Fumarate	$5.4x10^4 \pm 7.7x10^2$	$4.4x10^4 \pm 1.3x10^3$
Glucose	$7.0x10^4 \pm 1.7x10^3$	$5.3x10^4 \pm 1.6x10^3$

Table S1a continued

Metabolite	½ OD_{max}	
	WT	**Δ262-kb**
Glucose-6-phosphate	$1.5x10^4 \pm 8.8x10^2$	$1.2x10^4 \pm 5.1x10^2$
Glutamate	$5.9x10^7 \pm 1.0x10^6$	$5.7x10^7 \pm 1.1x10^6$
Glutamine	$3.9x10^6 \pm 2.3x10^5$	$3.3x10^6 \pm 2.9x10^5$
Glutarate	$2.6x10^4 \pm 1.1x10^3$	$2.1x10^4 \pm 1.1x10^3$
Glycerol-3-phosphate	$2.5x10^5 \pm 1.2x10^4$	$3.0x10^5 \pm 1.9x10^4$
Glycerophosphoglycerol	$9.1x10^4 \pm 4.2x10^3$	$9.9x10^4 \pm 4.7x10^3$
Glycine	$3.4x10^5 \pm 1.7x10^4$	$3.2x10^5 \pm 1.3x10^4$
Glycylglycine	$1.2x10^5 \pm 1.6x10^4$	$6.2x10^4 \pm 1.1x10^4$
Glycylproline	$6.3x10^3 \pm 9.8x10^2$	$3.1x10^4 \pm 6.5x10^3$
GMP	$6.4x10^4 \pm 1.5x10^3$	$6.9x10^4 \pm 1.7x10^3$
Guanine	$2.6x10^4 \pm 9.6x10^2$	$2.4x10^4 \pm 1.2x10^3$
Histidine	$4.9x10^4 \pm 2.0x10^3$	$7.4x10^4 \pm 3.7x10^3$
Isoleucine	$4.1x10^5 \pm 1.2x10^4$	$3.5x10^5 \pm 2.5x10^4$
Leucine	$3.7x10^5 \pm 2.4x10^4$	$2.9x10^5 \pm 2.2x10^4$
Lysine	$2.9x10^5 \pm 9.1x10^3$	$3.4x10^5 \pm 1.1x10^4$
Malate	$7.0x10^4 \pm 2.1x10^3$	$5.2x10^4 \pm 1.1x10^3$
Methionine	$1.5x10^5 \pm 1.6x10^4$	$1.3x10^5 \pm 1.7x10^4$
NA_1703.1	$2.1x10^4 \pm 1.5x10^3$	$4.6x10^4 \pm 2.8x10^3$
NA_1705.1	$1.3x10^4 \pm 1.3x10^3$	$1.1x10^4 \pm 6.5x10^3$
NA199017_1996.71	$3.2x10^4 \pm 1.3x10^3$	$2.5x10^4 \pm 1.6x10^3$
NA261	$1.0x10^5 \pm 5.1x10^3$	$1.1x10^5 \pm 5,2x10^3$
NA714	n.d.	$2.4x10^5 \pm 1.6x10^4$
N-acetyl-glutamate	$9.7x10^3 \pm 4.7x10^2$	$1.0x10^4 \pm 7.2x10^2$
Nicotinamide	$1.3x10^5 \pm 3.0x10^3$	$1.1x10^5 \pm 4.8x10^3$
Ornithine	$3.3x10^4 \pm 8.6x10^2$	$5.4x10^4 \pm 4.9x10^3$
Phenylalanine	$3.4x10^5 \pm 1.4x10^4$	$3.7x10^5 \pm 1.4x10^4$
Phosphate-monomethyl ester	$3.4x10^4 \pm 1.1x10^3$	$4.4x10^4 \pm 1.0x10^3$
Phosphoenolpyruvate	$4.9x10^3 \pm 6.9x10^2$	$2.2x10^4 \pm 1.1x10^3$
Pipecolate	$9.3x10^5 \pm 2.6x10^4$	$3.2x10^6 \pm 7.6x10^4$
Proline	$7.4x10^5 \pm 5.7x10^4$	$5.8x10^5 \pm 7.7x10^4$
Putrescine	$6.5x10^4 \pm 3.9x10^3$	$3.0x10^4 \pm 3.6x10^3$
Pyroglutamate	$7.1x10^6 \pm 3.4x10^5$	$6.0x10^6 \pm 2.3x10^5$
Serine	$8.2x10^4 \pm 3.6x10^3$	$2.2x10^5 \pm 5.5x10^3$
Spermidine	$2.7x10^4 \pm 1.2x10^3$	$2.3x10^4 \pm 1.1x10^3$
Succinate	$6.8x10^4 \pm 8.9x10^2$	$5.9x10^4 \pm 1.3x10^3$
Threonine	$2.0x10^5 \pm 2.1x10^4$	$2.9x10^5 \pm 2.7x10^4$
Thymine	$3.3x10^4 \pm 8.8x10^2$	$2.5x10^4 \pm 6.2x10^2$

Table S1a continued

Metabolite	½ OD_{max}	
	WT	**Δ262-kb**
Tyrosine	$1.4x10^6 \pm 4.5x10^4$	$6.3x10^5 \pm 3.0x10^4$
UMP	$2.2x10^5 \pm 1.2x10^4$	$1.8x10^5 \pm 1.5x10^4$
Unknown#1169.8-pae-bth_013	$7.4x10^4 \pm 3.9x10^3$	$6.6x10^4 \pm 2.9x10^3$
Unknown#1248.7-cgl-sst_008	$1.2x10^5 \pm 7.5x10^3$	$1.3x10^5 \pm 1.2x10^4$
Unknown#1361.3-pin-mhe_010	$2.9x10^4 \pm 1.3x10^3$	$2.0x10^4 \pm 1.0x10^3$
Unknown#1830.2-pin-mhe_038	$1.6x10^4 \pm 5.4x10^2$	$1.4x10^4 \pm 8.4x10^2$
Unknown#2018.7-pin-mhe_028	$4.0x10^4 \pm 2.2x10^3$	$3.6x10^4 \pm 1.3x10^3$
Unknown#2148.0-pin-mhe_047	$1.5x10^4 \pm 6.3x10^2$	$1.9x10^4 \pm 1.3x10^3$
Unknown#2394.5-pin-mhe_056	$1.7x10^4 \pm 6.0x10^2$	$2.7x10^4 \pm 7.5x10^2$
Unknown#2442.5-pin-mhe_059	n.d.	$2.5x10^4 \pm 1.7x10^3$
Unknown#2548.1-pin-mhe_066	$1.2x10^4 \pm 1.0x10^3$	$9.9x10^3 \pm 1.1x10^3$
Uracil	$5.2x10^4 \pm 1.8x10^3$	$4.7x10^4 \pm 1.7x10^3$
Uric acid	$1.3x10^4 \pm 6.9x10^2$	$5.7x10^3 \pm 2.2x10^2$
Valine	$4.3x10^6 \pm 2.4x10^5$	$3.3x10^6 \pm 2.9x10^5$
Xanthine	$1.7x10^4 \pm 1.1x10^3$	$1.4x10^4 \pm 7.6x10^2$

Table S1b Normalized peak areas of intracellularly detected metabolites of the wild-type and Δ262-kb mutant strain at OD_{max} with casamino acids as carbon source (cultivation in process-controlled bioreactors). Normalized peak areas are listed with corresponding standard error for all identified metabolites detectable at least in one of both strains. n.d.: not detected. Cultivation and sampling were performed by the working group of Ralf Rabus (ICBM).

Metabolite	OD_{max}	
	WT	Δ262-kb
2,4-diaminobutanoate	$5.3x10^4 \pm 6.3x10^3$	$1.6x10^4 \pm 3.8x10^3$
2,6-diamino-pimelate	$1.7x10^5 \pm 2.3x10^4$	$3.6x10^4 \pm 4.4x10^3$
2-aminoadipic-acid	$1.4x10^5 \pm 6.9x10^3$	$3.6x10^4 \pm 2.3x10^3$
2-isopropylmalic acid	$3.4x10^4 \pm 3.6x10^3$	$5.2x10^3 \pm 2.8x10^2$
2-oxoglutarate	$8.4x10^3 \pm 8.7x10^2$	$8.4x10^3 \pm 6.4x10^2$
3-hydroxybutanoate	$1.8x10^4 \pm 2.8x10^3$	$4.1x10^4 \pm 2.4x10^3$
3-hydroxy-decanoate	$9.4x10^3 \pm 7.8x10^2$	$8.4x10^3 \pm 3.9x10^2$
5-aminopentanoic-acid	$3.8x10^6 \pm 5.9x10^5$	$1.1x10^6 \pm 1.2x10^5$
Adenine	$8.3x10^4 \pm 5.4x10^3$	$6.1x10^4 \pm 3.6x10^3$
Alanine	$7.7x10^6 \pm 7.1x10^5$	$2.9x10^6 \pm 3.3x10^5$
Alanyl-alanine	$4.0x10^5 \pm 2.7x10^4$	$1.6x10^5 \pm 7.5x10^3$
AMP	$6.6x10^5 \pm 3.1x10^4$	$5.1x10^5 \pm 2.3x10^4$
Arginine	$9.1x10^3 \pm 6.3x10^2$	$1.1x10^4 \pm 8.3x10^2$
Asparagine	$1.4x10^4 \pm 1.4x10^3$	$2.1x10^4 \pm 1.3x10^3$
Aspartate	$3.6x10^6 \pm 7.6x10^5$	$1.0x10^6 \pm 1.3x10^5$
Cadaverine	$1.4x10^6 \pm 3.4x10^5$	$8.1x10^5 \pm 6.9x10^4$
Cis-vaccenic acid	$2.0x10^4 \pm 3.5x10^3$	$1.3x10^4 \pm 9.9x10^2$
Citrate	$3.7x10^4 \pm 2.3x10^3$	$3.8x10^4 \pm 4.4x10^3$
Cysteine	$1.1x10^3 \pm 1.1x10^3$	$1.8x10^4 \pm 3.9x10^3$
Cysteinyl-glycine	$1.0x10^5 \pm 8.4x10^3$	$6.4x10^4 \pm 3.0x10^3$
Cytosine	$8.2x10^4 \pm 5.3x10^3$	$6.3x10^4 \pm 4.1x10^3$
D200302_2009.31	n.d.	$5.1x10^4 \pm 3.3x10^3$
Ethanolamine	$2.9x10^4 \pm 2.6x10^3$	$6.4x10^4 \pm 6.6x10^3$
Fumarate	$5.0x10^4 \pm 4.1x10^3$	$3.6x10^4 \pm 1.8x10^3$
Glucose	$7.5x10^4 \pm 3.2x10^3$	$4.2x10^4 \pm 3.0x10^3$
Glutamate	$3.3x10^7 \pm 3.0x10^6$	$2.9x10^7 \pm 2.0x10^6$
Glutamine	$9.6x10^5 \pm 1.1x10^5$	$4.9x10^5 \pm 7.2x10^4$
Glutarate	$2.6x10^4 \pm 2.4x10^3$	$7.7x10^3 \pm 5.3x10^2$
Glycerate	$3.0x10^3 \pm 3.0x10^2$	$4.7x10^3 \pm 3.5x10^2$
Glycerol-3-phosphate	$2.0x10^5 \pm 2.1x10^4$	$2.1x10^5 \pm 2.2x10^4$
Glycerophosphoglycerol	$2.9x10^4 \pm 4.1x10^3$	$4.2x10^4 \pm 5.2x10^3$
Glycine	$6.0x10^5 \pm 8.7x10^4$	$4.4x10^5 \pm 3.9x10^4$

Table S1b continued

Metabolite	OD_{max}	
	WT	**Δ262-kb**
Glycylglycine	$1.6x10^4 \pm 1.9x10^3$	$7.8x10^4 \pm 1.5x10^4$
Glycyl-proline	n.d.	$7.0x10^4 \pm 4.1x10^3$
GMP	$5.0x10^4 \pm 3.5x10^3$	$4.9x10^4 \pm 2.7x10^3$
Guanine	$1.8x10^4 \pm 1.7x10^3$	$1.7x10^4 \pm 8.8x10^2$
Histidine	$3.7x10^4 \pm 2.9x10^3$	$3.5x10^4 \pm 4.8x10^3$
Homoserine	$2.2x10^4 \pm 4.3x10^3$	n.d.
Isoleucine	$1.1x10^6 \pm 1.1x10^5$	$1.6x10^5 \pm 2.0x10^4$
Leucine	$1.2x10^6 \pm 9.8x10^4$	$2.0x10^5 \pm 3.0x10^4$
Lysine	$2.4x10^5 \pm 1.7x10^4$	$5.8x10^5 \pm 6.2x10^4$
Malate	$7.0x10^4 \pm 8.1x10^3$	$2.9x10^4 \pm 1.8x10^3$
Methionine	$1.4x10^5 \pm 2.0x10^4$	$5.5x10^4 \pm 6.9x10^3$
NA_1703.1	$1.1x10^4 \pm 1.1x10^3$	$3.2x10^4 \pm 4.8x10^3$
NA199017_1996.71	$4.8x10^4 \pm 2.4x10^3$	$1.4x10^4 \pm 2.3x10^3$
NA261	$7.8x10^4 \pm 1.1x10^4$	$8.5x10^4 \pm 8.2x10^3$
NA714	n.d.	$1.0x10^6 \pm 6.0x10^4$
N-acetyl-glutamate	$1.2x10^4 \pm 5.2x10^2$	$1.3x10^4 \pm 1.4x10^3$
Nicotinamide	$1.5x10^5 \pm 1.1x10^4$	$1.3x10^5 \pm 1.0x10^4$
Octadecanoate	$7.0x10^3 \pm 5.5x10^2$	$6.3x10^3 \pm 3.9x10^2$
Ornithine	$4.0x10^4 \pm 2.7x10^3$	$3.3x10^4 \pm 2.5x10^3$
Phenylalanine	$3.8x10^5 \pm 3.6x10^4$	$1.1x10^5 \pm 9.5x10^3$
Phosphate-monomethyl ester	$2.9x10^4 \pm 1.6x10^3$	$2.6x10^4 \pm 2.9x10^3$
Pipecolate	$1.7x10^6 \pm 9.3x10^4$	$8.0x10^6 \pm 4.5x10^5$
Proline	$4.2x10^5 \pm 1.4x10^4$	$1.8x10^5 \pm 5.4x10^4$
Putrescine	$2.3x10^4 \pm 2.5x10^3$	$9.4x10^3 \pm 8.0x10^2$
Pyroglutamate	$4.3x10^6 \pm 4.7x10^5$	$3.0x10^6 \pm 2.4x10^5$
Pyruvate	$5.5x10^3 \pm 5.5x10^2$	$2.6x10^3 \pm 8.2x10^2$
Serine	$6.6x10^4 \pm 6.1x10^3$	$2.3x10^4 \pm 1.9x10^3$
Succinate	$5.6x10^4 \pm 3.4x10^3$	$4.4x10^4 \pm 2.3x10^3$
Threonine	$1.8x10^5 \pm 1.8x10^4$	$2.4x10^5 \pm 3.7x10^4$
Thymine	$3.4x10^4 \pm 1.8x10^3$	$2.5x10^4 \pm 1.2x10^3$
Tyrosine	$2.1x10^6 \pm 1.1x10^5$	$5.1x10^5 \pm 5.4x10^4$
UMP	$2.1x10^5 \pm 1.3x10^4$	$1.1x10^5 \pm 8.8x10^3$
Unknown#1169.8-pae-bth_013	$4.6x10^4 \pm 4.9x10^3$	$4.6x10^4 \pm 3.7x10^3$
Unknown#1248.7-cgl-sst_008	$1.0x10^5 \pm 1.2x10^4$	$8.2x10^4 \pm 7.1x10^3$
Unknown#1830.2-pin-mhe_038	$1.3x10^5 \pm 9.1x10^3$	$9.0x10^4 \pm 6.8x10^3$
Unknown#2148.0-pin-mhe_047	$8.4x10^3 \pm 8.0x10^2$	$1.5x10^4 \pm 9.6x10^2$
Unknown#2260-cgl-sst_001	$1.3x10^5 \pm 1.3x10^4$	n.d.

Table S1b continued

Metabolite	OD_{max}	
	WT	**Δ262-kb**
Unknown#2394.5-pin-mhe_056	$2.4x10^4 \pm 1.4x10^3$	$3.1x10^4 \pm 9.0x10^2$
Unknown#2442.5-pin-mhe_059	$3.0x10^4 \pm 2.2x10^3$	$4.9x10^4 \pm 5.2x10^3$
Unknown#2548.1-pin-mhe_066	$1.1x10^4 \pm 1.5x10^3$	$1.4x10^4 \pm 1.3x10^3$
Unknown#2557.6-pin-mhe_067	$2.6x10^4 \pm 4.5x10^3$	$1.7x10^5 \pm 1.1x10^4$
Uracil	$4.0x10^4 \pm 2.5x10^3$	$3.6x10^4 \pm 3.0x10^3$
Uric acid	$7.5x10^3 \pm 6.5x10^2$	$8.6x10^3 \pm 8.0x10^2$
Valine	$5.6x10^6 \pm 5.7x10^5$	$4.6x10^6 \pm 2.0x10^5$
Xanthine	$1.2x10^4 \pm 8.4x10^2$	$1.4x10^4 \pm 1.7x10^3$

Table S2a Normalized peak areas of extracellularly detected metabolites of the wild-type strain and of Δ262-kb mutant strain at ½ OD_{max} with casamino acids as carbon source (cultivation in process-controlled bioreactors). Normalized peak areas are listed with corresponding standard error for all identified metabolites detectable at least in one of both strains. n.d.: not detected

Metabolite	½ OD_{max}	
	WT	Δ262-kb
2-amino-2-methylpropane-1,3-diol	$3.2x10^5 \pm 6.8x10^3$	$1.9x10^5 \pm 1.5x10^4$
2-oxoisovaleric acid	$6.4x10^3 \pm 4.7x10^2$	n.d.
Alanine	$6.4x10^6 \pm 3.5x10^5$	$2.7x10^6 \pm 3.3x10^5$
Arginine	$3.8x10^4 \pm 1.6x10^3$	$3.0x10^4 \pm 2.2x10^3$
Aspartate	$3.6x10^5 \pm 1.2x10^4$	$7.6x10^3 \pm 2.7x10^3$
Glutamate	$3.0x10^6 \pm 4.2x10^4$	$1.7x10^6 \pm 2.0x10^5$
Glycerol	$5.2x10^4 \pm 2.7x10^4$	n.d.
Glycine	$2.5x10^6 \pm 1.5x10^5$	$7.5x10^3 \pm 2.5x10^3$
Histidine	$3.3x10^4 \pm 8.3x10^2$	$1.1x10^4 \pm 6.6x10^3$
Isoleucine	$2.8x10^6 \pm 8.8x10^4$	$1.8x10^6 \pm 7.1x10^4$
Leucine	$3.3x10^6 \pm 1.4x10^5$	$2.0x10^6 \pm 9.8x10^4$
Lysine	$3.0x10^6 \pm 3.3x10^4$	$2.6x10^6 \pm 1.2x10^5$
Methionine	$4.5x10^5 \pm 9.7x10^3$	$3.0x10^5 \pm 1.5x10^4$
N-acetyl-putrescine	$3.4x10^4 \pm 1.1x10^4$	n.d.
Phenylalanine	$1.4x10^6 \pm 1.7x10^4$	$9.3x10^5 \pm 5.8x10^4$
Pipecolate	n.d.	$5.2x10^4 \pm 4.4x10^3$
Proline	$1.6x10^7 \pm 5.0x10^5$	$9.1x10^6 \pm 5.8x10^5$
Pyroglutamate	$3.9x10^6 \pm 9.1x10^4$	$3.0x10^6 \pm 1.9x10^5$
Serine	$3.9x10^5 \pm 9.7x10^3$	$2.7x10^5 \pm 1.4x10^4$
Threonine	$2.4x10^5 \pm 1.3x10^4$	$1.7x10^5 \pm 3.9x10^3$
Tyrosine	$3.4x10^6 \pm 6.0x10^4$	$2.4x10^6 \pm 1.3x10^5$
Urea	$1.8x10^4 \pm 5.1x10^2$	$1.6x10^4 \pm 1.8x10^3$
Valine	$4.5x10^6 \pm 1.4x10^5$	$3.5x10^6 \pm 8.0x10^4$

Table S2b Normalized peak areas of extracellularly detected metabolites of the wild-type strain and of Δ262-kb mutant strain at OD_{max} with casamino acids as carbon source (cultivation in process-controlled bioreactors). Normalized peak areas are listed with corresponding standard error for all identified metabolites detectable at least in one of both strains. n.d.: not detected

Metabolite	OD_{max}	
	WT	Δ262-kb
2-amino-2-methylpropane-1,3-diol	$2.3x10^5 \pm 1.4x10^4$	$5.4x10^4 \pm 2.8x10^3$
2-isopropylmalic acid	$2.9x10^4 \pm 1.1x10^3$	$1.3x10^4 \pm 1.6x10^2$
2-oxo-isocaproic-acid	$1.8x10^4 \pm 4.6x10^2$	n.d.
2-oxoisovaleric acid	$1.8x10^4 \pm 9.4x10^2$	n.d.
3-methyl-2-oxopentanoic-acid	$1.5x10^4 \pm 5.8x10^2$	n.d.
Alanine	$4.7x10^6 \pm 2.5x10^5$	n.d.
Arginine	$2.9x10^4 \pm 1.4x10^3$	$1.5x10^4 \pm 8.0x10^2$
Aspartate	$2.3x10^4 \pm 3.2x10^3$	n.d.
Ethanolamine	n.d.	n.d.
Glutamate	$1.6x10^6 \pm 1.8x10^5$	$1.3x10^4 \pm 4.5x10^3$
Glycine	$7.5x10^4 \pm 3.9x10^4$	n.d.
Histidine	$2.2x10^4 \pm 2.6x10^3$	n.d.
Isoleucine	$2.7x10^6 \pm 6.4x10^4$	$3.9x10^5 \pm 8.8x10^4$
Leucine	$2.7x10^6 \pm 7.6x10^4$	$4.9x10^5 \pm 6.2x10^4$
Lysine	$2.4x10^6 \pm 6.7x10^4$	$1.3x10^6 \pm 9.1x10^4$
Methionine	$3.2x10^5 \pm 7.9x10^3$	$3.5x10^4 \pm 7.0x10^3$
N-acetyl-putrescine	$4.6x10^4 \pm 1.5x10^3$	n.d.
Phenylalanine	$1.2x10^6 \pm 4.1x10^4$	$2.3x10^5 \pm 3.7x10^4$
Pipecolate	$4.1x10^4 \pm 2.6x10^3$	$1.9x10^5 \pm 1.1x10^4$
Proline	$1.2x10^7 \pm 5.7x10^5$	$9.5x10^5 \pm 3.5x10^5$
Pyroglutamate	$3.3x10^6 \pm 6.6x10^4$	$1.5x10^6 \pm 7.8x10^4$
Serine	$3.6x10^5 \pm 7.8x10^3$	n.d.
Threonine	$2.1x10^5 \pm 6.9x10^3$	$5.0x10^4 \pm 6.2x10^3$
Tyrosine	$3.0x10^6 \pm 4.9x10^4$	$6.9x10^5 \pm 9.2x10^4$
Urea	$5.4x10^4 \pm 4.1x10^3$	$2.9x10^4 \pm 2.3x10^3$
Valine	$4.5x10^6 \pm 8.3x10^4$	$1.3x10^6 \pm 1.6x10^5$

Table S2c Normalized peak areas of extracellularly detected compounds in the casamino acids medium (cultivation in process-controlled bioreactors). Normalized peak areas are listed with corresponding standard error for all identified compounds detected in the medium prior to inoculation.

Metabolite	**medium**
2-amino-2-methylpropane-1,3-diol	$3.6x10^5 \pm 2.4x10^4$
Alanine	$6.4x10^6 \pm 8.3x10^5$
Arginine	$4.1x10^4 \pm 1.8x10^3$
Aspartate	$4.8x10^5 \pm 1.6x10^4$
Ethanolamine	$2.4x10^4 \pm 5.9x10^2$
Glutamate	$3.5x10^6 \pm 9.6x10^4$
Glycerol	$2.4x10^5 \pm 7.3x10^4$
Glycine	$2.9x10^6 \pm 6.0x10^4$
Histidine	$5.4x10^4 \pm 5.6x10^3$
Isoleucine	$2.9x10^6 \pm 4.6x10^4$
Leucine	$3.7x10^6 \pm 4.9x10^4$
Lysine	$3.5x10^6 \pm 4.3x10^4$
Methionine	$5.5x10^5 \pm 9.7x10^3$
Phenylalanine	$1.5x10^6 \pm 1.9x10^4$
Proline	$1.8x10^7 \pm 3.0x10^5$
Pyroglutamate	$4.2x10^6 \pm 6.4x10^4$
Serine	$4.1x10^5 \pm 4.9x10^3$
Threonine	$2.6x10^5 \pm 5.0x10^3$
Tyrosine	$3.7x10^6 \pm 4.3x10^4$
Valine	$4.7x10^6 \pm 5.1x10^4$

Table S3 Fold changes of intracellularly detected metabolites of the Δ262-kb mutant strain compared to the wild-type strain at ½ OD_{max} and OD_{max} with casamino acids as carbon source (cultivation in process-controlled bioreactors). Fold changes were determined with normalized peak areas and are listed with corresponding standard error. Significance was calculated with Wilcoxon-Mann-Whitney test. Metabolites only detected in the Δ262-kb mutant strain are listed with "+" and metabolites only detected in the wild-type strain with n.d. (not detected). Metabolites detected in none of both strains are listed with "-".

Metabolite	½ OD_{max}		OD_{max}	
	Fold change	p-value	Fold change	p-value
2,4-diaminobutanoate	1.37 ± 0.07	0.0001554	0.30 ± 0.08	0.0001554
2,6-diamino-pimelate	1.31 ± 0.09	0.00109	0.21 ± 0.04	0.0001554
2-aminoadipic-acid	0.12 ± 0.02	0.0001554	0.27 ± 0.02	0.0001554
2-isopropylmalic acid	0.50 ± 0.04	0.0001554	0.15 ± 0.02	0.0001554
2-oxoglutarate	0.91 ± 0.06	0.16053	1.00 ± 0.13	0.95913
3-aminoisobutanoate	1.13 ± 0.17	0.57374	-	-
3-hydroxybutanoate	1.52 ± 0.12	0.0006216	2.27 ± 0.38	0.0001554
3-hydroxy-decanoate	0.92 ± 0.08	0.64538	0.90 ± 0.09	0.38228
3-phosphoglycerate	1.69 ± 0.12	0.0001554	-	-
5-aminopentanoic-acid	1.46 ± 0.13	0.0001554	0.28 ± 0.06	0.0006216
6-phospho-gluconate	0.84 ± 0.13	0.13038	-	-
Adenine	0.77 ± 0.03	0.0001554	0.73 ± 0.06	0.03792
Alanine	0.81 ± 0.13	0.06496	0.38 ± 0.06	0.0001554
Alanylalanine	-	-	0.41 ± 0.03	0.0001554
AMP	1.00 ± 0.04	0.64538	0.78 ± 0.05	0.00109
Arginine	1.34 ± 0.07	0.0006216	1.16 ± 0.12	0.2345
Asparagine	1.53 ± 0.11	0.0001554	1.47 ± 0.17	0.00466
Aspartate	1.18 ± 0.11	0.13038	0.28 ± 0.07	0.00699
Beta-alanine	0.61 ± 0.10	0.00699	-	-
Cadaverine	6.64 ± 1.87	0.0001554	0.57 ± 0.14	0.04988
Cis-vaccenic acid	0.99 ± 0.13	0.95913	0.63 ± 0.12	0.27863
Citrate	1.59 ± 0.09	0.0001554	1.04 ± 0.14	0.7209
Cysteine	0.66 ± 0.20	0.27863	16.9 ± 17.3	0.0006216
Cysteinylglycine	0.91 ± 0.11	0.4418	0.63 ± 0.06	0.00295
Cytosine	0.85 ± 0.06	0.03792	0.77 ± 0.07	0.04988
D200302_2009.31	+	0.0001554	+	0.0001554
D-glucosaminate	0.52 ± 0.05	0.0001554	-	-
Ethanolamine	1.87 ± 0.12	0.0001554	2.20 ± 0.30	0.0006216

Table S3: continued

Metabolite	½ OD_{max}		OD_{max}	
	Fold change	p-value	Fold change	p-value
Fructose-1,6-bisphosphate	0.94 ± 0.17	0.7209	-	-
Fumarate	0.83 ± 0.03	0.0001554	0.72 ± 0.07	0.01041
Glucose	0.76 ± 0.03	0.0001554	0.56 ± 0.05	0.0001554
Glucose-6-phosphate	0.84 ± 0.06	0.06496	-	-
Glutamate	0.96 ± 0.02	0.19487	0.86 ± 0.10	0.4418
Glutamine	0.85 ± 0.09	0.16053	0.51 ± 0.09	0.00699
Glutarate	0.82 ± 0.05	0.02067	0.30 ± 0.03	0.0001554
Glycerate	-	-	1.56 ± 0.19	0.00466
Glycerol-3-phosphate	1.20 ± 0.10	0.19487	1.05 ± 0.16	0.87848
Glycerophosphoglycerol	1.09 ± 0.07	0.04988	1.43 ± 0.27	0.04988
Glycine	0.93 ± 0.06	0.2345	0.74 ± 0.12	0.08298
Glycylglycine	0.52 ± 0.12	0.00466	4.90 ± 1.11	0.0001554
Glycylproline	5.00 ± 1.30	0.0001554	+	0.0001554
GMP	1.08 ± 0.04	0.04988	0.99 ± 0.09	0.79845
Guanine	0.90 ± 0.06	0.2345	0.93 ± 0.10	0.64538
Histidine	1.51 ± 0.10	0.0003108	0.95 ± 0.15	0.7209
Homoserine	-	-	n.d.	0.0001554
Isoleucine	0.85 ± 0.07	0.03792	0.15 ± 0.03	0.0001554
Leucine	0.78 ± 0.08	0.02813	0.17 ± 0.03	0.0001554
Lysine	1.15 ± 0.05	0.00466	2.38 ± 0.31	0.0001554
Malate	0.74 ± 0.03	0.0001554	0.42 ± 0.05	0.0001554
Methionine	0.87 ± 0.15	0.32821	0.38 ± 0.07	0.00186
NA_1703.1	2.22 ± 0.21	0.0001554	2.79 ± 0.50	0.00699
NA_1705.1	0.85 ± 0.10	0.2345	-	-
NA199017_1996.71	0.79 ± 0.06	0.00466	0.29 ± 0.05	0.0001554
NA261	1.11 ± 0.08	0.16053	1.09 ± 0.18	0.87848
NA714	+	0.0001554	+	0.0001554
N-acetyl-glutamate	1.02 ± 0.09	0.7209	1.12 ± 0.13	0.57374
Nicotinamide	0.80 ± 0.04	0.00109	0.88 ± 0.09	0.16053
Octadecanoate	-	-	0.90 ± 0.09	0.16053
Ornithine	1.64 ± 0.15	0.0001554	0.82 ± 0.08	0.13038
Phenylalanine	1.08 ± 0.06	0.38228	0.28 ± 0.04	0.0001554
Phosphate-monomethyl ester	1.28 ± 0.05	0.0003108	0.87 ± 0.11	0.50536
Phosphoenolpyruvate	4.62 ± 0.69	0.0001554	-	-
Pipecolate	3.48 ± 0.13	0.0001554	4.86 ± 0.39	0.0001554
Proline	0.78 ± 0.12	0.19487	0.44 ± 0.13	0.02067

Table S3: continued

Metabolite	½ OD_{max}		OD_{max}	
	Fold change	p-value	Fold change	p-value
Putrescine	0.46 ± 0.06	0.0001554	0.41 ± 0.06	0.0006216
Pyroglutamate	0.85 ± 0.05	0.01476	0.71 ± 0.10	0.06496
Pyruvate	-	-	0.47 ± 0.16	0.02036
Serine	2.68 ± 0.13	0.0001554	0.35 ± 0.04	0.0001554
Spermidine	0.83 ± 0.05	0.02067	-	-
Succinate	0.86 ± 0.02	0.0001554	0.78 ± 0.06	0.01041
Threonine	1.43 ± 0.20	0.08298	1.34 ± 0.25	0.19487
Thymine	0.78 ± 0.03	0.0001554	0.75 ± 0.05	0.00186
Tyrosine	0.46 ± 0.03	0.0001554	0.25 ± 0.03	0.0001554
UMP	0.86 ± 0.09	0.1049	0.51 ± 0.05	0.0001554
Unknown#1169.8-pae-bth_013	0.89 ± 0.06	0.13038	1.01 ± 0.14	0.79845
Unknown#1248.7-cgl-sst_008	1.13 ± 0.12	0.32821	0.81 ± 0.12	0.50536
Unknown#1361.3-pin-mhe_010	0.67 ± 0.05	0.0003108	-	-
Unknown#1830.2-pin-mhe_038	0.86 ± 0.06	0.00699	0.69 ± 0.07	0.0006216
Unknown#2018.7-pin-mhe_028	0.91 ± 0.06	0.19487	-	-
Unknown#2148.0-pin-mhe_047	1.25 ± 0.10	0.00699	1.80 ± 0.21	0.0001554
Unknown#2260-cgl-sst_001	-	-	n.d.	0.0001554
Unknown#2394.5-pin-mhe_056	1.55 ± 0.07	0.0001554	1.28 ± 0.08	0.00186
Unknown#2442.5-pin-mhe_059	+	0.0001554	1.63 ± 0.21	0.00186
Unknown#2548.1-pin-mhe_066	0.82 ± 0.11	0.1049	1.34 ± 0.23	0.16053
Unknown#2557.6-pin-mhe_067	-	-	6.74 ± 1.26	0.0001554
Uracil	0.91 ± 0.05	0.16053	0.90 ± 0.09	0.27863
Uric acid	0.45 ± 0.03	0.0001554	1.16 ± 0.15	0.32821
Valine	0.78 ± 0.08	0.1049	0.82 ± 0.09	0.16053
Xanthine	0.82 ± 0.07	0.03792	1.21 ± 0.17	0.32821

Table S4 Expression levels of genes involved in dipeptide transport.

Locus tag	Enzyme function	WT		Δ262-kb	
		½ OD_{max}	OD_{max}	½ OD_{max}	OD_{max}
PGA1_262p01000	dipeptide transport ATP-binding protein DppF	72	36	0	0
PGA1_262p01010	dipeptide transport ATP-binding protein DppD	30	6	0	0
PGA1_262p01020	dipeptide transport system permease DppC	31	6	0	0
PGA1_262p01030	dipeptide transport system permease DppB	36	5	0	0
PGA1_262p01040	periplasmic dipeptide transport protein precursor (dipeptide-binding protein)	319	8	0	0

Table S5 Amino acid concentrations for the wild-type strain and the Δ262-kb mutant strain at ½ OD_{max} and OD_{max} in the casamino acid medium (cultivation in process-controlled bioreactors). Amino acid concentrations in mmol L^{-1} in medium prior to inoculation and at ½ OD_{max} and OD_{max} are listed with corresponding standard deviation.

Amino acid	medium	WT		Δ262-kb	
		½ OD_{max}	OD_{max}	½ OD_{max}	OD_{max}
Aspartate	2.19 ± 0.07	1.64 ± 0.02	0.03 ± 0.03	0.00 ± 0.00	0.00 ± 0.00
Glutamate	7.55 ± 0.27	6.59 ± 0.12	3.74 ± 0.70	4.32 ± 0.40	0.01 ± 0.00
Serine	1.49 ± 0.06	1.39 ± 0.03	1.30 ± 0.09	0.98 ± 0.07	0.04 ± 0.02
Glycine	2.80 ± 0.09	2.31 ± 0.04	0.11 ± 0.10	0.00 ± 0.00	0.01 ± 0.00
Threonine	1.87 ± 0.06	1.76 ± 0.04	1.67 ± 0.10	1.29 ± 0.08	0.32 ± 0.08
Histidine	0.99 ± 0.03	0.94 ± 0.02	0.88 ± 0.06	0.76 ± 0.04	0.24 ± 0.04
Alanine	8.33 ± 0.28	7.43 ± 0.17	6.20 ± 0.54	3.73 ± 0.69	0.01 ± 0.00
Arginine	1.57 ± 0.06	1.34 ± 0.03	1.09 ± 0.09	1.24 ± 0.07	0.80 ± 0.03
Tyrosine	1.92 ± 0.07	1.74 ± 0.03	1.72 ± 0.12	1.39 ± 0.09	0.53 ± 0.10
Valine	4.36 ± 0.14	4.09 ± 0.10	4.20 ± 0.27	3.25 ± 0.18	1.24 ± 0.19
Methionine	1.31 ± 0.05	1.09 ± 0.03	0.78 ± 0.06	0.75 ± 0.06	0.14 ± 0.04
Isoleucine	2.31 ± 0.05	2.17 ± 0.06	2.24 ± 0.15	1.56 ± 0.19	0.38 ± 0.10
Phenylalanine	2.04 ± 0.08	1.83 ± 0.04	1.66 ± 0.11	1.32 ± 0.10	0.35 ± 0.09
Leucine	4.54 ± 0.15	4.00 ± 0.09	3.54 ± 0.25	2.71 ± 0.20	0.64 ± 0.12
Lysine	3.66 ± 0.28	3.30 ± 0.22	2.77 ± 0.28	3.33 ± 0.25	2.03 ± 0.11
Proline	9.62 ± 0.62	8.39 ± 0.52	6.63 ± 0.59	5.76 ± 0.64	0.74 ± 0.46

Table S6 Expression levels of selected transcripts with relations to differences in metabolome. Shown are expression levels (Rockhopper) for the wild-type and the Δ262-kb mutant strain at ½ OD_{max} and OD_{max} for selected genes.

Locus tag	Enzyme function	WT		Δ262-kb	
		½ OD_{max}	OD_{max}	½ OD_{max}	OD_{max}
PGA1_c10280	Isovaleryl-CoA Dehydrogenase	555	58	212	309
PGA1_c10300	Acetyl-CoA Synthetase AcsA	30	5	32	39
PGA1_c10320	Methylcrotonyl-CoA carboxylase	88	14	98	70
PGA1_c11320	3-Hydroxyacyl-CoA dehydrogenase	108	11	88	75
PGA1_c13580	secretion protein, HlyD family	2	1	46	294
PGA1_c13590	ABC transporter ATP-binding protein	10	10	77	1062
PGA1_c13600	hypothetical protein	22	12	67	1059
PGA1_c13610	hypothetical protein	5	3	16	440
PGA1_c13630	hypothetical protein	4	3	25	298
PGA1_c13640	hypothetical protein	10	4	42	523
PGA1_c13650	hypothetical protein	5	3	23	256
PGA1_c13660	hypothetical protein	4	2	18	203
PGA1_c13670	hypothetical protein	6	9	14	213
PGA1_c13680	hypothetical protein	2	1	8	127
PGA1_c13690	hypothetical protein	5	3	17	326
PGA1_c13700	hypothetical protein	13	8	34	786
PGA1_c13710	diaminopimelate decarboxylase-like protein	12	9	34	811
PGA1_c13720	hypothetical protein	7	4	17	328
PGA1_c13730	hypothetical protein	6	4	15	245
PGA1_c13740	long-chain-fatty-acid- CoA ligase IcfB	5	4	15	285
PGA1_c13750	phosphopantetheine binding protein	16	12	34	608

Table S6: continued

Locus tag	Enzyme function	WT		Δ262-kb	
		½ OD_{max}	OD_{max}	½ OD_{max}	OD_{max}
PGA1_c13760	D-alanine--poly(phosphoribitol) ligase subunit	4	2	9	113
PGA1_c13770	cytochrome P450	19	13	41	828
PGA1_c13780	D-alanine--poly(phosphoribitol) ligase subunit	10	9	21	423
PGA1_c13790	hypothetical protein	9	8	16	273
PGA1_c13800	alkanesulfonate monooxygenase	32	29	56	1167
PGA1_c13810	long-chain specific acyl-CoA dehydrogenase	32	37	43	431
PGA1_c13820	4'-phosphopantetheinyl transferase-like protein	2	3	4	21
PGA1_c13830	hypothetical protein	3	3	41	560
PGA1_c15730	phosphate regulon transcriptional regulatory protein PhoB	89	82	78	606
PGA1_c15740	phosphate transport system protein PhoU	63	55	58	443
PGA1_c15750	phosphate import ATP-binding protein PstB	139	133	151	1057
PGA1_c15760	phosphate transport system permease protein PstA	35	31	31	365
PGA1_c15770	phosphate transport system permease protein PstC	20	13	11	210
PGA1_c15790	phosphate transporter, phosphate-binding protein	139	115	78	6865
PGA1_c15800	phosphate regulon sensor protein phoR-like protein	25	20	20	82
PGA1_c17070	acetyltransferase domain-containing protein	13	19	15	994
PGA1_c17340	acyl-CoA dehydrogenase AcdA	291	42	203	310
PGA1_c17350	3-hydroxyisobutyryl-CoA hydrolase	279	59	223	307
PGA1_c17360	3-hydroxyisobutyrate dehydrogenase	77	22	75	122
PGA1_c18210	phage late control gene D protein (GPD)	1	2	2	10
PGA1_c18220	phage tail protein X	1	3	3	11
PGA1_c18230	phage-related tail protein (gpU)	0	1	2	10

Table S6: continued

Locus tag	Enzyme function	WT		Δ262-kb	
		½ OD_{max}	OD_{max}	½ OD_{max}	OD_{max}
PGA1_c18240	phage tail tape measure protein	1	2	4	17
PGA1_c18250	hypothetical protein	6	8	13	238
PGA1_c18260	phage major tail tube protein	0	1	2	57
PGA1_c18270	major tail sheath protein	0	0	1	39
PGA1_c18280	hypothetical protein	3	5	4	21
PGA1_c18290	hypothetical protein	5	7	6	51
PGA1_c18300	hypothetical protein	8	11	13	85
PGA1_c18310	hypothetical protein	6	9	10	47
PGA1_c18320	phage tail protein I	2	3	5	25
PGA1_c18330	baseplate assembly protein J	0	1	1	9
PGA1_c18340	baseplate assembly protein W	1	1	1	13
PGA1_c18350	baseplate assembly protein V	2	3	4	12
PGA1_c18360	hypothetical protein	6	6	8	23
PGA1_c18370	hypothetical protein	1	1	3	11
PGA1_c18380	hypothetical protein	1	1	2	20
PGA1_c18390	hypothetical protein	10	13	13	437
PGA1_c18400	peptidase U35, phage prohead HK97-like protein	1	2	3	143
PGA1_c18410	phage portal protein, lambda family	0	0	2	18
PGA1_c18420	hypothetical protein	0	0	1	19
PGA1_c18430	phage terminase large subunit (GpA)	0	1	2	5
PGA1_c18440	terminase small subunit	2	3	5	15
PGA1_c18450	hypothetical protein	0	0	1	17

Table S6: continued

Locus tag	Enzyme function	WT		Δ262-kb	
		½ OD_{max}	OD_{max}	½ OD_{max}	OD_{max}
PGA1_c18460	hypothetical protein	0	0	1	14
PGA1_c18470	hypothetical protein	0	0	1	7
PGA1_c18480	hypothetical protein	107	48	142	73
PGA1_c18490	hypothetical protein	144	87	207	119
PGA1_c18500	hypothetical protein	1	1	3	20
PGA1_c18510	hypothetical protein	4	3	6	62
PGA1_c18520	hypothetical protein	3	4	7	73
PGA1_c18530	hypothetical protein	5	5	10	115
PGA1_c18540	hypothetical protein	3	4	5	60
PGA1_c18550	hypothetical protein	1	1	4	35
PGA1_c18560	hypothetical protein	1	1	5	30
PGA1_c22710	Acyl-CoA Dehydrogenase	1	2	1106	1192
PGA1_c32550	phenylacetate-CoA ligase PaaK	76	84	102	310
PGA1_c32560	high-affinity branched-chain amino acid transport ATP-binding protein	48	57	74	203
PGA1_c32570	branched-chain amino acid transport system	76	86	124	387
PGA1_c32580	high-affinity branched-chain amino acid transport permease	45	63	67	244
PGA1_c32610	high-affinity branched-chain amino acid transport permease	42	71	60	315
PGA1_c32620	high-affinity branched-chain amino acid transport ATP-binding protein	57	92	88	430
PGA1_c32630	long-chain-fatty-acid--CoA ligase	48	61	90	365
PGA1_c35540	alcohol dehydrogenase AlkJ	40	29	189	150
PGA1_c35550	medium-chain-fatty-acid--CoA ligase AlkK	83	56	559	449

Table S6: continued

Locus tag	Enzyme function	WT		Δ262-kb	
		½ OD_{max}	OD_{max}	½ OD_{max}	OD_{max}
PGA1_c35560	chemotaxis protein MotB-like protein	7	36	23	26
PGA1_c35570	flagellar hook protein FlgE	12	176	16	14
PGA1_c35580	flagellar hook-associated protein FlgK	2	45	5	8
PGA1_c35590	hypothetical protein	20	110	29	42
PGA1_c35600	flagellar P-ring protein FlgI	13	72	14	23
PGA1_c35610	flagellar biosynthetic protein FliP	3	12	6	5
PGA1_c35620	flagellar motor switch protein FliN	19	197	28	40
PGA1_c35630	flagellar biosynthesis protein	11	81	20	29
PGA1_c35640	flagellar M-ring protein FliF	3	52	9	10
PGA1_c35650	flagellar basal body-associated protein FliL	11	127	16	36
PGA1_c35660	hypothetical protein	13	75	16	51
PGA1_c35670	hypothetical protein	4	35	8	12
PGA1_c35680	chemotaxis protein MotA	5	46	11	14
PGA1_c35690	hypothetical protein	8	36	11	19
PGA1_c35700	transglycosylase, SLT family	0	9	2	2
PGA1_c35710	flagellar biosynthetic protein FlhA	3	25	6	7
PGA1_c35720	flagellar biosynthetic protein FliR	2	7	4	4
PGA1_c35730	flagellar biosynthetic protein FlhB	11	34	15	22
PGA1_c35740	hypothetical protein	13	33	17	16
PGA1_c35750	flagellar basal body-associated protein FliL	4	38	8	7
PGA1_c35760	flagellar L-ring protein FlgH	7	75	10	11

Table S6: continued

Locus tag	Enzyme function	WT		Δ262-kb	
		½ OD_{max}	OD_{max}	½ OD_{max}	OD_{max}
PGA1_c35770	flagella basal body P-ring formation protein FlgA	0	14	2	2
PGA1_c35780	flagellar basal-body rod protein FlgG	2	19	3	3
PGA1_c35790	flagellar basal-body rod protein FlgF	3	54	7	7
PGA1_c35800	flagellar biosynthetic protein FliQ	3	40	11	7
PGA1_c35810	flagellar hook-basal body complex protein FliE	3	38	6	6
PGA1_c35820	flagellar basal-body rod protein FlgC	2	55	7	8
PGA1_c35830	flagellar basal-body rod protein FlgB	2	22	4	5
PGA1_c35840	flagellum-specific ATP synthase FliI	14	23	16	25
PGA1_c35850	flagellar biosynthesis repressor FlbT	6	52	10	8
PGA1_c35860	flagellar protein FlaF	9	75	15	11
PGA1_c35870	flagellin	36	653	30	33
PGA1_c35880	FlgN-like protein	13	176	20	21
PGA1_c35890	rod-binding protein	13	158	18	17
PGA1_c35900	flagellar hook-length control protein	6	52	8	53
PGA1_c35910	flagellar hook capping protein	13	92	19	109

Table S7 Expression levels of putative TDA biosynthesis related genes. Shown are expression levels (Rockhopper) for the wild-type and the Δ262-kb mutant strain.

Locus tag	Enzyme function	WT		Δ262-kb	
		½ OD_{max}	OD_{max}	½ OD_{max}	OD_{max}
PGA1_262p00780	NAD dependent epimerase/dehydratase	1668	2546	0	1
PGA1_262p00790	hypothetical protein	0	0	0	0
PGA1_262p00800	phenylacetic acid degradation protein PaaZ	2665	4659	0	4
PGA1_262p00810	flavoprotein, HFCD family	2381	3188	0	1
PGA1_262p00820	hypothetical protein	157	91	0	0
PGA1_262p00830	hypothetical protein	78	82	0	0
PGA1_262p00840	hypothetical protein	3566	6020	0	3
PGA1_262p00850	sodium dependent symporter	1002	1131	0	0
PGA1_262p00860	hypothetical protein	992	1162	0	0
PGA1_262p00870	ABC transporter, extracellular solute-binding protein	1549	2268	0	1
PGA1_262p00880	ABC transporter, integral inner membrane component	314	578	0	0
PGA1_262p00890	ABC transporter, integral inner membrane component	448	641	0	0
PGA1_262p00900	ABC transporter ATP-binding protein	120	175	0	0
PGA1_262p00910	cation transport protein	4279	6255	0	5
PGA1_262p00920	hypothetical protein	5268	9133	0	5
PGA1_262p00930	hypothetical protein	7331	12269	0	7
PGA1_262p00940	acyl-CoA dehydrogenase TdaE	10147	16890	0	9
PGA1_262p00950	thioesterase superfamily protein TdaD	21564	31883	0	25
PGA1_262p00960	prephenate dehydratase TdaC-like protein	6074	13611	0	9

Table S7: continued

Locus tag	Enzyme function	WT		Δ262-kb	
		½ OD_{max}	OD_{max}	½ OD_{max}	OD_{max}
PGA1_262p00970	beta etherase TdaB	2450	1407	0	1
PGA1_262p00980	LysR family transcriptional regulator	1028	3340	0	1
PGA1_262p00990	LysR family transcriptional regulator	14	15	0	0
PGA1_262p01320	hypothetical protein	65	615	0	0
PGA1_262p01330	MarR family transcriptional regulator	45	336	0	0
PGA1_262p01340	hypothetical protein	45	10205	0	2
PGA1_262p01580	metal ion uptake regulator	55	824	0	0
PGA1_262p01590	hypothetical protein	235	3332	0	1
PGA1_262p01890	hypothetical protein	4544	5024	0	3
PGA1_262p01900	hypothetical protein	544	711	0	0
PGA1_262p01910	NADH:flavin oxidoreductase / NADH oxidase	100	262	0	0
PGA1_262p01920	NADH:flavin oxidoreductase / NADH oxidase	34	245	0	0
PGA1_262p01930	ArsR family transcriptional regulator	109	322	0	0
PGA1_262p01940	hypothetical protein	2715	1489	0	1
PGA1_c00840	glutathione transferase-like protein	28	491	15	18
PGA1_c00850	hypothetical protein	61	100	58	1017
PGA1_c00860	cystathionine beta-lyase PatB	285	142	334	201
PGA1_c04030	phenylacetic acid degradation protein paaA-like protein	67	67	41	68
PGA1_c04040	phenylacetic acid degradation NADH oxidoreductase PaaE	320	232	113	206
PGA1_c04050	phenylacetic acid degradation protein PaaD	160	112	75	82
PGA1_c04060	phenylacetic acid degradation protein PaaC	233	203	94	200

Table S7: continued

Locus tag	Enzyme function	WT		Δ262-kb	
		½ OD_{max}	OD_{max}	½ OD_{max}	OD_{max}
PGA1_c04070	phenylacetic acid degradation protein PaaB	168	137	76	162
PGA1_c04080	phenylacetic acid degradation protein PaaA	613	760	367	643
PGA1_c04090	beta-ketoadipyl-CoA thiolase PaaJ	350	333	213	218
PGA1_c07040	LysR family transcriptional regulator	2	3	6	5
PGA1_c07050	methyltransferase domain-containing protein	203	1181	173	292
PGA1_c07600	AsnC/LRP family transcriptional regulator	15	13	16	16
PGA1_c07610	4-hydroxyphenylpyruvate dioxygenase	3863	7041	793	1086
PGA1_c11690	thioesterase domain-containing protein	30	28	33	34
PGA1_c11700	5,10-methylenetetrahydrofolate reductase	201	983	310	445
PGA1_c11710	LysR family transcriptional regulator	46	55	36	52
PGA1_c20730	AsnC family transcriptional regulator	89	46	36	23
PGA1_c20740	uroporphyrinogen-III C-methyltransferase CobA	735	992	71	141
PGA1_c20750	hypothetical protein	1938	2389	232	445
PGA1_c20760	nitrite/sulfite reductase	2360	2881	263	798
PGA1_c20770	phosphoadenosine phosphosulfate reductase	2226	2242	202	605
PGA1_c20780	hypothetical protein	1164	1100	85	282
PGA1_c20790	ferredoxin--NADP reductase Fpr	1612	1475	381	370
PGA1_c22710	acyl-CoA dehydrogenase	1	2	1106	1192

Table S8. Proposed sum formula for intracellularly detected unidentified compounds at ½ OD_{max} and OD_{max} for the wild-type strain and Δ262-kb mutant strain. Predictions were performed with SmartFormula, implemented in DataAnalysis 4.0

Compound	m/z measured	Ion Formula	mSigma	m/z	Sum Formula
[M]269.2_RT464	270.1554	$C_{10}H_{24}NO_7$	14.6	270.1547	$C_{10}H_{23}NO_7$
[M]313.2_RT672	314.1820	$C_{12}H_{28}NO_8$	7.1	314.1809	$C_{12}H_{27}NO_8$
[M]357.2_RT846	358.2072	$C_{14}H_{32}NO_9$	8.6	358.2072	$C_{14}H_{31}NO_9$
[M]401.2_RT995	402.2332	$C_{16}H_{36}NO_{10}$	4.7	402.2334	$C_{16}H_{35}NO_{10}$
[M]445.3_RT1127	446.259	$C_{18}H_{40}NO_{11}$	6.4	446.2596	$C_{18}H_{39}NO_{11}$
[M]489.3_RT1244	490.285	$C_{20}H_{44}NO_{12}$	2.3	490.2858	$C_{20}H_{43}NO_{12}$
[M]533.3_RT1347	534.3109	$C_{22}H_{48}NO_{13}$	15.6	534.312	$C_{22}H_{47}NO_{13}$
[M]577.3_RT1428	578.3358	$C_{24}H_{52}NO_{14}$	4.1	578.3382	$C_{24}H_{51}NO_{14}$
[M]621.4_RT1472	622.3624	$C_{26}H_{56}NO_{15}$	3.4	622.3644	$C_{26}H_{55}NO_{15}$
[M]665.4_RT1501	666.3886	too less abundant			$C_{28}H_{59}NO_{16}$
[M]371.2_RT489	372.1853	$C_{14}H_{30}NO_{10}$	10.7	372.1864	$C_{14}H_{29}NO_{10}$
[M]415.2_RT667	416.212	$C_{16}H_{34}NO_{11}$	13.6	416.2126	$C_{16}H_{33}NO_{11}$
[M]459.2_RT818	460.2378	$C_{18}H_{38}NO_{12}$	10.9	460.2389	$C_{18}H_{37}NO_{12}$
[M]503.3_RT949	504.2629	$C_{20}H_{42}NO_{13}$	6.7	504.2651	$C_{20}H_{41}NO_{13}$
[M]547.3_RT1066	548.2902	$C_{22}H_{46}NO_{14}$	2	548.2913	$C_{22}H_{45}NO_{14}$
[M]591.3_RT1170	592.3136	$C_{24}H_{50}NO_{15}$	9.5	592.3178	$C_{24}H_{49}NO_{15}$
[M]635.3_RT1268	636.3446	too less abundant			$C_{26}H_{53}NO_{16}$
[M]679.4_RT1357	680.3709	too less abundant			$C_{28}H_{57}NO_{17}$

Table S9 Predicted genes coding for enzymes with possible function in L-lysine degradation via L-pipecolate/2-aminoadipate. S: Swiss-Prot, T:TrEMBL

Searched protein function					Predicted gene	Closest sequence (Swiss-Prot)			
EC nr.	**enzyme**	**organism**	**e-Value**	**Iden-tity**	**Gene locus**	**enzyme**	**organism**	**e-Value**	**Iden-tity**
4.3.1.28	L-lysine cyclodeaminase	*Streptomyces hygroscopicus* (S)	1e-25	28%	PGA1_c16390	Ornithine cyclodeaminase (arcB)	*Brucella suis biovar 1*	2.2e-180	72%
		Jannaschia aquimarina (T)	2e-123	61%	PGA1_c31650	1-pyrroline-2-carboxylate reductase	*Paracoccus denitrificans* PD1222	9e-81	44%
1.5.1.21	1-pyrroline/piperideine-2-carboxylate reductase	*Pseudomonas aeruginosa* PAO1 (S)	1e-27	38%	PGA1_262p01410	1-pyrroline-2-carboxylate reductase	*Pseudomonas fluorescens* Pf-5	7.5e-30	43%
2.6.1.84	Arginine-pyruvate transaminase AruH	*Pseudomonas aeruginosa* PAO1 (S)	2e-99	42%	PGA1_262p02330	Arginine-pyruvate transaminase AruH	*Pseudomonas aeruginosa* PAO1	2.8e-99	42%
1.5.3.7	L-pipecolate oxidase amaA PP5257	*Pseudomonas putida* KT2440 (T)	4e-97	40%	PGA1_262p02210	Probable oxidoreductase OrdL	*Sinorhizobium meliloti* 1021	1.9e-38	29%
	Pipecolate oxidase	*Salipiger mucosus* DSM 16094 (T)	3e-153	55%	PGA1_262p02210	Gamma-glutamylputrescine oxidoreductase	*Escherichia coli* K12	2.1e-33	30%
2.6.1.23	L-lysine-epsilon-aminotransferase	*Streptomyces clavuligerus*	2e-30	27%	PGA1_c24230	Acetylornithine aminotransferase	*Rhodobacter capsulatus SB1003*	0.0	72%

Table S10 Putative exopolysaccharide biosynthesis gene cluster. Shown are BLASTp hits against the genome of *Rhizobium meliloti* 1021 with corresponding e-Values and identities as well as sequence analyses with InterPro to predict domains.

Gene locus	Predicted enzyme	e-Value	Identity	InterPro
PGA1_262p00050	Succinoglycan biosynthesis protein ExoO	8.e-35	33%	nucleotide-diphospho-sugar transferase: glycosyltransferase 2-like (domain)
	Succinoglycan biosynthesis protein ExoU	12e-22	34%	
PGA1_262p00060	Succinoglycan biosynthesis protein ExoO	7e-31	30%	
	Succinoglycan biosynthesis protein ExoU	8e-26	29%	
PGA1_262p00070	Exopolysaccharide production protein ExoQ	8e-16	29%	O-antigen ligase-related (family)
PGA1_262p00080	-	-	-	p-loop containing nucleoside triphosphate hydrolase (domain)
PGA1_262p00090	Succinoglycan biosynthesis transport protein ExoP	1e-46	24%	Lipopolysaccharide biosynthesis, tyrosine kinase (G-rich), P-loop containing nucleoside triphosohate hydrolase: AAA: Exopolysaccharide synthesis protein
PGA1_262p00100	Succinoglycan biosynthesis protein ExoA	3e-71	44%	nucleotide-diphospho-sugar transferase: glycosyltransferase 2-like (domain)
PGA1_262p00110	Succinoglycan biosynthesis protein ExoM	7e-61	40%	
PGA1_262p00120	Succinoglycan biosynthesis protein ExoL	1e-43	33%	UDP-Glycosyltransferase/glycogen phosphorylase superfamily (unintegrated)
PGA1_262p00130	-	-	-	

Table S11 Normalized peak areas of intracellularly detected metabolites of the wild-typ, the Δ262-kb mutant and the *tdaE* transposon mutant strains with casamino acids as carbon source. Normalized peak areas are listed with corresponding standard error for all identified metabolites detectable at least in one of both strains. n.d.: not detected.

Metabolite	WT	Δ262-kb	*tdaE*
2,4-diaminobutanoate	$2.5x10^5 \pm 2x10^4$	$3.1x10^5 \pm 1x10^4$	$2.3x10^5 \pm 3x10^3$
2,6-diamino-pimelate	$3.1x10^5 \pm 2x10^4$	$2.0x10^5 \pm 1x10^4$	$1.7x10^5 \pm 6x10^3$
2-amino-2-deoxygalactose	$1.0x10^5 \pm 6x10^3$	$5.2x10^5 \pm 2x10^4$	$2.3x10^5 \pm 9x10^3$
2-amino-2-deoxy-gluconate	$4.0x10^5 \pm 2x10^4$	$2.0x10^5 \pm 4x10^3$	$1.3x10^5 \pm 4x10^3$
2-amino-2-deoxy-glucose	$7.8x10^4 \pm 7x10^3$	$3.6x10^5 \pm 2x10^4$	$1.6x10^5 \pm 8x10^3$
2-aminoadipic-acid	$5.4x10^4 \pm 2x10^3$	n.d.	$2.5x10^4 \pm 1x10^3$
2-isopropylmalic acid	$4.6x10^4 \pm 5x10^3$	$1.1x10^4 \pm 5x10^2$	$4.3x10^3 \pm 1x10^3$
2-oxoglutarate	$2.5x10^4 \pm 3x10^3$	$3.3x10^4 \pm 3x10^3$	$4.0x10^4 \pm 4x10^3$
3-aminoisobutanoate	$3.5x10^4 \pm 1x10^3$	$2.8x10^5 \pm 2x10^4$	$4.4x10^4 \pm 2x10^3$
3-hydroxybutanoate	$2.6x10^4 \pm 3x10^3$	$1.5x10^4 \pm 2x10^3$	$2.1x10^4 \pm 1x10^3$
3-hydroxy-decanoate	$1.3x10^4 \pm 8x10^2$	$2.5x10^4 \pm 6x10^2$	$1.6x10^4 \pm 1x10^3$
3-phosphoglycerate	$4.0x10^4 \pm 2x10^3$	$4.4x10^4 \pm 4x10^3$	$5.3x10^4 \pm 4x10^3$
5-aminopentanoic-acid	$6.9x10^6 \pm 7x10^5$	$1.9x10^7 \pm 1x10^6$	$5.0x10^6 \pm 8x10^5$
6-phospho-gluconate	$2.2x10^4 \pm 8x10^3$	$1.1x10^4 \pm 5x10^2$	$1.1x10^4 \pm 1x10^3$
Adenine	$8.5x10^4 \pm 3x10^3$	$7.7x10^4 \pm 2x10^3$	$7.3x10^4 \pm 3x10^3$
Alanine	$8.2x10^6 \pm 6x10^5$	$1.0x10^7 \pm 4x10^5$	$5.1x10^6 \pm 2x10^5$
AMP	$1.1x10^6 \pm 6x10^4$	$1.1x10^6 \pm 5x10^4$	$9.7x10^5 \pm 4x10^4$
Arginine	$2.0x10^4 \pm 1x10^3$	$3.8x10^4 \pm 1x10^3$	$2.4x10^4 \pm 1x10^3$
Asparagine	$2.4x10^4 \pm 1x10^3$	$4.3x10^4 \pm 2x10^3$	$2.1x10^4 \pm 8x10^2$
Aspartate	$1.2x10^7 \pm 6x10^5$	$3.6x10^7 \pm 2x10^6$	$1.3x10^7 \pm 1x10^6$
Beta-Alanine	$4.1x10^4 \pm 1x10^3$	$8.7x10^4 \pm 4x10^3$	$6.2x10^4 \pm 2x10^3$
Cadaverine	$4.7x10^5 \pm 2x10^4$	$2.5x10^6 \pm 4x10^5$	$4.7x10^5 \pm 3x10^4$
Citrate	$1.4x10^5 \pm 4x10^3$	$4.8x10^4 \pm 3x10^3$	$6.7x10^4 \pm 3x10^3$
Cysteine	$1.8x10^4 \pm 6x10^2$	$7.4x10^3 \pm 2x10^3$	$8.8x10^3 \pm 1x10^3$
Cysteinyl-glycine	$6.2x10^4 \pm 8x10^3$	$1.9x10^5 \pm 2x10^4$	$1.3x10^5 \pm 1x10^4$
Cytosine	$5.9x10^4 \pm 5x10^3$	$1.2x10^5 \pm 9x10^3$	$5.8x10^4 \pm 2x10^3$
D200302	n.d.	$2.8x10^4 \pm 8x10^2$	n.d.
Ethanolamine	$3.3x10^4 \pm 4x10^3$	$3.9x10^4 \pm 3x10^3$	$4.1x10^4 \pm 3x10^3$
Fructose-1,6-bisphosphate	$1.7x10^4 \pm 1x10^3$	$4.5x10^4 \pm 3x10^3$	$3.1x10^4 \pm 2x10^3$
Fumarate	$1.0x10^5 \pm 3x10^3$	$6.6x10^4 \pm 2x10^3$	$5.9x10^4 \pm 2x10^3$
Glucose	$7.5x10^3 \pm 5x10^2$	$7.9x10^3 \pm 5x10^2$	$6.0x10^3 \pm 1x10^3$
Glucose-6-phosphate	$1.5x10^4 \pm 9x10^2$	$2.6x10^4 \pm 1x10^3$	$2.2x10^4 \pm 1x10^3$
Glutamate	$1.1x10^8 \pm 3x10^6$	$1.5x10^8 \pm 2x10^7$	$1.4x10^8 \pm 2x10^6$

Table S11 continued

Metabolite	WT	Δ262-kb	*tdaE*
Glutamine	$2.0x10^6 \pm 1x10^5$	$2.1x10^6 \pm 2x10^5$	$4.6x10^6 \pm 1x10^5$
Glycerol-3-phosphate	$2.2x10^5 \pm 2x10^4$	$9.8x10^4 \pm 8x10^3$	$1.8x10^5 \pm 8x10^3$
Glycerophosphoglycerol	$1.2x10^5 \pm 1x10^4$	$5.9x10^4 \pm 5x10^3$	$9.3x10^4 \pm 6x10^3$
Glycine	$8.7x10^5 \pm 8x10^4$	$1.5x10^6 \pm 1x10^5$	$1.2x10^6 \pm 6x10^4$
Guanine	$1.7x10^4 \pm 1x10^3$	$1.9x10^4 \pm 1x10^3$	$1.8x10^4 \pm 1x10^3$
Guanosine-5-monophosphate	$6.0x10^4 \pm 3x10^3$	$8.4x10^4 \pm 3x10^3$	$5.9x10^4 \pm 5x10^3$
Homoserine	$6.0x10^4 \pm 3x10^3$	$5.8x10^4 \pm 2x10^3$	$4.1x10^4 \pm 2x10^3$
Isoleucine	$8.4x10^5 \pm 4x10^4$	$1.1x10^6 \pm 5x10^4$	$2.3x10^5 \pm 9x10^3$
Leucine	$8.7x10^5 \pm 5x10^4$	$5.1x10^5 \pm 3x10^4$	$1.5x10^5 \pm 1x10^4$
Lysine	$1.6x10^5 \pm 8x10^3$	$4.3x10^5 \pm 3x10^4$	$2.0x10^5 \pm 8x10^3$
Malate	$1.6x10^5 \pm 8x10^3$	$1.1x10^5 \pm 7x10^3$	$1.0x10^5 \pm 6x10^3$
Methionine	$2.2x10^5 \pm 2x10^4$	$2.6x10^5 \pm 2x10^4$	$1.4x10^5 \pm 5x10^3$
N-acetyl-glutamate	$4.9x10^4 \pm 1x10^3$	$4.1x10^4 \pm 1x10^3$	$4.4x10^4 \pm 1x10^3$
N-acetyl-ornithine	$5.1x10^4 \pm 2x10^3$	$9.2x10^4 \pm 5x10^3$	$8.9x10^4 \pm 3x10^3$
N-acetyl-serine	$7.3x10^4 \pm 4x10^3$	n.d.	n.d.
Nicotinamide	$2.7x10^5 \pm 2x10^4$	$1.9x10^5 \pm 1x10^4$	$1.9x10^5 \pm 2x10^4$
Ornithine	$1.8x10^5 \pm 8x10^3$	$2.9x10^5 \pm 9x10^3$	$2.7x10^5 \pm 1x10^4$
Phenylalanine	$1.0x10^6 \pm 3x10^4$	$3.4x10^5 \pm 7x10^4$	$7.6x10^5 \pm 7x10^4$
Phosphate-monomethylester	$4.7x10^4 \pm 2x10^3$	$7.3x10^4 \pm 3x10^3$	$5.6x10^4 \pm 1x10^3$
Pipecolate	$7.4x10^5 \pm 4x10^4$	$2.0x10^6 \pm 1x10^5$	$3.6x10^5 \pm 2x10^4$
Proline	$1.4x10^6 \pm 1x10^5$	$3.9x10^6 \pm 3x10^5$	$1.6x10^6 \pm 1x10^5$
Putrescine	$2.7x10^4 \pm 8x10^2$	$5.2x10^4 \pm 2x10^3$	$9.5x10^4 \pm 3x10^3$
Pyroglutamate	$1.9x10^7 \pm 8x10^5$	$4.8x10^7 \pm 2x10^6$	$2.6x10^7 \pm 2x10^6$
Serine	$8.2x10^4 \pm 2x10^3$	$3.6x10^5 \pm 1x10^4$	$1.4x10^5 \pm 2x10^3$
Threonine	$3.2x10^5 \pm 7x10^3$	$4.7x10^5 \pm 2x10^4$	$2.3x10^5 \pm 8x10^3$
Thymine	$4.0x10^4 \pm 1x10^3$	$4.1x10^4 \pm 1x10^3$	$3.3x10^4 \pm 1x10^3$
Tyrosine	$2.6x10^6 \pm 4x10^5$	$4.7x10^5 \pm 4x10^4$	$6.3x10^5 \pm 2x10^4$
Uric acid	$1.5x10^4 \pm 1x10^3$	n.d.	$8.1x10^3 \pm 8x10^2$
Uridine 5'-monophosphate	$1.1x10^5 \pm 8x10^3$	$2.1x10^5 \pm 1x10^4$	$1.1x10^5 \pm 1x10^4$
Valine	$6.1x10^6 \pm 2x10^5$	$1.0x10^7 \pm 7x10^5$	$1.7x10^6 \pm 9x10^4$
Xanthine	$1.4x10^4 \pm 8x10^2$	$7.5x10^3 \pm 3x10^2$	$1.9x10^4 \pm 9x10^3$

Table S12 Amino acid concentrations for the wild-type strain, the Δ262-kb and *tdaA*, *tdaB*, *tdaC*, *tdaE* mutant strain at OD_{max} with casamino acids as carbon source. Amino acid concentrations in mmol L^{-1} in medium prior to inoculation and at OD_{max} are listed with corresponding standard deviation.

Amino acid	medium	WT	Δ262-kb	*tdaA*	*tdaB*	*tdaC*	*tdaE*
Aspartate	3.25 ± 0.11	0.85 ± 0.29	0.05 ± 0.05	n.d.	n.d.	n.d.	n.d.
Glutamate	8.89 ± 0.32	n.d.	n.d.	n.d.	n.d.	n.d.	n.d.
Serine	2.84 ± 0.10	1.02 ± 0.48	n.d.	n.d.	n.d.	n.d.	n.d.
Glycine	1.41 ± 0.05	n.d.	n.d.	n.d.	n.d.	n.d.	n.d.
Threonine	1.81 ± 0.06	0.25 ± 0.16	n.d.	n.d.	n.d.	n.d.	n.d.
Histidine	0.71 ± 0.03	0.45 ± 0.02	n.d.	n.d.	n.d.	n.d.	n.d.
Alanine	2.02 ± 0.07	n.d.	n.d.	n.d.	n.d.	n.d.	n.d.
Arginine	0.87 ± 0.03	0.14 ± 0.05	0.08 ± 0.09	n.d.	n.d.	n.d.	n.d.
Tyrosine	0.15 ± 0.02	0.05 ± 0.02	n.d.	n.d.	n.d.	n.d.	n.d.
Valine	2.05 ± 0.07	0.95 ± 0.15	n.d.	n.d.	n.d.	n.d.	n.d.
Methionine	0.80 ± 0.03	0.13 ± 0.03	n.d.	n.d.	n.d.	n.d.	n.d.
Isoleucine	1.24 ± 0.04	0.65 ± 0.05	n.d.	n.d.	n.d.	n.d.	n.d.
Phenylalanine	0.94 ± 0.03	0.21 ± 0.06	n.d.	n.d.	n.d.	n.d.	n.d.
Leucine	2.38 ± 0.09	0.88 ± 0.08	n.d.	n.d.	n.d.	n.d.	n.d.
Lysine	2.09 ± 0.15	0.44 ± 0.08	0.16 ± 0.18	n.d.	n.d.	n.d.	n.d.
Proline	5.75 ± 0.43	n.d.	n.d.	n.d.	n.d.	n.d.	n.d.

Table S13 Amino acid concentrations for the wild-type strain, the Δ262-kb and *tdaE* mutant strain at ½ OD_{max} with casamino acids as carbon source. Amino acid concentrations in mmol L^{-1} at ½ OD_{max} (harvesting point for metabolome analysis) are listed with corresponding standard deviation.

Amino acid	WT	Δ262-kb	*tdaE*
Aspartate	2.05 ± 0.05	1.52 ± 0.09	2.10 ± 0.05
Glutamate	3.12 ± 0.19	6.37 ± 0.18	6.11 ± 0.21
Serine	2.35 ± 0.02	1.95 ± 0.08	2.23 ± 0.03
Glycine	0.45 ± 0.01	0.14 ± 0.03	0.45 ± 0.04
Threonine	1.31 ± 0.15	0.19 ± 0.09	0.60 ± 0.05
Histidine	0.72 ± 0.02	0.64 ± 0.01	0.59 ± 0.02
Alanine	1.01 ± 0.04	0.39 ± 0.08	0.98 ± 0.05
Arginine	0.39 ± 0.01	0.57 ± 0.01	0.49 ± 0.01
Tyrosine	0.15 ± 0.01	0.03 ± 0.01	0.06 ± 0.00
Valine	1.60 ± 0.02	1.17 ± 0.11	1.44 ± 0.04
Methionine	0.44 ± 0.00	0.45 ± 0.02	0.52 ± 0.01
Isoleucine	0.91 ± 0.01	0.82 ± 0.03	0.91 ± 0.02
Phenylalanine	0.54 ± 0.03	0.12 ± 0.05	0.28 ± 0.03
Leucine	1.19 ± 0.02	1.07 ± 0.04	1.27 ± 0.03
Lysine	1.10 ± 0.03	1.54 ± 0.07	1.38 ± 0.03
Proline	1.36 ± 0.05	2.39 ± 0.14	2.73 ± 0.13

Table S14 Oxygen consumption dependent on TDA presence. Shown are determined oxygen uptake rates with corresponding growth physiology for the wild-type, the Δ262-kb and *tdaE* mutant strains at ⅛OD_{max}, ¼ OD_{max}, ½ OD_{max}, ¾ OD_{max} and shortly before reaching OD_{max} for cultivation with casamino acids.

		WT	**Δ262-kb**	***tdaE***
⅛ OD_{max}	Time [h]	9.5 ± 0.1	8.6 ± 0.1	11.1 ± 0.3
	CDW [g L^{-1} h^{-1}]	0.18 ± 0.00	0.33± 0.00	0.28 ± 0.01
	μ [h^{-1}]	0.15 ± 0.00	0.40 ± 0.00	0.33 ± 0.02
	OUR [$mmol_{O2}$ L^{-1} h^{-1}]	1.9 ± 0.3	4.0 ± 0.7	2.7 ± 0.7
	q_{O2} [$mmol_{O2}$ g^{-1} h^{-1}]	10.3 ± 1.5	12.2 ± 2.1	9.7 ± 2.5
	O_2 consumption [$mmol_{O2}$ g^{-1}]	67 ± 10	30 ± 6	30 ± 9
¼ OD_{max}	Time [h]	13.6 ± 0.1	10.4 ± 0.1	13.4 ± 0.4
	CDW [g L^{-1} h^{-1}]	0.36 ± 0.00	0.65 ± 0.00	0.55 ± 0.00
	μ [h^{-1}]	0.18 ± 0.00	0.35 ± 0.00	0.29 ± 0.02
	OUR [$mmol_{O2}$ L^{-1} h^{-1}]	4.5 ± 0.6	7.4 ± 0.3	6.2 ± 1.0
	q_{O2} [$mmol_{O2}$ g^{-1} h^{-1}]	12.4 ± 1.5	11.4 ± 0.4	11.2 ± 1.9
	O_2 consumption [$mmol_{O2}$ g^{-1}]	68 ± 10	32 ± 1	40 ± 9
½ OD_{max}	Time [h]	17.5 ± 0.3	12.5 ± 0.2	15.9 ± 0.6
	CDW [g L^{-1} h^{-1}]	0.72 ± 0.00	1.29 ± 0.01	1.09 ± 0.01
	μ [h^{-1}]	0.13 ± 0.01	0.27 ± 0.00	0.22 ± 0.02
	OUR [$mmol_{O2}$ L^{-1} h^{-1}]	8.3 ± 0.8	14.3 ± 0.7	13.2 ± 1.7
	q_{O2} [$mmol_{O2}$ g^{-1} h^{-1}]	11.5 ± 1.1	11.1 ± 0.6	12.1 ± 1.7
	O_2 consumption [$mmol_{O2}$ g^{-1}]	91 ± 14	40 ± 2	55 ± 11
¾ OD_{max}	Time [h]	20.9 ± 0.5	14.2 ± 0.2	17.9 ± 0.7
	CDW [g L^{-1} h^{-1}]	1.03 ± 0.00	1.94 ± 0.01	1.65 ± 0.00
	μ [h^{-1}]	0.07 ± 0.01	0.20 ± 0.00	0.16 ± 0.01
	OUR [$mmol_{O2}$ L^{-1} h^{-1}]	11.7 ± 1.2	22.4 ± 0.3	19.9 ± 0.8
	q_{O2} [$mmol_{O2}$ g^{-1} h^{-1}]	11.3 ± 1.2	11.5 ± 0.1	12.1 ± 1.7
	O_2 consumption [$mmol_{O2}$ g^{-1}]	169 ± 37	59 ± 1	78 ± 15
~ OD_{max}	Time [h]	25.6 ± 1.6	15.2 ± 0.2	19.2 ± 0.9
	CDW [g L^{-1} h^{-1}]	1.24 ± 0.01	2.34 ± 0.02	1.99 ± 0.01
	μ [h^{-1}]	0.03 ± 0.01	0.14 ± 0.00	0.11 ± 0.01
	OUR [$mmol_{O2}$ L^{-1} h^{-1}]	13.2 ± 1.2	22.7 ± 3.6	23.1 ± 2.4
	q_{O2} [$mmol_{O2}$ g^{-1} h^{-1}]	10.6 ± 1.1	9.7 ± 1.5	11.6 ± 1.2
	O_2 consumption [$mmol_{O2}$ g^{-1}]	446 ± 156	68 ± 12	107 ± 18.5

Table S15 Biomass composition for the wild-type, Δ262-kb mutant and *tdaE* transposon mutant strains for cells growing with L-alanine, L-phenylalanine or L-leucine as sole carbon source, respectively. Listed are mean values of 6 biological replicates for DNA, RNA, lipids, protein and polyhydroxybutyrate, respectively. Peptidoglycan content was estimated by quantification of *meso*-diaminopimelate (1.7% of CDW) of cell hydrolysates over all strains and carbon sources. All values are listed in % of biomass.

Component	Alanine			Phenylalanine			Leucine			Reference
	WT	Δ262	*tdaE*	WT	Δ262	*tdaE*	WT	Δ262	*tdaE*	
DNA	1.6 ± 0.1	1.4 ± 0.3	1.2 ± 0.2	1.3 ± 0.2	2.0 ± 0.3	1.1 ± 0.2	1.4 ± 0.2	1.6 ± 0.3	0.9 ± 0.3	this work
RNA	4.5 ± 0.3	6.8 ± 0.9	5.9 ± 0.5	5.4 ± 0.8	5.8 ± 0.3	3.9 ± 0.7	3.4 ± 0.3	4.3 ± 0.8	3.7 ± 0.1	this work
Lipids	6.8 ± 0.4	5.9 ± 0.5	5.3 ± 0.6	6.1 ± 0.6	5.3 ± 0.9	5.9 ± 0.5	5.6 ± 0.6	5.9 ± 0.7	3.4 ± 0.5	this work
Protein	54 ± 3	56 ± 3	59 ± 4	55 ± 3	52 ± 4	51 ± 4	53 ± 4	59 ± 5	50 ± 4	this work
Polyhydroxybutyrate	7 ± 2	7 ± 0.5	7 ± 1	13 ± 1	14 ± 3	24 ± 2	17 ± 2	14 ± 4	23 ± 3	this work
Peptidoglycan	12 ± 2	12 ± 2	12 ± 2	12 ± 2	12 ± 2	12 ± 2	12 ± 2	12 ± 2	12 ± 2	this work
Lipopolysaccharide	3.4	3.4	3.4	3.4	3.4	3.4	3.4	3.4	3.4	Feist et al 2007
Glutamate	4	4	4	4	4	4	4	4	4	Kleist et al 2016
Soluble pool	2	2	2	2	2	2	2	2	2	
Sum	95 ± 8	99 ± 7	100 ± 8	102 ± 8	100 ± 11	107 ± 9	102 ± 9	106 ± 13	102 ± 10	

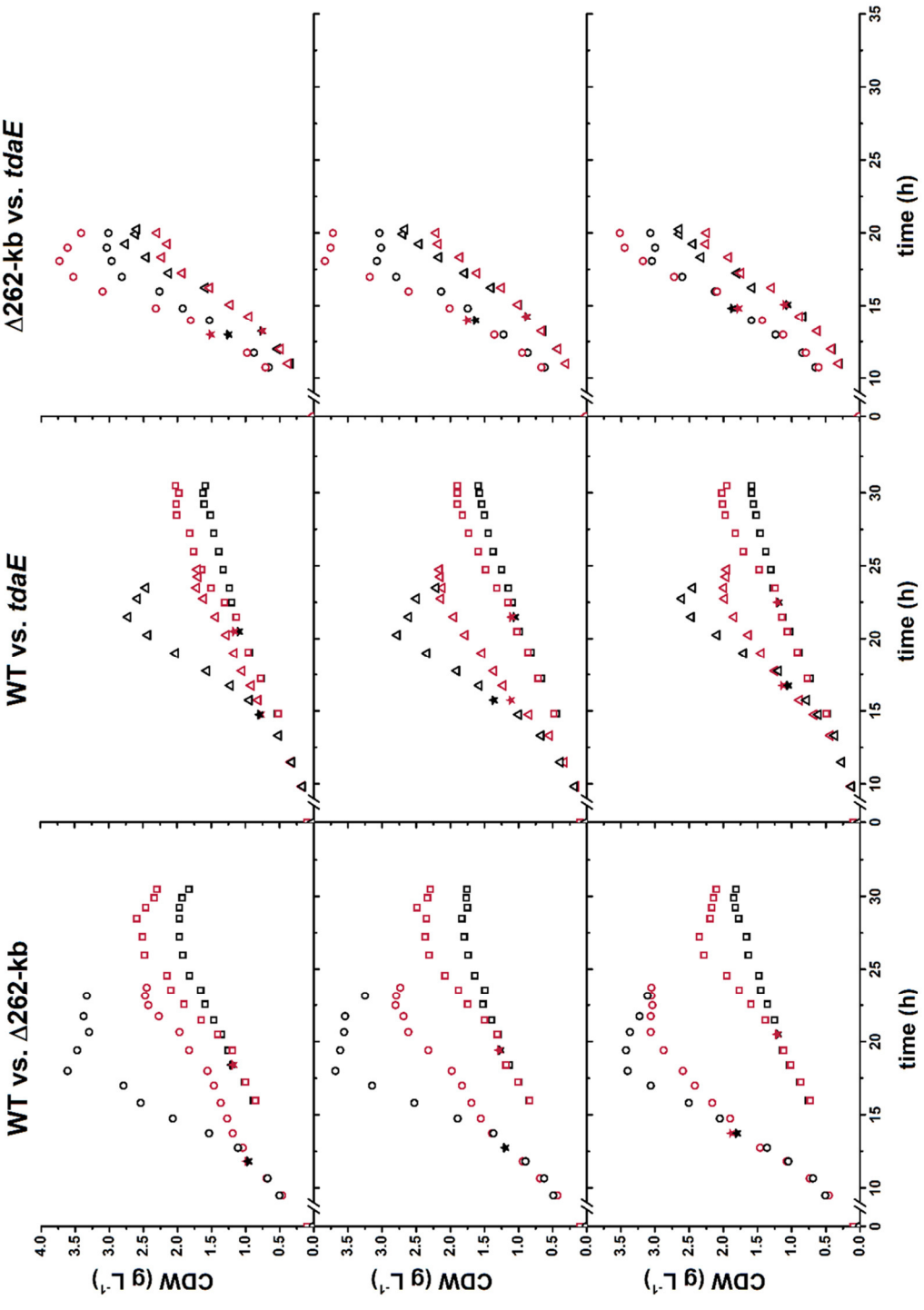

Figure S1 Medium exchange experiment. Shown are CDW values for the wild-type (squares), the Δ262-kb mutant (circles) and the *tdaE* transposon mutant (triangles) strains for exchanged cultures (red) and references (black). Stars: time point of exchange.

Figure S2 Growth and OUR of the wild-type strain, the Δ262-kb and *tdaE* mutant strains with casamino acids as carbon source.

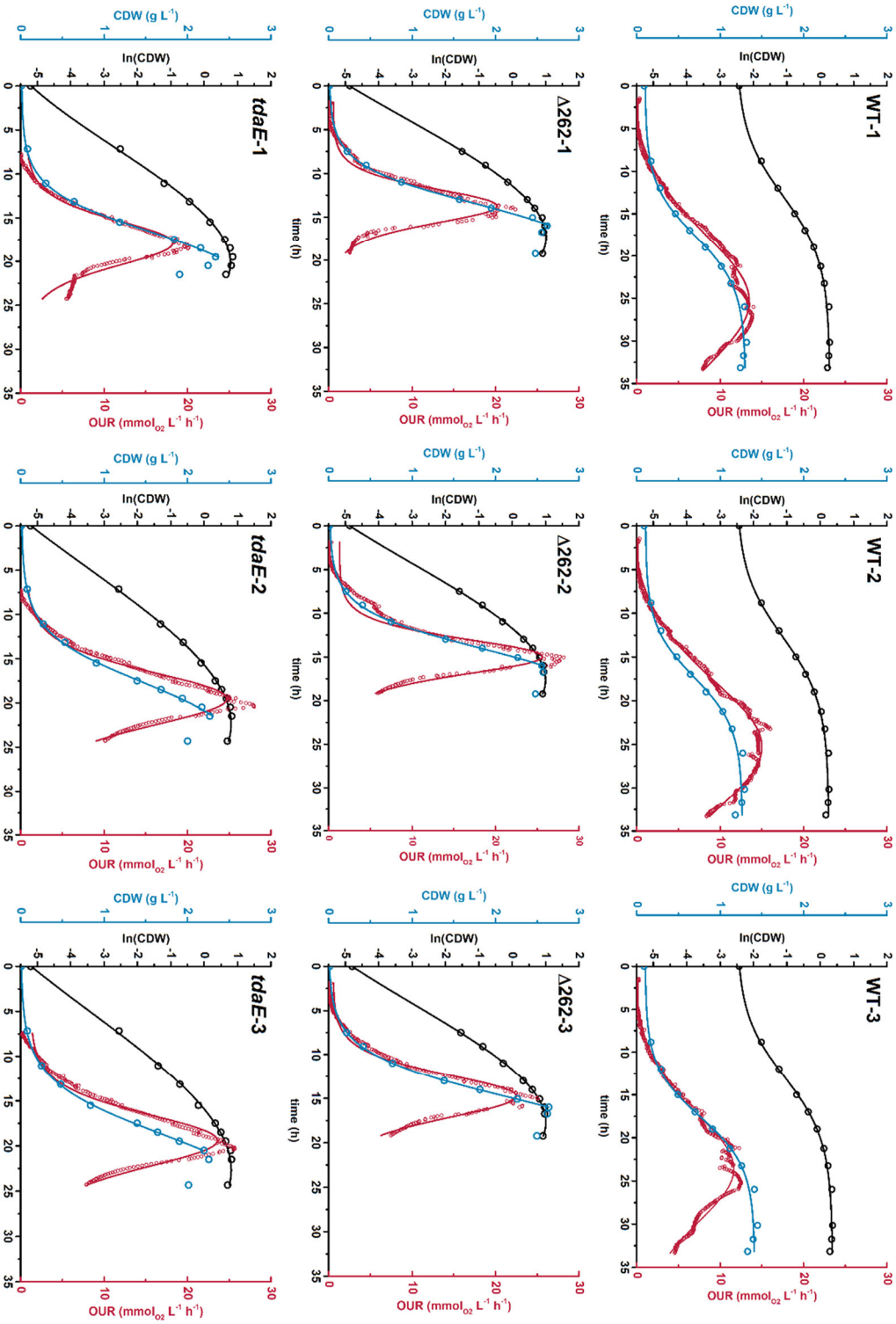

Model *i*Pin571

model: iPin571
organism: Phaeobacter inhibens
strain: DSM 17395
updated: 171213
modeler: swi

 # EMP
glycolysis_2.7.1.2_GLUCOKIN-RXN: 1 ATP + 1 beta-D-glucose --> 1 ADP + 1 H+ + 1 beta-D-glucose-6-phosphate
glycolysis_5.3.1.9_PGLUCISOM-RXN: 1 beta-D-glucose-6-phosphate <=> 1 D-fructose-6-phosphate
glycolysis_4.1.2.13_F16ALDOLASE-RXN: 1 fructose-1,6-bisphosphate <=> 1 dihydroxyacetone_phosphate + 1 D-glyceraldehyde-3-phosphate
glycolysis_5.3.1.1_TRIOSEPISOMERIZATION-RXN: 1 D-glyceraldehyde-3-phosphate <=> 1 dihydroxyacetone_phosphate
~no-pathway_1.2.1.12_GAPDHSYNEC-RXN_NAD: 1 NAD+ + 1 D-glyceraldehyde-3-phosphate + 1 phosphate <=> 1 1,3-bisphospho-D-glycerate + 1 NADH + 1 H+
glycolysis_2.7.2.3_PHOSGLYPHOS-RXN: 1 ATP + 1 3-phospho-D-glycerate <=> 1 1,3-bisphospho-D-glycerate + 1 ADP
glycolysis_5.4.2.12_3PGAREARR-RXN: 1 3-phospho-D-glycerate <=> 1 2-phospho-D-glycerate
glycolysis_4.2.1.11_2PGADEHYDRAT-RXN: 1 2-phospho-D-glycerate <=> 1 phosphoenolpyruvate + 1 H2O
glycolysis_2.7.1.40_PEPDEPHOS-RXN: 1 ATP + 1 pyruvate <-- 1 H+ + 1 phosphoenolpyruvate + 1 ADP

 # gluconeogenesis
~no-pathway_1.1.1.39_1.1.1.39-RXN: 1 NAD+ + 1 (S)-malate --> 1 NADH + 1 pyruvate + 1 CO2
gluconeogenesis_C4-photosynthetic-carbon-assimilation-cycle_1.1.1.39_1.1.1.40_MALIC-NADP-RXN: 1 (S)-malate + 1 NADP+ --> 1 pyruvate + 1 NADPH + 1 CO2
superpathway-of-glyoxylate-cycle_gluconeogenesis_4.1.1.49_PEPCARBOXYKIN-RXN: 1 ATP + 1 oxaloacetate --> 1 CO2 + 1 ADP + 1 phosphoenolpyruvate
C4_photosynthetic_carbon_assimilation_cycle-2.7.9.1-PYRUVATEORTHOPHOSPHATE-DIKINASE-RXN: 1 ATP + 1 phosphate + 1 pyruvate --> 1 AMP + 1 phosphoenolpyruvate + 1 diphosphate + 1 H+
Calvin-Benson-Bassham-cycle_1.2.1.59_1.2.1.13-RXN: 1 NADP+ + 1 D-glyceraldehyde-3-phosphate + 1 phosphate <-- 1 NADPH + 1 H+ + 1 1,3-bisphospho-D-glycerate
glycolysis_3.1.3.11_F16BDEPHOS-RXN: 1 fructose-1,6-bisphosphate + 1 H2O --> 1 phosphate + 1 D-fructose-6-phosphate

 # EDP
~multiple-pathways_1.1.1.49_GLU6PDEHYDROG-RXN: 1 beta-D-glucose-6-phosphate + 1 NADP+ <=> 1 6-phospho-D-glucono-1,5-lactone + 1 NADPH + 1 H+
~multiple-pathways_3.1.1.31_6PGLUCONOLACT-RXN: 1 H2O + 1 6-phospho-D-glucono-1,5-lactone --> 1 H+ + 1 6-phospho-D-gluconate
Entner-Doudoroff-pathway-I_4.2.1.12_PGLUCONDEHYDRAT-RXN: 1 6-phospho-D-gluconate --> 1 H2O + 1 2-dehydro-3-deoxy-D-gluconate-6-phosphate
Entner-Doudoroff-pathway_4.1.2.14_KDPGALDOL-RXN: 1 2-dehydro-3-deoxy-D-gluconate-6-phosphate --> 1 D-glyceraldehyde-3-phosphate + 1 pyruvate

 # PPP
~multiple-pathways_5.1.3.1_RIBULP3EPIM-RXN: 1 D-ribulose-5-phosphate <=> 1 D-xylulose-5-phosphate
~multiple-pathways_5.3.1.6_RIB5PISOM-RXN: 1 D-ribose-5-phosphate <=> 1 D-ribulose-5-phosphate
~multiple-pathways_2.2.1.1_1TRANSKETO-RXN: 1 D-sedoheptulose-7-phosphate + 1 D-glyceraldehyde-3-phosphate <=> 1 D-xylulose-5-phosphate + 1 D-ribose-5-phosphate

~multiple-pathways_2.2.1.1_2TRANSKETO-RXN: 1 D-xylulose-5-phosphate + 1 D-erythrose-4-phosphate <=> 1 D-glyceraldehyde-3-phosphate + 1 D-fructose-6-phosphate
~multiple-pathways_2.2.1.2_TRANSALDOL-RXN: 1 D-sedoheptulose-7-phosphate + 1 D-glyceraldehyde-3-phosphate <=> 1 D-fructose-6-phosphate + 1 D-erythrose-4-phosphate

 # PDH comnplex
acetyl-CoA-biosynthesis-(from-pyruvate)_1.2.4.1_RXN0-1134 : 1 lipoamide + 1 pyruvate + 1 H+ --> 1 S-acetyldihydrolipoamide + 1 CO2
glycine-cleavage-complex_1.8.1.4_RXN-8629: 1 NAD+ + 1 dihydrolipoamide --> 1 NADH + 1 lipoamide + 1 H+
~no-pathway_2.3.1.12_DIHYDLIPACETRANS-RXN: 1 acetyl-CoA + 1 dihydrolipoamide <=> 1 S-acetyldihydrolipoamide + 1 coenzyme_A

 # CAC
TCA-cycle_2.3.3.1_CITSYN-RXN: 1 H2O + 1 acetyl-CoA + 1 oxaloacetate --> 1 H+ + 1 coenzyme_A + 1 citrate
TCA-cycle_4.2.1.3_ACONITATEDEHYDR-RXN: 1 citrate <=> 1 cis-aconitate + 1 H2O
TCA-cycle_4.2.1.3_ACONITATEHYDR-RXN: 1 cis-aconitate + 1 H2O <=> 1 D-threo-isocitrate
reductive-TCA-cycle_1.1.1.42_ISOCITDEH-RXN : 1 D-threo-isocitrate + 1 NADP+ --> 1 CO2 + 1 NADPH + 1 2-oxoglutarate
2-ketoglutarate-dehydrogenase-complex_2.3.1.61_RXN0-1147: 1 H+ + 1 dihydrolipoamide + 1 succinyl-CoA <=> 1 |Oxo-glutarate-dehydro-suc-DH-lipoyl| + 1 coenzyme_A
2-ketoglutarate-dehydrogenase-complex_1.2.4.2_2OXOGLUTDECARB-RXN: 1 2-oxoglutarate + 1 lipoamide + 2 H+ --> 1 |Oxo-glutarate-dehydro-suc-DH-lipoyl| + 1 CO2
TCA-cycle_6.2.1.5_SUCCCOASYN-RXN: 1 coenzyme_A + 1 ATP + 1 succinate <=> 1 ADP + 1 succinyl-CoA + 1 phosphate
TCA-cycle_1.3.5.1_SUCCINATE-DEHYDROGENASE-UBIQUINONE-RXN: 1 succinate + 1 ubiquinone-10 --> 1 fumarate + 1 ubiquinol-10
TCA-cycle_4.2.1.2_FUMHYDR-RXN: 1 (S)-malate <=> 1 fumarate + 1 H2O
TCA-cycle_1.1.1.37_MALATE-DEH-RXN: 1 (S)-malate + 1 NAD+ <=> 1 H+ + 1 oxaloacetate + 1 NADH
TCA-cycle-variation_2.3.3.9_MALSYN-RXN: 1 acetyl-CoA + 1 H2O + 1 glyoxylate --> 1 H+ + 1 (S)-malate + 1 coenzyme_A
anapleurotic_synthesis_of_oxalacetate-6.4.1.1-PYRUVATE-CARBOXYLASE-RXN: 1 ATP + 1 bicarbonate + 1 pyruvate --> 1 ADP + 1 oxaloacetate + 1 phosphate + 1 H+

 # pyruvate metabolism
~multiple-pathways_2.3.1.8_PHOSACETYLTRANS-RXN: 1 phosphate + 1 acetyl-CoA <=> 1 coenzyme_A + 1 acetylphosphate
~multiple-pathways_2.7.2.1_ACETATEKIN-RXN: 1 ATP + 1 acetate --> 1 ADP + 1 acetylphosphate
~multiple-pathways_6.2.1.1_ACETATE--COA-LIGASE-RXN: 1 acetate + 1 ATP + 1 coenzyme_A --> 1 acetyl-CoA + 1 diphosphate + 1 AMP
oxidative-ethanol-degradation_1.2.1.3_RXN66-3: 1 H2O + 1 NAD+ + 1 acetaldehyde --> 1 NADH + 2 H+ + 1 acetate

 # oxidative phosphorylation
~multiple-pathways_1.6.5.3_NADH-DEHYDROG-A-RXN: 1 NADH + 5 H+ + 1 ubiquinone-10 <=> 1 NAD+ + 1 ubiquinol-10 + 4 H+_rc
aerobic-respiration----electron-donor-II_1.10.2.2_1.10.2.2-RXN: 2 |Cytochromes-C-Oxidized| + 1 ubiquinol-10 + 2 H+ <=> 2 |Cytochromes-C-Reduced| + 1 ubiquinone-10 + 2 H+_rc
aerobic-respiration----electron-donor-II_1.9.3.1_CYTOCHROME-C-OXIDASE-RXN: 1 oxygen + 4 |Cytochromes-C-Reduced| + 4 H+ --> 2 H2O + 4 |Cytochromes-C-Oxidized| + 4 H+_rc
~no-pathway_1.6.99.5_NADH-DEHYDROGENASE-RXN: 1 NADH + 1 H+ + 1 ubiquinone-10 --> 1 ubiquinol-10 + 1 NAD+
oxidative_phosphorylation-3.6.3.27-3.6.3.27-RXN: 1 ATP + 1 phosphate_ex + 1 H2O --> 1 ADP + 2 phosphate + 1 H+
~no-pathway_3.6.1.1_INORGPYROPHOSPHAT-RXN: 1 diphosphate + 1 H2O --> 1 H+ + 2 phosphate
oxidative_phosphorylation-3.6.3.14-ATPSYN-RXN: 1 ATP + 3 H+ + 1 H2O <=> 1 ADP + 1 phosphate + 4 H+_rc

 # shikimate pathway
~no-pathway_2.5.1.54_DAHPSYN-RXN: 1 H2O + 1 D-erythrose-4-phosphate + 1 phosphoenolpyruvate --> 1 phosphate + 1 3-deoxy-D-arabino-heptulosonate-7-phosphate
~no-pathway_4.2.3.4_3-DEHYDROQUINATE-SYNTHASE-RXN: 1 3-deoxy-D-arabino-heptulosonate-7-phosphate --> 1 3-dehydroquinate + 1 phosphate
quinate-degradation_4.2.1.10_3-DEHYDROQUINATE-DEHYDRATASE-RXN: 1 3-dehydroquinate <=> 1 H2O + 1 3-dehydroshikimate
~no-pathway_1.1.1.25_RXN-7968_NADP: 1 NADP+ + 1 shikimate <-- 1 3-dehydroshikimate + 1 NADPH + 1 H+
~no-pathway_2.7.1.71_SHIKIMATE-KINASE-RXN: 1 shikimate + 1 ATP --> 1 shikimate-3-phosphate + 1 H+ + 1 ADP
~no-pathway_2.5.1.19_2.5.1.19-RXN: 1 phosphoenolpyruvate + 1 shikimate-3-phosphate <=> 1 5-enolpyruvyl-shikimate-3-phosphate + 1 phosphate
~no-pathway_4.2.3.5_CHORISMATE-SYNTHASE-RXN: 1 5-enolpyruvyl-shikimate-3-phosphate --> 1 chorismate + 1 phosphate

 # ethylmalonyl-CoA pathway
~multiple-pathways_2.3.1.9_ACETYL-COA-ACETYLTRANSFER-RXN: 2 acetyl-CoA <=> 1 coenzyme_A + 1 acetoacetyl-CoA
acetyl-CoA-fermentation-to-butyrate_glutaryl-CoA-degradation_1.1.1.35_RXN-11662: 1 NAD+ + 1 (S)-3-hydroxybutanoyl-CoA <=> 1 NADH + 1 H+ + 1 acetoacetyl-CoA
~multiple-pathways_1.1.1.36_RXN-5901: 1 (R)-3-hydroxybutanoyl-CoA + 1 NADP+ <-- 1 H+ + 1 NADPH + 1 acetoacetyl-CoA
acetyl-CoA-fermentation-to-butyrate_ethylmalonyl-pathway_4.2.1.55_1.1.1.36_4.2.1.17_3-HYDROXBUTYRYL-COA-DEHYDRATASE-RXN: 1 (R)-3-hydroxybutanoyl-CoA --> 1 H2O + 1 crotonyl-CoA
~multiple-pathways_4.2.1.55_4.2.1.17_RXN-11667: 1 (S)-3-hydroxybutanoyl-CoA <=> 1 crotonyl-CoA + 1 H2O
~no-pathway_5.1.2.3_5.1.2.3-RXN: 1 (S)-3-hydroxybutanoyl-CoA <=> 1 (R)-3-hydroxybutanoyl-CoA
ethylmalonyl-pathway_1.3.1.85_RXN-8957: 1 NADP+ + 1 (2S)-ethylmalonyl-CoA <=> 1 NADPH + 1 crotonyl-CoA + 1 CO2
ethylmalonyl-pathway_5.4.99.2_RXN-8958: 1 (2S)-ethylmalonyl-CoA --> 1 methylsuccinyl-CoA
ethylmalonyl-CoA_pathway-RXN-8959: 1 methylsuccinyl-CoA --> 1 mesaconyl-CoA + 2 H+
ethylmalonyl-CoA_pathway-RXN-8960 : 1 mesaconyl-CoA + 1 H2O <=> 1 beta-methylmalyl-CoA
glyoxylate-assimilation_ethylmalonyl-pathway_4.1.3.24_RXN-8961: 1 beta-methylmalyl-CoA <=> 1 glyoxylate + 1 propanoyl-CoA
3-hydroxypropionate-cycle_methylmalonyl-pathway_6.4.1.3_PROPIONYL-COA-CARBOXY-RXN: 1 ATP + 1 propanoyl-CoA + 1 bicarbonate --> 1 H+ + 1 (S)-methylmalonyl-CoA + 1 ADP + 1 phosphate
~multiple-pathways_5.1.99.1_METHYLMALONYL-COA-EPIM-RXN: 1 (R)-methylmalonyl-CoA <=> 1 (S)-methylmalonyl-CoA
~multiple-pathways_5.4.99.2_METHYLMALONYL-COA-MUT-RXN: 1 (R)-methylmalonyl-CoA <=> 1 succinyl-CoA

 # PHB
PHB_biosynthesis-PhaC-2.3.1.-RXN: 1 (R)-3-hydroxybutanoyl-CoA --> 1 [PHB] + 1 coenzyme_A
PHB_degradation-3.1.1.75-3.1.1.75-RXN: 1 [PHB] + 1 H2O --> 1 (R)-3-hydroxybutanoate
-no_pathway-1.1.1.30-3-HYDROXYBUTYRATE-DEHYDROGENASE-RXN: 1 (R)-3-hydroxybutanoate + 1 NAD+ <=> 1 acetoacetate + 1 NADH + 1 H+

##

 # fatty acid biosynthesis

starter molecule
~multiple-pathways_6.4.1.2_ACETYL-COA-CARBOXYLTRANSFER-RXN: 1 bicarbonate + 1 ATP + 1 acetyl-CoA --> 1 malonyl-CoA + 1 H+ + 1 phosphate + 1 ADP
fatty-acid-biosynthesis-initiation_fatty-acid-biosynthesis_2.3.1.39_MALONYL-COA-ACP-TRANSACYL-RXN : 1 ACP + 1 malonyl-CoA <=> 1 malonyl-[ACP] + 1 coenzyme_A

fatty-acid-biosynthesis-initiation-I_2.3.1.180_2.3.1.180-RXN : 1 malonyl-[ACP] + 1 acetyl-CoA + 1 H+ --> 1 Acetoacetyl-[ACP] + 1 CO2 + 1 coenzyme_A

octanoic acid
palmitate-biosynthesis_1.1.1.100_RXN-9514 : 1 Acetoacetyl-[ACP]+ 1 NADPH + 1 H+ --> 1 (R)-3-hydroxy-butanoyl-[ACP] + 1 NADP+
palmitate-biosynthesis_4.2.1.59_4.2.1.58-RXN : 1 (R)-3-hydroxy-butanoyl-[ACP] --> 1 trans-D2-butenoyl-[ACP] + 1 H2O
palmitate-biosynthesis-II-(bacteria-and-plants)_1.3.1.9_RXN-9657 : 1 NAD+ + 1 Butanoyl-[ACP] <-- 1 trans-D2-butenoyl-[ACP] + 1 H+ + 1 NADH
palmitate-biosynthesis-II-(bacteria-and-plants)_2.3.1.180_2.3.1.41_RXN-9516 : 1 Butanoyl-[ACP] + 1 malonyl-[ACP] + 1 H+ --> 1 CO2 + 1 ACP + 1 3-oxo-hexanoyl-[ACP]
palmitate-biosynthesis_1.1.1.100_RXN-9518 : 1 (R)-3-hydroxy-hexanoyl-[ACP] + 1 NADP+ <-- 1 3-oxo-hexanoyl-[ACP] + 1 H+ + 1 NADPH
palmitate-biosynthesis_4.2.1.59_RXN-9520 : 1 (R)-3-hydroxy-hexanoyl-[ACP] --> 1 trans-D2-hexenoyl-[ACP] + 1 H2O
palmitate-biosynthesis-II-(bacteria-and-plants)_1.3.1.9_RXN-9658 : 1 NAD+ + 1 Hexanoyl-[ACP] <-- 1 H+ + 1 trans-D2-hexenoyl-[ACP] + 1 NADH
palmitate-biosynthesis-II-(bacteria-and-plants)_2.3.1.180_2.3.1.41_RXN-9523 : 1 Hexanoyl-[ACP] + 1 malonyl-[ACP] + 1 H+ --> 1 ACP + 1 CO2 + 1 3-oxo-octanoyl-[ACP]
palmitate-biosynthesis_1.1.1.100_RXN-9524 : 1 NADP+ + 1 (R)-3-hydroxy-octanoyl-[ACP] <-- 1 NADPH + 1 H+ + 1 3-oxo-octanoyl-[ACP]
palmitate-biosynthesis_4.2.1.59_4.2.1.59-RXN : 1 (R)-3-hydroxy-octanoyl-[ACP] --> 1 trans-D2-octenoyl-[ACP] + 1 H2O
palmitate-biosynthesis-II-(bacteria-and-plants)_1.3.1.9_RXN-9659 : 1 NAD+ + 1 Octanoyl-[ACP] <-- 1 trans-D2-octenoyl-[ACP] + 1 NADH + 1 H+

decanoic acid
palmitate-biosynthesis-II-(bacteria-and-plants)_2.3.1.180_2.3.1.41_RXN-9527 : 1 Octanoyl-[ACP] + 1 malonyl-[ACP] + 1 H+ --> 1 ACP + 1 3-oxo-decanoyl-[ACP] + 1 CO2
palmitate-biosynthesis_1.1.1.100_RXN-9528 : 1 NADP+ + 1 (R)-3-hydroxy-decanoyl-[ACP] <-- 1 H+ + 1 3-oxo-decanoyl-[ACP] + 1 NADPH
cis-dodecenoyl-biosynthesis_palmitate-biosynthesis_4.2.1.59_RXN-9655 : 1 (R)-3-hydroxy-decanoyl-[ACP] --> 1 trans-D2-decenoyl-[ACP] + 1 H2O
palmitate-biosynthesis-II-(bacteria-and-plants)_1.3.1.9_RXN-9660: 1 NAD+ + 1 Decanoyl-[ACP] <-- 1 H+ + 1 NADH + 1 trans-D2-decenoyl-[ACP]

dodecanoic acid
palmitate-biosynthesis-II-(bacteria-and-plants)_2.3.1.180_2.3.1.41_RXN-9531 : 1 Decanoyl-[ACP] + 1 malonyl-[ACP] + 1 H+ --> 1 ACP + 1 CO2 + 1 3-oxo-dodecanoyl-[ACP]
palmitate-biosynthesis_1.1.1.100_RXN-9532 : 1 NADP+ + 1 (R)-3-hydroxy-dodecanoyl-[ACP] <-- 1 NADPH + 1 3-oxo-dodecanoyl-[ACP] + 1 H+
palmitate-biosynthesis_4.2.1.59_RXN-9533 : 1 (R)-3-hydroxy-dodecanoyl-[ACP] --> 1 H2O + 1 trans-D2-dodecenoyl-[ACP]
palmitate-biosynthesis-II-(bacteria-and-plants)_1.3.1.9_RXN-9661 : 1 NAD+ + 1 Dodecanoyl-[ACP] <-- 1 H+ + 1 trans-D2-dodecenoyl-[ACP] + 1 NADH
tetradecanoic acid
palmitate-biosynthesis-II-(bacteria-and-plants)_2.3.1.180_2.3.1.41_RXN-9535 : 1 Dodecanoyl-[ACP] + 1 malonyl-[ACP] + 1 H+ --> 1 ACP + 1 CO2 + 1 3-oxo-tetradecanoyl-[ACP]
palmitate-biosynthesis_1.1.1.100_RXN-9536 : 1 NADP+ + 1 (R)-3-hydroxy-tetradecanoyl-[ACP] <-- 1 NADPH + 1 3-oxo-tetradecanoyl-[ACP] + 1 H+
palmitate-biosynthesis_4.2.1.59_RXN-9537 : 1 (R)-3-hydroxy-tetradecanoyl-[ACP] --> 1 H2O + 1 trans-D2-tetradecenoyl-[ACP]
palmitate-biosynthesis-II-(bacteria-and-plants)_1.3.1.9_RXN-9662 : 1 NAD+ + 1 Tetradecanoyl-[ACP] <-- 1 H+ + 1 trans-D2-tetradecenoyl-[ACP] + 1 NADH

hexadecanoic acid
palmitate-biosynthesis-II-(bacteria-and-plants)_2.3.1.41_RXN-9539 : 1 Tetradecanoyl-[ACP] + 1 malonyl-[ACP] + 1 H+ --> 1 ACP + 1 CO2 + 1 3-oxo-hexadecanoyl-[ACP]
palmitate-biosynthesis_1.1.1.100_RXN-9540 : 1 NADP+ + 1 (R)-3-hydroxy-hexadecanoyl-[ACP] <-- 1 NADPH + 1 3-oxo-hexadecanoyl-[ACP] + 1 H+
palmitate-biosynthesis_4.2.1.59_4.2.1.61-RXN : 1 (R)-3-hydroxy-hexadecanoyl-[ACP] --> 1 H2O + 1 trans-D2-hexadecenoyl-[ACP]
palmitate-biosynthesis-II-(bacteria-and-plants)_1.3.1.9_RXN-9663 : 1 NAD+ + 1 Hexadecanoyl-[ACP] <-- 1 H+ + 1 trans-D2-hexadecenoyl-[ACP] + 1 NADH

octadecanoic acid
stearate-biosynthesis-II-(bacteria-and-plants)_2.3.1.41_RXN-9632 : 1 Hexadecanoyl-[ACP] + 1 malonyl-[ACP] + 1 H+ --> 1 ACP + 1 CO2 + 1 3-oxo-octadecanoyl-[ACP]
stearate-biosynthesis_1.1.1.100_RXN-9633 : 1 NADP+ + 1 (R)-3-hydroxy-octadecanoyl-[ACP] <-- 1 NADPH + 1 3-oxo-octadecanoyl-[ACP] + 1 H+
stearate-biosynthesis_4.2.1.59_RXN-9634 : 1 (R)-3-hydroxy-octadecanoyl-[ACP] --> 1 H2O + 1 trans-D2-octadecenoyl-[ACP]
stearate-biosynthesis-II-(bacteria-and-plants)_1.3.1.9_RXN-9635 : 1 NAD+ + 1 Octadecanoyl-[ACP] <-- 1 H+ + 1 trans-D2-octadecenoyl-[ACP] + 1 NADH

cis-D5-dodecenoyl-[ACP]
cis-dodecenoyl-biosynthesis_5.3.3.14_5.3.3.14-RXN : 1 trans-D2-decenoyl-[ACP] --> 1 cis-D3-decenoyl-[ACP]
cis-dodecenoyl-biosynthesis_fabB_RXN : 1 cis-D3-decenoyl-[ACP] + 1 malonyl-[ACP] --> 1 3-oxo-cis-D5-dodecenoyl-[ACP] + ACP + CO2
cis-dodecenoyl-biosynthesis_1.1.1.100_RXN0-2142 : 1 (3R)-hydroxy-cis-D5-dodecenoyl-[ACP] + 1 NADP+ <-- 1 H+ + 1 3-oxo-cis-D5-dodecenoyl-[ACP] + 1 NADPH
cis-dodecenoyl-biosynthesis_4.2.1.59_RXN0-2144 : 1 (3R)-hydroxy-cis-D5-dodecenoyl-[ACP] --> 1 H2O + 1 trans-D3-cis-D5-dodecenoyl-[ACP]
cis-dodecenoyl-biosynthesis_1.3.1.9_RXN0-2145 : 1 cis-D5-dodecenoyl-[ACP] + 1 NAD+ <-- 1 H+ + 1 trans-D3-cis-D5-dodecenoyl-[ACP] + 1 NADH

Palmitoleoyl-[ACP] ((Z)-hexadec-11-enoyl-[ACP])
palmitoleate-biosynthesis-I_2.3.1.41_RXN-10654 : 1 cis-D5-dodecenoyl-[ACP] + 1 malonyl-[ACP] + 1 H+ --> 1 ACP + 1 CO2 + 1 3-oxo-cis-D7-tetradecenoyl-[ACP]
palmitoleate-biosynthesis-I_1.1.1.100_RXN-10655 : 1 NADP+ + 1 (3R)-hydroxy-cis-D7-tetradecenoyl-[ACP] <-- 1 3-oxo-cis-D7-tetradecenoyl-[ACP] + 1 NADPH + 1 H+
palmitoleate-biosynthesis-I_4.2.1.59_RXN-10656 : 1 (3R)-hydroxy-cis-D7-tetradecenoyl-[ACP] --> 1 trans-D3-cis-D7-tetradecenoyl-[ACP] + 1 H2O
palmitoleate-biosynthesis-I_1.3.1.9_RXN-10657 : 1 cis-D7-tetradecenoyl-[ACP] + 1 NAD+ <-- 1 trans-D3-cis-D7-tetradecenoyl-[ACP] + 1 H+ + 1 NADH
palmitoleate-biosynthesis-I_2.3.1.41_RXN-10658 : 1 cis-D7-tetradecenoyl-[ACP] + 1 malonyl-[ACP] + 1 H+ --> 1 CO2 + 1 3-oxo-cis-D9-hexadecenoyl-[ACP] + 1 ACP
palmitoleate-biosynthesis-I_1.1.1.100_RXN-10659 : 1 NADP+ + 1 (3R)-hydroxy-cis-D9-hexaecenoyl-[ACP] <-- 1 3-oxo-cis-D9-hexadecenoyl-[ACP] + 1 H+ + 1 NADPH
palmitoleate-biosynthesis-I_4.2.1.59_RXN-10660 : 1 (3R)-hydroxy-cis-D9-hexaecenoyl-[ACP] --> 1 H2O + 1 trans-D3-cis-D9-hexadecenoyl-[ACP]
palmitoleate-biosynthesis-I_1.3.1.9_RXN-10661 : 1 Palmitoleoyl-[ACP] + 1 NAD+ <-- 1 H+ + 1 trans-D3-cis-D9-hexadecenoyl-[ACP] + 1 NADH

cis-vaccenic acid ((Z)-octadec-11-enoic acid)
cis-vaccenate-biosynthesis_2.3.1.179_2.3.1.179-RXN : 1 Palmitoleoyl-[ACP] + 1 malonyl-[ACP] + 1 H+ --> 1 3-oxo-cis-vaccenoyl-[ACP] + 1 CO2 + 1 ACP
cis-vaccenate-biosynthesis_1.1.1.100_RXN-9556 : 1 (R)-3-hydroxy-cis-vaccenoyl-[ACP] + 1 NADP+ <-- 1 3-oxo-cis-vaccenoyl-[ACP] + 1 H+ + 1 NADPH
cis-vaccenate-biosynthesis_4.2.1.59_RXN-9557 : 1 (R)-3-hydroxy-cis-vaccenoyl-[ACP] --> 1 H2O + 1 cis-vaccen-2-enoyl-[ACP]

cis-vaccenate-biosynthesis_1.3.1.9_RXN-9558 : 1 NADH + 1 H+ + 1 cis-vaccen-2-enoyl-[ACP] --> 1 NAD+ + 1 cis-vaccenoyl-[ACP]

##

 # phospholipids

phosphatidylglycerol
CDP-diacylglycerol-biosynthesis_1.1.1.94_GLYC3PDEHYDROGBIOSYN-RXN_NAD : 1 NAD+ + 1 sn-glycerol_3-phosphate <-- 1 dihydroxyacetone_phosphate + 1 NADH + 1 H+
CDP-diacylglycerol-biosynthesis_1.1.1.94_GLYC3PDEHYDROGBIOSYN-RXN_NADP : 1 sn-glycerol_3-phosphate + 1 NADP+ <-- 1 NADPH + 1 dihydroxyacetone_phosphate + 1 H+
CDP-diacylglycerol-biosynthesis-II_2.3.1.15_RXN-10462 : 1 cis-vaccenoyl-[ACP] + 1 sn-glycerol_3-phosphate --> 1 cis-vaccenoyl-sn-glycerol-3-phosphate + 1 ACP
CDP-diacylglycerol-biosynthesis_2.3.1.51_1-ACYLGLYCEROL-3-P-ACYLTRANSFER-RXN : 1 cis-vaccenoyl-sn-glycerol-3-phosphate + 1 cis-vaccenoyl-[ACP] --> 1 1,2-di-cis-vaccenoyl-sn-glycerol-3-phosphate + 1 ACP
~no-pathway_2.7.7.41_RXN0-5515 : 1 CTP + 1 1,2-di-cis-vaccenoyl-sn-glycerol-3-phosphate + 1 H+ --> 1 diphosphate + 1 CDP-1,2-di-cis-vaccenoylglycerol
PG_I-2.7.8.5-PHOSPHAGLYPSYN-RXN : 1 CDP-1,2-di-cis-vaccenoylglycerol + 1 sn-glycerol_3-phosphate --> 1 H+ + 1 CMP + 1 L-1-phosphatidylglycerol-phosphate
~no-pathway_3.1.3.27_RXN-13313 : 1 L-1-phosphatidylglycerol-phosphate + 1 H2O --> 1 L-1-phosphatidylglycerol + 1 phosphate

phosphatidylethanolamine
PE_2.7.8.8_RXN : 1 CDP-1,2-di-cis-vaccenoylglycerol + 1 L-serine --> 1 H+ + 1 CMP + 1 L-1-phosphatidylserine
phosphatidylethanolamine-biosynthesis-I_4.1.1.65_PHOSPHASERDECARB-RXN : 1 L-1-phosphatidylserine + 1 H+ --> 1 CO2 + 1 L-1-phosphatidylethanolamine

phosphatidylcholine
phosphatidylcholine-biosynthesis-V_2.1.1.17_2.1.1.17-RXN : 1 L-1-phosphatidylethanolamine + 1 S-adenosyl-L-methionine --> 1 phosphatidyl-N-methylethanolamine + 1 S-adenosyl-L-homocysteine + 1 H+
phosphatidylcholine-biosynthesis_2.1.1.71_2.1.1.71-RXN : 1 phosphatidyl-N-methylethanolamine + 1 S-adenosyl-L-methionine --> 1 H+ + 1 phosphatidyl-N-dimethylethanolamine + 1 S-adenosyl-L-homocysteine
phosphatidylcholine-biosynthesis_2.1.1.17_2.1.1.71_RXN4FS-2 : 1 phosphatidyl-N-dimethylethanolamine + 1 S-adenosyl-L-methionine --> 1 phosphatidylcholine + 1 H+ + 1 S-adenosyl-L-homocysteine

cardiolipin
cardiolipin-biosynthesis-I_2.7.8.-_CARDIOLIPSYN-RXN : L-1-phosphatidylglycerol + CDP-1,2-di-cis-vaccenoylglycerol --> 1 cardiolipin + 1 CMP + H+

##

 # amino acids biosynthesis

aspartate and asparagine biosynthesis
~multiple-pathways_2.6.1.1_ASPAMINOTRANS-RXN : 1 2-oxoglutarate + 1 L-aspartate <=> 1 oxaloacetate + 1 L-glutamate
~metabolism-of-asparagine_3.5.1.1_ASPARAGHYD-RXN : 1 L-asparagine + 1 H2O --> 1 L-aspartate + 1 ammonia + 1 H+
~no-pathway_6.1.1.-_RXN490-3616 : 1 L-aspartate + 1 |ASN-tRNAs| + 1 ATP --> 1 diphosphate + 1 |L-aspartyl-tRNAAsn| + 1 AMP

~no-pathway_6.3.5.6_6.3.5.6-RXN : 1 L-glutamine + 1 |L-aspartyl-tRNAAsn| + 1 H2O + 1 ATP --> 1 L-glutamate + 1 |Charged-ASN-tRNAs| + 2 H+ + 1 phosphate + 1 ADP
~no-pathway_3.1.1.29_RXN-12460 : 1 |Charged-ASN-tRNAs| + 1 H2O --> 2 H+ + 1 |ASN-tRNAs| + 1 L-asparagine

glutamate and glutamine biosynthesis
~multiple-pathways_1.4.1.3_GLUTAMATE-DEHYDROGENASE-NADP+-RXN_NAD : 1 L-glutamate + 1 H2O + 1 NAD+ <=> 1 2-oxoglutarate + 1 NADH + 2 H+ + 1 ammonia
~multiple-pathways_1.4.1.3_GLUTAMATE-DEHYDROGENASE-NADP+-RXN_NADP : 1 L-glutamate + 1 H2O + 1 NADP+ <-- 1 ammonia + 1 NADPH + 1 2-oxoglutarate + 2 H+
glutamate-biosynthesis_glutamine-degradation_1.4.1.13_GLUTAMATESYN-RXN : 1 NADP+ + 2 L-glutamate <-- 1 H+ + 1 2-oxoglutarate + 1 NADPH + 1 L-glutamine
glutamine-biosynthesis_nitrate-reduction_6.3.1.2_GLUTAMINESYN-RXN : 1 ATP + 1 ammonia + 1 L-glutamate --> 1 ADP + 1 phosphate + 1 L-glutamine

proline biosynthesis
proline-biosynthesis_citrulline-biosynthesis_2.7.2.11_GLUTKIN-RXN : 1 ATP + 1 L-glutamate --> 1 ADP + 1 L-glutamate-5-phosphate
proline-biosynthesis_citrulline-biosynthesis_1.2.1.41_GLUTSEMIALDEHYDROG-RXN : 1 NADP+ + 1 L-glutamate-5-semialdehyde + 1 phosphate <-- 1 NADPH + 1 L-glutamate-5-phosphate + 1 H+
proline-biosynthesis_arginine-degradation_1.5.1.2_PYRROLINECARBREDUCT-RXN_NAD : 1 NAD+ + 1 L-proline <-- 1 (S)-1-pyrroline-5-carboxylate + 1 NADH + 2 H+
proline-biosynthesis_arginine-degradation_1.5.1.2_PYRROLINECARBREDUCT-RXN_NADP : 1 NADP+ + 1 L-proline <-- 2 H+ + 1 NADPH + 1 (S)-1-pyrroline-5-carboxylate

arginine biosynthesis
ornithine-biosynthesis_arginine-biosynthesis_2.3.1.1_N-ACETYLTRANSFER-RXN : 1 acetyl-CoA + 1 L-glutamate --> 1 H+ + 1 coenzyme_A + 1 N-acetyl-L-glutamate
arginine-biosynthesis-II-(acetyl-cycle)_2.3.1.35_GLUTAMATE-N-ACETYLTRANSFERASE-RXN : 1 N-acetyl-L-ornithine + 1 L-glutamate --> 1 L-ornithine + 1 N-acetyl-L-glutamate
ornithine-biosynthesis_arginine-biosynthesis_2.7.2.8_ACETYLGLUTKIN-RXN : 1 ATP + 1 N-acetyl-L-glutamate --> 1 N-acetylglutamyl-phosphate + 1 ADP
ornithine-biosynthesis_arginine-biosynthesis_1.2.1.38_N-ACETYLGLUTPREDUCT-RXN : 1 NADP+ + 1 N-acetyl-L-glutamate_5-semialdehyde + 1 phosphate <=> 1 H+ + 1 N-acetylglutamyl-phosphate + 1 NADPH
ornithine-biosynthesis_arginine-biosynthesis_2.6.1.11_ACETYLORNTRANSAM-RXN : 1 2-oxoglutarate + 1 N-acetyl-L-ornithine <=> 1 L-glutamate + 1 N-acetyl-L-glutamate_5-semialdehyde
ornithine-biosynthesis_3.5.1.16_ACETYLORNDEACET-RXN : 1 N-acetyl-L-ornithine + 1 H2O --> 1 acetate + 1 L-ornithine
~multiple-pathways_2.1.3.3_ORNCARBAMTRANSFER-RXN : 1 carbamoyl-phosphate + 1 L-ornithine <=> 1 H+ + 1 L-citrulline + 1 phosphate
~multiple-pathways_6.3.4.5_ARGSUCCINSYN-RXN : 1 L-aspartate + 1 L-citrulline + 1 ATP --> 1 diphosphate + 1 L-arginino-succinate + 1 H+ + 1 AMP
~multiple-pathways_4.3.2.1_ARGSUCCINLYA-RXN : 1 L-arginino-succinate <=> 1 fumarate + 1 L-arginine
de-novo-biosynthesis-of-uridine-5'-monophosphate_arginine-biosynthesis_6.3.5.5_CARBPSYN-RXN : 2 ATP + 1 L-glutamine + 1 H2O + 1 bicarbonate --> 1 phosphate + 2 ADP + 2 H+ + 1 L-glutamate + 1 carbamoyl-phosphate

valine biosynthesis
valine-biosynthesis_2.2.1.6_ACETOLACTSYN-RXN : 2 pyruvate + 1 H+ --> 1 CO2 + 1 (S)-2-acetolactate
valine-biosynthesis_1.1.1.86_ACETOLACTREDUCTOISOM-RXN : 1 NADP+ + 1 (R)-2,3-dihydroxy-3-methylbutanoate <=> 1 NADPH + 1 H+ + 1 (S)-2-acetolactate
valine-biosynthesis_4.2.1.9_DIHYDROXYISOVALDEHYDRAT-RXN : 1 (R)-2,3-dihydroxy-3-methylbutanoate --> 1 H2O + 1 2-oxoisovalerate
~multiple-pathways_2.6.1.42_BRANCHED-CHAINAMINOTRANSFERVAL-RXN : 1 2-oxoglutarate + 1 L-valine <=> 1 L-glutamate + 1 2-oxoisovalerate

leucine biosynthesis
leucine-biosynthesis_2.3.3.13_2-ISOPROPYLMALATESYN-RXN : 1 acetyl-CoA + 1 H2O + 1 2-oxoisovalerate --> 1 coenzyme_A + 1 H+ + 1 (2S)-2-isopropylmalate
leucine-biosynthesis_4.2.1.33_3-ISOPROPYLMALISOM-RXN : 1 (2S)-2-isopropylmalate --> 1 2-isopropylmaleate + 1 H2O
leucine_metabolism-4.2.1.33-RXN-8991 : 1 (2R,3S)-3-isopropylmalate <-- 1 2-isopropylmaleate + 1 H2O
leucine-biosynthesis_1.1.1.85_3-ISOPROPYLMALDEHYDROG-RXN : 1 (2R,3S)-3-isopropylmalate + 1 NAD+ <=> 1 H+ + 1 NADH + 1 (2S)-2-isopropyl-3-oxosuccinate
leucine-biosynthesis_1.1.1.85_RXN-7800 : 1 (2S)-2-isopropyl-3-oxosuccinate + 1 H+ --> 1 CO2 + 1 4-methyl-2-oxopentanoate
leucine-biosynthesis_2.6.1.42_BRANCHED-CHAINAMINOTRANSFERLEU-RXN : 1 2-oxoglutarate + 1 L-leucine <=> 1 L-glutamate + 1 4-methyl-2-oxopentanoate

isoleucine biosynthesis
isoleucine-biosynthesis-from-threonine_isoleucine-biosynthesis_2.2.1.6_ACETOOHBUTSYN-RXN: 1 H+ + 1 2-oxobutanoate + 1 pyruvate --> 1 CO2 + 1 2-aceto-2-hydroxy-butanoate
isoleucine-biosynthesis-from-threonine_isoleucine-biosynthesis_1.1.1.86_ACETOOHBUTREDUCTOISOM-RXN : 1 NADP+ + 1 2,3-dihydroxy-3-methylvalerate <=> 1 H+ + 1 NADPH + 1 2-aceto-2-hydroxy-butanoate
isoleucine-biosynthesis-from-threonine_isoleucine-biosynthesis_4.2.1.9_DIHYDROXYMETVALDEHYDRAT-RXN : 1 2,3-dihydroxy-3-methylvalerate --> 1 H2O + 1 2-keto-3-methyl-valerate
~metabolism-of-isoleucine_2.6.1.42_BRANCHED-CHAINAMINOTRANSFERILEU-RXN : 1 2-oxoglutarate + 1 L-isoleucine <=> 1 L-glutamate + 1 2-keto-3-methyl-valerate
isoleucine-biosynthesis-from-threonine_threonine-degradation_4.3.1.19_THREDEHYD-RXN : 1 L-threonine --> 1 H+ + 1 2-oxobutanoate + 1 ammonia

threonine biosynthesis
~metabolism-of-biosynthesis_2.7.2.4_ASPARTATEKIN-RXN : 1 ATP + 1 L-aspartate --> 1 L-aspartyl-4-phosphate + 1 ADP
~metabolism-of-biosynthesis_1.2.1.11_ASPARTATE-SEMIALDEHYDE-DEHYDROGENASE-RXN : 1 phosphate + 1 NADP+ + 1 L-aspartate-semialdehyde <=> 1 NADPH + 1 L-aspartyl-4-phosphate + 1 H+
homoserine-biosynthesis_1.1.1.3_HOMOSERDEHYDROG-RXN_NAD : 1 NAD+ + 1 L-homoserine <-- 1 L-aspartate-semialdehyde + 1 NADH + 1 H+
homoserine-biosynthesis_1.1.1.3_HOMOSERDEHYDROG-RXN_NADP : 1 L-homoserine + 1 NADP+ <-- 1 H+ + 1 NADPH + 1 L-aspartate-semialdehyde
methionine-biosynthesis_threonine-biosynthesis-from-homoserine_2.7.1.39_HOMOSERKIN-RXN : 1 L-homoserine + 1 ATP --> 1 H+ + 1 O-phospho-L-homoserine + 1 ADP
threonine-biosynthesis-from-homoserine_4.2.3.1_THRESYN-RXN : 1 O-phospho-L-homoserine + 1 H2O --> 1 L-threonine + 1 phosphate

methionine biosynthesis
methionine-biosynthesis-I_2.3.1.46_HOMSUCTRAN-RXN : 1 L-homoserine + 1 succinyl-CoA --> 1 coenzyme_A + 1 O-succinyl-L-homoserine
methionine-biosynthesis-I_2.5.1.48_O-SUCCHOMOSERLYASE-RXN : 1 L-cysteine + 1 O-succinyl-L-homoserine --> 1 L-cystathionine + 1 succinate + 1 H+
methionine-biosynthesis_homocysteine-and-cysteine-interconversion_4.4.1.8_CYSTATHIONINE-BETA-LYASE-RXN : 1 H2O + 1 L-cystathionine --> 1 L-homocysteine + 1 ammonia + 1 H+ + 1 pyruvate
~multiple-pathways_2.1.1.13_HOMOCYSMETB12-RXN : 1 5-methyl-tetrahydrofolate + 1 L-homocysteine --> 1 tetrahydrofolate + 1 L-methionine
S-adenosyl-L-methionine-cycle_methionine-biosynthesis_2.1.1.14_HOMOCYSMET-RXN : 1 5-methyltetrahydropteroyltri-L-glutamate + 1 L-homocysteine <=> 1 L-methionine + 1 tetrahydropteroyl_tri-L-glutamate
~multiple-pathways_2.5.1.6_S-ADENMETSYN-RXN : 1 L-methionine + 1 ATP + 1 H2O --> 1 phosphate + 1 diphosphate + 1 S-adenosyl-L-methionine
S-adenosyl-L-methionine-cycle_methionine-degradation_3.3.1.1_ADENOSYLHOMOCYSTEINASE-RXN: 1 S-adenosyl-L-homocysteine + 1 H2O <=> 1 L-homocysteine + 1 adenosine

S-methyl-5-thio-alpha-D-ribose-1-phosphate-degradation-II_2.5.1.49_O-ACETYLHOMOSERINE-THIOL-LYASE-RXN : 1 O-acetyl-L-homoserine + 1 methanethiol --> 1 acetate + 1 H+ + 1 L-methionine
homocysteine-biosynthesis_2.5.1.49_ACETYLHOMOSER-CYS-RXN : 1 O-acetyl-L-homoserine + 1 hydrogen_sulfide <=> 1 H+ + 1 acetate + 1 L-homocysteine

lysine biosynthesis
lysine-biosynthesis_4.3.3.7_DIHYDRODIPICSYN-RXN : 1 L-aspartate-semialdehyde + 1 pyruvate --> 1 H2O + 1 H+ + 1 (2S,4S)-4-hydroxy-2,3,4,5-tetrahydrodipicolinate
~no-pathway_1.17.1.8_RXN-14014 : 1 NADP+ + 1 H2O + 1 (S)-2,3,4,5-tetrahydrodipicolinate <-- 1 H+ + 1 (2S,4S)-4-hydroxy-2,3,4,5-tetrahydrodipicolinate + 1 NADPH
lysine-biosynthesis-I_2.3.1.117_TETHYDPICSUCC-RXN : 1 (S)-2,3,4,5-tetrahydrodipicolinate + 1 succinyl-CoA + 1 H2O --> 1 coenzyme_A + 1 N-succinyl-2-amino-6-ketopimelate
lysine-biosynthesis-I_2.6.1.17_SUCCINYLDIAMINOPIMTRANS-RXN : 1 2-oxoglutarate + 1 N-succinyl-L,L-2,6-diaminopimelate <=> 1 N-succinyl-2-amino-6-ketopimelate + 1 L-glutamate
lysine-biosynthesis-I_3.5.1.18_SUCCDIAMINOPIMDESUCC-RXN : 1 N-succinyl-L,L-2,6-diaminopimelate + 1 H2O --> 1 succinate + 1 L,L-diaminopimelate
lysine-biosynthesis_5.1.1.7_DIAMINOPIMEPIM-RXN : 1 L,L-diaminopimelate <=> 1 meso-diaminopimelate
lysine-biosynthesis_4.1.1.20_DIAMINOPIMDECARB-RXN : 1 meso-diaminopimelate + 1 H+ --> 1 L-lysine + 1 CO2

serine and glycine biosynthesis
serine-biosynthesis_1.1.1.95_PGLYCDEHYDROG-RXN : 1 3-phospho-D-glycerate + 1 NAD+ <=> 1 H+ + 1 NADH + 1 3-phospho-hydroxypyruvate
serine-biosynthesis_2.6.1.52_PSERTRANSAM-RXN : 1 3-phospho-L-serine + 1 2-oxoglutarate <=> 1 L-glutamate + 1 3-phospho-hydroxypyruvate
serine-biosynthesis_3.1.3.3_RXN0-5114 : 1 3-phospho-L-serine + 1 H2O --> 1 phosphate + 1 L-serine
~multiple-pathways_2.1.2.1_GLYOHMETRANS-RXN : 1 L-serine + 1 tetrahydrofolate <=> 1 H2O + 1 5,10-methylenetetrahydrofolate + 1 glycine

cysteine and alanine biosynthesis
cysteine-biosynthesis-I_2.3.1.30_SERINE-O-ACETTRAN-RXN : 1 L-serine + 1 acetyl-CoA <=> 1 coenzyme_A + 1 O-acetyl-L-serine
cysteine-biosynthesis-I_2.5.1.47_ACSERLY-RXN : 1 O-acetyl-L-serine + 1 hydrogen_sulfide <=> 1 L-cysteine + 1 H+ + 1 acetate
alanine-biosynthesis-III_2.8.1.7_RXN0-308 : 1 L-cysteine + 1 |L-Cysteine-Desulfurases| --> 1 |Persulfurated-L-cysteine-desulfurases| + 1 L-alanine

tyrosine and phenylalanine biosynthesis
phenylalanine-biosynthesis_tyrosine-biosynthesis_5.4.99.5_CHORISMATEMUT-RXN : 1 chorismate <=> 1 prephenate
tyrosine-biosynthesis-I_1.3.1.12_PREPHENATEDEHYDROG-RXN : 1 NAD+ + 1 prephenate --> 1 NADH + 1 4-hydroxyphenylpyruvate + 1 CO2
~multiple-pathways_2.6.1.57_TYROSINE-AMINOTRANSFERASE-RXN : 1 2-oxoglutarate + 1 L-tyrosine <=> 1 L-glutamate + 1 4-hydroxyphenylpyruvate
phenylalanine-biosynthesis-I_4.2.1.51_PREPHENATEDEHYDRAT-RXN : 1 prephenate + 1 H+ --> 1 keto-phenylpyruvate + 1 CO2 + 1 H2O
phenylalanine-biosynthesis_2.6.1.57_PHEAMINOTRANS-RXN : 1 L-glutamate + 1 keto-phenylpyruvate <=> 1 L-phenylalanine + 1 2-oxoglutarate

tryptophan biosynthesis
tryptophan-biosynthesis_4.1.3.27_ANTHRANSYN-RXN : 1 chorismate + 1 L-glutamine <=> 1 H+ + 1 pyruvate + 1 L-glutamate + 1 anthranilate
tryptophan-biosynthesis_2.4.2.18_PRTRANS-RXN : 1 N-(5'-phosphoribosyl)-anthranilate + 1 diphosphate <-- 1 5-phospho-alpha-D-ribose_1-diphosphate + 1 anthranilate
tryptophan-biosynthesis_5.3.1.24_PRAISOM-RXN : 1 N-(5'-phosphoribosyl)-anthranilate --> 1 1-(o-carboxyphenylamino)-1'-deoxyribulose-5'-phosphate

tryptophan-biosynthesis_4.1.1.48_IGPSYN-RXN : 1 H+ + 1 1-(o-carboxyphenylamino)-1'-deoxyribulose-5'-phosphate --> 1 (1S,2R)-1-C-(indol-3-yl)glycerol_3-phosphate + 1 H2O + 1 CO2
IAA-biosynthesis_tryptophan-biosynthesis_4.2.1.20_RXN0-2381 : 1 (1S,2R)-1-C-(indol-3-yl)glycerol_3-phosphate <=> 1 D-glyceraldehyde-3-phosphate + 1 indole
tryptophan-biosynthesis_4.2.1.20_RXN0-2382 : 1 indole + 1 L-serine --> 1 L-tryptophan + 1 H2O

histidine biosynthesis
PRPP-biosynthesis-II_5.4.2.7_PPENTOMUT-RXN : 1 alpha-D-ribose-1-phosphate <=> 1 D-ribose-5-phosphate
PRPP-biosynthesis-I_2.7.6.1_PRPPSYN-RXN : 1 ATP + 1 D-ribose-5-phosphate <=> 1 5-phospho-alpha-D-ribose_1-diphosphate + 1 H+ + 1 AMP
histidine-biosynthesis-I_2.4.2.17_ATPPHOSPHORIBOSYLTRANS-RXN : 1 phosphoribosyl-ATP + 1 diphosphate <-- 1 5-phospho-alpha-D-ribose_1-diphosphate + 1 ATP
histidine-biosynthesis-I_3.6.1.31_HISTPRATPHYD-RXN : 1 phosphoribosyl-ATP + 1 H2O --> 1 H+ + 1 diphosphate + 1 1-(5-phospho-D-ribosyl)-AMP
histidine-biosynthesis-I_3.5.4.19_HISTCYCLOHYD-RXN : 1 1-(5-phospho-D-ribosyl)-AMP + 1 H2O --> 1 1-(5-phosphoribosyl)-5-[(5-phosphoribosylamino)methylideneamino]imidazole-4-carboxamide
histidine-biosynthesis-I_5.3.1.16_PRIBFAICARPISOM-RXN : 1 1-(5-phosphoribosyl)-5-[(5-phosphoribosylamino)methylideneamino]imidazole-4-carboxamide --> 1 phosphoribulosylformimino-AICAR-P
histidine-biosynthesis-I_4.1.3.-_2.4.2.-_GLUTAMIDOTRANS-RXN : 1 phosphoribulosylformimino-AICAR-P + 1 L-glutamine --> 1 D-erythro-imidazole-glycerol-phosphate + 1 L-glutamate + 1 H+ + 1 aminoimidazole_carboxamide_ribonucleotide
histidine-biosynthesis-I_4.2.1.19_IMIDPHOSDEHYD-RXN : 1 D-erythro-imidazole-glycerol-phosphate --> 1 H2O + 1 imidazole_acetol-phosphate
histidine-biosynthesis-I_2.6.1.9_HISTAMINOTRANS-RXN : 1 L-glutamate + 1 imidazole_acetol-phosphate <=> 1 2-oxoglutarate + 1 L-histidinol-phosphate
histidine-biosynthesis-I_3.1.3.15_HISTIDPHOS-RXN : 1 L-histidinol-phosphate + 1 H2O --> 1 phosphate + 1 histidinol
histidine-biosynthesis-I_1.1.1.23_HISTOLDEHYD-RXN : 1 histidinol + 1 NAD+ --> 1 histidinal + 1 H+ + 1 NADH
histidine-biosynthesis-I_1.1.1.23_HISTALDEHYD-RXN : 1 H2O + 1 NAD+ + 1 histidinal --> 1 NADH + 2 H+ + 1 L-histidine

beta-alanine biosynthesis
beta-alanine-biosynthesis-II_1.3.8.-_PROPCOASYN-RXN : 1 FAD + 1 propanoyl-CoA --> 1 FADH2 + 1 acryloyl-CoA
~multiple-pathways_4.2.1.116_RXN-6383 : 1 3-hydroxypropanoyl-CoA <=> 1 H2O + 1 acryloyl-CoA
beta-alanine-biosynthesis-II_3.1.2.4_RXN-6384 : 1 3-hydroxypropanoyl-CoA + 1 H2O --> 1 coenzyme_A + 1 3-hydroxypropionate + 1 H+
acrylate-degradation_beta-alanine-biosynthesis_1.1.1.59_3-HYDROXYPROPIONATE-DEHYDROGENASE-RXN : 1 3-hydroxypropionate + 1 NAD+ --> 1 H+ + 1 malonate_semialdehyde + 1 NADH
beta-alanine-degradation_beta-alanine-biosynthesis_2.6.1.18_2.6.1.18-RXN: 1 L-alanine + 1 malonate_semialdehyde <=> 1 beta-alanine + 1 pyruvate
~multiple-pathways_2.6.1.19_BS353590 : 1 2-oxoglutarate + 1 beta-alanine <=> 1 L-glutamate + 1 malonate_semialdehyde

##

 # purine metabolism
~no-pathway_2.4.2.14_PRPPAMIDOTRANS-RXN : 1 L-glutamate + 1 diphosphate + 1 5-phospho-beta-D-ribosyl-amine <-- 1 L-glutamine + 1 5-phospho-alpha-D-ribose_1-diphosphate + 1 H2O
~no-pathway_6.3.4.13_GLYRIBONUCSYN-RXN : 1 glycine + 1 5-phospho-beta-D-ribosyl-amine + 1 ATP --> 1 ADP + 1 H+ + 1 5-phospho-ribosyl-glycineamide + 1 phosphate

~no-pathway_6.3.5.3_FGAMSYN-RXN : 1 ATP + 1 L-glutamine + 1 5'-phosphoribosyl-N-formylglycineamide + 1 H2O --> 1 H+ + 1 ADP + 1 phosphate + 1 5-phosphoribosyl-N-formylglycineamidine + 1 L-glutamate
~no-pathway_6.3.3.1_AIRS-RXN : 1 ATP + 1 5-phosphoribosyl-N-formylglycineamidine --> 1 H+ + 1 phosphate + 1 ADP + 1 5-amino-1-(5-phospho-D-ribosyl)imidazole
~no-pathway_6.3.4.18_RXN0-742 : 1 ATP + 1 5-amino-1-(5-phospho-D-ribosyl)imidazole + 1 bicarbonate --> 2 H+ + 1 phosphate + 1 N5-carboxyaminoimidazole_ribonucleotide + 1 ADP
~no-pathway_5.4.99.18_RXN0-743 : 1 N5-carboxyaminoimidazole_ribonucleotide --> 1 5-amino-1-(5-phospho-D-ribosyl)imidazole-4-carboxylate
~no-pathway_6.3.2.6_SAICARSYN-RXN : 1 ATP + 1 5-amino-1-(5-phospho-D-ribosyl)imidazole-4-carboxylate + 1 L-aspartate --> 1 H+ + 1 ADP + 1 phosphate + 1 5'-phosphoribosyl-4-(N-succinocarboxamide)-5-aminoimidazole
~no-pathway_4.3.2.2_AICARSYN-RXN : 1 5'-phosphoribosyl-4-(N-succinocarboxamide)-5-aminoimidazole <=> 1 aminoimidazole_carboxamide_ribonucleotide + 1 fumarate
~no-pathway_2.1.2.3_AICARTRANSFORM-RXN : 1 10-formyl-tetrahydrofolate + 1 aminoimidazole_carboxamide_ribonucleotide <=> 1 phosphoribosyl-formamido-carboxamide + 1 tetrahydrofolate
~no-pathway_3.5.4.10_2.1.2.3_IMPCYCLOHYDROLASE-RXN : 1 IMP + 1 H2O <=> 1 phosphoribosyl-formamido-carboxamide
purine-nucleotides-de-novo-biosynthesis-II_6.3.4.4_ADENYLOSUCCINATE-SYNTHASE-RXN : 1 L-aspartate + 1 GTP + 1 IMP --> 1 GDP + 1 phosphate + 2 H+ + 1 adenylo-succinate
purine-nucleotides-de-novo-biosynthesis-II_4.3.2.2_AMPSYN-RXN : 1 adenylo-succinate <=> 1 fumarate + 1 AMP
salvage-pathways-of-purine-and-pyrimidine-nucleotides_2.7.4.3_ADENYL-KIN-RXN : 1 AMP + 1 ATP <=> 2 ADP
~no-pathway_1.17.4.1_ADPREDUCT-RXN : 1 dADP + 1 H2O + 1 |Ox-Thioredoxin| <-- 1 |Red-Thioredoxin| + 1 ADP
~no-pathway_2.7.4.6_DADPKIN-RXN : 1 dADP + 1 ATP --> 1 dATP + 1 ADP
purine-nucleotides-de-novo-biosynthesis_urate-biosynthesis_1.1.1.205_IMP-DEHYDROG-RXN : 1 NAD+ + 1 H2O + 1 IMP <=> 1 NADH + 1 H+ + 1 XMP
purine-nucleotides-de-novo-biosynthesis-II_6.3.5.2_GMP-SYN-GLUT-RXN : 1 XMP + 1 H2O + 1 ATP + 1 L-glutamine --> 1 L-glutamate + 1 diphosphate + 1 AMP + 2 H+ + 1 GMP
salvage-pathways-of-purine-and-pyrimidine-nucleotides_2.7.4.8_GUANYL-KIN-RXN : 1 ATP + 1 GMP --> 1 GDP + 1 ADP
~no-pathway_2.7.4.8_GMKALT-RXN : 1 ATP + 1 dGMP --> 1 dGDP + 1 ADP
~no-pathway_1.17.4.1_GDPREDUCT-RXN : 1 H2O + 1 dGDP + 1 |Ox-Thioredoxin| <-- 1 |Red-Thioredoxin| + 1 GDP
~no-pathway_2.7.4.6_DGDPKIN-RXN : 1 ATP + 1 dGDP --> 1 dGTP + 1 ADP
ppGpp-biosynthesis_2.7.4.6_GDPKIN-RXN : 1 GDP + 1 ATP --> 1 GTP + 1 ADP
salvage-pathways-of-adenine,-hypoxanthine,-and-their-nucleosides_3.1.3.5_AMP-DEPHOSPHORYLATION-RXN : 1 H2O + 1 AMP --> 1 phosphate + 1 adenosine
~no-pathway_3.1.3.5_RXN-7609 : 1 H2O + 1 GMP --> 1 phosphate + 1 guanosine
urate-biosynthesis_3.1.3.5_XMPXAN-RXN : 1 H2O + 1 XMP --> 1 xanthosine + 1 phosphate
~no-pathway_3.1.3.5_RXN-7607 : 1 IMP + 1 H2O --> 1 phosphate + 1 inosine
~no-pathway_3.1.3.5_RXN-14142 : 1 dGMP + 1 H2O --> 1 phosphate + 1 deoxyguanosine
~no-pathway_3.1.3.5_RXN-14161 : 1 H2O + 1 dAMP --> 1 phosphate + 1 deoxyadenosine
purine-deoxyribonucleosides-degradation_2.4.2.1_DEOXYADENPHOSPHOR-RXN : 1 deoxyadenosine + 1 phosphate <=> 1 adenine + 1 2-deoxy-alpha-D-ribose_1-phosphate
purine-deoxyribonucleosides-degradation_2.4.2.1_DEOXYGUANPHOSPHOR-RXN : 1 phosphate + 1 deoxyguanosine <=> 1 guanine + 1 2-deoxy-alpha-D-ribose_1-phosphate
purine-deoxyribonucleosides-degradation_2.4.2.1_DEOXYINOPHOSPHOR-RXN : 1 deoxyinosine + 1 phosphate <=> 1 hypoxanthine + 1 2-deoxy-alpha-D-ribose_1-phosphate
~metabolism-of-purine_2.4.2.1_ADENPHOSPHOR-RXN : 1 adenosine + 1 phosphate <=> 1 alpha-D-ribose-1-phosphate + 1 adenine
~multiple-pathways_2.4.2.1_INOPHOSPHOR-RXN : 1 phosphate + 1 inosine <=> 1 alpha-D-ribose-1-phosphate + 1 hypoxanthine
~metabolism-of-purine_2.4.2.1_RXN0-5199 : 1 guanosine + 1 phosphate <=> 1 alpha-D-ribose-1-phosphate + 1 guanine

~multiple-pathways_2.4.2.1_XANTHOSINEPHOSPHORY-RXN : 1 xanthosine + 1 phosphate <=> 1 xanthine + 1 alpha-D-ribose-1-phosphate
~no-pathway_3.5.4.2_ADENINE-DEAMINASE-RXN : 1 adenine + 1 H2O --> 1 ammonia + 1 hypoxanthine
purine-degradation_3.5.4.3_GUANINE-DEAMINASE-RXN : 1 guanine + 1 H2O --> 1 xanthine + 1 ammonia
~metabolism-of-salvage-pathways-purine_2.4.2.7_ADENPRIBOSYLTRAN-RXN: 1 AMP + 1 diphosphate <-- 1 5-phospho-alpha-D-ribose_1-diphosphate + 1 adenine
~no-pathway_2.4.2.8_HYPOXANPRIBOSYLTRAN-RXN : 1 diphosphate + 1 IMP <-- 1 5-phospho-alpha-D-ribose_1-diphosphate + 1 hypoxanthine
salvage-pathways-of-purine-and-pyrimidine-nucleotides_2.4.2.8_2.4.2.22_GUANPRIBOSYLTRAN-RXN : 1 GMP + 1 diphosphate <-- 1 5-phospho-alpha-D-ribose_1-diphosphate + 1 guanine
salvage-pathways-of-guanine,-xanthine,-and-their-nucleosides_2.4.2.8_2.4.2.22_XANPRIBOSYLTRAN-RXN : 1 diphosphate + 1 XMP <-- 1 xanthine + 1 5-phospho-alpha-D-ribose_1-diphosphate
~multiple-pathways_1.17.1.4_RXN0-901: 1 NAD+ + 1 H2O + 1 xanthine <=> 1 H+ + 1 urate + 1 NADH
~multiple-pathways_1.17.1.4_RXN-7682: 1 hypoxanthine + 1 NAD+ + 1 H2O --> 1 NADH + 1 H+ + 1 xanthine
~no-pathway_3.6.1.19_RXN0-1603 : 1 XTP + 1 H2O --> 1 H+ + 1 XMP + 1 diphosphate
~no-pathway_3.6.1.19_RXN0-6382 : 1 ITP + 1 H2O --> 1 H+ + 1 diphosphate + 1 IMP
~no-pathway_3.6.1.19_RXN-14140 : 1 GTP + 1 H2O --> 1 diphosphate + 1 H+ + 1 GMP
~no-pathway_3.6.1.19_RXN0-385 : 1 dGTP + 1 H2O --> 1 H+ + 1 diphosphate + 1 dGMP
~no-pathway_3.6.1.19_RXN0-384 : 1 dATP + 1 H2O --> 1 H+ + 1 diphosphate + 1 dAMP
~no-pathway_3.1.5.1_DGTPTRIPHYDRO-RXN : 1 dGTP + 1 H2O --> 1 H+ + 1 PPPi + 1 deoxyguanosine
ppGpp-biosynthesis_3.1.7.2_PPGPPSYN-RXN : 1 ppGpp + 1 H2O --> 1 H+ + 1 diphosphate + 1 GDP
ppGpp-biosynthesis_3.1.7.2_RXN0-6427 : 1 H2O + 1 pppGpp --> 1 diphosphate + 1 H+ + 1 GTP
ppGpp-biosynthesis_2.7.6.5_GDPPYPHOSKIN-RXN : 1 GDP + 1 ATP --> 1 ppGpp + 1 AMP
ppGpp-biosynthesis_2.7.6.5_GTPPYPHOSKIN-RXN : 1 GTP + 1 ATP --> 1 pppGpp + 1 AMP
ppGpp-biosynthesis_3.6.1.11_3.6.1.40_PPPGPPHYDRO-RXN : 1 H2O + 1 pppGpp --> 1 H+ + 1 phosphate + 1 ppGpp

 # pyrimidine metabolism
de-novo-biosynthesis-of-uridine-5'-monophosphate_2.1.3.2_ASPCARBTRANS-RXN : 1 carbamoyl-phosphate + 1 L-aspartate <=> 1 H+ + 1 N-carbamoyl-L-aspartate + 1 phosphate
de-novo-biosynthesis-of-uridine-5'-monophosphate_3.5.2.3_DIHYDROOROT-RXN : 1 (S)-dihydroorotate + 1 H2O <=> 1 H+ + 1 N-carbamoyl-L-aspartate
de-novo-biosynthesis-of-uridine-5'-monophosphate_1.3.5.2_RXN0-6491 : 1 ubiquinone-10 + 1 (S)-dihydroorotate --> 1 ubiquinol-10 + 1 orotate
de-novo-biosynthesis-of-uridine-5'-monophosphate_2.4.2.10_OROPRIBTRANS-RXN : 1 orotidine-5'-phosphate + 1 diphosphate <=> 1 5-phospho-alpha-D-ribose_1-diphosphate + 1 orotate
de-novo-biosynthesis-of-uridine-5'-monophosphate_4.1.1.23_OROTPDECARB-RXN : 1 orotidine-5'-phosphate + 1 H+ --> 1 CO2 + 1 UMP
de-novo-biosynthesis-of-pyrimidine-deoxyribonucleotides_2.7.4.6_DCDPKIN-RXN : 1 ATP + 1 dCDP --> 1 dCTP + 1 ADP
de-novo-biosynthesis-of-pyrimidine-deoxyribonucleotides_2.7.4.6_DTDPKIN-RXN : 1 dTDP + 1 ATP --> 1 dTTP + 1 ADP
de-novo-biosynthesis-of-pyrimidine-deoxyribonucleotides_2.7.4.6_DUDPKIN-RXN : 1 dUDP + 1 ATP --> 1 dUTP + 1 ADP
pyrimidine-ribonucleotides-interconversion_2.7.4.6_UDPKIN-RXN : 1 ATP + 1 UDP --> 1 UTP + 1 ADP
~metabolism-of-ribonucleotides-pyrimidine_2.7.4.6_CDPKIN-RXN : 1 ATP + 1 CDP <=> 1 CTP + 1 ADP
~no-pathway_2.7.4.22_2.7.4.25_RXN-12002 : 1 UMP + 1 ATP --> 1 UDP + 1
pyrimidine-ribonucleotides-interconversion_6.3.4.2_CTPSYN-RXN : 1 H2O + 1 ATP + 1 UTP + 1 L-glutamine --> 2 H+ + 1 ADP + 1 CTP + 1 L-glutamate + 1 phosphate
thioredoxin-pathway_1.8.1.9_THIOREDOXIN-REDUCT-NADPH-RXN : 1 |Red-Thioredoxin| + 1 NADP+ <-- 1 |Ox-Thioredoxin| + 1 H+ + 1 NADPH
de-novo-biosynthesis-of-pyrimidine-deoxyribonucleotides_1.17.4.1_CDPREDUCT-RXN : 1 H2O + 1 dCDP + 1 |Ox-Thioredoxin| <-- 1 |Red-Thioredoxin| + 1 CDP

de-novo-biosynthesis-of-pyrimidine-deoxyribonucleotides_1.17.4.1_UDPREDUCT-RXN : 1 H2O + 1 dUDP + 1 |Ox-Thioredoxin| <-- 1 UDP + 1 |Red-Thioredoxin|
de-novo-biosynthesis-of-pyrimidine-deoxyribonucleotides_3.5.4.13_DCTP-DEAM-RXN : 1 H2O + 1 dCTP --> 1 dUTP + 1 ammonia
~no-pathway_3.5.4.13_3.5.4.5_RXN-14118 : 1 CTP + 1 H+ + 1 H2O --> 1 UTP + 1 ammonium
~no-pathway_3.6.1.19_DCTP-PYROPHOSPHATASE-RXN : 1 H2O + 1 dCTP --> 1 diphosphate + 1 H+ + 1 dCMP
~no-pathway_3.6.1.19_RXN0-383 : 1 CTP + 1 H2O --> 1 CMP + 1 diphosphate + 1 H+
~no-pathway_3.6.1.19_RXN0-5107 : 1 dTTP + 1 H2O --> 1 H+ + 1 dTMP + 1 diphosphate
de-novo-biosynthesis-of-pyrimidine-deoxyribonucleotides_3.6.1.19_3.6.1.23_DUTP-PYROP-RXN : 1 dUTP + 1 H2O --> 1 H+ + 1 diphosphate + 1 dUMP
~metabolism-of-pyrimidine_2.7.4.9_DTMPKI-RXN : 1 ATP + 1 dTMP --> 1 ADP + 1 dTDP
~no-pathway_2.7.4.22_2.7.4.9_2.7.4.25_RXN-14122 : 1 dUMP + 1 ATP --> 1 dUDP + 1 ADP
~metabolism-of-salvage-pathways-pyrimidine_2.7.4.25_RXN-11832 : 1 CMP + 1 ATP --> 1 CDP + 1 ADP
~no-pathway_2.7.4.25_RXN-7913 : 1 dCMP + 1 ATP --> 1 dCDP + 1 ADP
~no-pathway_3.1.3.5_THYMIDYLATE-5-PHOSPHATASE-RXN : 1 dTMP + 1 H2O --> 1 thymidine + 1 phosphate
~no-pathway_3.1.3.5_RXN-14026 : 1 H2O + 1 CMP --> 1 phosphate + 1 cytidine
~no-pathway_3.1.3.5_RXN-14025 : 1 H2O + 1 UMP --> 1 phosphate + 1 uridine
~no-pathway_3.1.3.5_RXN0-5292 : 1 dCMP + 1 H2O --> 1 phosphate + 1 deoxycytidine
~metabolism-of-pyrimidine_3.5.4.5_CYTIDEAM-RXN : 1 deoxycytidine + 1 H2O --> 1 ammonia + 1 deoxyuridine
~metabolism-of-pyrimidine_3.5.4.5_CYTIDEAM2-RXN : 1 H2O + 1 cytidine --> 1 uridine + 1 ammonia
salvage-pathways-of-pyrimidine-deoxyribonucleotides_2.7.1.21_DURIDKI-RXN : 1 deoxyuridine + 1 ATP --> 1 H+ + 1 dUMP + 1 ADP
~metabolism-of-salvage-pathways-pyrimidine_2.7.1.21_THYKI-RXN : 1 thymidine + 1 ATP --> 1 dTMP + 1 H+ + 1 ADP
~metabolism-of-pyrimidine_2.4.2.1_2.4.2.4_URA-PHOSPH-RXN : 1 phosphate + 1 deoxyuridine <=> 1 uracil + 1 2-deoxy-alpha-D-ribose_1-phosphate
~metabolism-of-pyrimidine_2.4.2.4_THYM-PHOSPH-RXN : 1 phosphate + 1 thymidine <=> 1 thymine + 1 2-deoxy-alpha-D-ribose_1-phosphate
~metabolism-of-salvage-pathways-pyrimidine_2.4.2.9_URACIL-PRIBOSYLTRANS-RXN : 1 diphosphate + 1 UMP <=> 1 uracil + 1 5-phospho-alpha-D-ribose_1-diphosphate

##

 # methylerythritol phosphate pathway
~multiple-pathways_2.2.1.7_DXS-RXN : 1 pyruvate + 1 D-glyceraldehyde-3-phosphate + 1 H+ --> 1 CO2 + 1 1-deoxy-D-xylulose_5-phosphate
methylerythritol-phosphate-pathway_1.1.1.267_DXPREDISOM-RXN : 1 NADP+ + 1 2-C-methyl-D-erythritol_4-phosphate <=> 1 H+ + 1 NADPH + 1 1-deoxy-D-xylulose_5-phosphate
methylerythritol-phosphate-pathway_2.7.7.60_2.7.7.60-RXN : 1 2-C-methyl-D-erythritol_4-phosphate + 1 H+ + 1 CTP --> 1 4-(cytidine_5'-diphospho)-2-C-methyl-D-erythritol + 1 diphosphate
methylerythritol-phosphate-pathway_2.7.1.148_2.7.1.148-RXN : 1 4-(cytidine_5'-diphospho)-2-C-methyl-D-erythritol + 1 ATP --> 1 H+ + 1 2-phospho-4-(cytidine_5'-diphospho)-2-C-methyl-D-erythritol + 1 ADP
methylerythritol-phosphate-pathway_4.6.1.12_RXN0-302 : 1 2-phospho-4-(cytidine_5'-diphospho)-2-C-methyl-D-erythritol --> 1 CMP + 1 2-C-methyl-D-erythritol-2,4-cyclodiphosphate
methylerythritol-phosphate-pathway_1.17.7.1_RXN0-882 : 1 1-hydroxy-2-methyl-2-(E)-butenyl_4-diphosphate + 2 |Oxidized-flavodoxins| + 1 H2O <-- 1 H+ + 1 2-C-methyl-D-erythritol-2,4-cyclodiphosphate + 2 |Reduced-flavodoxins|
methylerythritol-phosphate-pathway_1.17.1.2_ISPH2-RXN_NAD : 1 NAD+ + 1 H2O + 1 isopentenyl_diphosphate <-- 1 H+ + 1 1-hydroxy-2-methyl-2-(E)-butenyl_4-diphosphate + 1 NADH
methylerythritol-phosphate-pathway_1.17.1.2_ISPH2-RXN_NADP : 1 H2O + 1 isopentenyl_diphosphate + 1 NADP+ <-- 1 H+ + 1 1-hydroxy-2-methyl-2-(E)-butenyl_4-diphosphate + 1 NADPH

methylerythritol-phosphate-pathway_1.17.1.2_RXN0-884_NAD : 1 H2O + 1 NAD+ + 1 dimethylallyl_diphosphate <-- 1 NADH + 1 H+ + 1 1-hydroxy-2-methyl-2-(E)-butenyl_4-diphosphate
methylerythritol-phosphate-pathway_1.17.1.2_RXN0-884_NADP : 1 NADP+ + 1 H2O + 1 dimethylallyl_diphosphate <-- 1 H+ + 1 1-hydroxy-2-methyl-2-(E)-butenyl_4-diphosphate + 1 NADPH
~multiple-pathways_5.3.3.2_IPPISOM-RXN : 1 isopentenyl_diphosphate <=> 1 dimethylallyl_diphosphate
~no-pathway_1.18.1.2_FLAVONADPREDUCT-RXN : 1 H+ + 1 NADPH + 1 |Oxidized-flavodoxins| <=> 1 |Reduced-flavodoxins| + 1 NADP+

##

 # tetrahydrofolate biosynthesis
~multiple-pathways_2.1.1.45_THYMIDYLATESYN-RXN : 1 dUMP + 1 5,10-methylenetetrahydrofolate --> 1 dTMP + 1 7,8-dihydrofolate
~multiple-pathways_3.5.4.9_METHENYLTHFCYCLOHYDRO-RXN : 1 5,10-methenyltetrahydrofolate + 1 H2O <=> 1 H+ + 1 10-formyl-tetrahydrofolate
~no-pathway_2.1.2.2_GART-RXN : 1 5-phospho-ribosyl-glycineamide + 1 10-formyl-tetrahydrofolate <=> 1 H+ + 1 tetrahydrofolate + 1 5'-phosphoribosyl-N-formylglycineamide
~no-pathway_2.6.1.85_PABASYN-RXN : 1 chorismate + 1 L-glutamine <=> 1 L-glutamate + 1 4-amino-4-deoxychorismate
~no-pathway_4.1.3.38_ADCLY-RXN : 1 4-amino-4-deoxychorismate <=> 1 pyruvate + 1 4-aminobenzoate + 1 H+
~no-pathway_2.5.1.15_H2PTEROATESYNTH-RXN : 1 6-hydroxymethyl-dihydropterin_diphosphate + 1 4-aminobenzoate --> 1 diphosphate + 1 7,8-dihydropteroate
formylTHF-biosynthesis-I_6.3.2.12_DIHYDROFOLATESYNTH-RXN : 1 L-glutamate + 1 ATP + 1 7,8-dihydropteroate --> 1 ADP + 1 H+ + 1 phosphate + 1 7,8-dihydrofolate
formylTHF-biosynthesis_1.5.1.3_DIHYDROFOLATEREDUCT-RXN : 1 tetrahydrofolate + 1 NADP+ <-- 1 NADPH + 1 H+ + 1 7,8-dihydrofolate
tetrahydrobioprein-biosynthesis_3.5.4.16_GTP-CYCLOHYDRO-I-RXN : 1 H2O + 1 GTP --> 1 H+ + 1 formate + 1 7,8-dihydroneopterin_triphosphate
~no-pathway_3.6.1.-_DIHYDRONEOPTERIN-MONO-P-DEPHOS-RXN : 1 7,8-dihydroneopterin_3'-phosphate + 1 H2O --> 1 phosphate + 1 7,8-dihydro-D-neopterin
~no-pathway_3.6.1.-_H2NEOPTERINP3PYROPHOSPHOHYDRO-RXN : 1 7,8-dihydroneopterin_triphosphate + 1 H2O --> 1 diphosphate + 1 7,8-dihydroneopterin_3'-phosphate + 1 H+
~no-pathway_4.1.2.25_H2NEOPTERINALDOL-RXN : 1 7,8-dihydro-D-neopterin --> 1 6-hydroxymethyl-7,8-dihydropterin + 1 glycolaldehyde
~no-pathway_2.7.6.3_H2PTERIDINEPYROPHOSPHOKIN-RXN : 1 ATP + 1 6-hydroxymethyl-7,8-dihydropterin --> 1 H+ + 1 6-hydroxymethyl-dihydropterin_diphosphate + 1 AMP
~multiple-pathways_6.3.4.3_FORMATETHFLIG-RXN : 1 tetrahydrofolate + 1 formate + 1 ATP --> 1 10-formyl-tetrahydrofolate + 1 ADP + 1 phosphate
~multiple-pathways_1.5.1.5_METHYLENETHFDEHYDROG-NADP-RXN : 1 5,10-methylenetetrahydrofolate + 1 NADP+ <=> 1 NADPH + 1 5,10-methenyltetrahydrofolate
formylTHF-biosynthesis_folate-transformations_1.5.1.20_1.5.1.20-RXN : 1 5-methyl-tetrahydrofolate + 1 NAD+ <=> 1 NADH + 1 5,10-methylenetetrahydrofolate + 1 H+
D-arabinose-degradation_ethylene-glycol-degradation_1.2.1.21_GLYCOLALD-DEHYDROG-RXN : 1 H2O + 1 glycolaldehyde + 1 NAD+ --> 1 glycolate + 2 H+ + 1 NADH
~metabolism-of-degradation_1.1.1.26_BR29285 : 1 glycolate + 1 NAD+ <=> 1 H+ + 1 NADH + 1 glyoxylate

 # flavin biosynthesis
flavin-biosynthesis_3.5.4.25_GTP-CYCLOHYDRO-II-RXN : 3 H2O + 1 GTP --> 1 2,5-diamino-6-(5-phospho-D-ribosylamino)pyrimidin-4(3H)-one + 2 H+ + 1 formate + 1 diphosphate
flavin-biosynthesis_4.1.99.12_DIOHBUTANONEPSYN-RXN : 1 D-ribulose-5-phosphate --> 1 1-deoxy-L-glycero-tetrulose_4-phosphate + 1 H+ + 1 formate
flavin-biosynthesis_3.5.4.26_RIBOFLAVINSYNDEAM-RXN : 1 2,5-diamino-6-(5-phospho-D-ribosylamino)pyrimidin-4(3H)-one + 1 H2O --> 1 ammonia + 1 5-amino-6-(5-phospho-D-ribosylamino)uracil

flavin-biosynthesis_1.1.1.193_RIBOFLAVINSYNREDUC-RXN: 1 5-amino-6-(5-phospho-D-ribitylamino)uracil + 1 NADP+ <-- 1 NADPH + 1 H+ + 1 5-amino-6-(5-phospho-D-ribosylamino)uracil
flavin_biosynthesis-RIBOPHOSPHAT-RXN : 1 5-amino-6-(5-phospho-D-ribitylamino)uracil + 1 H2O --> 1 5-amino-6-(D-ribitylamino)uracil + 1 phosphate
flavin-biosynthesis_2.5.1.78_LUMAZINESYN-RXN : 1 5-amino-6-(D-ribitylamino)uracil + 1 1-deoxy-L-glycero-tetrulose_4-phosphate --> 1 H+ + 1 6,7-dimethyl-8-(1-D-ribityl)lumazine + 1 phosphate + 2 H2O
flavin-biosynthesis_2.5.1.9_RIBOFLAVIN-SYN-RXN : 2 6,7-dimethyl-8-(1-D-ribityl)lumazine + 1 H+ --> 1 riboflavin + 1 5-amino-6-(D-ribitylamino)uracil
flavin-biosynthesis_5,6-dimethylbenzimidazole-biosynthesis_2.7.1.26_RIBOFLAVINKIN-RXN : 1 riboflavin + 1 ATP --> 1 H+ + 1 FMN + 1 ADP
flavin-biosynthesis_2.7.7.2_FADSYN-RXN : 1 ATP + 2 H+ + 1 FMN --> 1 FAD + 1 diphosphate

 # NAD biosynthesis
NAD-biosynthesis-I-(from-aspartate)_1.4.3.16_L-ASPARTATE-OXID-RXN : 1 L-aspartate + 1 oxygen --> 1 H+ + 1 hydrogen_peroxide + 1 alpha-iminosuccinate
NAD-biosynthesis-I-(from-aspartate)_2.5.1.72_QUINOLINATE-SYNTHA-RXN : 1 dihydroxyacetone_phosphate + 1 alpha-iminosuccinate --> 2 H2O + 1 phosphate + 1 quinolinate
NAD-biosynthesis-from-2-amino-3-carboxymuconate-semialdehyde_NAD-biosynthesis_2.4.2.19_QUINOPRIBOTRANS-RXN : 2 H+ + 1 5-phospho-alpha-D-ribose_1-diphosphate + 1 quinolinate --> 1 diphosphate + 1 CO2 + 1 nicotinate_D-ribonucleotide
~multiple-pathways_2.7.7.18_NICONUCADENYLYLTRAN-RXN : 1 ATP + 1 nicotinate_D-ribonucleotide + 1 H+ --> 1 nicotinate_adenine_dinucleotide + 1 diphosphate
~multiple-pathways_6.3.5.1_NAD-SYNTH-GLN-RXN : 1 H2O + 1 nicotinate_adenine_dinucleotide + 1 ATP + 1 L-glutamine --> 1 L-glutamate + 1 NAD+ + 1 AMP + 1 H+ + 1 diphosphate
~metabolism-of-phosphorylation-dephosphorylation_2.7.1.23_NAD-KIN-RXN : 1 ATP + 1 NAD+ --> 1 H+ + 1 ADP + 1 NADP+
NAD_NADP-1.6.1.2-RXN : 1 NAD+ + 1 NADPH + 1 H+ <-- 1 NADH + 1 NADP+ + 1 H+_ex

 # ubiquinol-10 biosynthesis
~metabolism-of-biosynthesis_2.5.1.1_GPPSYN-RXN : 1 dimethylallyl_diphosphate + 1 isopentenyl_diphosphate <=> 1 diphosphate + 1 geranyl_diphosphate
~metabolism-of-biosynthesis_2.5.1.10_FPPSYN-RXN : 1 isopentenyl_diphosphate + 1 geranyl_diphosphate <=> 1 diphosphate + 1 (2E,6E)-farnesyl_diphosphate
all-trans-decaprenyl-diphosphate-biosynthesis_2.5.1.91_RXN-9106 : 7 isopentenyl_diphosphate + 1 (2E,6E)-farnesyl_diphosphate <=> 1 all-trans-decaprenyl_diphosphate + 7 diphosphate
ubiquinol-8-biosynthesis_4-hydroxybenzoate-biosynthesis_4.1.3.40_CHORPYRLY-RXN : 1 chorismate --> 1 pyruvate + 1 4-hydroxybenzoate
ubiquinol-10-biosynthesis_2.5.1.39_RXN-9230 : 1 4-hydroxybenzoate + 1 all-trans-decaprenyl_diphosphate --> 1 diphosphate + 1 3-decaprenyl-4-hydroxybenzoate
ubiquinol-10-biosynthesis-(prokaryotic)_4.1.1.-_RXN-9231 : 1 3-decaprenyl-4-hydroxybenzoate + 1 H+ --> 1 2-decaprenylphenol + 1 CO2
ubiquinol-10-biosynthesis-(prokaryotic)_1.14.13.-_RXN-9232 : 1 oxygen + 1 NADPH + 1 H+ + 1 2-decaprenylphenol --> 1 NADP+ + 1 3-(all-trans-decaprenyl)benzene-1,2-diol + 1 H2O
ubiquinol-10-biosynthesis-(prokaryotic)_2.1.1.222_RXN-9233 : 1 S-adenosyl-L-methionine + 1 3-(all-trans-decaprenyl)benzene-1,2-diol --> 1 2-methoxy-6-(all-trans-decaprenyl)phenol + 1 H+ + 1 S-adenosyl-L-homocysteine
ubiquinol-10-biosynthesis_1.14.13.-_RXN-9234 : 1 NADPH + 1 2-methoxy-6-(all-trans-decaprenyl)phenol + 1 H+ + 1 oxygen --> 1 H2O + 1 NADP+ + 1 2-methoxy-6-all_trans-decaprenyl-2-methoxy-1,4-benzoquinol
ubiquinol-10-biosynthesis_2.1.1.201_RXN-9235 : 1 2-methoxy-6-all_trans-decaprenyl-2-methoxy-1,4-benzoquinol + 1 S-adenosyl-L-methionine --> 1 H+ + 1 6-methoxy-3-methyl-2-all-trans-decaprenyl-1,4-benzoquinol + 1 S-adenosyl-L-homocysteine
ubiquinol-10-biosynthesis_1.14.-.-_RXN-9236 : 1 oxygen + 1 NADPH + H+ + 1 6-methoxy-3-methyl-2-all-trans-decaprenyl-1,4-benzoquinol --> 1 3-demethylubiquinol-10 + 1 H2O + 1 NADP+
ubiquinol-10-biosynthesis_2.1.1.64_RXN-9237 : 1 S-adenosyl-L-methionine + 1 3-demethylubiquinol-10 --> 1 ubiquinol-10 + 1 H+ + 1 S-adenosyl-L-homocysteine

 # pantothenate biosynthesis
phosphopantothenate-biosynthesis_2.1.2.11_3-CH3-2-OXOBUTANOATE-OH-CH3-XFER-RXN : 1 2-oxoisovalerate + 1 5,10-methylenetetrahydrofolate + 1 H2O <=> 1 2-dehydropantoate + 1 tetrahydrofolate
phosphopantothenate-biosynthesis_1.1.1.169_2-DEHYDROPANTOATE-REDUCT-RXN : 1 (R)-pantoate + 1 NADP+ <-- 1 H+ + 1 NADPH + 1 2-dehydropantoate
phosphopantothenate-biosynthesis-I_6.3.2.1_PANTOATE-BETA-ALANINE-LIG-RXN : 1 ATP + 1 (R)-pantoate + 1 beta-alanine --> 1 (R)-pantothenate + 1 diphosphate + 1 AMP + 1 H+

 # coenzyme A biosynthesis
phosphopantothenate-biosynthesis_2.7.1.33_PANTOTHENATE-KIN-RXN : 1 (R)-pantothenate + 1 ATP --> 1 ADP + 1 H+ + 1 D-4'-phosphopantothenate
coenzyme-A-biosynthesis_6.3.2.5_P-PANTOCYSLIG-RXN : 1 L-cysteine + 1 D-4'-phosphopantothenate + 1 CTP --> 1 diphosphate + 1 H+ + 1 R-4'-phosphopantothenoyl-L-cysteine + 1 CMP
coenzyme-A-biosynthesis_4.1.1.36_P-PANTOCYSDECARB-RXN : 1 H+ + 1 R-4'-phosphopantothenoyl-L-cysteine --> 1 4'-phosphopantetheine + 1 CO2
coenzyme-A-biosynthesis_2.7.7.3_PANTEPADENYLYLTRAN-RXN : 1 ATP + 1 H+ + 1 4'-phosphopantetheine --> 1 3'-dephospho-CoA + 1 diphosphate
coenzyme-A-biosynthesis_2.7.1.24_DEPHOSPHOCOAKIN-RXN : 1 3'-dephospho-CoA + 1 ATP --> 1 H+ + 1 coenzyme_A + 1 ADP

##

 # N-acetyl-glucosamine
CMP-legionaminate-biosynthesis_UDP-N-acetyl-D-glucosamine-biosynthesis_2.6.1.16_L-GLN-FRUCT-6-P-AMINOTRANS-RXN : 1 D-fructose-6-phosphate + 1 L-glutamine <=> 1 L-glutamate + 1 alpha-D-glucosamine_6-phosphate
CMP-legionaminate-biosynthesis_UDP-N-acetyl-D-glucosamine-biosynthesis_5.4.2.10_5.4.2.10-RXN : 1 D-glucosamine_1-phosphate <=> 1 alpha-D-glucosamine_6-phosphate
UDP-N-acetyl-D-glucosamine-biosynthesis-I_2.3.1.157_2.3.1.157-RXN : 1 acetyl-CoA + 1 D-glucosamine_1-phosphate --> 1 H+ + 1 N-acetyl-alpha-D-glucosamine_1-phosphate + 1 coenzyme_A
~metabolism-of-biosynthesis_2.7.7.23_NAG1P-URIDYLTRANS-RXN : 1 N-acetyl-alpha-D-glucosamine_1-phosphate + 1 UTP + 1 H+ --> 1 UDP-N-acetyl-alpha-D-glucosamine + 1 diphosphate

 # peptidoglycan biosynthesis
UDP-N-acetylmuramoyl-pentapeptide-biosynthesis_2.5.1.7_UDPNACETYLGLUCOSAMENOLPYRTRANS-RXN : 1 phosphoenolpyruvate + 1 UDP-N-acetyl-alpha-D-glucosamine --> 1 UDP-N-acetyl-alpha-D-glucosamine-enolpyruvate + 1 phosphate
UDP-N-acetylmuramoyl-pentapeptide-biosynthesis_1.3.1.98_UDPNACETYLMURAMATEDEHYDROG-RXN : 1 NADP+ + 1 UDP-N-alpha-D-acetylmuramate <-- 1 H+ + 1 NADPH + 1 UDP-N-acetyl-alpha-D-glucosamine-enolpyruvate
UDP-N-acetylmuramoyl-pentapeptide-biosynthesis_6.3.2.8_UDP-NACMUR-ALA-LIG-RXN : 1 UDP-N-alpha-D-acetylmuramate + 1 L-alanine + 1 ATP --> 1 H+ + 1 phosphate + 1 ADP + 1 UDP-N-acetylmuramoyl-L-alanine
UDP-N-acetylmuramoyl-pentapeptide-biosynthesis_5.1.1.3_GLUTRACE-RXN : 1 L-glutamate <=> 1 D-glutamate
UDP-N-acetylmuramoyl-pentapeptide-biosynthesis_6.3.2.9_UDP-NACMURALA-GLU-LIG-RXN: 1 UDP-N-acetylmuramoyl-L-alanine + 1 ATP + 1 D-glutamate --> 1 H+ + 1 phosphate + 1 ADP + 1 UDP-N-acetylmuramoyl-L-alanyl--D-glutamate
UDP-N-acetylmuramoyl-pentapeptide-biosynthesis-III-(meso-DAP-containing)_6.3.2.13_UDP-NACMURALGLDAPLIG-RXN : 1 ATP + 1 meso-diaminopimelate + 1 UDP-N-acetylmuramoyl-L-alanyl--D-glutamate --> 1 phosphate + 1 ADP + 1 UDP-N-acetylmuramoyl-L-alanyl-gamma-D-glutamyl-meso-2,6-diaminopimelate + 1 H+
alanine-degradation_alanine-biosynthesis_5.1.1.1_ALARACECAT-RXN : 1 L-alanine <=> 1 D-alanine

UDP-N-acetylmuramoyl-pentapeptide-biosynthesis_6.3.2.4_DALADALALIG-RXN : 1 ATP + 2 D-alanine --> 1 phosphate + 1 H+ + 1 ADP + 1 D-alanyl-D-alanine
UDP-N-acetylmuramoyl-pentapeptide-biosynthesis-III-(meso-DAP-containing)_6.3.2.10_UDP-NACMURALGLDAPAALIG-RXN : 1 ATP + 1 UDP-N-acetylmuramoyl-L-alanyl-gamma-D-glutamyl-meso-2,6-diaminopimelate + 1 D-alanyl-D-alanine --> 1 ADP + 1 UDP-N-acetylmuramoyl-L-alanyl-gamma-D-glutamyl-meso-2,6-diaminopimelyl-D-alanyl-D-alanine + 1 H+ + 1 phosphate
di-trans,poly-cis-undecaprenyl-phosphate-biosynthesis_2.5.1.31_RXN-8999 : 8 isopentenyl_diphosphate + 1 (2E,6E)-farnesyl_diphosphate <=> 8 diphosphate + 1 di-trans,octa-cis-undecaprenyl_diphosphate
~no-pathway_3.6.1.27_UNDECAPRENYL-DIPHOSPHATASE-RXN : 1 H2O + 1 di-trans,octa-cis-undecaprenyl_diphosphate --> 1 H+ + 1 phosphate + 1 di-trans,octa-cis-undecaprenyl_phosphate
peptidoglycan-biosynthesis-I-(meso-diaminopimelate-containing)_2.7.8.13_PHOSNACMURPENTATRANS-RXN : 1 UDP-N-acetylmuramoyl-L-alanyl-gamma-D-glutamyl-meso-2,6-diaminopimelyl-D-alanyl-D-alanine + 1 di-trans,octa-cis-undecaprenyl_phosphate --> 1 UMP + 1 undecaprenyldiphospho-N-acetylmuramoyl-L-alanyl-gamma-D-glutamyl-meso-2,6-diaminopimelyl-D-alanyl-D-alanine
peptidoglycan-biosynthesis-I-(meso-diaminopimelate-containing)_2.4.1.227_NACGLCTRANS-RXN : 1 undecaprenyldiphospho-N-acetylmuramoyl-L-alanyl-gamma-D-glutamyl-meso-2,6-diaminopimelyl-D-alanyl-D-alanine + 1 UDP-N-acetyl-alpha-D-glucosamine <=> 1 UDP + 1 H+ + 1 undecaprenyldiphospho-N-acetyl-(N-acetylglucosaminyl)muramoyl-L-alanyl-gamma-D-glutamyl-meso-2,6-diaminopimelyl-D-alanyl-D-alanine
peptidoglycan-biosynthesis-I-(meso-diaminopimelate-containing)_2.4.1.129_RXN0-5405 : 2 undecaprenyldiphospho-N-acetyl-(N-acetylglucosaminyl)muramoyl-L-alanyl-gamma-D-glutamyl-meso-2,6-diaminopimelyl-D-alanyl-D-alanine --> 1 a_peptidoglycan_dimer_(meso-diaminopimelate_containing) + 1 di-trans,octa-cis-undecaprenyl_diphosphate + 1 H+
peptidoglycan-biosynthesis-I-(meso-diaminopimelate-containing)_3.4.16.4_RXN-11302 : 2 a_peptidoglycan_dimer_(meso-diaminopimelate_containing) --> 1 a_peptidoglycan_with_D,D_cross-links_(meso-diaminopimelate_containing) + 1 D-alanine

 # KDO-lipidA
CMP-KDO-biosynthesis-I_5.3.1.13_DARAB5PISOM-RXN : 1 D-arabinose_5-phosphate <=> 1 D-ribulose-5-phosphate
CMP-KDO-biosynthesis_2.5.1.55_KDO-8PSYNTH-RXN : 1 phosphoenolpyruvate + 1 D-arabinose_5-phosphate + 1 H2O --> 1 phosphate + 1 3-deoxy-D-manno-octulosonate_8-phosphate
CMP-KDO-biosynthesis_3.1.3.45_KDO-8PPHOSPHAT-RXN : 1 3-deoxy-D-manno-octulosonate_8-phosphate + 1 H2O --> 1 3-deoxy-D-manno-octulosonate + 1 phosphate
CMP-KDO-biosynthesis_2.7.7.38_CPM-KDOSYNTH-RXN : 1 3-deoxy-D-manno-octulosonate + 1 CTP --> 1 diphosphate + 1 CMP-3-deoxy-D-manno-octulosonate
lipid-IVA-biosynthesis_2.3.1.129_UDPNACETYLGLUCOSAMACYLTRANS-RXN : 1 (R)-3-hydroxy-tetradecanoyl-[ACP] + 1 UDP-N-acetyl-alpha-D-glucosamine --> 1 UDP-3-O-[(3R)-3-hydroxymyristoyl]-N-acetyl-alpha-D-glucosamine + ACP
lipid-IVA-biosynthesis_3.5.1.108_UDPACYLGLCNACDEACETYL-RXN : 1 UDP-3-O-[(3R)-3-hydroxymyristoyl]-N-acetyl-alpha-D-glucosamine + 1 H2O --> 1 UDP-3-O-(3-hydroxymyristoyl)-alpha-D-glucosamine + 1 acetate
lipid-IVA-biosynthesis_2.3.1.191_UDPHYDROXYMYRGLUCOSAMNACETYLTRANS-RXN : 1 UDP-3-O-(3-hydroxymyristoyl)-alpha-D-glucosamine + 1 (R)-3-hydroxy-tetradecanoyl-[ACP] --> 1 ACP + 1 H+ + 1 UDP-2,3-bis[O-(3R)-3-hydroxymyristoyl]-alpha-D-glucosamine
lipid-IVA-biosynthesis_3.6.1.54_LIPIDXSYNTHESIS-RXN : 1 H2O + 1 UDP-2,3-bis[O-(3R)-3-hydroxymyristoyl]-alpha-D-glucosamine --> 2 H+ + 1 UMP + 1 2,3-bis[(3R)-3-hydroxymyristoyl]-alpha-D-glucosaminyl_1-phosphate
lipid-IVA-biosynthesis_2.4.1.182_LIPIDADISACCHARIDESYNTH-RXN : 1 2,3-bis[(3R)-3-hydroxymyristoyl]-alpha-D-glucosaminyl_1-phosphate + 1 UDP-2,3-bis[O-(3R)-3-hydroxymyristoyl]-alpha-D-glucosamine --> 1 UDP + 1 lipid_A_disaccharide + 1 H+
lipid-IVA-biosynthesis_2.7.1.130_TETRAACYLDISACC4KIN-RXN : 1 lipid_A_disaccharide + 1 ATP --> 1 lipid_IVA + 1 H+ + 1 ADP
KDO-transfer-to-lipid-IVA-I_2.4.99.12_2.4.99.13_KDOTRANS-RXN : 1 CMP-3-deoxy-D-manno-octulosonate + 1 lipid_IVA --> 1 H+ + 1 alpha-Kdo-(2rarr6)-lipid_IVA + 1 CMP

KDO-transfer-to-lipid-IVA-I_2.4.99.13_KDOTRANS2-RXN : 1 CMP-3-deoxy-D-manno-octulosonate + 1 alpha-Kdo-(2rarr6)-lipid_IVA --> 1 alpha-Kdo-(2->4)-alpha-Kdo-(2->6)-lipid_IVA + 1 H+ + 1 CMP
superpathway-of-(KDO)2-lipid-A-biosynthesis_(KDO)2-lipid-A-biosynthesis_2.3.1.-_LAUROYLACYLTRAN-RXN : 1 alpha-Kdo-(2->4)-alpha-Kdo-(2->6)-lipid_IVA + 1 Dodecanoyl-[ACP] --> 1 ACP + 1 (KDO)2-(lauroyl)-lipid_IVA
superpathway-of-(KDO)2-lipid-A-biosynthesis_(KDO)2-lipid-A-biosynthesis_2.3.1.-_MYRISTOYLACYLTRAN-RXN : 1 (KDO)2-(lauroyl)-lipid_IVA + 1 Tetradecanoyl-[ACP] --> 1 (KDO)2-lipid_A + 1 ACP
~multiple-pathways_5.4.2.2_PHOSPHOGLUCMUT-RXN : 1 alpha-D-glucose_1-phosphate <=> 1 alpha-D-glucose_6-phosphate
~multiple-pathways_2.7.7.9_GLUC1PURIDYLTRANS-RXN : 1 H+ + 1 alpha-D-glucose_1-phosphate + 1 UTP <=> 1 UDP-alpha-D-glucose + 1 diphosphate

##########

 # SECONDARY METABOLITES

 # TDA biosynthesis (based on Brock et al 2014)
TDA_biosynthesis-RXN : 3-oxo-5,6-dehydrosuberyl-CoA_semialdehyde + 2 L-cysteine + 2 H2O + 4 NAD+ --> 1 TDA + 2 L-serine + 1 coenzyme_A + 4 NADH + 4 H+

##########

 # detoxification
methanol-oxidation-to-formaldehyde_superoxide-radicals-degradation_1.11.1.21_CATAL-RXN : 2 hydrogen_peroxide --> 1 oxygen + 2 H2O
~no-pathway_1.14.12.17_R621-RXN_NAD : 1 NADH + 2 nitric_oxide + 2 oxygen --> 1 NAD+ + 2 nitrate + 1 H+
~no-pathway_1.14.12.17_R621-RXN_NADP: 2 nitric_oxide + 2 oxygen + 1 NADPH --> 2 nitrate + 1 NADP+ + 1 H+
~multiple-pathways_1.7.2.1_NITRITE-REDUCTASE-CYTOCHROME-RXN : 1 nitric_oxide + 1 H2O + 1 |Cytochromes-C-Oxidized| <=> 1 |Cytochromes-C-Reduced| + 1 nitrite + 2 H+
nitrate-reduction_nitrifier-denitrification_1.7.2.5_NITRIC-OXIDE-REDUCTASE-RXN : 1 nitrous_oxide + 2 |Cytochromes-C-Oxidized| + 1 H2O <=> 2 |Cytochromes-C-Reduced| + 2 H+ + 2 nitric_oxide

##########

 # sulfate assimilation
sulfate-reduction-I-(assimilatory)_1.8.1.2_SULFITE-REDUCT-RXN: 3 NADP+ + 3 H2O + 1 hydrogen_sulfide <=> 5 H+ + 3 NADPH + 1 sulfite
thiosulfate-disproportionation-III-(rhodanese)_2.8.1.1_THIOSULFATE-SULFURTRANSFERASE-RXN : 1 hydrogen_cyanide + 1 thiosulfate <=> 1 sulfite + 2 H+ + 1 thiocyanate (E.coli)
~multiple-pathways_2.7.7.4_SULFATE-ADENYLYLTRANS-RXN : 1 ATP + 1 sulfate + 1 H+ <=> 1 diphosphate + 1 adenosine_5'-phosphosulfate
sulfate-activation-for-sulfonation_2.7.1.25_ADENYLYLSULFKIN-RXN : 1 adenosine_5'-phosphosulfate + 1 ATP --> 1 phosphoadenosine-5'-phosphosulfate + 1 H+ + 1 ADP
sulfate-reduction-I-(assimilatory)_1.8.4.8_1.8.4.8-RXN : 1 |Ox-Thioredoxin| + 2 H+ + 1 adenosine_3',5'-bisphosphate + 1 sulfite <=> 1 |Red-Thioredoxin| + 1 phosphoadenosine-5'-phosphosulfate
~no-pathway_3.1.3.7_325-BISPHOSPHATE-NUCLEOTIDASE-RXN : 1 adenosine_3',5'-bisphosphate + 1 H2O --> 1 phosphate + 1 AMP

##########

 # DEGRADATION PATHWAYS

 # amino acid degradation

tryptophan degradation
~metabolism-of-tryptophan-degradation_1.13.11.11_RXN-8665 : 1 oxygen + 2 H+ + 1 L-tryptophan --> 1 N-formylkynurenine
~metabolism-of-tryptophan-degradation_3.5.1.9_ARYLFORMAMIDASE-RXN : 1 N-formylkynurenine + 1 H2O --> 1 formate + 3 H+ + 1 L-kynurenine
tryptophan-degradation_3.7.1.3_KYNURENINASE-RXN : 1 L-kynurenine + 1 H2O --> 1 L-alanine + 1 H+ + 1 anthranilate
alanine-degradation-IV_1.4.1.1_ALANINE-DEHYDROGENASE-RXN : 1 H2O + 1 L-alanine + 1 NAD+ <=> 1 H+ + 1 NADH + 1 ammonium + 1 pyruvate
~multiple-pathways_6.2.1.32_AMINOBENZCOALIG-RXN : 1 ATP + 1 anthranilate + 1 coenzyme_A --> 1 diphosphate + 1 2-aminobenzoyl-CoA + 1 AMP
anthranilate-degradation-II-(aerobic)_1.14.13.40_ANTHRANILOYL-COA-MONOOXYGENASE-RXN_NAD : 2 NADH + 2 H+ + 1 oxygen + 1 2-aminobenzoyl-CoA --> 1 2-amino-5-oxocyclohex-1-enecarboxyl-CoA + 1 H2O + 2 NAD+
anthranilate-degradation-II-(aerobic)_1.14.13.40_ANTHRANILOYL-COA-MONOOXYGENASE-RXN_NADP : 2 H+ + 2 NADPH + 1 oxygen + 1 2-aminobenzoyl-CoA --> 1 2-amino-5-oxocyclohex-1-enecarboxyl-CoA + 2 NADP+ + 1 H2O
#tryptophan-degradation1_RXN : 1 2-amino-5-oxocyclohex-1-enecarboxyl-CoA + 1 NADPH + 3 H+ + 2 oxygen --> 1 3-oxoadipate + 1 NADPH + 1 ammonia + 1 coenzyme_A + CO2
#tryptophan-degradation2_RXN : 1 2-amino-5-oxocyclohex-1-enecarboxyl-CoA + 1 NADP+ + 1 aspartate + 1 H+ + 2 oxygen --> 1 3-oxoadipate + 1 NADPH + 1 asparagine + 1 coenzyme_A + CO2
#tryptophan-degra_2.8.3.5_RXN : 1 3-oxoadipate + 1 succinyl-CoA <=> 1 3-oxoadipyl-CoA + 1 succinate
tryptophan-degra-grob-RXN : 1 2-amino-5-oxocyclohex-1-enecarboxyl-CoA + 1 coenzyme_A + 2 oxygen + 2 H+ + 1 NADPH --> 1 succinyl-CoA + 1 acetyl-CoA + 1 CO2 + 1 ammonium + 1 NADP+

phenylalanine degradation
phenylalanine-degradation_2.6.1.57_PHEAMINOTRANS-RXN : 1 L-glutamate + 1 keto-phenylpyruvate <=> 1 L-phenylalanine + 1 2-oxoglutarate
phenylalanine_degra_1.2.7.8_-RXN : 1 |Oxidized-ferredoxins| + 1 keto-phenylpyruvate + 1 coenzyme_A --> 1 phenylacetyl-CoA + 1 CO2 + 1 |Reduced-ferredoxins|
phenylacetate-degradation-I-(aerobic)_1.14.13.149_RXN0-2042 : 1 phenylacetyl-CoA + 1 H+ + 1 oxygen + 1 NADPH --> 1 H2O + 1 2-(1,2-epoxy-1,2-dihydrophenyl)acetyl-CoA + 1 NADP+
phenylacetate-degradation-I-(aerobic)_5.3.3.18_RXN0-6510 : 1 2-(1,2-epoxy-1,2-dihydrophenyl)acetyl-CoA <=> 1 2-oxepin-2(3H)-ylideneacetyl-CoA
phenylacetate-degradation-I-(aerobic)_3.3.2.12_RXNMETA-12671 : 1 2-oxepin-2(3H)-ylideneacetyl-CoA + 1 H2O --> 1 3-oxo-5,6-dehydrosuberyl-CoA_semialdehyde
phenylacetate-degradation-I-(aerobic)_1.17.1.7_RXNMETA-12672 : 1 H2O + 1 3-oxo-5,6-dehydrosuberyl-CoA_semialdehyde + 1 NADP+ --> 1 NADPH + 2 H+ + 1 3-oxo-5,6-didehydrosuberyl-CoA
phenylacetate-degradation-I-(aerobic)_2.3.1.223_RXN0-6512 : 1 acetyl-CoA + 1 2,3-didehydroadipyl-CoA <-- 1 coenzyme_A + 1 3-oxo-5,6-didehydrosuberyl-CoA
phenylacetate-degradation-I-(aerobic)_4.2.1.17_RXN0-6513 : 1 3-hydroxyadipyl-CoA <=> 1 2,3-didehydroadipyl-CoA + 1 H2O
benzoyl-CoA-degradation_phenylacetate-degradation_1.1.1.35_RXN0-2044 : 1 3-hydroxyadipyl-CoA + 1 NAD+ <=> 1 H+ + 1 NADH + 1 3-oxoadipyl-CoA
~metabolism-of-degradation_2.3.1.174_RXN-3641 : 1 acetyl-CoA + 1 succinyl-CoA <-- 1 coenzyme_A + 1 3-oxoadipyl-CoA
ubiquinol-6-biosynthesis-from-4-aminobenzoate_1.18.1.2_1.18.1.2-RXN : 1 NADP+ + 2 |Reduced-ferredoxins| + 1 H+ --> 1 NADPH + 2 |Oxidized-ferredoxins|
phenylalanine-degra_1.13.11.27_4-HYDROXYPHENYLPYRUVATE-DIOXYGENASE-RXN : 1 keto-phenylpyruvate + 1 oxygen --> 1 2-hydroxyphenylacetate + 1 CO2
phenylalanine_degra_3.2.1.-_THIOESTERASE-RXN : 1 phenylacetyl-CoA + 1 H2O --> 1 phenylacetate + 1 coenzyme_A + 1 H+

phenylacetate-degradation_phenylalanine-degradation_6.2.1.30_RXN-10819 : 1 coenzyme_A + 1 phenylacetate + 1 ATP --> 1 phenylacetyl-CoA + 1 diphosphate + 1 AMP
phenylalanine_degra_3.2.1.-_THIOESTERASE2-RXN : 1 2-(1,2-epoxy-1,2-dihydrophenyl)acetyl-CoA + 1 H2O --> 1 2-(1,2-epoxy-1,2-dihydrophenyl)acetate + 1 coenzyme_A + 1 H+
phenylalanine_degra_spontaneous-RXN : 1 2-(1,2-epoxy-1,2-dihydrophenyl)acetate --> 1 2-hydroxyphenylacetate

methionine degradation
methionine-degradation-II_4.4.1.11_METHIONINE-GAMMA-LYASE-RXN : 1 L-methionine + 1 H2O <=> 1 methanethiol + 1 ammonium + 1 2-oxobutanoate
2-oxobutanoate-degradation_PDH-RXN : 1 2-oxobutanoate + 1 NAD+ + 1 coenzyme_A --> 1 propanoyl-CoA + 1 NADH + 1 CO2

leucine degradation
~no-pathway_1.4.1.9_LEUCINE-DEHYDROGENASE-RXN : 1 NAD+ + 1 H2O + 1 L-leucine <=> 1 NADH + 1 ammonium + 1 H+ + 1 4-methyl-2-oxopentanoate
leucine-degra_1.2.7.8-RXN : 1 4-methyl-2-oxopentanoate + 1 coenzyme_A + 1 |Oxidized-ferredoxins| --> 1 |Reduced-ferredoxins| + 1 isovaleryl-CoA + 1 CO2
~no-pathway_1.3.8.4_RXN-14264 : 1 isovaleryl-CoA + 1 FAD + 1 H+ <=> 1 3-methylcrotonyl-CoA + 1 FADH2
leucine-degradation-I_6.4.1.4_METHYLCROTONYL-COA-CARBOXYLASE-RXN : 1 3-methylcrotonyl-CoA + 1 bicarbonate + 1 ATP --> 1 phosphate + 1 3-methylglutaconyl-CoA + 1 H+ + 1 ADP
leucine-degradation-I_4.2.1.18_METHYLGLUTACONYL-COA-HYDRATASE-RXN : 1 (S)-3-hydroxy-3-methylglutaryl-CoA <=> 1 3-methylglutaconyl-CoA + 1 H2O
~multiple-pathways_4.1.3.4_HYDROXYMETHYLGLUTARYL-COA-LYASE-RXN : 1 (S)-3-hydroxy-3-methylglutaryl-CoA --> 1 acetoacetate + 1 acetyl-CoA
TCA-cycle_2.8.3.5_RXNI-2 : 1 acetoacetate + 1 succinyl-CoA <=> 1 succinate + 1 acetoacetyl-CoA

isoleucine degradation
~no-pathway_1.4.1.9_ILEDEAMINE-RXN : 1 H2O + 1 NAD+ + 1 L-isoleucine --> 1 H+ + 1 (S)-3-methyl-2-oxopentanoate + 1 ammonium + 1 NADH
isoleucine-degradation_2.6.1.42_BRANCHED-CHAINAMINOTRANSFERILEU-RXN : 1 2-oxoglutarate + 1 L-isoleucine <=> 1 L-glutamate + 1 (S)-3-methyl-2-oxopentanoate
isoleucine-degra_1.2.7.8-RXN : 1 (S)-3-methyl-2-oxopentanoate + 1 coenzyme_A + 1 |Oxidized-ferredoxins| --> 1 |Reduced-ferredoxins| + 1 2-methylbutanoyl-CoA + 1 CO2
isoleucine-degra_1.3.8.4_RXN-14264 : 1 FAD + 1 H+ + 1 2-methylbutanoyl-CoA <=> 1 (E)-2-methylcrotonoyl-CoA + 1 FADH2
isoleucine-degradation_2-methylbutyrate-biosynthesis_4.2.1.17_TIGLYLCOA-HYDROXY-RXN : 1 2-methyl-3-hydroxybutyryl-CoA <=> 1 (E)-2-methylcrotonoyl-CoA + 1 H2O
isoleucine-degradation_2-methylbutyrate-biosynthesis_1.1.1.178_1.1.1.178-RXN : 1 2-methyl-3-hydroxybutyryl-CoA + 1 NAD+ <=> 1 NADH + 1 H+ + 1 2-methylacetoacetyl-CoA
isoleucine-degradation_2-methylbutyrate-biosynthesis_2.3.1.9_METHYLACETOACETYLCOATHIOL-RXN : 1 2-methylacetoacetyl-CoA + 1 coenzyme_A <=> 1 propanoyl-CoA + 1 acetyl-CoA

valine degradation
~no-pathway_1.4.1.9_RXN-13184 : 1 NAD+ + 1 L-valine + 1 H2O <=> 1 ammonium + 1 3-methyl-2-oxobutanoate + 1 H+ + 1 NADH
valine-degra_2.6.1.42_BRANCHED-CHAINAMINOTRANSFERVAL-RXN : 1 2-oxoglutarate + 1 L-valine <=> 1 L-glutamate + 1 3-methyl-2-oxobutanoate
valine-degra_1.2.7.8_1.2.7.8-RXN : 1 coenzyme_A + 1 3-methyl-2-oxobutanoate + 1 |Oxidized-ferredoxins| --> 1 isobutanoyl-CoA + 1 CO2 + 1 |Reduced-ferredoxins|
valine-degra_1.3.8.4_RXN-14264 : 1 isobutanoyl-CoA + 1 FAD + 1 H+ <=> 1 FADH2 + 1 methylacrylyl-CoA
valine-degradation-I_4.2.1.17_METHYLACYLYLCOA-HYDROXY-RXN : 1 (S)-3-hydroxy-isobutanoyl-CoA <=> 1 methylacrylyl-CoA + 1 H2O
valine-degradation-I_3.1.2.4_3-HYDROXYISOBUTYRYL-COA-HYDROLASE-RXN : 1 (S)-3-hydroxy-isobutanoyl-CoA + 1 H2O --> 1 H+ + 1 (S)-3-hydroxy-isobutanoate + 1 coenzyme_A

valine-degradation-I_1.1.1.31_3-HYDROXYISOBUTYRATE-DEHYDROGENASE-RXN : 1 NAD+ + 1 (S)-3-hydroxy-isobutanoate --> 1 H+ + 1 NADH + 1 (S)-methylmalonate-semialdehyde
2,4-dinitrotoluene-degradation_1.2.1.27_1.2.1.27-RXN : 1 (S)-methylmalonate-semialdehyde + 1 coenzyme_A + 1 NAD+ + 1 H2O --> 1 bicarbonate + 1 NADH + 1 propanoyl-CoA + 1 H+

histidine degradation
histidine-degradation_4.3.1.3_HISTIDINE-AMMONIA-LYASE-RXN : 1 L-histidine --> 1 urocanate + 1 ammonium
histidine-degradation_4.2.1.49_UROCANATE-HYDRATASE-RXN : 1 4-imidazolone-5-propionate <-- 1 urocanate + 1 H2O
histidine-degradation_3.5.2.7_IMIDAZOLONEPROPIONASE-RXN : 1 4-imidazolone-5-propionate + 1 H2O --> 1 N-formimino-L-glutamate
histidine-degradation-II_3.5.3.13_FORMIMINOGLUTAMATE-DEIMINASE-RXN : 1 N-formimino-L-glutamate + 1 H2O --> 1 ammonium + 1 N-formyl-L-glutamate
histidine-degradation-II_3.5.1.68_N-FORMYLGLUTAMATE-DEFORMYLASE-RXN : 1 N-formyl-L-glutamate + 1 H2O --> 1 L-glutamate + 1 formate

lysine degradation
~multiple-pathways_4.1.1.18_LYSDECARBOX-RXN : 1 L-lysine + 1 H+ --> 1 CO2 + 1 cadaverine
lysine-degradation-X_2.6.1.-_RXN-10853 : 1 cadaverine + 1 pyruvate --> 1 H+ + 1 L-alanine + 1 H2O + 1 1-piperideine
lysine-degra_2.6.1.-_RXN : 1 cadaverine + 1 pyruvate --> 1 L-alanine + 1 5-aminopentanal
lysine-degradation-X_1.5.1.-_RXN-10854 : 1 1-piperideine + 1 NAD+ + 2 H2O --> 1 NADH + 1 H+ + 1 5-aminopentanoate
lysine-degra_1.2.1.-_RXN : 1 5-aminopentanal + 1 NAD+ + 1 H2O --> 1 5-aminopentanoate + 1 NADH + 1 H+
L-lysine-degradation_2.6.1.48_VAGL-RXN : 1 5-aminopentanoate + 1 2-oxoglutarate <=> 1 L-glutamate + 1 glutarate_semialdehyde
lysine-degradation_1.2.1.-_RXN-8182 : 1 glutarate_semialdehyde + 1 H2O + 1 NADP+ --> 1 glutarate + 1 NADPH + 2 H+
lysine-degradation_2.8.3.13_RXN-14724 : 1 succinyl-CoA + 1 glutarate --> 1 succinate + 1 glutaryl-CoA
lysine-degradation-VI_2.6.1.36_L-LYSINE-AMINOTRANSFERASE-RXN : 1 pyruvate + 1 L-lysine --> 1 (S)-2-amino-6-oxohexanoate + 1 L-alanine
spontaneous_lysine-degradation_lysine-biosynthesis_1.4.1.18_RXN-8173 : 1 (S)-2-amino-6-oxohexanoate <=> 1 H2O + 1 (S)-2,3,4,5-tetrahydropiperidine-2-carboxylate + 1 H+
lysine-degradation_1.2.1.-_RXN-8162 : 1 (S)-2,3,4,5-tetrahydropiperidine-2-carboxylate + 1 NAD+ + 2 H2O --> 1 H+ + 1 L-2-aminoadipate + 1 NADH
lysine-degradation_lysine-biosynthesis_2.6.1.39_2-AMINOADIPATE-AMINOTRANSFERASE-RXN : 1 pyruvate + 1 L-2-aminoadipate <=> 1 L-alanine + 1 2-oxoadipate
lysine-degra_1.2.4.4._RXN : 1 2-oxoadipate + 1 NAD+ + 1 coenzyme_A --> 1 glutaryl-CoA + 1 NADH + 1 H+ + 1 CO2
~no-pathway_1.3.8.6_RXN-14211 : 2 H+ + 1 glutaryl-CoA + 1 FAD --> 1 crotonyl-CoA + 1 CO2 + 1 FADH2
~no-pathway_4.3.1.28_RXN-13654 : 1 L-lysine <=> 1 L-pipecolate + 1 ammonium
lysine-degradation-V_1.5.3.7_L-PIPECOLATE-OXIDASE-RXN : 1 L-pipecolate + 1 oxygen --> 1 hydrogen_peroxide + 1 H+ + 1 (S)-2,3,4,5-tetrahydropiperidine-2-carboxylate

threonine degradation
threonine-degradation_aminopropanol-phosphate-biosynthesis_1.1.1.103_THREODEHYD-RXN : 1 L-threonine + 1 NAD+ --> 2 H+ + 1 NADH + 1 2-amino-3-oxobutanoate
threonine-degradation-II_2.3.1.29_AKBLIG-RXN : 1 acetyl-CoA + 1 glycine <=> 1 H+ + 1 coenzyme_A + 1 2-amino-3-oxobutanoate
~multiple-pathways_1.8.1.4_1.4.4.2_2.1.2.10_GCVMULTI-RXN : 1 tetrahydrofolate + 1 NAD+ + 1 glycine --> 1 ammonium + 1 NADH + 1 5,10-methylenetetrahydrofolate + 1 CO2
~metabolism-of-degradation_4.3.1.17_4.3.1.17-RXN: 1 L-serine --> 1 ammonium + 1 pyruvate
~no-pathway_4.1.2.5_LTAA-RXN : 1 L-threonine --> 1 glycine + 1 acetaldehyde

arginine and proline degradation
~multiple-pathways_3.5.3.1_ARGINASE-RXN : 1 L-arginine + 1 H2O <=> 1 urea + 1 L-ornithine
putrescine-biosynthesis_superpathway-of-ornithine-degradation_4.1.1.17_ORNDECARBOX-RXN : 1 L-ornithine + 1 H+ --> 1 putrescine + 1 CO2
arginine-degradation_ornithine-degradation_4.3.1.12_ORNITHINE-CYCLODEAMINASE-RXN : 1 L-ornithine --> 1 L-proline + 1 ammonium
~multiple-pathways_1.5.99.8_RXN-821 : 1 L-proline + 1 ubiquinone-10 --> 1 (S)-1-pyrroline-5-carboxylate + 1 H+ + 1 ubiquinol-10
spontaneous_multiple-pathways_SPONTPRO-RXN : 1 (S)-1-pyrroline-5-carboxylate + 1 H+ + 1 H2O <=> 1 L-glutamate-5-semialdehyde
~multiple-pathways_1.2.1.88_RXN-14116 : 1 L-glutamate-5-semialdehyde + 1 NAD+ + 1 H2O <=> 1 NADH + 1 L-glutamate + 2 H+
arginine-degradation-X-(arginine-monooxygenase-pathway)_1.13.12.1_ARGININE-2-MONOOXYGENASE-RXN : 1 L-arginine + 1 oxygen --> 1 H2O + 1 4-guanidinobutyramide + 1 CO2
arginine-degradation-X-(arginine-monooxygenase-pathway)_3.5.1.4_GUANIDINOBUTANAMIDE-NH3-RXN : 1 4-guanidinobutyramide + 1 H2O --> 1 ammonium + 1 4-guanidinobutyrate
arginine-degradation_3.5.3.7_GUANIDINOBUTYRASE-RXN : 1 4-guanidinobutyrate + 1 H2O --> 1 4-aminobutanoate + 1 urea

cysteine degradation
hydrogen-sulfide-biosynthesis_L-cysteine-degradation_2.6.1.1_CYSTEINE-AMINOTRANSFERASE-RXN: 1 2-oxoglutarate + 1 L-cysteine <=> 1 L-glutamate + 1 3-mercaptopyruvate
TCA-cycle_2.8.1.2_BR48100: 1 3-mercaptopyruvate + 1 hydrogen_cyanide <=> 1 thiocyanate + 1 pyruvate + 1 H+
L-cysteine-degradation-II_4.4.1.1_LCYSDESULF-RXN : 1 H2O + 1 L-cysteine --> 1 hydrogen_sulfide + 1 pyruvate + 1 ammonium

tyrosine degradation
~multiple-pathways_1.13.11.27_4-HYDROXYPHENYLPYRUVATE-DIOXYGENASE-RXN : 1 oxygen + 1 4-hydroxyphenylpyruvate --> 1 homogentisate + 1 CO2
tyrosine-degradation-I_1.13.11.5_HOMOGENTISATE-12-DIOXYGENASE-RXN : 1 homogentisate + 1 oxygen --> 1 4-maleyl-acetoacetate + 1 H+
tyrosine-degradation-I_5.2.1.2_MALEYLACETOACETATE-ISOMERASE-RXN: 1 4-maleyl-acetoacetate --> 1 4-fumaryl-acetoacetate
tyrosine-degradation-I_3.7.1.2_FUMARYLACETOACETASE-RXN: 1 4-fumaryl-acetoacetate + 1 H2O --> 1 fumarate + 1 H+ + 1 acetoacetate

 # carbohydrate degradation

N-acetyl-glucosamine degradation
chitin-derivatives-degradation_N-acetylglucosamine-degradation_2.7.1.59_N-ACETYLGLUCOSAMINE-KINASE-RXN : 1 ATP + 1 N-acetyl-beta-D-glucosamine --> 1 ADP + 1 N-acetyl-D-glucosamine_6-phosphate + 1 H+
chitin-derivatives-degradation_N-acetylglucosamine-degradation_3.5.1.25_NAG6PDEACET-RXN: 1 N-acetyl-D-glucosamine_6-phosphate + 1 H2O --> 1 alpha-D-glucosamine_6-phosphate + 1 acetate

xylose degradation
xylose-degradation-I_5.3.1.5_XYLISOM-RXN : 1 D-xylose <=> 1 D-xylulose
~metabolism-of-degradation_2.7.1.17_XYLULOKIN-RXN : 1 ATP + 1 D-xylulose --> 1 ADP + 1 H+ + 1 D-xylulose-5-phosphate

sucrose degradation
~no-pathway_3.2.1.20_RXN-2141 : 1 sucrose + 1 H2O --> 1 alpha-D-glucose + 1 beta-D-fructofuranose
~multiple-pathways_2.7.1.4_FRUCTOKINASE-RXN : 1 ATP + 1 beta-D-fructofuranose --> 1 ADP + 1 D-fructose-6-phosphate + 1 H+

mannitol degradation
mannitol-degra_1.1.1.67_MANNDEHYDR-RXN : 1 mannitol + 1 NAD+ --> 1 beta-D-fructofuranose + 1 NADH + 1 H+

 # 4-aminobutanoate degradation
~multiple-pathways_2.6.1.19_GABATRANSAM-RXN : 1 2-oxoglutarate + 1 4-aminobutanoate <=> 1 succinate_semialdehyde + 1 L-glutamate
4-aminobutyrate-degradation-III_1.2.1.16_RXN0-5293_NAD : 1 H2O + 1 succinate_semialdehyde + 1 NAD+ --> 1 succinate + 1 NADH + 2 H+
4-aminobutyrate-degradation-III_1.2.1.16_RXN0-5293_NADP : 1 succinate_semialdehyde + 1 H2O + 1 NADP+ --> 1 NADPH + 1 succinate + 2 H+

 # allantoin degradation
allantoin-degradation-to-ureidoglycolate_3.5.2.5_ALLANTOINASE-RXN : 1 H2O + 1 (S)-(+)-allantoin --> 1 H+ + 1 allantoate
allantoin-degradation-to-ureidoglycolate-II-(ammonia-producing)_3.5.3.9_ALLANTOATE-DEIMINASE-RXN : 1 H2O + 2 H+ + 1 allantoate --> 1 ammonium + 1 S-ureidoglycine + 1 CO2
allantoin-degradation-to-glyoxylate_allantoin-degradation-to-ureidoglycolate_3.5.3.26_URUR-RXN : 1 S-ureidoglycine + 1 H2O --> 1 S-ureidoglycolate + 1 ammonium
~no-pathway_3.5.1.116_BR29521 : 1 S-ureidoglycolate + 1 H2O --> 1 glyoxylate + 1 CO2 + 2 ammonia
allantoin-degradation-to-glyoxylate_4.3.2.3_UREIDOGLYCOLATE-LYASE-RXN : 1 S-ureidoglycolate --> 1 urea + 1 glyoxylate
 # myo-inositol degradation
~multiple-pathways_1.1.1.18_MYO-INOSITOL-2-DEHYDROGENASE-RXN : 1 myo-inositol + 1 NAD+ <=> 1 NADH + 1 scyllo-inosose + 1 H+
myo-inositol-degradation-I_4.2.1.44_MYO-INOSOSE-2-DEHYDRATASE-RXN : 1 scyllo-inosose --> 1 3D-(3,5_4)-trihydroxycyclohexane-1,2-dione + 1 H2O
myo-inositol-degradation-I_3.7.1.22_RXN-14149 : 1 H2O + 1 3D-(3,5_4)-trihydroxycyclohexane-1,2-dione --> 1 H+ + 1 5-deoxy-D-glucuronate
myo-inositol-degradation-I_5.3.1.30_RXN-14150 : 1 5-deoxy-D-glucuronate <=> 1 2-deoxy-5-dehydro-D-gluconate
myo-inositol-degradation-I_2.7.1.92_5-DEHYDRO-2-DEOXYGLUCONOKINASE-RXN : 1 ATP + 1 2-deoxy-5-dehydro-D-gluconate --> 1 H+ + 1 5-dehydro-2-deoxy-D-gluconate_6-phosphate + 1 ADP
myo-inositol-degradation-I_4.1.2.29_4.1.2.29-RXN: 1 5-dehydro-2-deoxy-D-gluconate_6-phosphate --> 1 dihydroxyacetone_phosphate + 1 malonate_semialdehyde
myo-inositol-degradation_beta-alanine-degradation_1.2.1.18_RXN-2902 : 1 coenzyme_A + 1 NAD+ + 1 malonate_semialdehyde --> 1 CO2 + 1 NADH + 1 acetyl-CoA
~no-pathway_1.2.1.18_1.2.1.18-RXN : 1 coenzyme_A + 1 malonate_semialdehyde + 1 NADP+ --> 1 NADPH + 1 CO2 + 1 acetyl-CoA

 # butanoate degradation
methyl-ketone-biosynthesis_6.2.1.2_BS143 : 1 n-butanoate + 1 coenzyme_A + 1 ATP --> 1 AMP + 1 diphosphate + 1 butanoyl-CoA
~no-pathway_1.3.8.1_RXN-14193 : 1 butanoyl-CoA + 1 H+ + 1 FAD <=> 1 FADH2 + 1 crotonyl-CoA

 # uracil degradation
#uracil-degradation-I-(reductive)_1.3.1.2_1.3.1.2-RXN: 1 NADP+ + 1 5,6-dihydrouracil <=> 1 H+ + 1 uracil + 1 NADPH
#uracil-degradation-I-(reductive)_3.5.2.2_DIHYDROPYRIMIDINASE-RXN : 1 H2O + 1 5,6-dihydrouracil <=> 1 H+ + 1 3-ureidopropionate
#uracil-degradation-I-(reductive)_3.5.1.6_BETA-UREIDOPROPIONASE-RXN : 2 H+ + 1 H2O + 1 3-ureidopropionate --> 1 CO2 + 1 ammonium + 1 beta-alanine

##

 # additional reactions
~metabolism-of-biosynthesis_6.3.2.2_GLUTCYSLIG-RXN: 1 L-cysteine + 1 ATP + 1 L-glutamate --> 1 H+ + 1 L-gamma-glutamylcysteine + 1 phosphate + 1 ADP
glutathione-biosynthesis_6.3.2.3_GLUTATHIONE-SYN-RXN: 1 glycine + 1 L-gamma-glutamylcysteine + 1 ATP --> 1 ADP + 1 phosphate + 1 glutathione + 1 H+
~no-pathway_3.6.1.25_TRIPHOSPHATASE-RXN: 1 PPPi + 1 H2O --> 1 diphosphate + 1 phosphate
~no-pathway_4.2.1.1_CARBODEHYDRAT-RXN: 1 bicarbonate <=> 1 CO2 + 1 H2O
5,6-dimethylbenzimidazole-biosynthesis_1.5.1.38_FMNREDUCT-RXN_NADP : 1 FMNH2 + 1 NADP+ <-- 1 FMN + 1 NADPH + 2 H+
~no-pathway_1.5.5.1_1.5.5.1-RXN: 1 FADH2 + 1 ubiquinone-10 <=> 1 ubiquinol-10 + 1 FAD
glycerol-degradation_glycerophosphodiester-degradation_1.1.5.3_RXN0-5258 : 1 sn-glycerol_3-phosphate + 1 ubiquinone-10 <=> 1 ubiquinol-10 + 1 dihydroxyacetone_phosphate
~multiple-pathways_1.2.1.2_1.2.1.2-RXN : 1 formate + 1 NAD+ --> 1 NADH + 1 CO2

 # spontaneous
spontaneous_metabolism-of-degradation_5.1.3.3_ALDOSE-1-EPIMERASE-RXN : 1 alpha-D-glucose <=> 1 beta-D-glucose
spontaneous_multiple-pathways_5.1.3.15_5.3.1.9_GLUCOSE-6-PHOSPHATE-1-EPIMERASE-RXN: 1 alpha-D-glucose_6-phosphate <=> 1 beta-D-glucose-6-phosphate
spontaneous_no-pathway_RXN-1181 : 1 ammonia + 1 H+ <=> 1 ammonium
spontaneous_sulfate-reduction-IV-(dissimilatory)_RXN-8315: 1 sulfite + 1 H+ <=> 1 bisulfite

##

 # transport reactions

carbohydrate uptake
T_ex_C_beta-D-glucose : 1 beta-D-glucose_ex <=>
T_trans_C_beta-D-glucose : 1 beta-D-glucose + 1 ADP + 1 phosphate + 1 H+ <-- 1 beta-D-glucose_ex + 1 ATP + 1 H2O
T_ex_C_N-acetyl-beta-D-glucosamine : 1 N-acetyl-beta-D-glucosamine_ex <=>
T_trans_C_N-acetyl-beta-D-glucosamine : 1 N-acetyl-beta-D-glucosamine + 1 ADP + 1 phosphate + 1 H+ <-- 1 N-acetyl-beta-D-glucosamine_ex + 1 ATP + 1 H2O
T_ex_C_D-xylose : 1 D-xylose_ex <=>
T_trans_C_D-xylose : 1 D-xylose + 1 ADP + 1 phosphate + 1 H+ <-- 1 D-xylose_ex + 1 ATP + 1 H2O
T_ex_C_sucrose : 1 sucrose_ex <=>
T_trans_C_sucrose : 1 sucrose + 1 ADP + 1 phosphate + 1 H+ <-- 1 sucrose_ex + 1 ATP + 1 H2O
T_ex_C_mannitol : 1 mannitol_ex <=>
T_trans_C_mannitol : 1 mannitol + 1 ADP + 1 phosphate + 1 H+ <-- 1 mannitol_ex + 1 ATP + 1 H2O

amino acid uptake
T_ex_C_L-alanine : 1 L-alanine_ex <=>
T_trans_C_L-alanine : 1 L-alanine + 1 Na+ <-- 1 L-alanine_ex + 1 Na+_ex
T_ex_C_L-arginine : 1 L-arginine_ex <=>
T_trans_C_L-arginine : 1 L-arginine + 1 ADP + 1 phosphate + 1 H+ <-- 1 L-arginine_ex + 1 ATP + 1 H2O
T_ex_C_L-asparagine : 1 L-asparagine_ex <=>
T_trans_C_L-asparagine : 1 L-asparagine + 1 ADP + 1 phosphate + 1 H+ <-- 1 L-asparagine_ex + 1 ATP + 1 H2O
T_ex_C_L-aspartate : 1 L-aspartate_ex <=>
T_trans_C_L-aspartate : 1 L-aspartate + 1 ADP + 1 phosphate + 1 H+ <-- 1 L-aspartate_ex + 1 ATP + 1 H2O
T_ex_C_L-cysteine : 1 L-cysteine_ex <=>
T_trans_C_L-cysteine : 1 L-cysteine + 1 ADP + 1 phosphate + 1 H+ <-- 1 L-cysteine_ex + 1 ATP + 1 H2O
T_ex_C_L-glutamine : 1 L-glutamine_ex <=>

T_trans_C_L-glutamine : 1 L-glutamine + 1 ADP + 1 phosphate + 1 H+ <-- 1 L-glutamine_ex + 1 ATP + 1 H2O
T_ex_C_L-glutamate : 1 L-glutamate_ex <=>
T_trans_C_L-glutamate : 1 L-glutamate + 1 ADP + 1 phosphate + 1 H+ <-- 1 L-glutamate_ex + 1 ATP + 1 H2O
T_ex_C_glycine : 1 glycine_ex <=>
T_trans_C_glycine : 1 glycine + 1 Na+ <-- 1 glycine_ex + 1 Na+_ex
T_ex_C_L-histidine : 1 L-histidine_ex <=>
T_trans_C_L-histidine : 1 L-histidine + 1 ADP + 1 phosphate + 1 H+ <-- 1 L-histidine_ex + 1 ATP + 1 H2O
T_ex_C_L-isoleucine : 1 L-isoleucine_ex <=>
T_trans_C_L-isoleucine : 1 L-isoleucine + 1 ADP + 1 phosphate + 1 H+ <-- 1 L-isoleucine_ex + 1 ATP + 1 H2O
T_ex_C_L-leucine : 1 L-leucine_ex <=>
T_trans_C_L-leucine : 1 L-leucine + 1 ADP + 1 phosphate + 1 H+ <-- 1 L-leucine_ex + 1 ATP + 1 H2O
T_ex_C_L-lysine : 1 L-lysine_ex <=>
T_trans_C_L-lysine : 1 L-lysine + 1 ADP + 1 phosphate + 1 H+ <-- 1 L-lysine_ex + 1 ATP + 1 H2O
T_ex_C_L-methionine : 1 L-methionine_ex <=>
T_trans_C_L-methionine : 1 L-methionine + 1 ADP + 1 phosphate + 1 H+ <-- 1 L-methionine_ex + 1 ATP + 1 H2O
T_ex_C_L-phenylalanine : 1 L-phenylalanine_ex <=>
T_trans_C_L-phenylalanine : 1 L-phenylalanine + 1 ADP + 1 phosphate + 1 H+ <-- 1 L-phenylalanine_ex + 1 ATP + 1 H2O
T_ex_C_L-proline : 1 L-proline_ex <=>
T_trans_C_L-proline : 1 L-proline + 1 ADP + 1 phosphate + 1 H+ <-- 1 L-proline_ex + 1 ATP + 1 H2O
T_ex_C_L-serine : 1 L-serine_ex <=>
T_trans_C_L-serine : 1 L-serine + 1 ADP + 1 phosphate + 1 H+ <-- 1 L-serine_ex + 1 ATP + 1 H2O
T_ex_C_L-threonine : 1 L-threonine_ex <=>
T_trans_C_L-threonine : 1 L-threonine + 1 ADP + 1 phosphate + 1 H+ <-- 1 L-threonine_ex + 1 ATP + 1 H2O
T_ex_C_L-tryptophan : 1 L-tryptophan_ex <=>
T_trans_C_L-tryptophan : 1 L-tryptophan + 1 ADP + 1 phosphate + 1 H+ <-- 1 L-tryptophan_ex + 1 ATP + 1 H2O
T_ex_C_L-tyrosine : 1 L-tyrosine_ex <=>
T_trans_C_L-tyrosine : 1 L-tyrosine + 1 ADP + 1 phosphate + 1 H+ <-- 1 L-tyrosine_ex + 1 ATP + 1 H2O
T_ex_C_L-valine : 1 L-valine_ex <=>
T_trans_C_L-valine : 1 L-valine + 1 ADP + 1 phosphate + 1 H+ <-- 1 L-valine_ex + 1 ATP + 1 H2O

additional C-sources
T_ex_C_succinate : 1 succinate_ex <=>
T_trans_C_succinate : 1 succinate + 1 H+ <-- 1 succinate_ex + 1 H+_ex
T_ex_C_acetate : 1 acetate_ex <=>
T_trans_C_acetate : 1 acetate + 1 H+ <-- 1 acetate_ex + 1 H+_ex
T_ex_C_pyruvate : 1 pyruvate_ex <=>
T_trans_C_pyruvate : 1 pyruvate + 1 H+ <-- 1 pyruvate_ex + 1 H+_ex
T_ex_C_2-oxoglutarate : 1 2-oxoglutarate_ex <=>
T_trans_C_2-oxoglutarate : 1 2-oxoglutarate + 1 H+ <-- 1 2-oxoglutarate_ex + 1 H+_ex
T_ex_C_4-aminobutanoate : 1 4-aminobutanoate_ex <=>
T_trans_C_4-aminobutanoate : 1 4-aminobutanoate + 1 Na+ <-- 1 4-aminobutanoate_ex + 1 Na+_ex
T_ex_C_myo-inositol : 1 myo-inositol_ex <=>
T_trans_C_myo-inositol : 1 myo-inositol + 1 Na+ <-- 1 myo-inositol_ex + 1 Na+_ex
T_ex_C_n-butanoate : 1 n-butanoate_ex <=>
T_trans_C_n-butanoate : 1 n-butanoate + 1 Na+ <-- 1 n-butanoate_ex + 1 Na+_ex

additional N-sources
T_ex_N_(S)-(+)-allantoin : 1 (S)-(+)-allantoin_ex <=>
T_trans_N_(S)-(+)-allantoin: 1 (S)-(+)-allantoin + 1 Na+ <-- 1 (S)-(+)-allantoin_ex + 1 Na+_ex

mineral and organic ion
T_ex_ammonium : 1 ammonium_ex <=>
T_trans_ammonium : 1 ammonium <=> 1 ammonium_ex
T_ex_sulfate : 1 sulfate_ex <=>
T_trans_sulfate : 1 sulfate + 1 ADP + 1 phosphate + 1 H+ <-- 1 sulfate_ex + 1 ATP + 1 H2O
T_ex_phosphate : 1 phosphate_ex <=>
T_trans_Na+ : 1 Na+ + 2 H+_ex --> 1 Na+_ex + 2 H+

others
T_ex_oxygen : 1 oxygen_ex <=>
T_trans_oxygen : 1 oxygen <=> 1 oxygen_ex
T_ex_H2O : 1 H2O_ex <=>
T_trans_H2O : 1 H2O <=> 1 H2O_ex
T_ex_H+ : 1 H+ -->
T_ex_H+_ex : 1 H+_ex <=>

secondary metabolites
T_ex_TDA : 1 TDA_ex <=>
T_trans_TDA : 1 TDA --> 1 TDA_ex

by-products/intermediates
T_ex_CO2 : 1 CO2_ex <=>
T_trans_CO2 : 1 CO2 <=> 1 CO2_ex
T_ex_methanethiol : 1 methanethiol_ex <=>
T_trans_methanethiol : 1 methanethiol --> 1 methanethiol_ex
T_ex_hydrogen_sulfide : 1 hydrogen_sulfide_ex <=>
T_trans_hydrogen_sulfide : 1 hydrogen_sulfide --> 1 hydrogen_sulfide_ex
T_ex_nitrate : 1 nitrate_ex <=>
T_trans_nitrate : 1 nitrate --> 1 nitrate_ex
T_ex_nitrite : 1 nitrite_ex <=>
T_trans_nitrite : 1 nitrite --> 1 nitrite_ex
T_ex_formate : 1 formate_ex <=>
T_trans_formate : 1 formate --> 1 formate_ex
T_ex_fumarate : 1 fumarate_ex <=>
T_trans_fumarate : 1 fumarate --> 1 fumarate_ex
T_ex_urea : 1 urea_ex <=>
T_trans_urea : 1 urea --> 1 urea_ex
T_ex_(2S)-2-isopropylmalate : 1 (2S)-2-isopropylmalate_ex <=>
T_trans_(2S)-2-isopropylmalate : 1 (2S)-2-isopropylmalate --> 1 (2S)-2-isopropylmalate_ex
T_ex_2-hydroxyphenylacetate : 1 2-hydroxyphenylacetate_ex <=>
T_trans_2-hydroxyphenylacetate : 1 2-hydroxyphenylacetate --> 1 2-hydroxyphenylacetate_ex
T_ex_cadaverine : 1 cadaverine_ex <=>
T_trans_cadaverine : 1 cadaverine --> 1 cadaverine_ex
T_ex_anthranilate : 1 anthranilate_ex <=>
T_trans_anthranilate : 1 anthranilate --> 1 anthranilate_ex
T_ex_L-kynurenine : 1 L-kynurenine_ex <=>
T_trans_L-kynurenine : 1 L-kynurenine --> 1 L-kynurenine_ex
T_ex_keto-phenylpyruvate : 1 keto-phenylpyruvate_ex <=>
T_trans_keto-phenylpyruvate : 1 keto-phenylpyruvate --> 1 keto-phenylpyruvate_ex

T_ex_hydrogen_peroxide : 1 hydrogen_peroxide_ex <=>
T_trans_hydrogen_peroxide : 1 hydrogen_peroxide --> 1 hydrogen_peroxide_ex

##

 # NGAM

NGAM : 1 ATP + 1 H2O --> 1 ADP + 1 phosphate + 1 H+

 # biomass

biomass_Ala_WT : 0.54 proteins + 0.016 dna + 0.045 rna + 0.068 phospholipids + 0.12 peptidoglycan + 0.034 LPS + 0.07 PHB + 0.04 L-glutamate + 0.02 solublepool + 85 ATP + 85 H2O --> 85 ADP + 85 phosphate + 85 H+
biomass_Phe_WT : 0.55 proteins + 0.013 dna + 0.054 rna + 0.061 phospholipids + 0.12 peptidoglycan + 0.034 LPS + 0.13 PHB + 0.04 L-glutamate + 0.02 solublepool + 85 ATP + 85 H2O --> 85 ADP + 85 phosphate + 85 H+
biomass_Leu_WT : 0.53 proteins + 0.014 dna + 0.034 rna + 0.056 phospholipids + 0.12 peptidoglycan + 0.034 LPS + 0.17 PHB + 0.04 L-glutamate + 0.02 solublepool + 85 ATP + 85 H2O --> 85 ADP + 85 phosphate + 85 H+
biomass_Ala_D262 : 0.56 proteins + 0.014 dna + 0.068 rna + 0.059 phospholipids + 0.12 peptidoglycan + 0.034 LPS + 0.07 PHB + 0.04 L-glutamate + 0.02 solublepool + 85 ATP + 85 H2O --> 85 ADP + 85 phosphate + 85 H+
biomass_Phe_D262 : 0.52 proteins + 0.02 dna + 0.058 rna + 0.053 phospholipids + 0.12 peptidoglycan + 0.034 LPS + 0.14 PHB + 0.04 L-glutamate + 0.02 solublepool + 85 ATP + 85 H2O --> 85 ADP + 85 phosphate + 85 H+
biomass_Leu_D262 : 0.59 proteins + 0.016 dna + 0.043 rna + 0.059 phospholipids + 0.12 peptidoglycan + 0.034 LPS + 0.14 PHB + 0.04 L-glutamate + 0.02 solublepool + 85 ATP + 85 H2O --> 85 ADP + 85 phosphate + 85 H+
biomass_Ala_tdaE : 0.59 proteins + 0.012 dna + 0.059 rna + 0.053 phospholipids + 0.12 peptidoglycan + 0.034 LPS + 0.07 PHB + 0.04 L-glutamate + 0.02 solublepool + 85 ATP + 85 H2O --> 85 ADP + 85 phosphate + 85 H+
biomass_Phe_tdaE : 0.51 proteins + 0.011 dna + 0.039 rna + 0.059 phospholipids + 0.12 peptidoglycan + 0.034 LPS + 0.24 PHB + 0.04 L-glutamate + 0.02 solublepool + 85 ATP + 85 H2O --> 85 ADP + 85 phosphate + 85 H+
biomass_Leu_tdaE : 0.50 proteins + 0.009 dna + 0.037 rna + 0.034 phospholipids + 0.12 peptidoglycan + 0.034 LPS + 0.23 PHB + 0.04 L-glutamate + 0.02 solublepool + 85 ATP + 85 H2O --> 85 ADP + 85 phosphate + 85 H+

PROTEIN : 0.6256 L-alanine + 0.4762 L-arginine + 0.3040 L-asparagine + 0.6993 L-aspartate + 0.1329 L-cysteine + 0.2499 L-glutamine + 0.3999 L-glutamate + 0.9359 glycine + 0.1343 L-histidine + 0.3658 L-isoleucine + 0.6430 L-leucine + 0.2375 L-lysine + 0.1185 L-methionine + 0.3173 L-phenylalanine + 0.5352 L-proline + 0.4893 L-serine + 0.5569 L-threonine + 0.1049 L-tryptophan + 0.1994 L-tyrosine + 0.5625 L-valine --> proteins

DNA : 0.6604 dTMP + 1.0343 dCMP + 0.6414 dAMP + 0.9085 dGMP --> dna

RNA : 0.6561 UMP + 0.9800 CMP + 0.6102 AMP + 0.8664 GMP --> rna

PHOSPHOLIPIDS : 0.4360 L-1-phosphatidylethanolamine + 0.4712 L-1-phosphatidylglycerol + 0.2062 phosphatidylcholine + 0.0070 cardiolipin --> phospholipids

PEPTIDOGLYCAN : 0.174855744 a_peptidoglycan_with_D,D_cross-links_(meso-diaminopimelate_containing) --> peptidoglycan

LPS : 0.0371 (KDO)2-lipid_A + 3.6196 UDP-alpha-D-glucose + 1.6176 UDP-N-acetyl-alpha-D-glucosamine --> 1 LPS + 5.2372 UDP + 1 H+

SOLUBLE POOL : 0.107 NAD+ + 0.00645 NADP+ + 0.0025 NADH + 0.0199 NADPH + 0.24876 tetrahydrofolate + 0.0005 FAD + 0.00295 riboflavin + 0.00295 coenzyme_A + 0.00295 ubiquinol-10 + 0.00295 S-adenosyl-L-methionine + 0.00015 succinyl-CoA + 0.0025 acetyl-CoA --> solublepool

PHB: 11.50 [PHB] --> 1 PHB

Danksagung

Ich möchte mich bei meinem Mentor Prof. Dietmar Schomburg für die Bereitstellung dieses Themas und die zahlreichen wissenschaftlichen und hilfreichen Diskussionen bedanken. Zudem danke ich Prof. Dieter Jahn für die Übernahme des Zweitgutachtens sowie Prof. Michael Hust für die Übernahme des Vorsitzes der Prüfungskommission.

Meinen Kooperationspartnern aus der Arbeitsgruppe von Prof. Rabus, insbesondere Dr. Kathleen Trautwein, danke ich für die Zusammenarbeit bei einigen Experimenten. Ein großer Dank geht auch an die Arbeitsgruppe von PD Dr. Jörn Petersen, insbesondere Pascal Bartling und Victoria Michael, für die Bereitstellung aller *Phaeobacter inhibens* Stämme.

Ein besonderer Dank gebührt Dr. Meina Neumann-Schaal für die große Unterstützung bei wissenschaftlichen Fragestellungen und das Korrekturlesen meiner Arbeit. Sabine Kaltenhäuser danke ich für die Instandhaltung der Analytik sowie des Kaffeevorrates. Sabine Noppenberger danke ich für allerlei Tätigkeiten, die einem den Laboralltag vereinfachten. Für die Hilfe bei einigen Experimenten sowie einiger *Phaeobacter*-spezifischer Diskussionen möchte ich mich bei Elisabeth Majer bedanken. Zudem danke ich Leopold Heydorn für seine hilfreiche Unterstützung im Labor. Bei Dr. Michael Hensler bedanke ich mich für seine hilfreichen Tipps, die mir den Einstieg erleichtert haben. Ein großer Dank geht raus an meine BRICS-Bürokollegin Julia Hofmann für die gemeinsame Achterbahnfahrt mit allen Höhen und Tiefen. Allen aktuellen und ehemaligen Mitarbeitern der Arbeitsgruppe gebührt ein großer Dank für die gute Arbeitsatmosphäre und stetige Hilfsbereitschaft untereinander sowie für die fachlichen aber auch fachfremden Diskussionen. Es wurde viel gearbeitet und verzweifelt, sodass ein Ausgleich zusammen in der Freizeit bei unvergessenen Lasertag Sessions, Spieleabenden und dem gemeinsamen Rätsel lösen unausweichlich war.

Zuletzt möchte ich mich bei meiner Familie und Freunden für die Unterstützung bedanken. Meinem Bruder Christoph danke ich für die Bereitschaft Teile meiner Arbeit Korrektur zu lesen. Zum Abschluss bedanke ich mich bei Jonas für die Geduld, den Rückhalt und die aufmunternden und motivierenden Worte und Taten.